

ALMA MATER STUDIORUM - UNIVERSITÀ DI BOLOGNA

FACOLTA' DI INGEGNERIA

CORSO DI LAUREA IN CIVIL ENGINEERING

DICAM

TESI DI LAUREA

in

Advanced Design of Concrete Structures

**NUMERICAL ANALYSIS AND EXPERIMENTAL
TESTS ON REINFORCED CONCRETE GRID WALL SYSTEMS**

CANDIDATO

Rita Borgognoni

RELATORE:

Chiar.mo Prof. Marco Savoia

CORRELATORI

Chiar.mo Prof. Claudio Mazzotti

Dott. Ing. Marco Bovo

Anno Accademico 2011/2012

Sessione I

INDEX

Numerical analysis and experimental tests on reinforced concrete grid wall systems

Abstract..... 11

Introduction.....15

Chapter 1

THE R.C. GRID WALL SYSTEM: NATIONAL AND INTERNATIONAL NORMATIVE CONTEXT AND BACKGROUND.....17

Object..... 18

1.1 The grid-wall system..... 18

1.1.1 *The construction technique*..... 19

1.1.2 *The Structural Behaviour in ETAG 009*.....22

1.2 The U.S. background24

1.2.1 *Design of Grid-wall in U.S.A*.....28

1.3 The Italian and European normative context for design purposes.....31

1.3.1 *Definitions*.....32

1.3.2 *Normal and shear stresses*.....32

1.3.3 *Behaviour factor*.....32

Chapter 2

THE EXPERIMENTAL TESTS.....41

Object.....42

2.1 The blocks object of experimental campaign.....43

2.2 Mechanical characterization of the materials: steel and concrete.....46

2.2.1 *Compression tests on concrete cubic specimen*.....46

2.2.2 *Traction test on reinforcing steel bars*.....49

2.3 The compression test.....52

2.3.1 The compression centered test.....	53
2.3.2 The diagonal tests.....	54

Chapter 3

EVALUATION OF THE EQUIVALENT CONTINUOUS WALL.....	55
--	-----------

Background.....	56
------------------------	-----------

Object.....	56
--------------------	-----------

Introduction.....	56
--------------------------	-----------

3.1 Characteristics of materials.....	57
--	-----------

3.2 Analysis of the results on 14 cm width panels.....	58
---	-----------

3.2.1 Equivalent thickness s_{eg} and Mean Axial Stiffness ΔK_{14} of the continuous wall 14 cm width (Block 25/18).....	58
--	----

3.2.2 Results of centered compression tests on panels 14 cm width: CC14_01 and CC14_02.....	59
---	----

3.3 Interpretation of the compression tests on 14 cm width panels.....	61
---	-----------

3.3.1 Equivalent Young Modulus E' of the continuous wall with $s_{eg}=9.8$ cm.....	61
--	----

3.3.2 Results of compressive diagonal tests on panels 14 cm width: CD14_01 and CD14_02.....	62
---	----

3.3.3 Equivalent Elastic Tangential Modulus G' of the continuous wall.....	64
--	----

3.4 Analysis of the results on 18 cm width panels.....	67
---	-----------

3.4.1 Equivalent thickness s_{eg} and Mean Axial Stiffness ΔK_{18} of the continuous wall 18 cm width (Block 32/22).....	67
--	----

3.4.2 Results of centered compression tests on panels 18 cm width: CC18_01 and CC18_02.....	68
---	----

3.5 Interpretation of the centered compression tests on 18cm width panels.....	70
---	-----------

3.5.1 Equivalent Young Modulus E' of the continuous wall with $s_{eg}=11.88$ cm.....	70
3.5.2 Results of compressive diagonal tests on panels 14 cm width: CD18_01 and CD18_02.....	72
3.5.3 Equivalent Elastic Tangential Modulus G' of the continuous wall.....	72
3.6 Summary.....	75
3.6.1 Definition of equivalent geometric thickness s_{eg}	75
3.6.2 Correction coefficient α and β	76
3.7 Equivalent continuous numerical models.....	77
3.7.1 Implementation and results on continuous wall 14.....	78
3.7.2 Implementation and results on continuous wall 18.....	79
.	
Chapter 4	
CONSTITUTIVE MODELS FOR MODELING PURPOSE.....	81
Background.....	82
Object.....	82
Introduction.....	82
4.1 Experimental behavior of the concrete.....	83
4.1.1 Concrete subject to uniaxial compression.....	83
4.1.2 Concrete subject to uniaxial tension.....	85
4.1.3 Behavior of concrete subjected to a biaxial state of stress.....	86
4.1.4 Behavior of concrete subjected to a triaxial state of stress.....	88
4.2 Constitutive models of concrete.....	89
4.3 Constitutive models in Abaqus: Concrete Damage Plasticity model(CDP).....	91
4.3.1 The main features of CDP model.....	91
4.3.2 Strain rate decomposition.....	92
4.3.3 Stress-strain relations.....	92
4.3.4 Postfailure stress-strain relation in traction.....	92
4.3.5 Fracture energy.....	94
4.3.6 Defining compressive behavior: $\sigma_{c_inel}-\epsilon_{c_inel}$; damage variable d_c	96

4.3.7 Hardening variables.....	98
4.3.8 Yield condition.....	98
4.3.9 The flow rule.....	102
4.4 Definition of plasticity parameters of CDP.....	103
4.5 Concrete compression behavior: Kent-Park formulation.....	104
4.6 Concrete traction behaviors implemented.....	105
4.6.1 Cornelissen's theoretical formulation on the post peak traction behavior of concrete(1986)	105
4.6.2 Experimental results on traction proof on plain concrete specimen.....	110
4.7 Numerical simulation of a simple tensile test.....	112
4.7.1 Implementation of simple tensile test (Reinhard 1986)with smeared cracking model.....	115
4.7.2 The CDP "concrete damage plasticity" model based on Lee and Fenver theory.....	124
Chapter 5	
BOND-SLIP FORMULATION.....	127
Background.....	128
Object.....	128
Introduction.....	128
5.1 Bond-slip Relationship.....	129
5.2 Current Study and Existing Models.....	133
5.2.1 FE Model of Reinforced Concrete.....	133
5.2.2 FE Model of Bond.....	134
5.2.3 Interaction Module of ABAQUS.....	135
5.2.3.1 Friction.....	136

5.2.3.2 Cohesive based surface modeling.....	137
5.3 The pull-out test.....	140
5.3.1 The test equipment.....	140
5.3.2 Load and boundary condition.....	141
5.3.4 Bond-slip formulation in the pull-out test.....	142
5.4 Bond-slip law implemented in the Pull-out test.....	144
5.5 The results of the Pull-out numerical test.....	146
5.6 Bond-slip law implemented in the grid-wall.....	148
Chapter 6	
NUMERICAL MODELS IN ABAQUS.....	149
<i>Background.....</i>	<i>150</i>
<i>Object.....</i>	<i>151</i>
<i>Introduction.....</i>	<i>151</i>
<i>FE model for panels subjected to centered axial compression.....</i>	<i>153</i>
6.1 The "Part" module.....	153
6.1.1 The Units.....	154
6.1.2 The two bases.....	154
6.1.3 The concrete core.....	155
6.1.4 The steel bars.....	156
6.1.5 The wood-concrete cores.....	157
6.2 Mechanical characterization of the materials.....	158
6.2.1 Steel.....	158
6.2.2 Concrete.....	160
6.2.2.1 Kent-Park formulation implemented for compressive behavior.....	160

6.2.2.2 Formulation implemented for traction behavior.....	162
6.2.3 The high strength concrete bases.....	164
6.2.4 The wood-concrete elements.....	165
6.3 The assembly.....	167
6.4 The "Step" module.....	169
6.5The "Interaction" module.....	174
6.6. The load and the boundary conditions.....	181
6.7 The mesh.....	182
Chapter 7	
RESULTS OF THE NUMERICAL MODEL IN ABAQUS.....	187
<i>Introduction.....</i>	<i>188</i>
7.1 Comparison P-ΔL curves.....	189
7.1.1 P- Vertical Δ L comparison.....	189
7.1.2 P-Horizontal Δ L comparison.....	190
7.2 Active yield flag.....	192
7.3 Main stresses on the pillars.....	194
7.4 Main stresses on the connector-beams.....	195
7.5 Main stresses on the wood-concrete elements.....	197
7.6 Strain distribution on concrete grid-wall.....	199
7.7 Comparison between cracking pattern of the test and numerical results.....	201
7.8 Collapse mechanism and stress history on steel bars.....	206
Chapter 8	
SUMMARY, CONCLUSIONS AND RECOMMENDATIONS FOR FUTURE STUDY.....	209
Bibliografy.....	213

*"La preoccupazione
dell'uomo e del suo destino
devono sempre costituire
l'interesse principale di tutti
gli sforzi tecnici. Non
dimenticatelo mai in mezzo a
tutti i vostri diagrammi e alle
vostre equazioni."*

A. Einstein

Acknowledgments

This thesis would not have been possible without the support of Prof. Claudio Mazzotti, who served me as my supervisors, and to Dr. Maddalena Dall'Agata who encouraged and helped me throughout all my university student career. Appreciation is also extended to, Dr. Marco Bovo and Dr. Luca Patruno, who offered guidance and support. Finally, thanks to my sister and to my friends, who endured this process with me, always offering support and love.

Abstract

Over the 2000-2010 decade, insulated concrete form (ICF) construction, has been growing in popularity in most all over Northern countries Europe (mainly in Germany, Austria, Belgium, U.S.A. and Canada). ICF is an innovative macro-category comprehensive of several type of walling system. Starting in residential house construction, this building method has now also started to expand into high density urban areas in the form of multi-story commercial and residential structures. Typically, Insulated concrete form walls (ICF) are characterized by the presence of different layers: one for structural purposes typically made of plain or reinforced concrete , combined with one or more insulating prefabricated layers for thermal and sound barriers purposes.

One of the ICF emerging structural systems that addresses sustainability from the structural and construction point of view have been the **insulated concrete form grid walls**, the object of this thesis, which are built using prefabricated stay-in-place formwork that provide improved thermal insulation over conventional methods, thereby reducing the energy requirements throughout the life of the building.



Figure a) – The shuttering kit formwork

The constructive system is composed of formwork blocks (or, “shuttering”) in mineralized wood (a mix of compressed crushed mineralized wood with water and cement slurry) that are properly assembled and filled with polystyrene for sound-

insulation purpose and of reinforced concrete as can be seen in *Figure a*). After curing of the concrete, the structure that is obtained (referred to in the following as the “structural concrete formation”) is a concrete bearing wall with horizontal and vertical steel reinforcement mesh. The structural components of the grid walls so obtained consist of horizontal and vertical reinforced concrete cores, as can be seen in the following in *Figure b*).

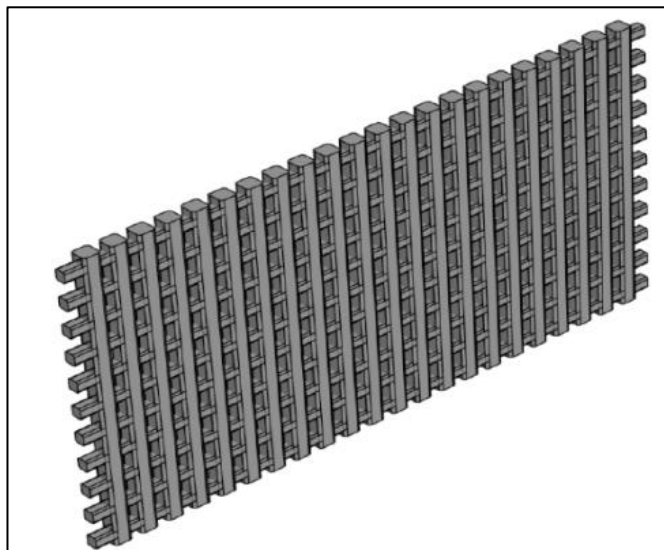


Figure b)– Grid type shear wall system

As before mentioned, ICF grid walls, are a little subset of ICF, that provides enhancements of ICF by using up to 40% less concrete respect to typical r.c. walls, and by near elimination of temporary formwork through the use modular erection methods based on the use of wood-concrete hollow blocks . Moreover the prefabricated blocks can be made from recycled materials, further enhancing the green building component of their use.

Building structures which make use of structural systems obtained filling with wood-concrete hollow bricks from the structural point of view can be seen as of **grid type shear wall systems** that are “historically” rearranged as “**Large Lightly Reinforced Concrete Walls**” (LLRCW, as defined in both Eurocode 2 and Eurocode 8) to best fit with Building Codes and to recall a more “design oriented”, consolidated and simplified theory.

It 'important to underline that even if walling systems provide high performances from structural point of view this type of wall does not come directly from a structural

requirement, but to improve the performance of buildings in terms of thermal insulation and to reduce the construction time.

Currently the use of Large Lightly Reinforced concrete walls (“pareti estese debolmente armate” in NTC 2008) placed on the perimeter of the building is spreading in Italy, introduced for small and medium size buildings with few floors, in a European Normative context that **from 2021** will **oblige all new** building to be **energetically-certified** and to be characterized from **high standards of energetic saving** because, as a matter of fact, the innovative feature of these type of walling system is to provide high level of thermal insulation with a consequent energetic saving. An American brand producer ICF, provided the following Energy costs:

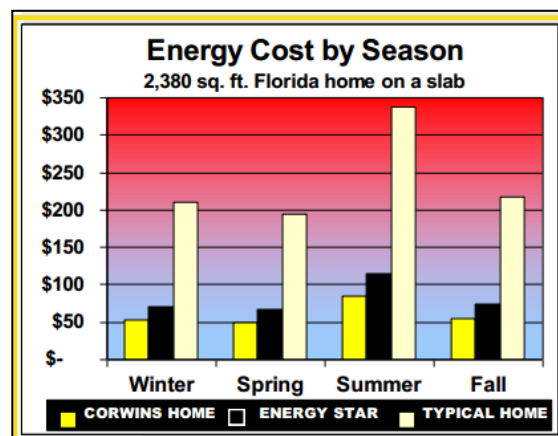


Figure c) Energy costs

In Europe the issue has been introduced by the Directive 2010/31/CE: among the EU countries all the Public buildings should be made with “almost zero energy criteria” from 2019, while from 2021 the requirement will cover all buildings, without making any distinctions. The “almost zero energy buildings” definition, covers all buildings whose energy requirement – very low or almost null – is predominantly covered by renewable sources.

For this reason the demand for green buildings construction is growing from commercial multi-story buildings to condominiums and single family houses, also because the most advanced Governments incentive for LEED certified buildings. The primary advantages are the occupancy-energy- savings with requirements of 40% less energy to heat/cool, and a significantly quieter inside environment than frame construction. To provide one example of this application connected with

LEED certifications the new center of Oregon University in 2007 can be mentioned [2].

Another important aspect must be introduced. The catastrophic seismic event of l'Aquila 2009 unfortunately emphasized how quite recent buildings suffered severe structural damages (and some cases even structural collapses), despite of the presence of reinforced concrete frames; moreover the expulsions of in-fill wall due to the lack of connection between the secondary and primary structure, caused the inaccessibility of the buildings and in some cases even deaths.

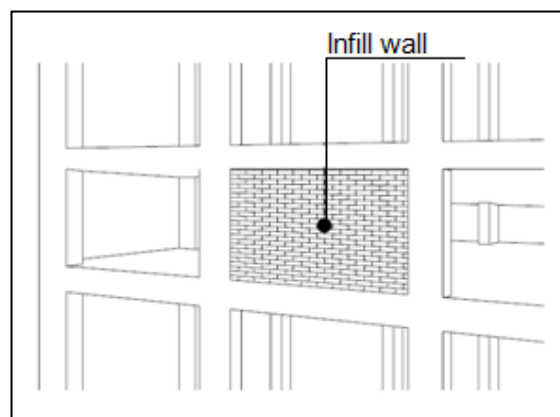


Figure d – Typical in-fill wall

For what concerns Italy the need of implementation of official formulation brought in July 2011 to development of the “*Linee guida per sistemi costruttivi a pannelli portanti basati sull’impiego di blocchi cassero e calcestruzzo debolmente armato*” promoted by Consiglio Superiore dei Lavori Pubblici.

In this context a producing company di wood-concrete shuttering blocks commissioned to C.I.R.I (Centro Interdipartimentale di Ricerca Industriale Edilizia e Costruzioni), an experimental campaign to test their Structural reliability and the effective performances of their grid type shear walls systems.

Introduction

In the present work the structural behavior of shear type grid wall system was investigated, in a first instance through experimental tests aimed at carrying-out the characteristics of the equivalent continuous wall, in a second phase thanks to non-linear simulations able to correctly simulate the experimental tests for an in-depth understanding of the collapse phase, of the stress-strain distribution inside the grid-wall and of the coactive state between steel and concrete.

For the numerical simulation the program ABAQUS was used.

The blocks and the related grid-walls considered were of two type: block 25/18 related to 14 cm width grid-walls, and blocks 30/22 related to 18 cm width grid-walls.

The structure of this thesis can be divided into two main parts: *Chapters 1, 2, 3* concern the description and the elaboration of the experimental results. *Chapters 4, 5, 6, 7* are completely focused on the numerical modeling theory and implementation in ABAQUS.

In the following a list of the subjects treated in the Chapters:

Chapter 1: *The Grid-wall Systems were introduced defining their main characteristics, their construction phases and inserting them in the Italian and worldwide normative context with particular attention to American scenario.*

Chapter 2: *The formwork blocks and the set of experimental results aimed at the characterization of the two main materials, concrete and steel-bars, used for the 1x1 m Grid Walls object of the Experimental campaign were described. Moreover a brief report of the compression tests (centered and diagonal), as suggested by CSLP Italian Guidelines, was provided.*

Chapter 3: *The Load-Vertical ΔL graphs and the Shear- γ curves were outlined and exploited to define the correction-factors α and β to be applied on mechanical properties E and G that define the grid-wall system response. The equivalent continuous wall thicknesses s_{eg} were defined. The goal was to model, in the design phase, the grid wall as a continuous elastic element. Two simple numerical proofs were conceived to have the confirmations on the reliability of these results.*

Chapter 4: *The primary objective of this chapter was to provide the complete framework in the definition of the non-linear constitutive model used, with the goal to*

describe the behavior of the concrete for a better matching between numerical model and experimental proof. The theoretical framework for concrete rely on Kent and Park [23] and Cornellissen et al. [26] formulations. The damaged plasticity model (CDP) used considers Lee and Fenves[20] formulation.

Chapter 5: The bond-slip interaction between steel bars and concrete was introduced so as reported in CEB-FIP2000. A numerical pull-out test was implemented in Abaqus for a better understanding of bond behavior simulation, with the aim to insert in the RC wall model, the best modeling techniques available in Abaqus.

Chapter 6: A finite element model which could correctly simulate the experimental test conducted on 1 m x 1 m grid-wall subjected to compression, for an in deep understanding of the collapse phase was developed. The experimental test chosen to be reproduced was the CC14_02 because it shown the most reliable data of the experimental campaign. All the steps to build the model are presented.

Chapter 7: The numerical results obtained are analyzed in order to compare the output-data of the model with experimental observations and measurements obtained during the investigation performed at the Laboratory of CIRI-Building Department of the University of Bologna. All the output of the numerical model are reported.

Chapter 8: the results, the conclusions and the recommendations for future study are depicted.

Chapter 1

The r.c. grid-wall system: national and international normative context and background

Object

The object of this Chapter is to introduce the Grid-wall Systems, defining their main characteristics, the construction phases and inserting them in the worldwide normative context with particular attention to American scenario.

1.1 The grid-wall system

The grid-wall-system object of this thesis can be categorized in the family of Insulated Concrete Formwork building technique.

The ICF construction systems consist of formwork of insulating material that produce both structural performance of the walls and the functional currency of the building. The market offers a variety of these systems that can be divided into three main categories:

- Formwork-to lose -systems of insulating material and partially prepared reinforcement, in which to cast concrete;

- Sandwich systems in which the insulating material is inserted between two layers of reinforced concrete; this solution can be achieved with prefabricated panels or by applying filling with concrete the sides of an insulating panel with prepared reinforcement;

- Formwork blocks made of material with good thermal insulation properties incremented adding additional filling materials, in which the reinforcement is predisposed to make the concrete casting; the blocks are shaped in order to ensure horizontal and vertical continuity of the casting and of the steel.

The above solutions do not present all the same problems and the same structural behavior, but certainly the only one that can be completely assimilated to the Large Lightly Reinforced Concrete Wall as will be better explained in the following, is one in which adopt the formwork of insulating material.

1.1.1. The construction technique

The wall elements tested in the experimental campaign, were obtained using the specific construction techniques described in the following. The constructive system is composed of formwork blocks (or, “shuttering”) in mineralized wood (a mix of compressed crushed mineralized wood with water and cement slurry) which are currently produced in conformity with EU standard PrEN 15498:2006 (see Figure a). This material provide high levels of acoustic and thermal insulation. When the hollows of the blocks are filled with appropriate (a) steel reinforcement and (b) concrete, it is possible to obtain a reinforced concrete grid walls (also referred to as “concrete formation”) of various characteristics, depending upon the type of blocks, reinforcement and concrete used in the construction.

Different brands proposes different but similar shuttering-kit-blocks. In U.S.A. for example there are three different families of this blocks said “flat”, “waffle grid”, “screen grid” that are conceived more slim in the main parts(column and beams)respect to the European ones :

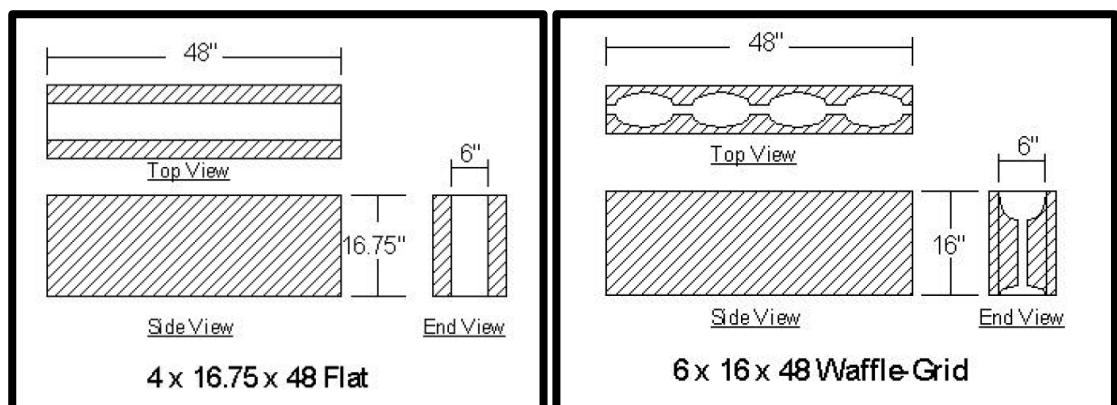


Figure. 1.1a – Most common shuttering kit formwork in U.S.A.- “Flat” and “Waffle” Grid Type

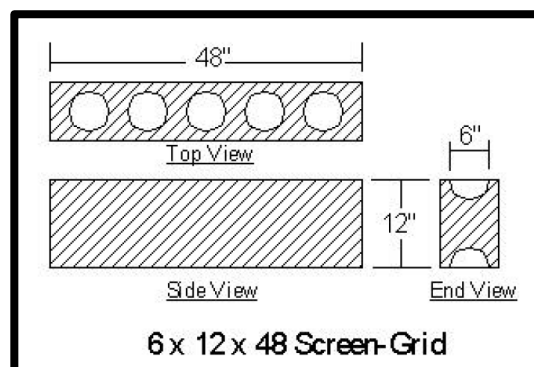


Figure. 1.1b – Most common shuttering kit formwork in U.S.A – Screen Grid Type

These particular type of blocks, once well posed, reinforced with horizontal and vertical bars, and filled with concrete, bring to the formation of a particular type of wall: **grid-type shear walls**, of which are reported some pictures in *Figure 1.2*:

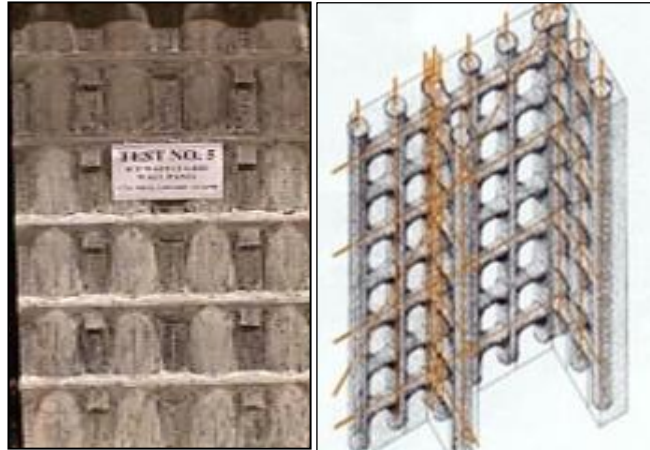


Fig.1.2(a) USA Waffle-Grid Fig.1.2(b)USA Screen Grid scheme



Fig.1.2(c)

Fig.1.2(d)USA Screen Grid

Figure 1.2 – The Grid walls after the removal of insulating layers

The typical construction sequence can be summarized as follows:

- after the completion of each horizontal layer of blocks, the basic horizontal reinforcement is inserted in the system by placing a single or double horizontal bars of relatively small diameter ($\Phi 8$ - $\Phi 10$) at the bottom of half moon indent of the blocks.

- after all the blocks are assembled together (to create the complete formwork) the basic vertical reinforcement is inserted in the system by placing a single or double vertical bar of relatively small diameter ($\Phi 8\text{--}\Phi 12$) in each vertical hole (each block is characterized by two vertical holes as shown in Figure a).



Figure 1.3 – Shear Type grid walls during construction phase

- after the insertion of all reinforcing bars (in addition to the “basic” reinforcement, typically additional bars are inserted around the openings and at both panel ends) the formwork thus obtained is filled with concrete of appropriate characteristics (typically concrete with $R_{ck} > 25 \text{ N/mm}^2$).



Figure 1.4 – Concrete casting phase

After curing, the structure obtained (referred to in the following as the “structural concrete formation”) is a concrete bearing wall with (horizontal and vertical) steel

reinforcement mesh characterized by a regular pattern of small horizontal holes (see *Figure 1.2*). All bearing walls are joined together with appropriate re-bars in order to obtain a cellular network of structural walls capable of allowing a “box behavior” of the structural system (i.e. all horizontal actions can be taken by each wall through an “in plane” action). For this reason, the theoretical framework presented in the following focuses mainly on in plane bending and shear strength of a single concrete formation panel.

In general, the constructive system is characterized by: (1) the insertion of a large amount of horizontal reinforcement to prevent shear failure, and (2) a rigid self imposed limitation upon the maximum vertical stress in the concrete, in order to prevent the brittle failure of the concrete in compression, even under bending. The “standard” vertical and horizontal re-bars lead to an area reinforcement ratio (w.r.t. the effective section of concrete) varying between 0,13 % and 0,3 %, or, in terms of weight, to about $0,25 \div 0,35$ KN of steel per cubic meter of concrete. This classifies the concrete formation as “concrete structures with small amount of reinforcement” or “lightly reinforced concrete structures” (according to EC).

1.1.2 The structural behavior in ETAG009 (2002)

The European Guideline ETAG009, concerning “*Non load-bearing permanent shuttering kits/systems based on hollow blocks or panels of insulating materials and sometimes concrete*” in Annex B offers a “Design Method for Grid-Type Shear wall” subjected to horizontal shear forces H_{sd} .

Three load bearing models may be applied according to the presence of reinforcement: frame model(a) or continuous strut model(b) for plain concrete or a beam model(c) for reinforced concrete.

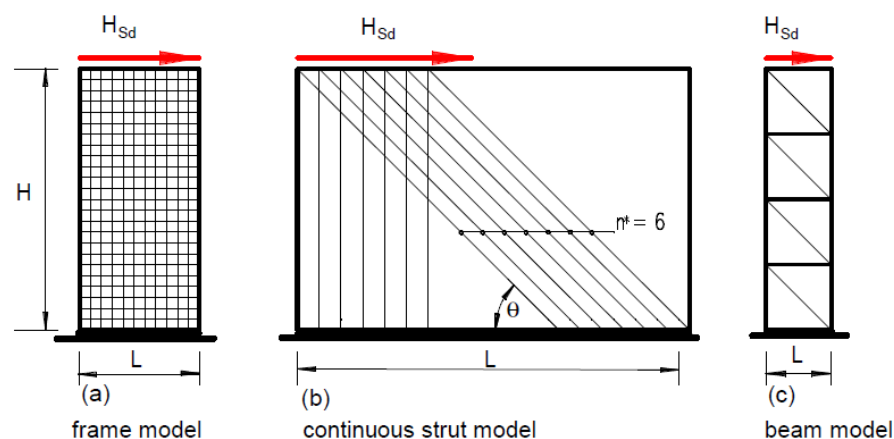


Fig. 1.5 Load bearing models in European Guideline ETAG009

The first observation is that in Italy for example is not allowed the use of plain concrete.(See Par. 1.3.1); it means that only "Beam model" can be conceived.

The design resistance H_{rd} according to the beam model. can be determined with the help of the design rules valid for reinforced concrete beams; the links are represented by horizontal bars passing along the connectors. A sufficient end anchorage of the horizontal bars – e.g. by hoop reinforcement – has to be verified.

The design resistance can be simply calculated as:

$$H_{rd}=A_{sh} f_{yd}$$

where A_{sh} is the horizontal reinforcing bar section and f_{yd} the design strength of steel. The guidelines suggest also that under a combined design action of horizontal and vertical loads the columns have to remain in stage I i.e. no tensile stress should occur, otherwise tensile vertical reinforcing bars in the columns have to be used by the designer (mandatory in Italy).

Another reference for a better understanding of the structural behavior of the grid-wall-system is [17] where the *connector beams* are simply conceived and designed with *strut and tie* model. The Load P on the wall generates a Shear force T on the connector beam and so a compression N_c on the compressed strut of concrete equal to $N_c= T/(\sin \alpha)$ where the angle α is the inclination of the compressed strut respect to the horizontal. The shear T also induces a tensile stress in the steel equal to $T \cot \alpha$. The experimental results on which the author relied also suggested a collapse of the joists for achievement of yield strength of steel.

1.2 The U.S. background

The efficient use of shear walls in residential construction subjected to wind and seismic loading is of great interest to designers and builders of homes in high hazard areas. Shear walls are the primary lateral force resisting system in residential construction. There has been considerable research aimed at optimizing the design of light-framed shear walls (wood and cold-formed steel) in recent years [4]. For relatively new types of wall systems, such as Insulating Concrete Form (ICF) wall construction, the technical information available is limited. There is a need to confirm or improve the use of traditional concrete shear wall design methods particularly in the context of ICF systems and residential construction practices. Thus, inefficiencies that result in conservative (uneconomical) or unconservative (unsafe) applications may be avoided.

Reinforced concrete shear walls can resist a large portion of the shear due to lateral loads on buildings. However, failures of reinforced concrete walls are not necessarily dominated by shear deformations. The balance between shear and flexure loading has a very significant role in overall deformation and strength characteristics. Walls with a height-to-length aspect ratio of more than about 2.0 possess flexure dominated deformational characteristics while walls with aspect ratios less than 2.0 are influenced more by the presence of high shear loads [5]. However, this rule may not apply to lightly reinforced concrete walls as found even in different codes [6] [7].

The use of reinforced concrete structural walls is common for resisting lateral loads imposed by wind and earthquakes. In practice there are two different types of structural concrete walls: cantilever shear walls and framed shear walls. Cantilever shear walls act as cantilever beams and are connected to the rest of the structure by floor diaphragms through which horizontal forces are transmitted to the wall. The design of cantilever shear walls is usually governed by flexural behavior. The design philosophy is to ensure a ductile flexural failure where the tensile steel in the boundary element reaches yielding before the web fails in shear.

The framed shear wall panel is considered to be an element that stiffens the shear resistance of a plane frame (enlightened respect to the case in which r.c frame is the sole structure). A framed shear wall is considered as part of the overall frame system except that it receives a larger portion of the shear loads due to its greater

stiffness. However, it is not considered to receive a large overturning moment as in the cantilever shear wall because it is constrained by the surrounding frame. It is essentially an in-fill wall that is designed to resist shear. Consequently, the framed shear wall behaves differently than does a cantilever wall – the predominant action is shear [8]. The grid-wall object of this thesis are conceived all around the World as framed shear wall panel.

The ultimate strength capacity of an individual shear wall element is a function of the material strengths, the applied loading, and the geometry of the wall, including the amount of reinforcement and the reinforcement detailing. Failure modes resulting from in-plane loads include shear friction, diagonal shear cracking, flexural reinforcement yielding, and web crushing. Other less desirable failure modes include reinforcement pullout (reinforcement development length failure) or concrete failure as a result of overturning tensile forces.

In the shear friction mode, the wall responds linearly until a horizontal crack forms, typically at the base of the wall, parallel to the applied load. At this point, the wall rotates as a rigid body, causing the reinforcing steel to yield. Because of the progressive yielding, when the loading is reversed, sliding displacement occurs along the horizontal crack. For this mode of failure to occur, a horizontal crack must form at the base of the wall before diagonal shear cracking forms. This mode typically controls the capacity of lightly reinforced low-rise shear walls [9].

Shear forces caused by lateral loads are accompanied by a moment applied in the plane of the wall. The presence of these moments requires that a flexural failure mode also be examined. The failure mode can result in either a crushing of the compression zone concrete (if the wall is heavily reinforced or constrained from overturning) or yielding of the tension bars. Typically, crushing of the concrete in the web is not considered because the percentages of reinforcement are kept below a balanced design value ensuring that the tension reinforcement will yield before crushing can occur [10]. To assess the strength of a shear wall, the capacity to withstand these various failure modes must be evaluated using mechanics-based expressions that have been empirically validated or modified.

Relatively little testing has been done to evaluate the performance of reinforced concrete walls with openings. Current building codes, such as the Uniform Building Code [11], include provisions for the design of symmetrical and unsymmetrical solid

concrete walls; however, it is often necessary to provide openings in the walls for doors and windows. If the openings are small relative to the wall dimensions, it may be reasonable to neglect the effects of the openings [12]. In many cases, the opening is relatively large or is located in a critical region where inelastic deformations are expected. In such cases, the influence of the opening on the overall wall behavior must be evaluated.

Since all the current codes do not provide exact design guidelines for walls with openings, considerable engineering judgment is required. In general, the influence of the opening on the flexural and shear strength, as well as the design requirements, should be considered. If the opening is near the middle of the wall, it will decrease the moment capacity of the wall only slightly; however, the shear strength may be significantly reduced. In contrast, an opening near a wall boundary may impact both the moment and shear strengths. Research conducted by Ali and Wight on one-quarter scale slender walls with staggered openings revealed the walls were vulnerable to shear compression failure in the narrow wall segment when the opening at the base was near the wall boundary [13]. One specimen was tested without openings and excellent behavior at large drift ratios was observed, even though only moderate detailing of the boundary zones was provided compared with ACI 318-95 requirements [13]. This improved behavior was explained using a displacement design approach [14]. Recently published research on the behavior of slender walls has shown that a displacement design approach provides a versatile design methodology [12] [14]. The procedure involves comparing the strain capacity of the wall with the estimated strains imposed on the wall as a result of a design earthquake. In general, providing additional transverse boundary reinforcement can increase the strain capacity of a wall. Thus, rather than providing an arbitrary amount of confining reinforcement at the wall boundaries, confinement is selected based on the deformation or strain demand. However, this method is not considered an efficient design approach for residential construction due to the increased complexity of reinforcement details required at the boundary elements.

Taylor et al. conducted two one-quarter scale tests to determine the effects of openings at the base of slender reinforced concrete walls [12]. The walls were 3.66 m high by 1.22 m long resulting in a height-to-length aspect ratio of 3. A 508 mm high by 229 mm long opening was provided at the base of each specimen located 89 mm from the edge of the wall. One specimen had a rectangular cross section

and one had a barbell cross-section. A constant axial load of approximately $0.1 f'_c A_g$ was applied to the walls for the duration of each test. This level of axial load was used to represent the dead load in a typical moderate-rise building. The research concluded that slender structural walls with openings can exhibit stable behavior and significant ductility, even for cases when the opening is in the flexural compression zone. The large opening at the base did not significantly influence the behavior or strength of the wall compared to the walls without openings. Vertical cracks above the door opening indicate that the reinforcement in this location was effective in providing a load path around the opening.

Lefas et al. tested 13 reinforced concrete shear walls with a constant thickness and a height-to-length aspect ratio ranging between 1 and 2. The vertical and horizontal reinforcement consisted of high tensile strength deformed bars. Additional horizontal reinforcement in the form of stirrups confined the wall edges. Three levels of constant axial load were applied in the testing program; they corresponded to $0.0 f'_c A_g$, $0.1 f'_c A_g$, and $0.2 f'_c A_g$. These load levels were considered to represent the amount of axial load at the base of the wall of a single story, a medium-height, and a high-rise building, respectively [15]. Failure of the walls occurred due to the nearly vertical splitting of the compression zone in the region of the inclined or deepest flexural crack, followed by splitting of the whole compressive zone. The failure region was more extensive with decreasing height-to-length aspect ratio and increasing axial load [15].

The ultimate shear capacity of the specimens with axial loads equal to $0.1 f'_c A_g$, and $0.2 f'_c A_g$ was higher than that of the walls subjected to shear load only by about 25 and 30 percent, respectively. The axial load also reduced the value of the horizontal displacement at peak load. Differences in compressive concrete strength as high as 35 percent resulted in almost negligible variation in wall strength. This may indicate that strength and deformation characteristics of the walls are not significantly affected by variability in concrete strength [15].

The observed maximum shear capacity sustained by the walls substantially exceeded the calculated flexural and shear capacities defined by ACI 318. Although ACI 318 provisions indicated a ductile flexural failure mode, the specimens actually exhibited a shear failure mode while remaining ductile. Specimens that utilized about half of the horizontal web reinforcement required by ACI 318 to safeguard against a non-ductile shear failure also failed by shear in a ductile manner. Such

behaviors indicated that significant reductions in the horizontal web reinforcement does not have a significant effect on shear capacity [15].

1.2.1 Design of Grid-wall in U.S.A

The current design of concrete shear walls for parallel (in-plane) shear follows the provisions outlined in ACI 318 – 99 Section 11.10 [6]. The equations below from Section 11.10 are used to check parallel (in-plane) shear. All vertical cores, both reinforced and unreinforced, are assumed to resist parallel wall shear. Dimensions are often simplified for waffle-grid and screen-grid wall systems that have complex cross sectional geometries. Generally, the web thickness (or effective web thickness) is not considered when evaluating the parallel shear resistance of ICF walls with non-uniform cross sections.

$$V_u > \Phi V_n$$

where V_u = Factored shear force at section, Φ = Shear strength reduction factor = 0.85 per ACI 9.3.2., V_n = Nominal shear strength per ACI 11.2. defined as follows:

$$V_n = V_c + V_s$$

where V_c = Nominal shear strength of concrete per ACI 11.10.5 V_s = Nominal shear strength of shear reinforcement per ACI 11.10.9:

$$V_s = \frac{A_v f_y d}{s_2} \quad \text{when} \quad V_u > \Phi V_c$$

$$V_c = 2 \sqrt{f'_c} h d$$

A_v = Area of horizontal shear reinforcement within a distance, s_2 , and a distance, d , per ACI 11.10; considering that s_2 is the Spacing of horizontal shear reinforcement and

$$d = 0.8 l_w$$

where l_w = Length of reinforced segment.

According to ACI-318, a larger value of d , equal to the distance from the extreme compression fiber to the center of force of all reinforcement in tension, is permitted when determined by strain compatibility analysis.

Where the factored shear force V_u exceeds shear strength ΦV_c , horizontal shear reinforcement shall be provided. The ratio of horizontal shear reinforcement area to gross concrete area of the vertical section shall not be less than 0.0025. According to ACI 318, spacing of horizontal reinforcement, s_2 , shall not exceed $l_w/5$, $3h$, nor 457 mm.

Due to the number and size of wall openings in residential construction, particularly on the street facing side of houses, there may be segments with height-to-length aspect ratios greater than or equal to 4:1. In such cases, the behavior of these segments may be dominated by flexural behavior rather than shear behavior. Therefore, the flexural response of such segments in ICF walls should be evaluated using the equations below in accordance with ACI Chapter 10. The amount of tensile reinforcing steel is limited such that it will yield before the concrete reaches its ultimate compressive strength as required by ACI 318 [6].

$$M_u \leq \Phi M_n$$

where M_u = moment induced by factored design loads, Φ = the strength reduction factor of 0.9 for flexure per ACI 9.3.2, M_n = nominal moment strength evaluated as:

$$\Phi M_n \leq \Phi A_s f_y \left(d - \frac{a}{2} \right)$$

A_s = area of tensile reinforcing steel, d = distance from extreme compression zone (top of beam or toe of wall) to centroid of tensile reinforcement, a = depth of equivalent rectangular stress block equal to:

$$a = \frac{A_s f_y}{0.85 f'_c b}$$

Regardless of the design conditions, ACI 318 requires a minimum amount of tensile reinforcing steel determined by the greater of the following equations:

$$A_{s,min} = \frac{3\sqrt{f'_c} b_w d}{f_y} \quad \text{ACI 318-99 Equation 10-3}$$

In practice, most design applications involve the use of multiple concrete shear wall segments to comprise a building wall line. In residential construction, the configuration and size of these segments (i.e., aspect ratio and wall opening dimensions) can vary significantly. This condition demands the consideration of stiffness of individual wall segments in determining the capacity of a wall line that may be comprised of segments with very different stiffness characteristics. Yet, the current approach favored in residential and low-rise concrete construction determines the capacity of a concrete (or masonry) shear wall by assuming that all solid portions of a wall, regardless of how far separated or to what degree they are coupled, act as a solid concrete wall of equal length. With this approach, only in cases with extremely scant amounts of solid wall (i.e., more representative of a concrete frame) does flexural capacity control the design solution. This questionable approach is represented in current code documents as well as the general engineering practice [14].

In the Prescriptive Method [1], a more conservative approach was used whereby wall bracing amounts in the prescriptive tables were controlled by limiting in-plane flexural capacity of the segments in the wall line in order to determine the required minimum percentage of wall length. An iterative process was used, whereby the length of the flexural elements were varied from 0.61 m to 2.4 m depending on the amount of solid wall length required.

1.3 The Italian and European Normative context for Design purposes

The followings considers some important hypothesis on the use and behavior of grid type shear walls:

- the grid type shear walls are ascribable to Large Lightly Reinforced Concrete Walls as mentioned in the Eurocodes
- the grid type shear walls are conceived to be designed in seismic zone.

The purpose of this paragraph is to provide a comparison between the most important design formulations existing in Italy and the Eurocode. The normative context referred to the design of this particular building system is not unified: different codes proposes similar but not equal provisions.

For what concerns Italy noteworthy are:

-NTC 2008

- Guidelines "*Linee guida per sistemi costruttivi a pannelli portanti basati sull'impiego di blocchi cassero e calcestruzzo debolmente armato*" promoted by Consiglio Superiore dei Lavori Pubblici (CSLP Luglio 2011 Guidelines).

-CNR 10024/84 "*Istruzioni per il progetto, l'esecuzione ed il controllo delle strutture prefabbricate in conglomerato cementizio e per le strutture costruite con sistemi industrializzati*"

In a wider context here are reported:

-EC2 / EC 8

1.3.1 Definitions:

The definition of “Lightly Reinforced Concrete” in Italian code is (4.1.11) strictly related to the quantity of reinforcement:

*“Il calcestruzzo a bassa percentuale di armatura è quello per il quale la percentuale di armatura messa in opera è minore di quella minima necessaria per il calcestruzzo armato o **la quantità media in peso di acciaio per metro cubo di calcestruzzo è inferiore a 0,3 kN.**”*

The CSLP Guidelines (Par. 7.8) instead suggest the quantity of reinforcement, but in order to ensure correct behavior with respect to the serviceability and ultimate limit states and towards local and global instability and it states that:

$$\rho_v \geq 0.20\%$$

$$\rho_0 \geq 0.20\%$$

where ρ_v and ρ_0 are the percentages obtained by dividing respectively the geometric area of vertical and horizontal reinforcement bars, for the area of concrete section.

In the Italian code NTC 2008 the Large Lightly Reinforced concrete walls are instead defined on the basis of geometrical requires and dynamical behavior:

*“Una struttura a pareti è da considerarsi come struttura a pareti estese debolmente armate se, nella direzione orizzontale d’interesse, essa ha un periodo fondamentale, calcolato nell’ipotesi di assenza di rotazioni alla base, non superiore a T_c , e comprende almeno due pareti con una dimensione orizzontale non inferiore al minimo tra 4,0m ed i 2/3 della loro altezza, che nella situazione sismica portano insieme almeno il 20% del carico gravitazionale. **Se una struttura non è classificata come struttura a pareti estese debolmente armate, tutte le sue pareti devono essere progettate come duttili.**”*

As here reported the Italian code seems to distinguish the LLRC walls from ductile walls even if, as it will be better explained, provide the same base behavior factor.

1.3.2 Normal and shear stresses

Italian code *NTC2008* provide also precise performance limits concerning “Lightly Reinforced Concrete” (4.1.11):

- 1- It is necessary to neglect the traction resistance

- 2- The compression stresses that raise under rare combination of load should be limited to:

$$\sigma_c \leq 0.3 f_{ck}$$

That means to allow a reduction factor more or less equal to 3 respect to the 1.5 of normal reinforced concrete in the evaluation of f_{cd} .

- 3- The shear stresses that raise under rare combination of load should be limited to:

$$\tau_c \leq 0.25 f_{ctk}$$

The *CSLP Guidelines* instead furnish similar limits making a difference between two sides or one way reinforcement in the width of the panel(7.3):

$$n_{sd} \leq 0,4 (f_{cd} A_{c,eff}) \quad \text{Two layers of reinforcement}$$

$$n_{sd} \leq 0,25 (f_{cd} A_{c,eff}) \quad \text{One layer of reinforcement(centered)}$$

It can be noticed how 0.3 of the NTC2008 is an average value between 0.25 and 0.4 suggested by *CSLP Guidelines*.

For what concerns shear, CSLP doesn't provide explicitly any formulas, but it states that the Shear strength should be carried out with reference to the equivalent thickness and in accordance with the provisions in the Technical Standards considering different failure modes:

- Shear-compression;
- Shear-traction;
- Shear and sliding.

In the CNR 10024/84 in the paragraph C.2.3.1.4 an interesting formulation of the N-V interaction is reported. If s is the width of the wall, V_d the shear action for unit of length and if:

$$\tau = \frac{V_d}{s}$$

$$\sigma = \frac{n_d}{s}$$

The condition that should be satisfied is:

$$\left| \frac{\sigma - \sqrt{\sigma^2 - 4\tau^2}}{2} \right| \leq f_{ctk}$$

For important shear actions (seismic forces, differential settlements..) is suggested to verify that the Mohr circle build starting from σ and τ , remains inside the intrinsic curve of the material.

More information about shear action can be found in EC8 (Par 5.4.2.5) where it's suggested to increase the shear force V'_{Ed} to ensure that flexural yielding precedes attainment of the ULS in shear. In order to obtain ductile crisis V_{Ed} can be calculated from the shear force V'_{Ed} from the analysis, in accordance with the following expression:

$$V_{ed} = v'_{ed} \frac{q + 1}{2}$$

This is strictly connected to the Capacity Design concept: both the Italian and the European codes confirm the need to amplify the Shear action in analogy with the design procedure for the walls designed in CD "B".

1.3.3 Behavior factor:

In this paragraph a comparison between NTC 2008, EC8 and CSLP Guidelines was reported. The NTC 2008 and EC8 Guidelines provide the same base-behaviour-factor, that must be multiplied for some coefficients (that takes into account the characteristic of regularity and the type of structure) smaller than 1 to reach the design behaviour factor. As will be better explained the only difference between the two Codes is in the difference in conceiving this system as ductile or not.

The CSLP 2011 Guidelines provide smaller value of base behaviour factor but the coefficients over mentioned are now defined bigger than 1.

Very interesting is the Research conducted by Pecce, Bibbò [16] that studied a building made of LLRC walls with a rectangular plant 20mx30m large and 3-storey 3m height ; the structure was made of a perimeter panels with a thickness of 15 cm, and by pillars of section 30cmx30cm on all three levels arranged with a distance of 5 m in both direction as can be seen in *Fig. 1.6*.

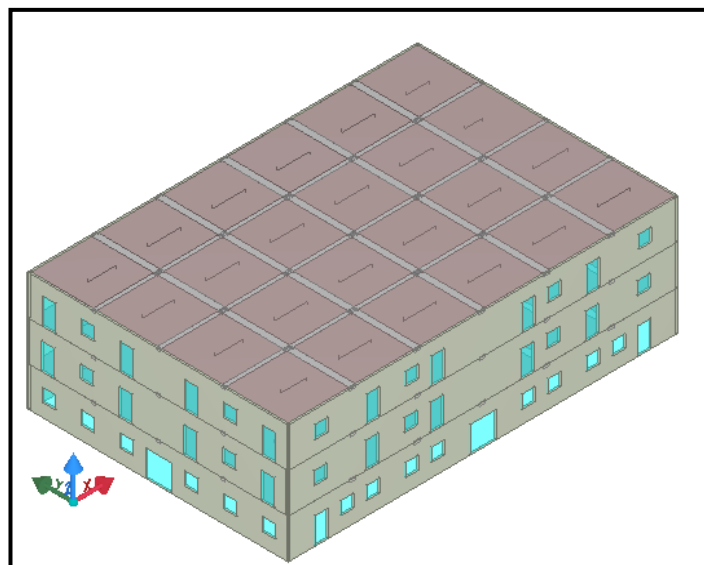


Figure 1.6 LLRC wall building

With reference to LLRCW system type in NTC 2008, and so to ductility class B, the *design behavior factor* was assumed to be equal to 1.50, once the shape factor of the walls k_w have been evaluated with reference to the size of the perimeter walls in absence of holes. The Reserchers performed a static non-linear analysis that revealed an effective behaviour factor of 2.5. This number is of course closer to the design behaviour factor provided by CSLP Guidelines for grid-wall systems.

To enter into much more details the Italian code clearly distinguishes Large Lightly Reinforced Concrete Wall from Ductile walls,

..”Se una struttura non è classificata come struttura a pareti estese debolmente armate, tutte le sue pareti devono essere progettate come duttili.”

nevertheless NTC 2008 allow to use the same base behavior factor, assuming equal ductility for both, as will be better explained following.

The EC8 instead furnishes clear indications about building details to guarantee the presence of fuses in the extremities of the sections in which concentrate flexural resistance and to guarantee a certain amount of ductility .

In favor of the assumption of the same behavior factor both for LLRCW and Ductile R.C Walls, are the research conducted in [1] where experimentally determined force/displacement envelope curves indicate that the panels tested were characterized by high level of kinematic ductility (the specimen developed maximum horizontal displacement corresponding to a kinematic ductility in the range between 8 and 10). Cause of the results the authors suggested to use, as reduction factor (for design purposes) for the structural system, the same reduction factor coefficient (“ $q_0 = 3$ ”) proposed by the Eurocode 8 for concrete wall buildings or even bigger if validated by additional experiments.

A different approach is suggested in the ***Italian Guidelines CSLP 2011***, the guidelines for building system based on the use of shuttering-wood-blocks and lightly reinforced concrete casted in situ that in the paragraph concerning “Provisions for structural design in seismic zone” propose a different structural behavior:

“... Poiché i meccanismi di collasso delle strutture in oggetto sono prevalentemente legati ai meccanismi di rottura per taglio o taglio-flessione, tali strutture si devono considerare appartenenti ad una classe di bassa duttilità.”

To be consistent with the above mentioned, in the paragraph 7.1 it states that for the building system under examination the base behavior factor q_0 must be assumed always smaller or equal than 2.0.

The design behavior factor q will be expressed as follows:

$$q=q_0 K_s K_r$$

where $K_s = \alpha_u / \alpha_l$ is the over-resistance factor that in absence of analytical formulations can be assumed equal to 1.2 for in plane regular structures and equal to 1.1 for irregular ones and K_r is the reducing factor connected to elevation irregularity that is equal to 1 for building regular in elevation, equal to 0.8 for irregular ones. That means that Italian Guidelines C.s.l.p 2011 suggests for a building regular both in plane and in elevation a design behaviour factor of 2.4.

Bigger values of base behavior factor q_0 are admitted only if justified by experimental results obtained by experimental studies and supported by a consistent numerical analysis. Nevertheless the value of the base behavior factor q_0 should never exceed values bigger than 3.0 .

For what concern the behavior factor for LLRC walls, the indications in **NTC2008** and **EC8** coincide, because the base behavior factor q_0 to be considered is the one of of the “strutture a pareti non accoppiate di classe B”,(par.7.4.3.2 NTC2008) which assumes values equal to 3.

The “Class B” is connected to the level of Dissipative Capacity or Ductility Classes(CD):

- High Ductility Class (CD”A”);
- Low Ductility Class (CD”B”).

The difference between the two classes lies in the extent of plasticization that is decided during the design stage; for both classes, in order to ensure to the structure a dissipative and ductile behavior avoiding brittle fractures and the formation of unstable unexpected mechanisms, it is possible to resort to the procedures typical of the hierarchy of strength.

Both in NTC 2008 and in EC8 the base behavior factor q_0 have to be corrected by a coefficient k_w :

$$q = q_0 k_w$$

Where k_w evaluated as follows:

$$k_w = \begin{cases} 1,00 & \text{for frame structures and mixed} \\ & \text{ones equivalent to frame} \\ 0,5 \leq \frac{(1 + \alpha_0)}{3} \leq 1 & \text{for structures made of walls,} \\ & \text{mixed ones equivalent to wall structure,} \\ & \text{torsionally deformable} \end{cases}$$

The coefficient α_0 is the value assumed by the ratio between the heights and the bases of the walls. In the event that the coefficients α_0 of the walls aren't significantly different, α_0 can be evaluated once for the whole, assuming the height as the sum of the heights of the different walls, and the base as the sum of all the bases. That means that α_0 has a value of $\frac{3}{4}$, the *design behavior factor* q will be 1.75.

For what concern the *Energy dissipation* the EC8 (in 5.11.1.3.2) state that in precast concrete structures the prevailing energy dissipation mechanism should be through plastic rotations within critical regions. Besides energy dissipation through plastic rotations in critical regions, precast structures can also dissipate energy through plastic shear mechanisms along joints, provided that both of the following conditions are satisfied:

- a) the restoring force should not degrade substantially during the seismic action; and
- b) the possible instabilities should be appropriately avoided.

For this purpose the EC8 in section 5.4.3.5.3 provide some specifics for the local ductility of LLRC walls:

1- Vertical bars necessary for the verification of the ULS in bending with axial force, or for the satisfaction of any minimum reinforcement provisions, should be engaged by a hoop or a cross-tie with a diameter of not less than 6 mm or one third of the vertical bar diameter, d_{bL} . Hoops and cross-ties should be at a vertical spacing of not more than 100 mm or $8d_{bL}$, whichever is less.

2- Vertical bars necessary for the verification of the ULS in bending with axial force and laterally restrained by hoops and cross-ties in accordance with (1) of this subclause should be concentrated in boundary elements at the ends of the cross-section. These elements should extend in the direction of the length l_w of the wall over a length not less than bw or $3b_w\sigma_{cm}/f_{cd}$, whichever is greater, where σ_{cm} is the mean value of the concrete stress in the compression zone in the ULS of bending with axial force. The diameter of the vertical bars should not be less than 12 mm in the lower storey of the building, or in any storey where the length l_w of the wall is reduced over that of the storey below by more than one-third of the storey height h_s . In all other storeys the diameter of vertical bars should not be less than 10 mm.

3- To avoid a change in the mode of behaviour from one controlled by flexure to another controlled by shear, the amount of vertical reinforcement placed in the wall section should not unnecessarily exceed the amount required for the verification of the ULS in flexure with axial load and for the integrity of concrete.

(4) Continuous steel ties, horizontal or vertical, should be provided: (a) along all intersections of walls or connections with flanges; (b) at all floor levels; and (c) around openings in the wall. As a minimum, these ties should satisfy EN 1992-1-1:2004, 9.10.

The Eurocode 8 provide explicitly the "Detailing for local ductility" for LLRC walls, NTC2008 in contrast, stresses the difference between the ductile walls and the Lightly Reinforced one, which shows that the armor should not comply with regulatory guidance aimed at achieving high ductility, as explicitly suggested in CSLP Guidelines.

Chapter 2

Experimental tests

Object

The object of this Chapter was to introduce the set of experimental results aimed at the characterization of the two materials, concrete and steel-bars, used for the 1x1 m Grid Walls object of the Experimental campaign. Moreover a brief description of the compression tests was provided.

2.1 The blocks object of the experimental campaign

The Laboratory tests carried out, were performed on 1mx1m walls constructed with the deployment of formwork blocks of 2 different sizes, the characteristics of which are listed below. These specimen are conceived for internal infill wall with structural capacity.

Formwork block 25/18

External Dimensions: length 50 cm

height 25 cm

width 25 cm

Width of the wood-concrete: external 4 cm

internal 3.5 cm

Width of the insulating material: 1.5 cm (foam polystyrene)

Width of concrete: 14 cm

Weight of the block: 0.64 kN/m²

Use of concrete: 118 lt/m²

Weight of the finite wall: 3.05 kN/m²(w/o plaster)

A scheme and a figure of the block 25/18 is here reported in Figure 2.1 .

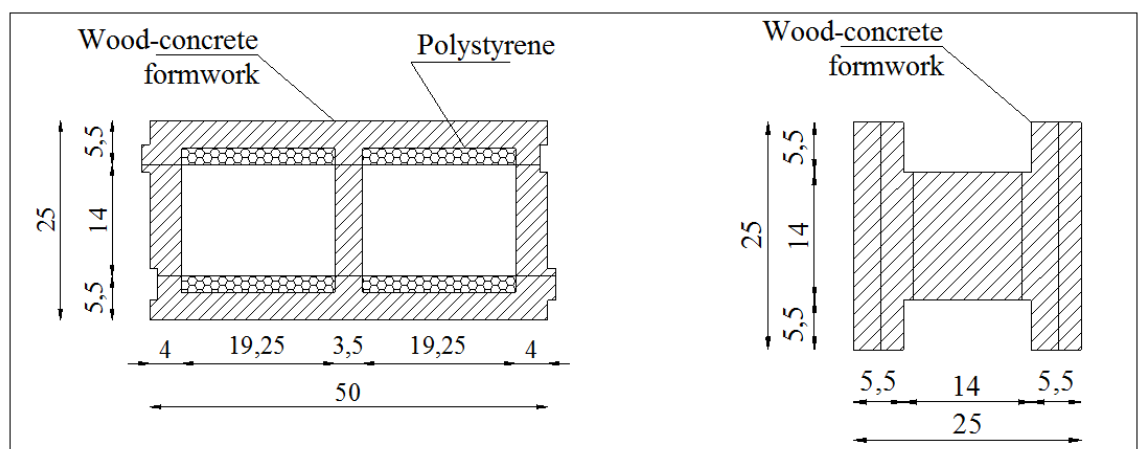


Fig.2.1 Scheme of formwork block of 25/18 used in the Lab.Tests

Formwork block 30/22

External Dimensions: length 50 cm

height 25 cm

width 30 cm

Width of the wood-concrete: external 4.5 cm

Internal 4 cm

Width of the insulating material: 1.5 cm (foam polystyrene)

Width of concrete: 18 cm

Weight of the block: 0.67 kN/m²

Use of concrete: 151 lt/m²

Weight of the finite wall: 4.24 kN/m² (w/o plaster)

A scheme of the block 30/22 is reported in the following Figure 2.2.

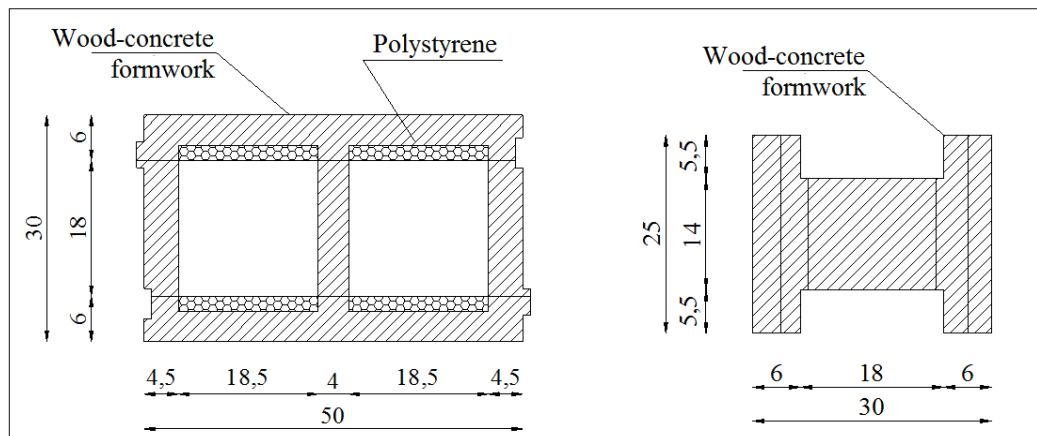


Fig.2.2 Scheme of formwork block of 30/22 used in the Lab. Tests



Fig.2.3 Formwork block of 25/18 used in the Lab.Tests



Fig.2.4 Disposition of the blocks for the creation of the grid-wall of the Lab.Tests

2.2 Mechanical characterization of the materials: concrete and steel

The structural skeleton of the grid walls object of this thesis is made of reinforced concrete. In order to obtain the strength-characteristics of the steel and of the concrete of which the grid-walls are made, a set of traction tests on \varnothing 8 mm bars, and different compression tests on 15 cm x 15 cm concrete cubes were performed.

2.2.1 Compression tests on concrete cubic specimen

Following the Italian code, to verify the compliance of the casted concrete with respect to the one established by the project and experimentally verified in the preliminary assessment, the so-called “controls acceptance” must be performed.

In our case the acceptance check is of type A, and it concerns quantities of homogeneous mixture not greater than 300 cm³ with the removal of 3 concrete specimens at least.

In this type of control two inequalities must be checked:

$$1) R_1 \geq R_{ck} - 3.5$$

$$2) R_m \geq R_{ck} + 3.5$$

with R_1 = lower resistance value of the samples (N/mm²)

R_m = average resistance of the samples (N/mm²)

The specimens subjected to the experimental tests, with dimensions 1x1 m, have been casted in two different days:

- 1) the samples to be subjected to diagonal test were casted in August 3rd, 2011;
- 2) the compression specimens were casted in September 23rd, 2011.

For each day of casting were collected 8 cubic concrete specimens, 4 of which have been tested in different days.

As described in the ASTM standard, on the same day of the test, it is necessary to measure the compressive resistance of the concrete with which the wall was built.

This resistance is measured on 4 of the 8 samples of concrete casted the same day of the wall, and aged in special cubic molds 15 cm x 15 cm x 15 cm long.

The concrete cubes are subjected to an axial compression by means of a press in load control condition. A sort of smoothing of the upper and bottom surfaces is performed in order to reduce as much as possible the irregularities that would distort the results. From compression tests is measured the mean compression resistance R_{cm} , in N/mm^2 that will be used in the numerical model to define the constitutive compression model.

For compression numerical test a peak compressive resistance of 31.3 Mpa was considered.

In the following *Table* all the results on compression tests cubic specimen are reported.

Table 2.1 Result of compressive test on concrete cubic specimen

CONCRETE OF THE SPECIMEN CC1_18, CC2_18, CC1_14, CC2_14									
Name	Dimensions[mm]	Date of casting	Date of the proof	Area[mm ²]	Ultimate load[kg]	Rcm[Mpa]	fcm[Mpa]	fck[Mpa]	Rck[Mpa]
P1	149	23/09/2011	25/11/2011(63 DAYS)	22201	85200	37.6474934	31.24741949	23.24742	28.00894
P2	150	23/09/2011	25/11/2011(63 DAYS)	22500	85600	37.3216	30.976928	22.97693	27.68305
P3	150	23/09/2011	07/12/2011(75 DAYS)	22500	86500	37.714	31.30262	23.30262	28.07545
P4	150	23/09/2011	07/12/2011(75 DAYS)	22500	87600	38.1936	31.700688	23.70069	28.55505
						MEAN	MEAN	Mean	
						37.7191733	31.30691387	23.30691	
						STAND.DEV			
						0.35977308			
CONCRETE OF THE SPECIMEN CD1_18, CD2_18, CD1_14, CD2_14									
Name	Dimensions[mm]	Date of casting	Date of the proof	Area[mm ²]	Ultimate load[kg]	Rcm[Mpa]	fcm[Mpa]	fck[Mpa]	Rck[Mpa]
P1	150	03/08/2011	19/9/2011(47 DAYS)	22500	91000	39.676	32.93108	24.93108	30.03745
P2	150	03/08/2011	19/9/2011(47 DAYS)	22500	91600	39.9376	33.148208	25.14821	30.29905
P3	150	03/08/2011	18/11/2011(107 DAYS)	22500	104200	45.4312	37.707896	29.7079	35.79265
P4	150	03/08/2011	18/11/2011(107 DAYS)	22500	104400	45.5184	37.780272	29.78027	35.87985
						MEAN	MEAN	Mean	
						42.6408	35.391864	27.39186	
						STAND.DEV			
						3.2743571			

C25/30
SCARCE QUALITY

C25/30

2.2.2 Traction test on reinforcing steel bars

The walls with dimensions 1m x1 m presented the following steel rebars:

- 2 Φ 8 for each concrete column (for each mt of wall there are 4 columns with a transversal sections 15x18 cm or 15x14 cm);
- 2 Φ 8 for each joist, which in the construction phase are leaned on each course of blocks(with an height of 14 cm).

For each wall, then, there are eight Φ 8 vertical bars and eight Φ 8 horizontal bars, the disposition of which can be observed in *Figure 2.5*.



Fig.2.5 Disposition of the steel inside the block

Three different traction proofs were performed in the CIRI laboratory to have the real σ - ϵ trend of the steel bars. The proof provided step by step the force applied and the correlated strain.

In each proof an extensimeter to provide the ΔL was posed, and then removed after the hardening phase. The laboratory equipment works in load control with a gradient load of $2.01204 \text{ e}+11 \text{ N}/(\text{mm}^2 \text{ sec})$ providing a force as output. To obtain the stresses, the forces has been divided for the nominal area of a Φ 8. Alternatively one could divide the force produced by the “fair-heavy” area: the 1 m long bars were weighted before each proof, to provide an equivalent diameter that resulted slightly

different from the nominal one. The comparison of the two methods emphasized the substantial equivalence of the two methods: the differences resulted negligible.

The result is represented in Fig.2.6 and reported in the numerical implementation phase as reported in Tab.2.1.

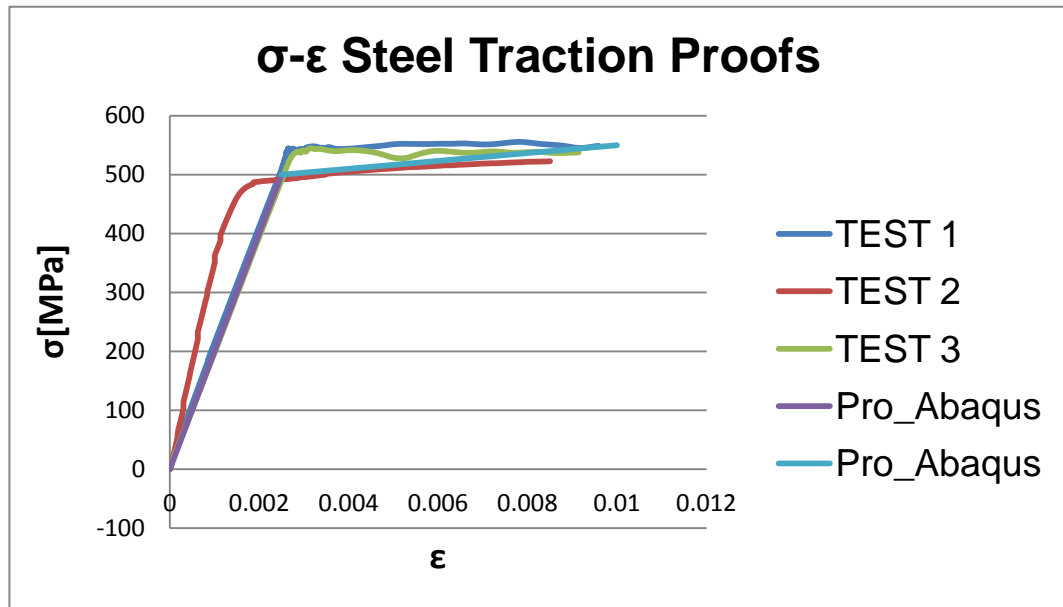


Fig.2.6 Experimental results of the 3 steel traction proofs on $\phi 8$ bars

The trend of Young's Modulus over the elastic branch is also reported in Fig.2.7

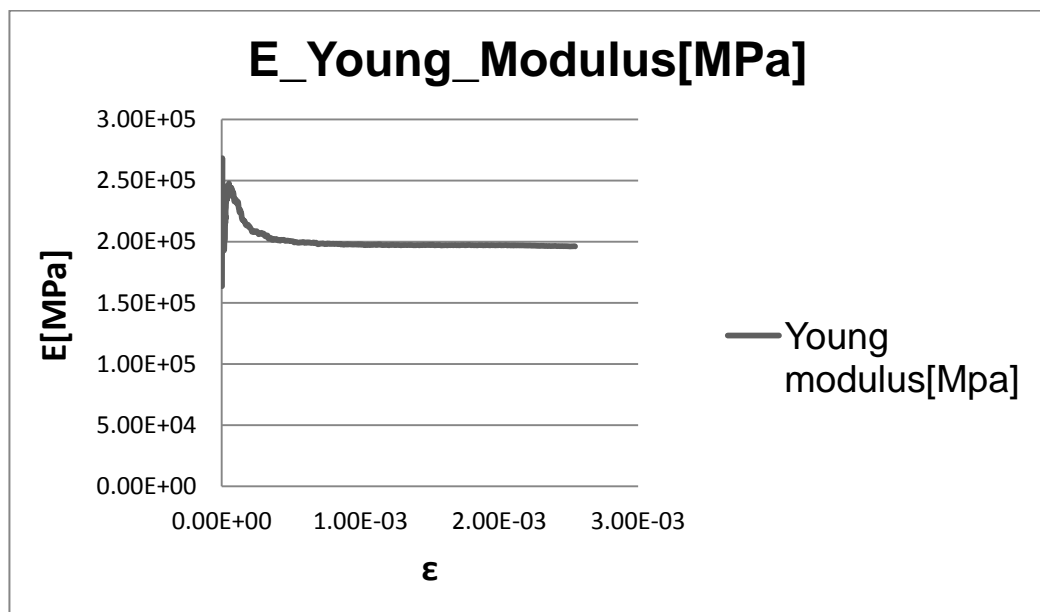


Fig.2.7 Young Modulus evaluation

The reference curve remain the one provided by the Italian Guidelines NTC 2008:

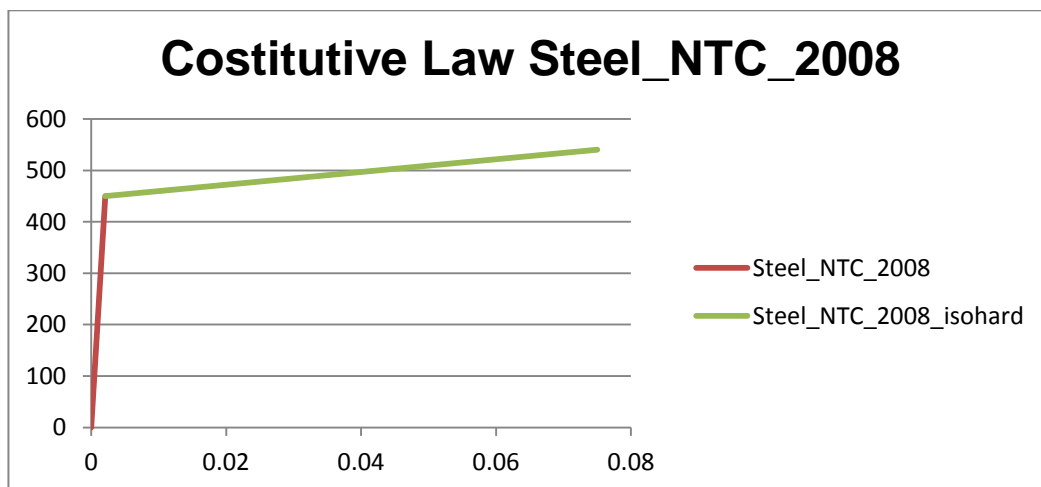


Fig.2.8. Constitutive law from Italian Guidelines NTC 2008

The Graph σ - ϵ implemented in the numerical models (that will be presented in Chapter 6) considered a mean trend among the 3 different traction tests:

Sigma[Mpa]	Eps
0	0
500	0.0025
550	0.01

Table.2.1 Constitutive law of steel implemented in Abaqus

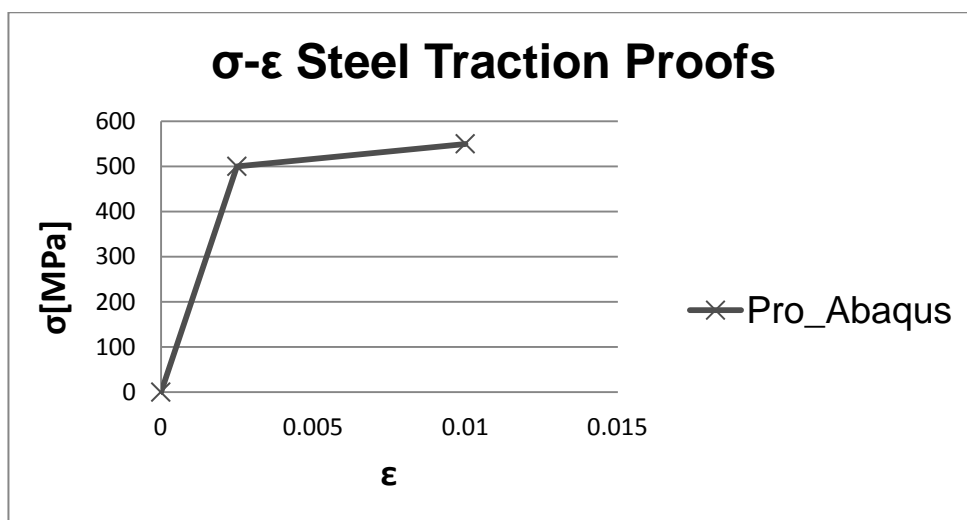


Fig.2.9 Graph σ - ϵ implemented in Abaqus

2.3 The compressive tests on 1mx1m walls

The mandatory tests, aimed at the characterization of the construction system, are imposed by the Italian Guidelines CSLP 2011. The 8 different proofs that are reported in this Thesis (*Chapter 3*) are part of TYPE 1 TEST("*Prove di tipo 1*") that must be conducted on panels of 1m x 1m long.

The load-application under monotonic and pseudo-static conditions must be of two types: axial centered compression and diagonal compression.

These tests are officially conceived to evaluate the longitudinal and transversal modules of elasticity, and to determine the relationship between the Secant stiffness evaluated at the maximum load and Secant stiffness to 30% of the maximum load.

2.3.1 The compression centered tests

In the Centered compression test the specimen is subjected to a uniform and vertical pressure through the work of a Load-equipment that works in load control conditions.



Figure 2.10 The Experimental set-up of compression tests

The presence of 4 LVDT allowed the measurement of vertical shortening of the specimen and of the horizontal expansion.

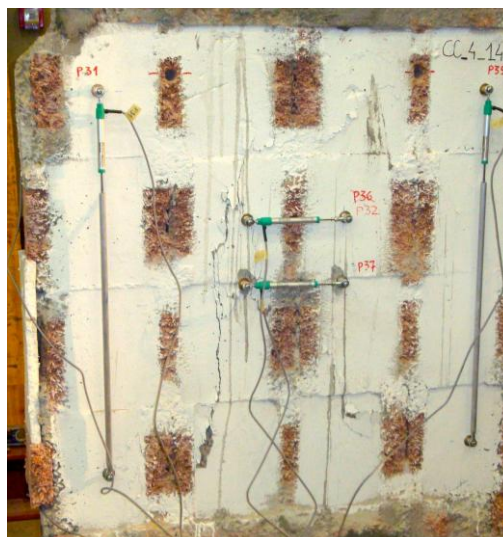


Figure 2.11 The LVDT measurement device

2.3.2 The diagonal tests

The diagonal compression test requires that the Load-equipment applies the pressure on one edge of the specimen, which must then be rotated 45 ° with respect to the position of the samples subjected to centered compression (because the press acts only in vertical direction).

To distribute the pressure in the most efficient way possible, and to limit the confinement of the specimen that would distort the test, the use of special "loading shoes" are recommended, as suggested by International ASTM E519 [18]

The measurements of the relative displacements of the specimen are measured by 4 LVDT. Each device, which length was in the range of 74 cm, was installed on each diagonal of each side in a centered position.



Figure 2.12 The diagonal experimental set-up with the LVDT measurement device

To ensure a more regular contact between the "loading-shoe" and the specimen, the latter is adjusted on the two loaded edges, by means of two L shape steel plates fixed with a high strength mortar.

Chapter 3

Evaluation of the equivalent continuous wall

Background

During the preliminary design phases there' s the need of simple tools for an immediate and effective global elastic analysis. In order to design a real structure making use of the grid-walls object of this thesis, it turns out to be useful the definition of equivalent continuous walls. This expedient allows both a simplification during the dimensioning/ modeling phase and to recall the Large Lightly reinforced concrete wall scheme of Eurocodes also called "Pareti estese debolmente armate" in Italian Guidelines NTC 2008.

Object

The object of this chapter is the definition of the correction-factors to be applied to geometric and mechanical properties that define the system formwork block, in order to model, in the design phase, the grid wall as a continuous elastic element.

Introduction

This chapter includes, as required by the Italian Guidelines " *Linee Guida per sistemi costruttivi a pannelli portanti basati sull'impiego di blocchi cassero e calcestruzzo debolmente armato in opera*" issued by the Consiglio Superiore dei Lavori Pubblici (August 2011), the elaborations and numerical modeling consequent to compression and diagonal centered tests conducted by CIRI Building and Construction Department of the Alma Mater Studiorum of Bologna. The experimental tests included:

- 1) No. 2 Centered Compression tests on r.c. panels 14 cm width called:
"CC14_01" and "CC14_02"
- 2) No. 2 Centered Compression tests on r.c. panels 18 cm width called:
"CC18_01" and "CC18_02"
- 3) No. 2 Diagonal Compression tests on r.c. panels 14 cm width called:
"CD14_01" and "CD14_02"
- 4) No. 2 Diagonal Compression tests on r.c. panels 18 cm width called:
"CD18_01" and "CD18_02"

3.1 Characteristics of materials

The materials used for the centered compression tests and diagonal compression are those already described in the previous chapter, the characteristics of are briefly reported in Table 3.1.

Characteristics Materials CC		Characteristics Materials CD	
Concrete	Steel	Concrete	Steel
R_{cm} 37.7 (MPa)	f_{ym} 500 (MPa)	R_{cm} 43.5 (MPa)	f_{yk} 450 (MPa)
f_{cm} 31.3 (MPa)	f_{tm} 550 (MPa)	f_{cm} 35.4 (MPa)	f_{tm} 550 (MPa)
f_{ck} 23.3 (MPa)	E_s 200000 (MPa)	f_{ck} 28.1 (MPa)	E_s 200000 (MPa)
f_{ctm} 2.9 (MPa)		f_{ctm} 3.2 (MPa)	
E_{cm} 30978 (MPa)		E_{cm} 32336 (MPa)	

Table 3.1. Materials characteristics

The Young's modulus E results from the formula provided by NTC 2008 once the mean compressive strength f_{cm} was evaluated from the compressive tests reported in Table 2.1 Chapter 2.

3.2 Analysis of the results on 14 cm width panels

3.2.1 Equivalent thickness s_{eg} and Mean Axial Stiffness ΔK_{14} of the continuous wall 14 cm width (Block 25/18)

The generic panel is composed of vertical pillars and horizontal beams. The *collaborating* geometrical area of each pillar, defined as the continuous vertical member from the lower to the upper base, is equal to 245 cm^2 . In *Fig. 3.1* is reported one of the wall tested: it can be noticed how the concrete pillars are not continuous due to the fitting procedure that foresee staggered blocks. In *Fig. 3.2* instead, are reported the effective dimensions of the typical 1 m cross-section.

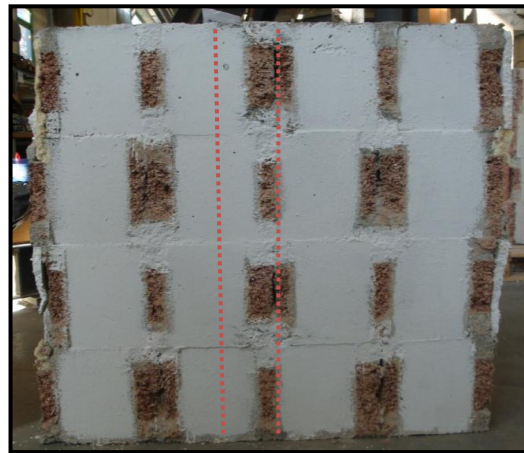


Fig.3.1 Geometry of the wall tested(1mx1m)

First of all is necessary to evaluate the geometrical concrete area A_{geom} :

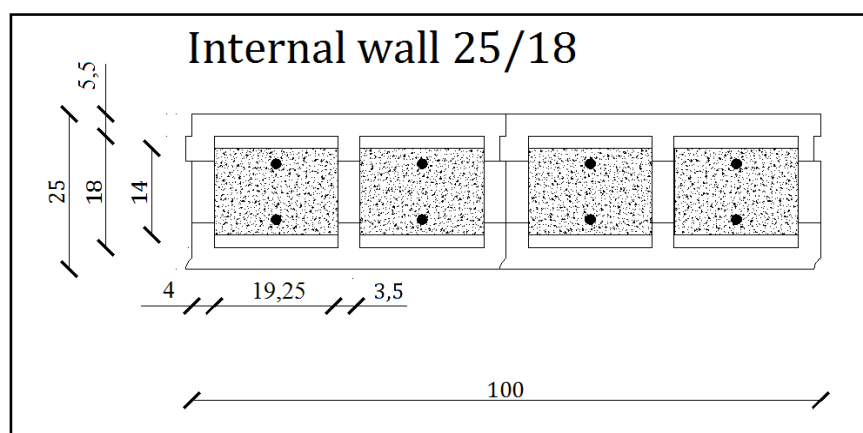


Fig.3.2 Cross-section of panel 14 cm width

In the case of wall 14 the concrete area per meter is:

$$A_{25/18}=980 \text{ cm}^2/\text{m}$$

The goal is to identify the continuous panel of equal cross section Area. According to the following expression the equivalent thickness of the panel can be defined:

$$s_{eg} = \frac{A_{c,eff}}{b} = \frac{980}{100} = 9.8 \text{ cm}$$

This definition completely rely on geometrical considerations. The equivalent geometrical thickness s_{eg} is the one to be used in the modeling phases, for the evaluation of the actions on the different elements.

3.2.2 Results of centered compression tests on panels 14 cm width: CC14_01 and CC14_02

Here below in *Figure 3.3 - Figure 3.4* and in *Table 3.2* and *Table 3.3* summarizes the results of experimental tests carried out in the laboratory.

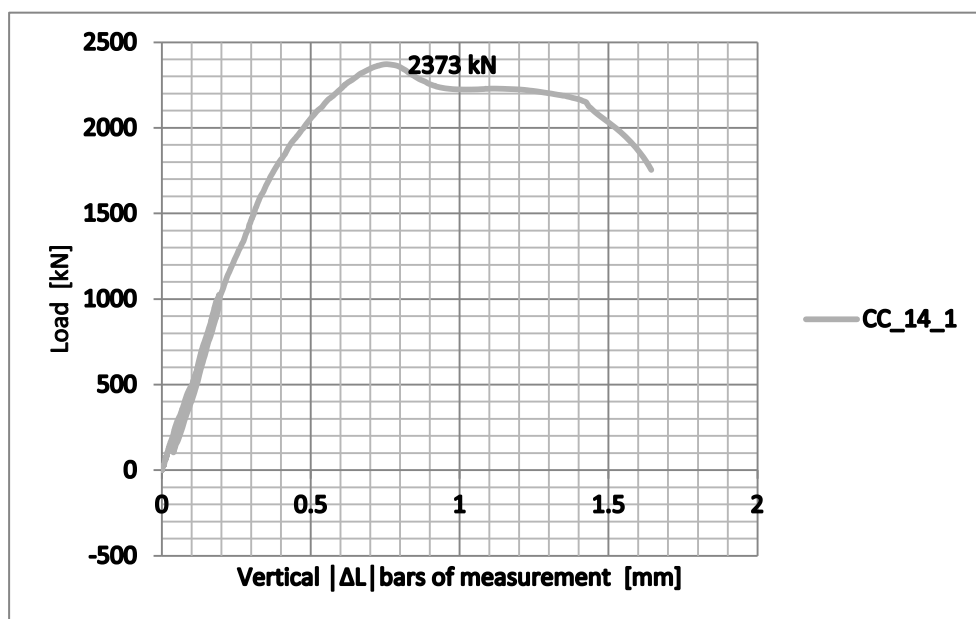


Figure 3.3. Load-Vertical Shortening graph of the centered compression test Panel CC14_01.

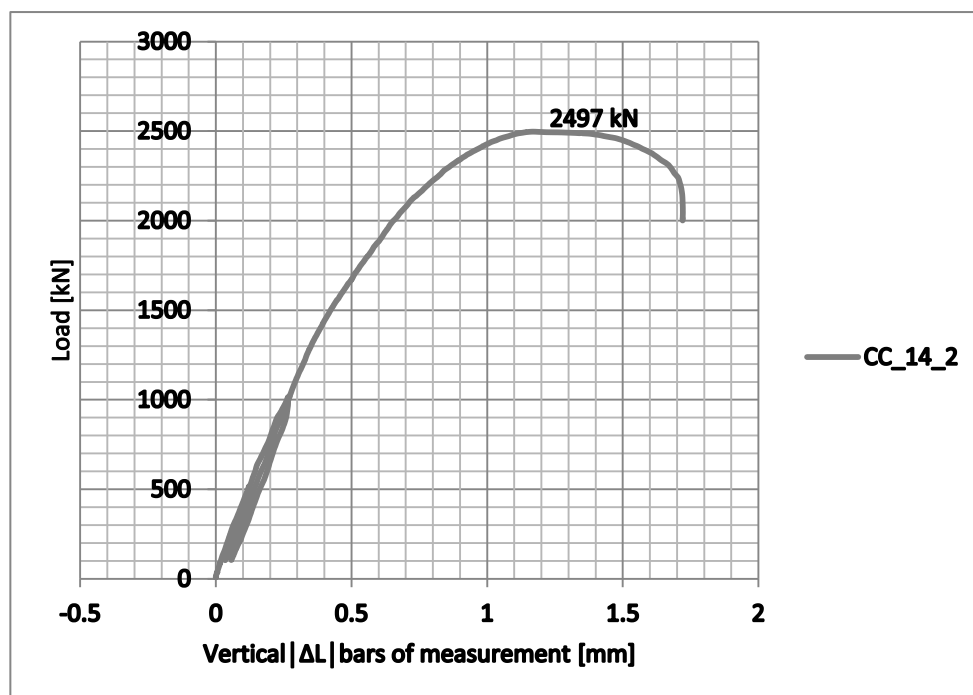


Figure 3.4. Load-Vertical Shortening graph of a centered compression test Panel CC14_02.

In the Table 3.2 and Table 3.3 are reported the values of the load P and vertical shortening Δl corresponding to the maximal Load P_{max} and to the 30% of P_{max} . These data were used to evaluate the secant stiffness of the panel in the two different load steps. It was evaluated also the ratio ΔK between the secant stiffness at 30% of P_{max} and P_{max} himself, in accordance with the Italian Guidelines "Linee Guida per sistemi costruttivi a pannelli portanti basati sull'impiego di blocchi cassero e calcestruzzo debolmente armato in opera" issued by the Consiglio Superiore dei Lavori Pubblici (August 2011).

CC14_01				CC14_02			
		$P_{30\%}$	P_{Max}			$P_{30\%}$	P_{Max}
P	(kN)	711.9	2373	P	(kN)	749	2497
δ	(mm)	0.144	0.755	δ	(mm)	0.189	1.17
K	(kN/mm)	4943	3143	K	(kN/mm)	3962.96	2135

ΔK	0.64
------------------------------	------

ΔK	0.53874
------------------------------	---------

Table 3.2. Panels CC14_01 and CC14_02 . results of Centered Compression tests on 14 cm panels

CC14_01 - CC14_02			
Valore Medio			
		P _{30%}	
K	(kN/mm)	4452.98	

Table 3.3. Mean value of the axial stiffness of the 14 cm panels.

3.3 Interpretation of the compression tests on 14 cm width panels

3.3.1 Equivalent Young Modulus E' of the continuous wall with s_{eg}=9.8 cm

Starting from the experimental results and making use of the equivalent geometric thickness defined in Par 3.2.1, we want to find the value of fictitious Young modulus E' able to match the experimental axial stiffness measured in linear elastic behavior. In particular, the fictitious elastic modulus is defined starting from the elastic modulus of concrete modified by a suitable correction coefficient α .

$$E' = \alpha E$$

This coefficient α takes into account that the wall build with formwork blocks is not continuous but presents a two-dimensional structure composed of vertical and horizontal elements. In accordance with the linear-elastic continuum model, the relation Force-Displacement can be expressed by the classical formulation:

$$F = K\delta$$

where the axial stiffness is equal to:

$$K = \frac{E' A}{l}$$

Starting from the experimental curves Load- Δl shown above, an average value of the secant stiffness (at 30% strength) of the panels tested was evaluated equal to $K = 4453 \text{ kN / mm}$. The inversion of the last equation, provides the dependence of the elastic modulus of such fictitious parameter according to the expression:

$$E' = \frac{Kl}{A}$$

from which, substituting into it the value of stiffness obtained experimentally, the cross-section area $A = 980 \text{ cm}^2$ and the length $l = 74 \text{ cm}$ of the measurement base of the transducers, can be obtained a value of fictitious elastic modulus $E' = 33\,625 \text{ MPa}$. The correction coefficient α results to be equal to:

$$\alpha_{14} = \frac{E'}{E} = \frac{33625}{30978} = 1.09$$

3.3.2 Results of compressive diagonal tests on panels 14 cm width: CD14_01 and CD14_02

Considering the Standards ASTM E519 "Standard Test Method for Diagonal Tension (Shear) in Masonry Assemblages", the shear-slip curve has been reconstructed for each test, by defining the following quantities:

- T = shear force acting on the generic section of the connector beams equal to:

$$T = P \cos 45^\circ$$

where P is the loading force.

- γ = slide defined by the ratio

$$\gamma = \frac{\delta_v - \delta_0}{g}$$

where δ_v is the measured vertical shortening of the specimen, δ_0 is the horizontal elongation and g is the basis of measurement (the length of measurement bar) used in the test, equal to 76.4 cm and can be seen in *Fig.3.5*.



Figure 3.5. Experimental set-up

All these quantities can be visualized in the following Figure 3.6.

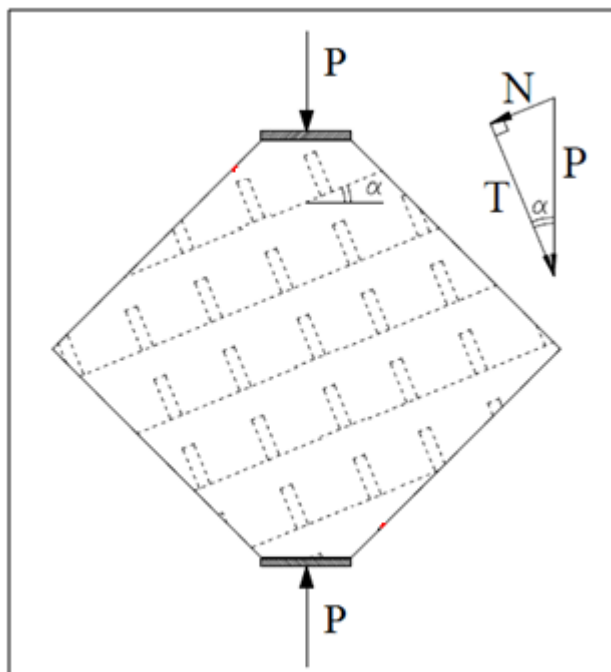


Figure 3.6. Diagonal test Scheme

In the test conducted in the CIRI laboratory α was equal to 45 degrees.

3.3.3 Equivalent Elastic Tangential Modulus G' of the continuous wall

Starting from the experimental results, and making use of the equivalent geometric thickness defined in paragraph 3.2.1, the goal of this paragraph is the definition of the value of fictitious shear modulus G' able to match the tangential stiffness measured during the tests on the grid-wall, with the one related to a continuous linear elastic model. In particular, the fictitious shear modulus G' was defined starting from the shear modulus of the concrete modified by a suitable correction coefficient β , according to the expression:

$$G' = \beta G$$

This β coefficient takes into account that the wall built with formwork blocks is not continuous, but has a discrete two-dimensional structure composed of vertical and horizontal elements. In accordance with the linear-elastic continuum model the relation T - γ can be expressed by the classical expression:

$$T = G' A \gamma,$$

where T can be evaluated as the Vertical Load P that the loading-machine impress on the upper corner of the wall, multiplied for $\cos 45^\circ$ to obtain the shear T on the joists; G' is the fictitious shear modulus, A is the geometrical cross section of the panel and γ is the slide. The shear elastic modulus of the concrete instead was defined starting from the Young's modulus according to the classic expression:

$$G = \frac{E_{cm}}{2(1 + \nu)}$$

where a Poisson's coefficient of 0.2 was considered, obtaining $G = 13473.3$ MPa considering a $E_{cm} = 32336$ MPa as Young's modulus.

In the following, the results of compressive diagonal test conducted on 14 cm grid-wall are reported.

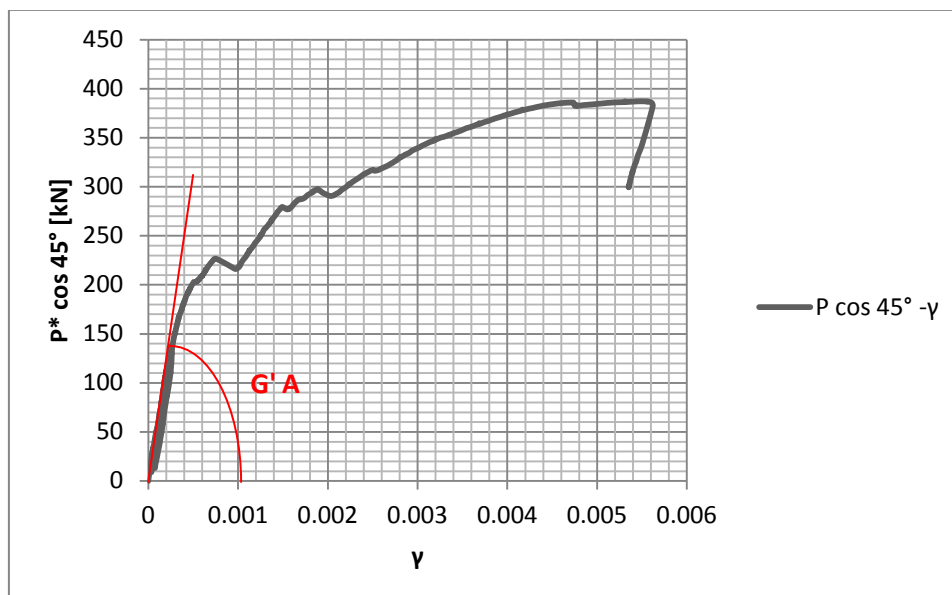


Fig.3.7 (T- γ) graph of CD14_01 test

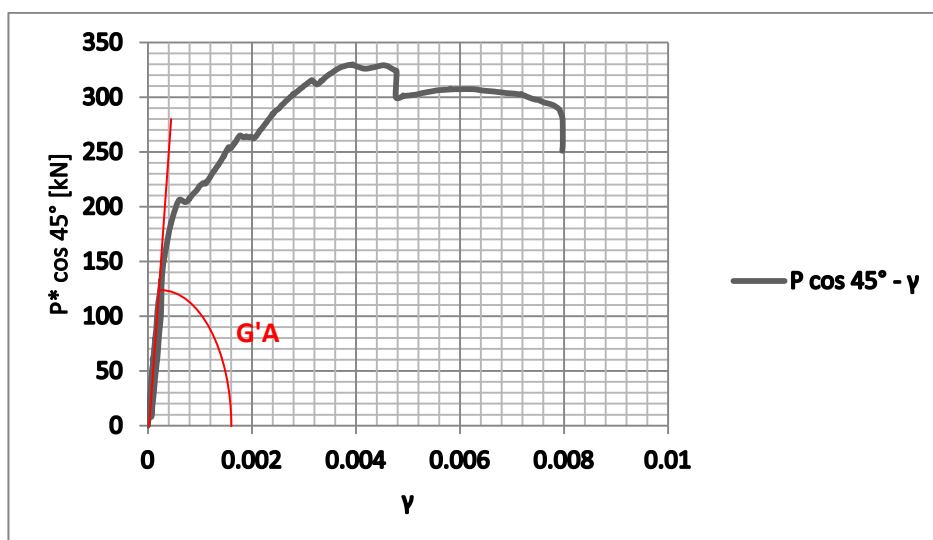


Fig.3.8 (T- γ) graph of CD14_02 test

From these two experimental curves was evaluated in the tangential stiffness $G'A$, which coincides with the inclination of the first section of the elastic part of the diagram T- γ .

Diagonal test(14)	G'A
	(kN)
CD14_01	575785
CD14_02	610359
Mean	593072

Table.3.4 Shear stiffness measured on diagonal tests on 14 cm specimen

In Table 3.4 are reported the tangential stiffness values evaluated. In order to obtain the coefficient β able to match the theoretical tangential stiffness connected to the concrete continuum theory with the experimental one related to the grid-wall, the following equation was imposed:

$$\beta = \frac{(G'A)_{\text{exp}}}{GA} = \frac{593072000}{13473.3 \cdot 98000} = 0.45$$

where the stiffness in the numerator is the mean value measured experimentally while in the denominator the concrete shear modulus and the effective cross section of the panel 14 cm width are reported.

3.4 Analysis of the results on 18 cm width panels

3.4.1 Equivalent thickness s_{eg} and Mean Axial Stiffness ΔK_{18} of the continuous wall 18 cm width (Block 32/22)

The generic panel made is composed of vertical pillars and horizontal beams. The *collaborating* geometrical area of each pillar, defined as the continuous vertical member from the lower to the upper base, is equal to 297 cm^2 . In Fig. 3.9 is reported one of the wall tested: it can be noticed how the concrete pillars are not continuous due to the fitting procedure that foresee staggered blocks. In Fig.3.10 instead, are reported the effective dimensions of the typical 1 m cross-section.



Fig.3.9 Geometry of the wall tested(1mx1m)

First of all is necessary to evaluate the geometrical concrete area A_{geom} :

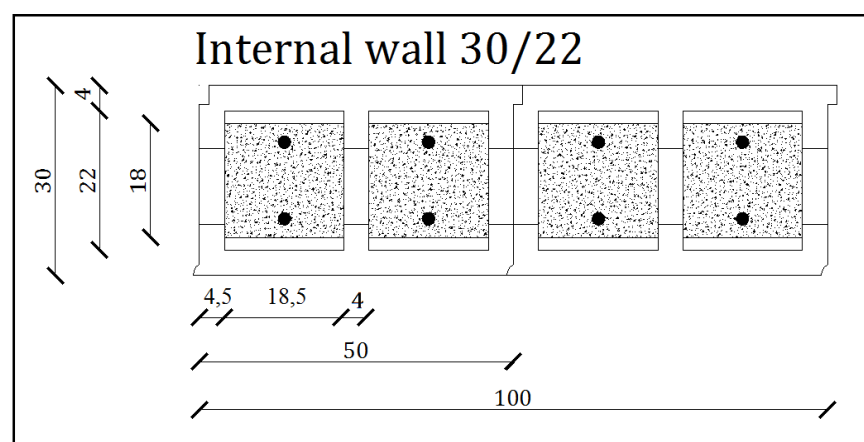


Fig.3.10 Cross-section of panel 18 cm width

In the case of wall 18 the concrete area per meter is:

$$A_{30/22}=1188 \text{ cm}^2/\text{m}$$

The goal is to identify the continuous panel of equal cross section Area. According to the following expression the equivalent thickness of the panel can be defined:

$$s_{eg} = \frac{A_{c,eff}}{b} = \frac{1188}{100} = 11.88 \text{ cm}$$

This definition completely rely on geometrical considerations. The equivalent geometrical thickness s_{eg} is the one to be used in the modeling phases, for the evaluation of the actions on the different elements.

3.4.2 Results of centered compression tests on panels 18 cm width: CC18_01 and CC18_02

Here below in *Figure 3.11 - Figure 3.12* and in *Table 3.5* and *Table 3.6* summarizes the results of experimental tests carried out in the laboratory.

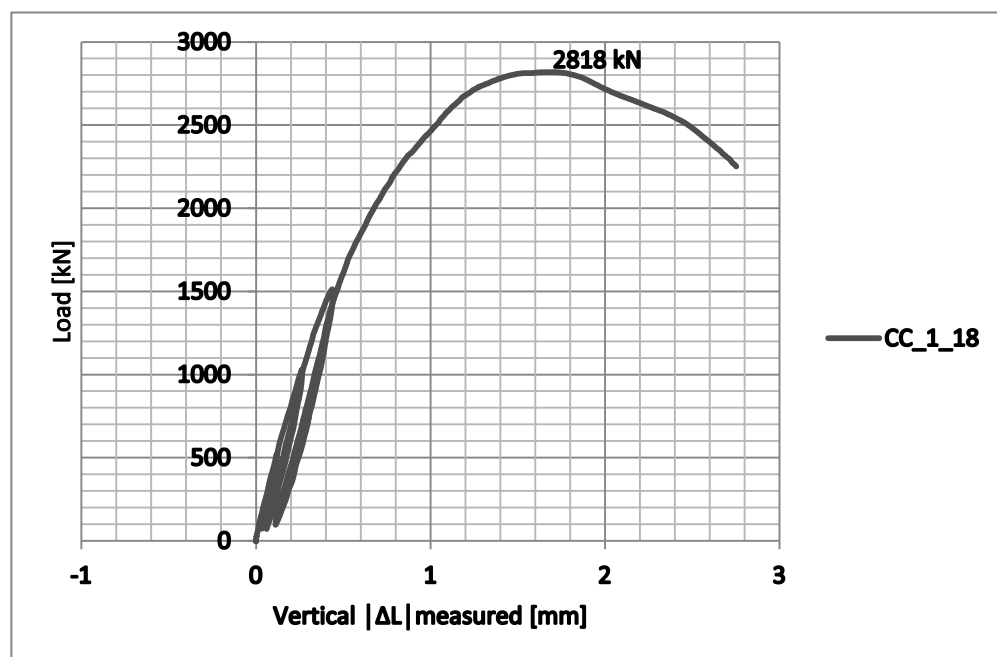


Figure 3.11. Load-Vertical Shortening graph of the centered compression test Panel CC18_01.

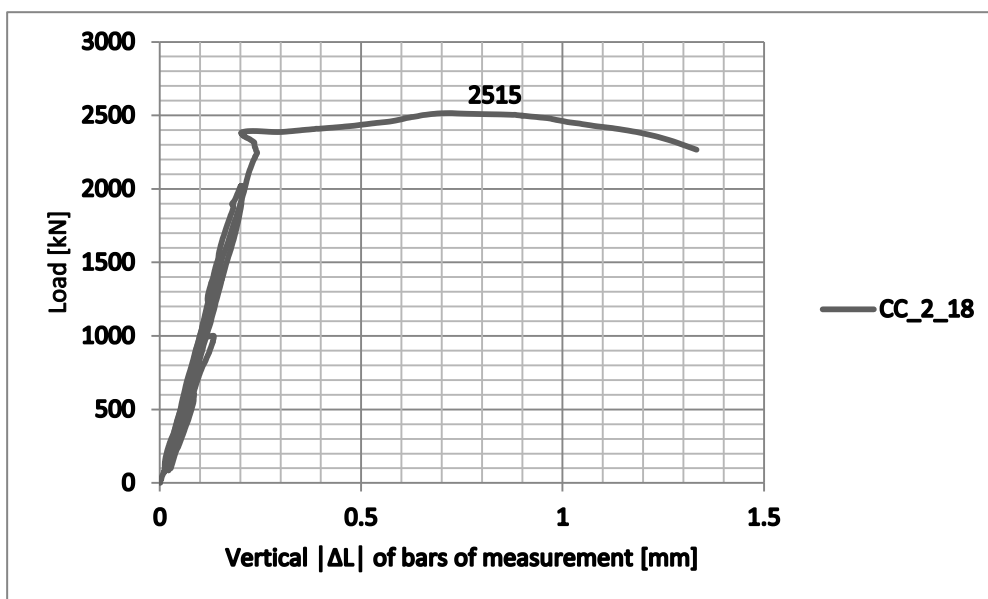


Figure 3.12. Load-Vertical Shortening graph of a centered compression test Panel CC18_02.

In the Table 3.5 and Table 3.6 are reported the values of the load P and vertical shortening Δl corresponding to the maximal Load P_{max} and to the 30% of P_{max} . These data were used to evaluate the secant stiffness of the panel in the two different load steps. It was evaluated also the ratio ΔK between the secant stiffness at 30% of P_{max} and P_{max} himself, in accordance with the Italian Guidelines "Linee Guida per sistemi costruttivi a pannelli portanti basati sull'impiego di blocchi cassero e calcestruzzo debolmente armato in opera" issued by the Consiglio Superiore dei Lavori Pubblici (August 2011).

CC18_01				CC18_02			
		$P_{30\%}$	P_{Max}			$P_{30\%}$	P_{Max}
P	(kN)	845	2818	P	(kN)	754	2515
δ	(mm)	0.209	1.704	δ	(mm)	0.101	0.721
K	(kN/mm)	4044	1654	K	(kN/mm)	7497	3486

ΔK	0.41
------------------------------	------

ΔK	0.47
------------------------------	------

Table 3.5. Panels CC18_01 and CC18_02 . results of Centered Compression tests on 18 cm panels

CC18_01 - CC18_02			
Mean value			
		P _{30%}	
K	(kN/mm)	5770.5	

Table 3.6. Mean value of the axial stiffness of the 18 cm panels.

3.5 Interpretation of the centered compression tests on 18cm width panels

3.5.1 Equivalent Young Modulus E' of the continuous wall with $s_{eg}=11.88$ cm

Starting from the experimental results and making use of the equivalent geometric thickness defined in *Par. 3.4.1*, we want to find the value of fictitious Young modulus E' able to match the experimental axial stiffness measured in linear elastic behavior. In particular, the fictitious elastic modulus is defined starting from the elastic modulus of concrete modified by a suitable correction coefficient α .

$$E' = \alpha E$$

This coefficient α takes into account that the wall build with formwork blocks is constituted not only by concrete pillars but presents a two-dimensional structure composed of vertical and horizontal elements. In accordance with the linear-elastic continuum model, the relation Force-Displacement can be expressed by the classical formulation:

$$F = K\delta$$

where the axial stiffness is equal to:

$$K = \frac{E' A}{l}$$

Starting from the experimental curves Load- Δl shown above, an average value of the secant stiffness (at 30% strength) of the panels tested was evaluated equal to $K = 5770.5$ kN / mm. The inversion of the last equation, provides the dependence of the elastic modulus of such fictitious parameter according to the expression:

$$E' = \frac{Kl}{A}$$

from which, substituting into it the value of stiffness obtained experimentally, the cross-section area $A = 1188 \text{ cm}^2$ and the length $l = 73.6 \text{ cm}$ of the measurement base of the transducers, can be obtained a value of fictitious elastic modulus $E' = 35749 \text{ MPa}$. The correction coefficient α results to be equal to:

$$\alpha_{18} = \frac{E'}{E} = \frac{35749}{30978} = 1.15$$

3.5.2 Results of compressive diagonal tests on panels 18 cm width: CD18_01 and CD18_02

Considering the Standards ASTM E519 "Standard Test Method for Diagonal Tension (Shear) in Masonry Assemblages", the shear-slip curve has been reconstructed for each test, by defining the following quantities:

- T = shear force acting on the generic section of the joists equal to:

$$T = P \cos 45^\circ$$

where P is the loading force.

- γ = slide defined by the ratio

$$\gamma = \frac{\delta_v - \delta_0}{g}$$

where δ_v is the measured vertical shortening of the specimen, δ_0 is the horizontal elongation and g is the basis of measurement (the length of measurement bar) used in the test, equal to 76.4 cm and can be seen in Fig.xxx.

3.5.3 Equivalent Elastic Tangential Modulus G' of the continuous wall

Starting from the experimental results, and making use of the equivalent geometric thickness defined in paragraph 3.4.1, the goal of this paragraph is the definition of the value of fictitious shear modulus G' able to match the tangential stiffness measured during the proof on the grid-wall, with the one related to a continuous linear elastic model. In particular, the fictitious shear modulus G' was defined starting from the shear modulus of the concrete modified by a suitable correction coefficient β , according to the expression:

$$G' = \beta G$$

This β coefficient takes into account that the wall built with formwork blocks is not continuous, but has a discrete two-dimensional structure composed of vertical and horizontal elements. In accordance with the linear-elastic continuum model the relation T - γ can be expressed by the classical expression:

$$T = G' A \gamma$$

where T can be evaluated as the Vertical Load P that the machine impress on the upper corner of the wall, multiplied for $\cos 45^\circ$ to obtain the shear T on the joists; G' is the fictitious shear modulus, A is the geometrical cross section of the panel and γ is the slide. The shear elastic modulus of the concrete instead was defined starting from the Young's modulus according to the classic expression:

$$G = \frac{E_{cm}}{2(1 + \nu)}$$

where a Poisson's coefficient of 0.2 was considered, obtaining $G=13473.3$ MPa considering a $E_{cm}=32336$ MPa as Young's modulus.

In the following, the results of compressive diagonal test conducted on 18 cm grid-wall are reported.

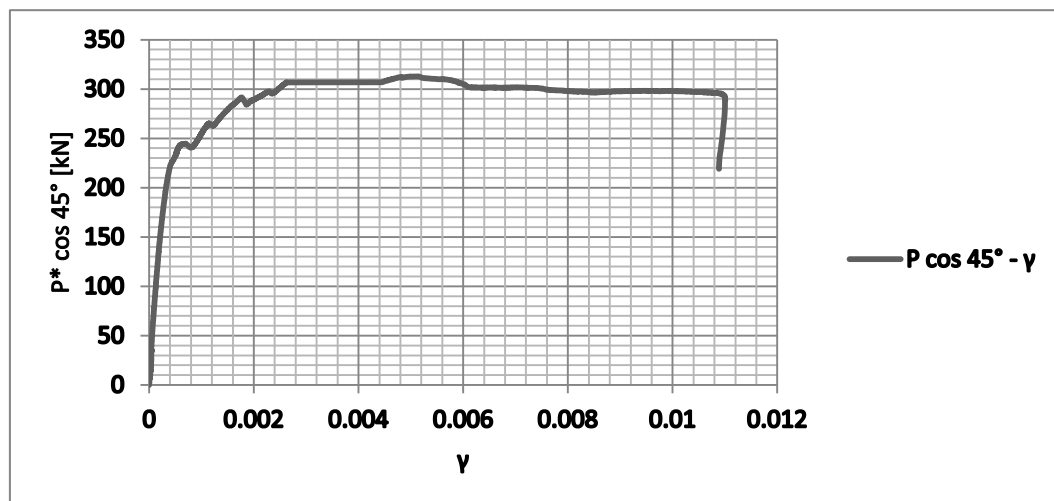


Fig.3.13 (T- γ) graph of CD18_01 test

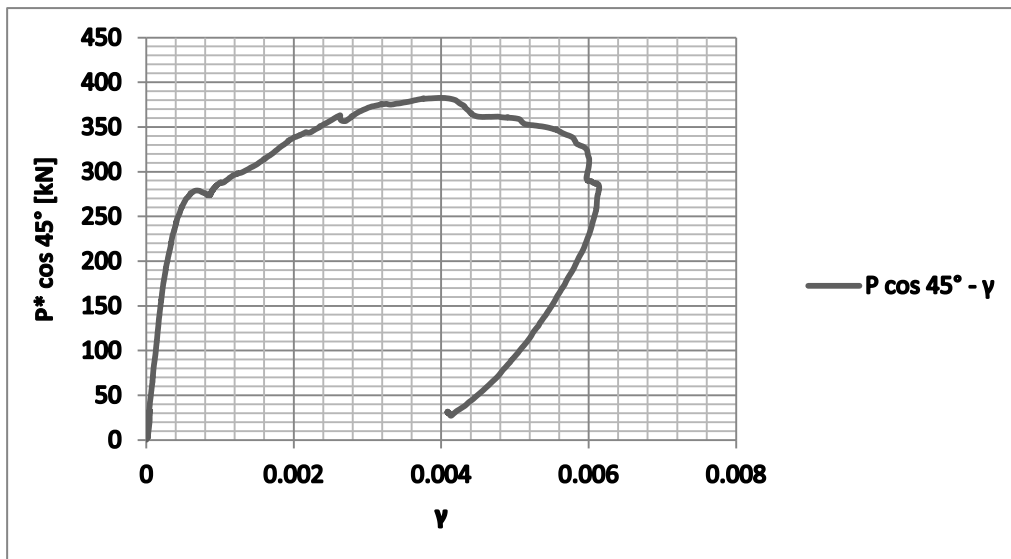


Fig.3.14 (T- γ) graph of CD18_02 test

From these two experimental curves was evaluated in the tangential stiffness $G'A$, which coincides with the inclination of the first section of the elastic part of the diagram T- γ .

Diagonal test(18)	$G'A$ (kN)
CD18_01	853262
CD18_02	800519
Mean	826890.5

Table.3.7 Shear stiffness measured on diagonal tests on 18 cm specimen

In Table 3.7 are reported the tangential stiffness values evaluated. In order to obtain the coefficient β able to match the theoretical tangential stiffness connected to the concrete continuum theory with the experimental one related to the grid-wall, the following equation was imposed:

$$\beta = \frac{(G'A)_{\text{exp}}}{GA} = \frac{826890500}{13473.3 \cdot 118800} = 0.51$$

where the stiffness in the numerator is the mean value measured experimentally while in the denominator the concrete shear modulus and the effective cross section of the panel 18 cm width are reported.

3.6 Summary

The experimental test, conducted on Large Lightly Reinforced Concrete Wall build with formwork block object of this Thesis, followed the n.1 typology the Italian Guidelines "*Linee Guida per sistemi costruttivi a pannelli portanti basati sull'impiego di blocchi cassero e calcestruzzo debolmente armato in opera*" issued by the Consiglio Superiore dei Lavori Pubblici (August 2011) on compression tests and diagonal compression tests. From the experimental tests some mechanical parameters identifying the elastic response of the grid-wall were defined. These parameters should be used during the design phase as a simplifying tool to build elastic continuum models.

A procedure which involves the use of corrective factors α and β was developed: it consist on multiplying respectively the values of the longitudinal elastic modulus E and transversal G , in order to model the r.c. grid-walls as continuous walls, devoid of holes, and characterized by a equivalent geometric thickness s_{eg} calculated as a function of the net area of concrete.

The results are listed below.

3.6.1 Definition of equivalent geometric thickness s_{eg}

The equivalent geometric thickness is defined as the net resistant area (the area of concrete casted on site) per unit length of the wall, divided by the length L . Proceeding in this way, the effective area of concrete $A_{c,eff}$ of the equivalent continuous wall suggested by Italian Guidelines, can be obtained according to the formula:

$$A_{c,eff} = s_{eg} L$$

For the two different typologies of blocks 25/18 (width 14 cm) and 30/22 (width 18 c), the equivalent geometrical thicknesses are evaluated as reported in Table 3.8.

	Width of panel	Equivalent continuous width
	(cm)	(cm)
Block 25/18	14	9.8
Block 30/22	18	11.88

Table 3.8 Values of the equivalent geometrical thickness to be considered in the design phase for the two different type of blocks

3.6.2 Correction coefficient α and β

The mechanical behavior of the grid walls can be compared to the behavior of a continuous wall, with the same length L and thickness coincident with the equivalent geometric one s_{eg} (defined according to the Guidelines). During the modeling and calculation phases the equivalent values $E' = \alpha E$ and $G' = \beta G$ must be used, using the correction coefficients indicated in Table 3.9:

	E	G	α	β
Panel 14	from Guidelines	from Guidelines	1.09	0.45
Panel 18	from Guidelines	from Guidelines	1.15	0.51

Table 3.9 Values of the correction factors to be applied during modeling phase to continuous equivalent wall

3.7 Equivalent continuous numerical models

Considering the result obtained and making reference to the *Table 3.8* and *Table 3.9* some simple numerical models able to test the reliability and effectiveness of the corrective coefficient obtained can be build. The F.E. program chosen to reproduce the equivalent wall was Abaqus, that will be used in the second part of this thesis for the micro-modeling attempt.

Both panels 14 cm and 18 cm were checked.

In both cases a continuous element were build. The dimensions are simply 1m x 1 m x s_{eg} as evaluated for the two cases in the previous paragraph and reported in *Table 3.8*. The mesh (characteristic dimension of 2 cm), the boundary conditions and the load used are reported in *Figure 3.15*.

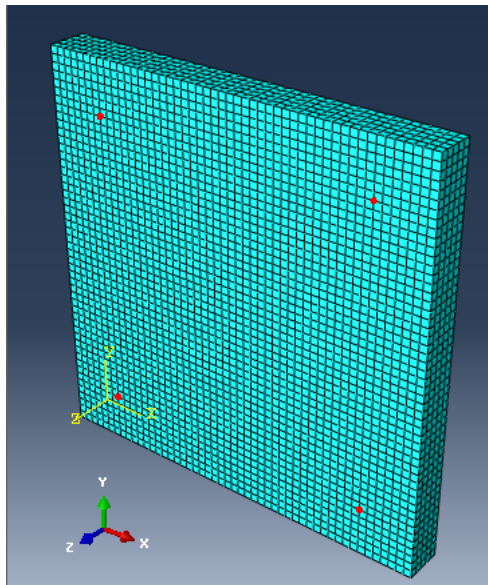


Fig.3.15 (a) The mesh and spy-nodes

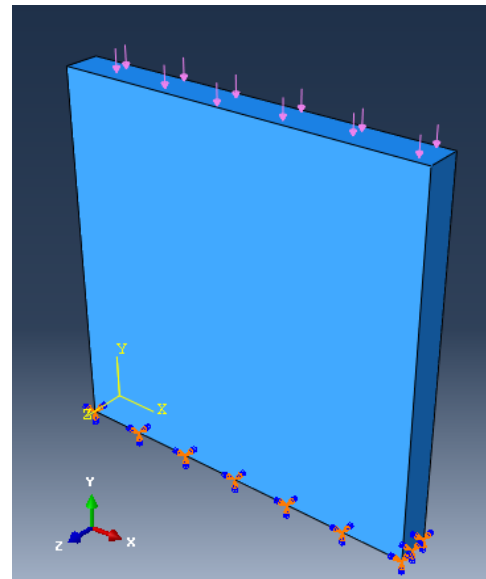


Fig.2.15 (b) The load and the B.C.

Fig.3.15 Continuous model for checking purpose

Four spy-nodes were introduced in each model to make a check between numerical Load-vertical shortening graph and experimental one. Abaqus elastic editor requests the Young's modulus E and the Poisson coefficient ν .

For what concern the Young modulus the corrected E' inserted following the over mentioned formula:

$$E' = \alpha E$$

For what concern the Poisson coefficient a corrected ν' was inserted. The new Poisson coefficient was evaluated as follows:

$$\nu' = \frac{1}{2} \left(\frac{E'}{G} - 2 \right)$$

3.7.1 Implementation and results on continuous wall 14

In *Table 3.10* the results on the elastic parameters implemented to reproduce the equivalent continuous wall 14 are reported.

Eq.wall_14	
E	30978
α_{14}	1.09
E'_14	33766.02
ν	0.2
G	12907.5
β_{14}	0.45
G'	5808.375
ν'	0.308

Table.3.10 Parameters considered for continuous numerical wall14

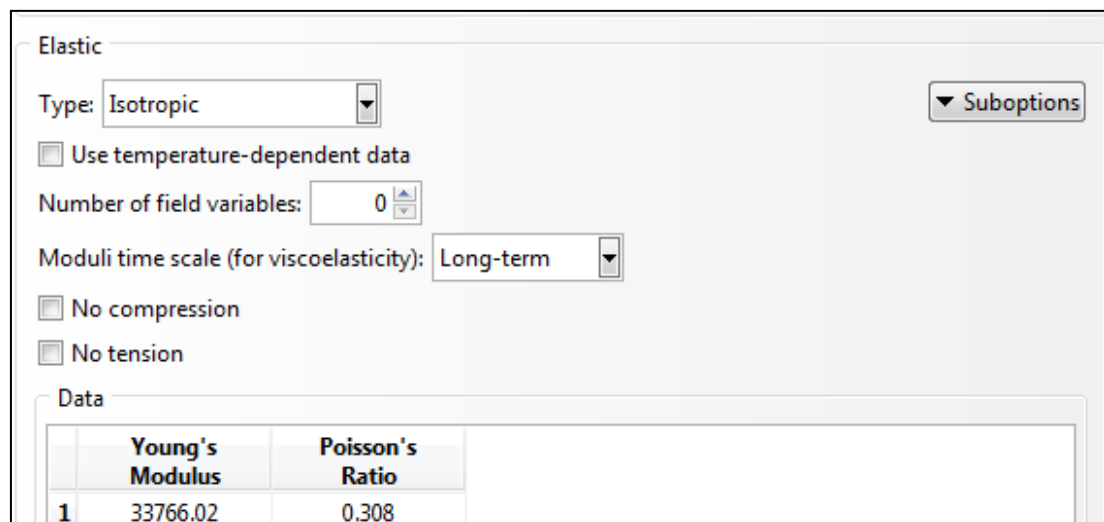


Fig.3.16 Abaqus material editor for continuous numerical wall14

The comparison with the experimental elastic part of the curve Load-Vertical ΔL shows good results. The numerical continuous wall implemented, falls perfectly in between the two experimental curves CC14_01 and CC14-02.

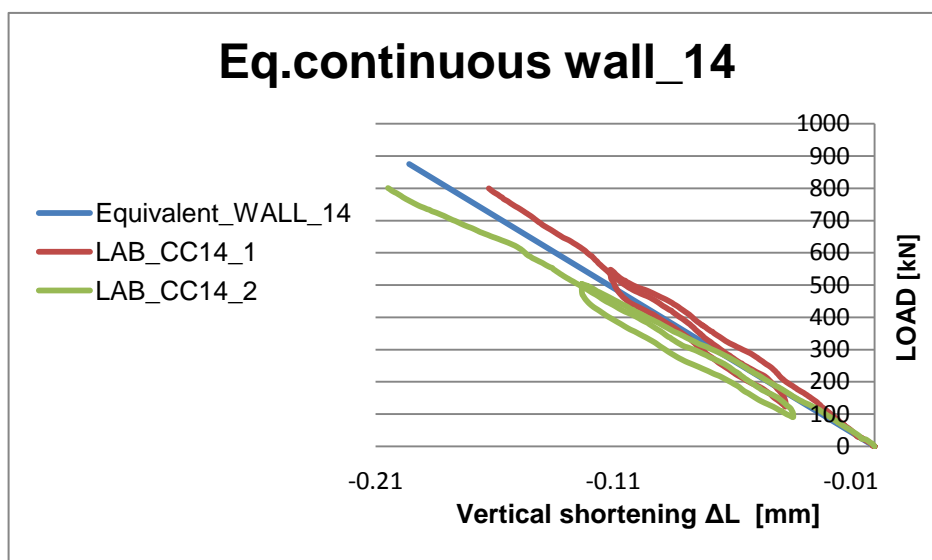


Fig.3.17 Comparison between numerical and experimental Load-Vertical ΔL curves for continuous wall14

3.7.2 Implementation and results on continuous wall 18

In Table 3.11 the results on the elastic parameters implemented to reproduce the equivalent continuous wall 18 are reported.

Eq.wall_18	
E	30978
α_{18}	1.15
E'_{18}	35624.7
ν	0.2
G	12907.5
β_{18}	0.51
G'	6582.83
ν'	0.38

Table.3.11 Parameters considered for continuous numerical wall14

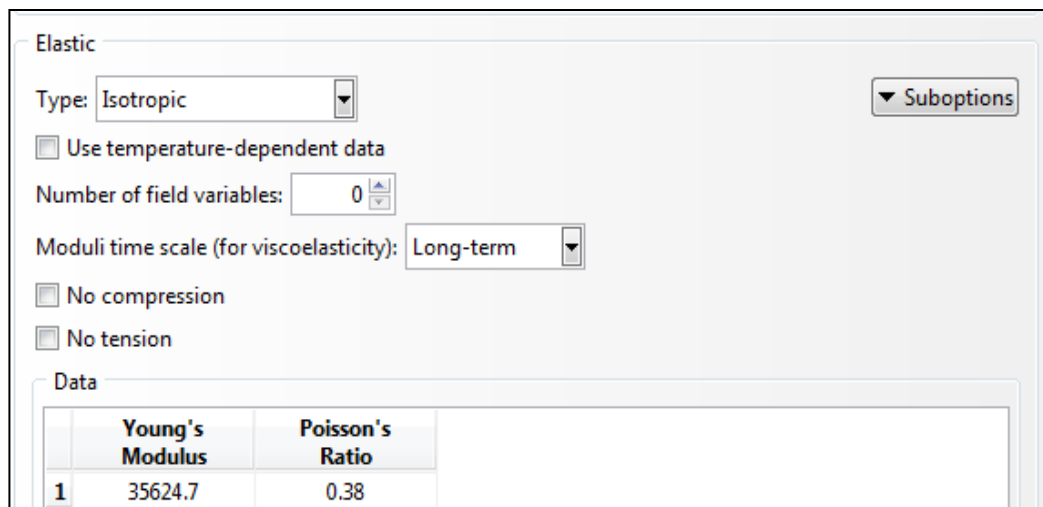


Fig.xx Abaqus material editor for continuous numerical wall18

The comparison with the experimental elastic part of the curve Load-Vertical ΔL shows good results. The numerical continuous wall implemented, falls perfectly in between the two experimental curves CC18_01 and CC18_02.

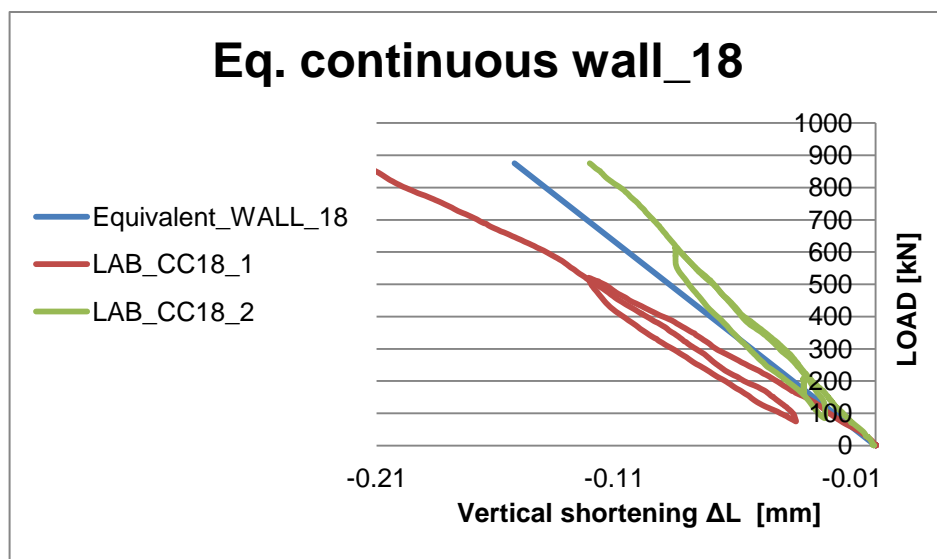


Fig.3.18 Comparison between numerical and experimental Load-Vertical ΔL curves for continuous wall18

Chapter 4

Constitutive laws for modeling purposes

Background

For a better and in-deep understanding of complex phenomena non-linear analysis is often used, especially in seismic design and collapse analysis. The non-linearity of the analysis introduce elements of complexity, but is the only way to capture the micro-behavior close to the collapse or, more in general, the phase after the elastic one. In practical design the use of sophisticated micro-modeling process is not used, cause of the unavoidable time-consuming problems connected with strong non-linearity.

In classical formulations two types of non-linearity are considered: the geometrical and the constitutive one. The constitutive non-linearity is the one used in the present thesis. The theoretical formulations available in literature are referred to experimental campaign on concrete behavior conducted by Kent and Park [23] , Cornellissen et al. [24].

The use of advanced “Arch-Length method” and the correct choice of the advancement-step is the only way to grant the convergence of this type of problems.

Object

The primary objective of this chapter was to provide the complete framework in the definition of the non-linear constitutive model used, with the goal to describe the behavior of the concrete for a better matching between numerical model and experimental proof.

Introduction

The definition of the constitutive model of the two material is one of the most important and tricky aspect of this study. In FE linear elastic analysis the definition of elastic parameters (Young's modulus E , Poisson ratio ν) and of the peak strength values is sufficient to ensure reliable and conservative solutions. In the non-linear analysis the definition of the σ - ϵ evolution-law, both in the pre-peak and moreover during the post-peak behavior is crucial for both convergence and accuracy aspects. Other important parameters concerns the *flow rule* and the *yield function*. All these laws must be well calibrated; that's imply that the more

experimental data are available the more the calibration process can be focused of the best fitting of a few number of parameters. For this purpose *Chapter 2* in which experimental data are provided will be often recalled.

4.1 Experimental behavior of concrete

4.1.1 Concrete subjected to uniaxial compression

The typical compressive stress-strain curve of the concrete is reported in *Fig.4.1*. Three different phases can be observed: the linear-elastic phase, the non elastic phase and the phase of the localization of the deformation. The first phase grows until a compression stress that is almost 30% of f'_c , the cylindrical compressive uniaxial strength. For bigger values, is observed a second phase, the non-linear response that becomes more evident close to the peak value f'_c beyond which the descending branch starts, in which the deformation decreases with increasing stress until rupture crushing. If the material is subjected to cyclic loading a residual strain and a degradation of stiffness can be observed.

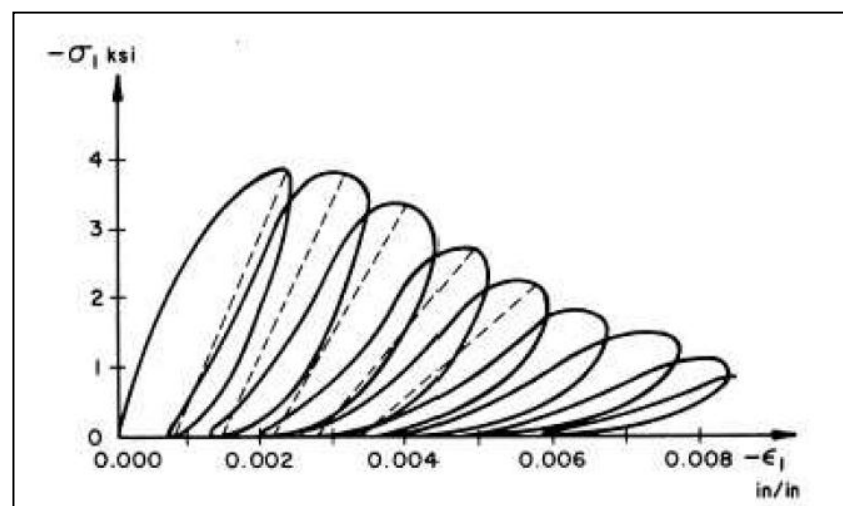
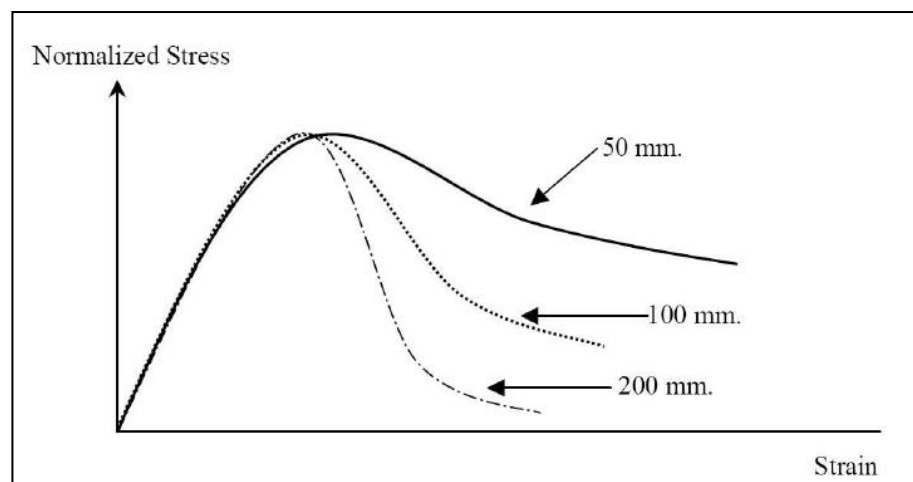


Fig. 4.1 Stress-strain curve for uniaxial cyclic proof (Chen[21])

Experimental observations show that in the after-peak phase, the deformation is no longer uniform, but tends to be localized in a section. In this phase a correct representation of the behavior must be done in terms of stress-displacements rather than stress-strain. This experimental evidence has been supported by studies

conducted by Van Mier [22] on the dependence of the stress-strain branch on the geometry element. The results are illustrated in *Fig.4.3*

It is noted that before the peak, the curves are identical. On the other hand after the peak, decreasing the height of the specimen there is a decrease in the slope of the stress-strain graph. On the contrary, if the same results are represented in terms of stress-displacement, the difference in the response of the samples disappears.



*Fig. 4.2: Dependence of the stress-strain curve of the size of the specimen
(Van Mier [22])*

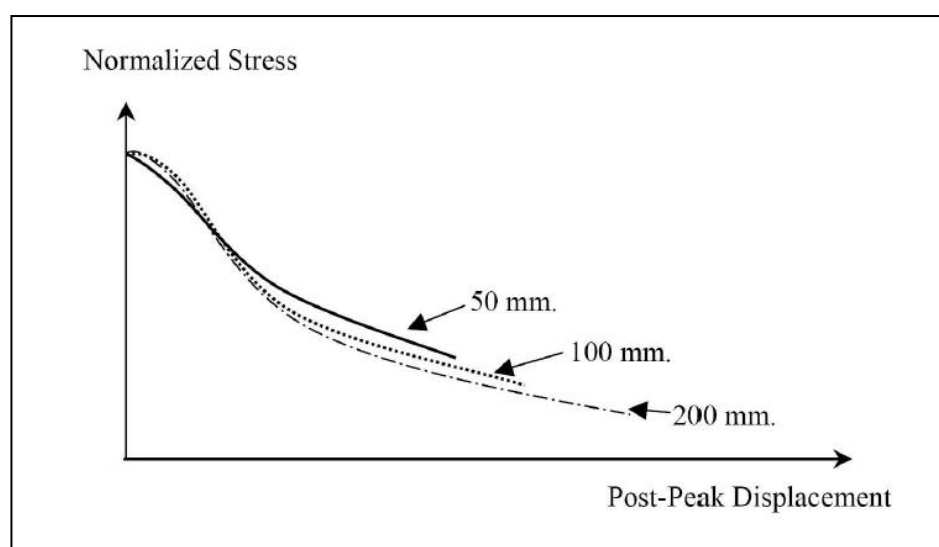


*Fig. 4.3: Independence of the stress-displacement curve of the size of the specimen
(Van Mier [22])*

4.1.2 Concrete subject to uniaxial tension

The typical stress-elongation curve for a concrete subject to uniaxial tension is illustrated in *Figure 4.4*.

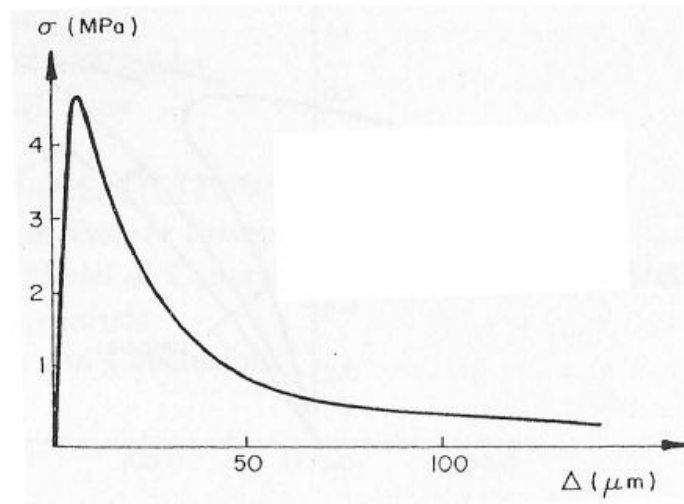


Fig. 4.4: Curve stress-elongation for uniaxial traction test

It is noted that the concrete has a nearly linear behavior up to the ultimate strength. Once reached the peak value, it is observed the formation of a crack. The stress, however, is not reduced instantaneously to zero as in brittle materials like glass, but decreases with increasing elongation. This phenomenon is known as traction softening. In this phase the deformation is no longer homogeneous in the specimen, but is localized in an area called "fracture zones", while the rest of the structure is discharged. The total deformation is composed of two distinct parts: the elastic deformation of the concrete between the microcracks and the deformation associated with the release of tension that acts over a width equal to the width of the fracture zones .

It has been shown experimentally that the stress-strain relationship depends on the size of the element. It is therefore appropriate to describe the cracking behavior with a stress-crack opening as shown in *Fig 4.6* . The area under this curve represents the specific energy of tensile fracture G_f , defined as the amount of energy required to create the unit area of a continuous crack. Since G_f is considered a property of the material, the energy dissipated at collapse is constant, and in this way we obtain a description of the material response independent of the element size.

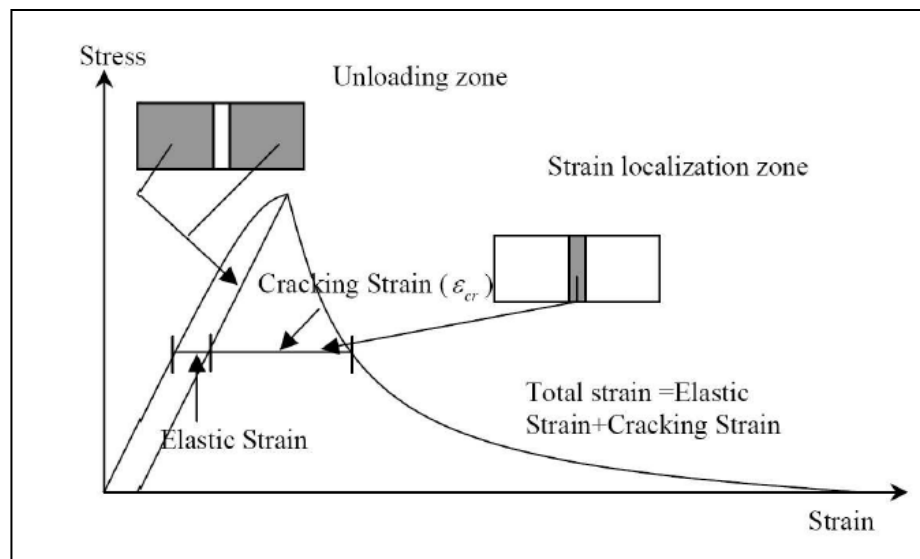


Fig. 4.5: Decomposition of the traction strain

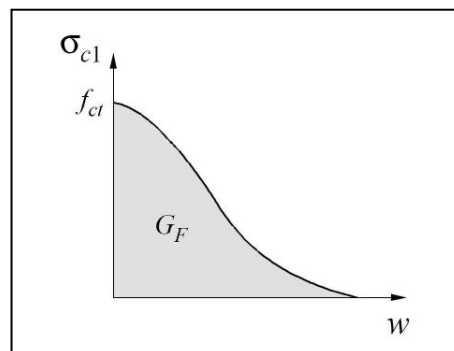


Fig. 4.6: Correlation stress-crack opening

4.1.3 Behavior of concrete subjected to a biaxial state of stress

The concrete subjected to biaxial compression exhibits a resistance and a stress-strain response different from the uniaxial loading conditions. Figure xx shows the failure surface biaxial proposed by Kupfer. For biaxial compression the concrete shows an increase of the resistance which is higher by 25% compared to the resistance uniaxial when $\sigma_1/\sigma_2=0.5$ and of the 16% when $\sigma_1/\sigma_2=1$. In the case of biaxial tensile strength is almost the same as the uniaxial tensile strength. In the case of traction-compression, the compressive strength decreases almost linearly with increasing of the principal tensile stress. The relationship between the principal

stresses σ_1/σ_2 also affects the ductility and expansion, that is, the increase of inelastic volume close to the breaking of concrete, as shown in Fig 4.8.

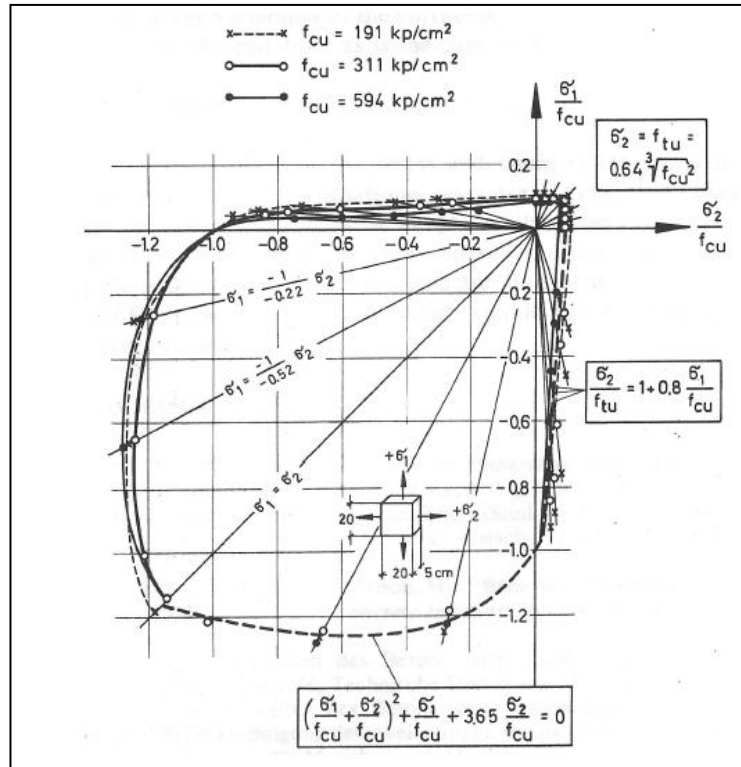


Fig. 4.7: Kupfer's failure surface

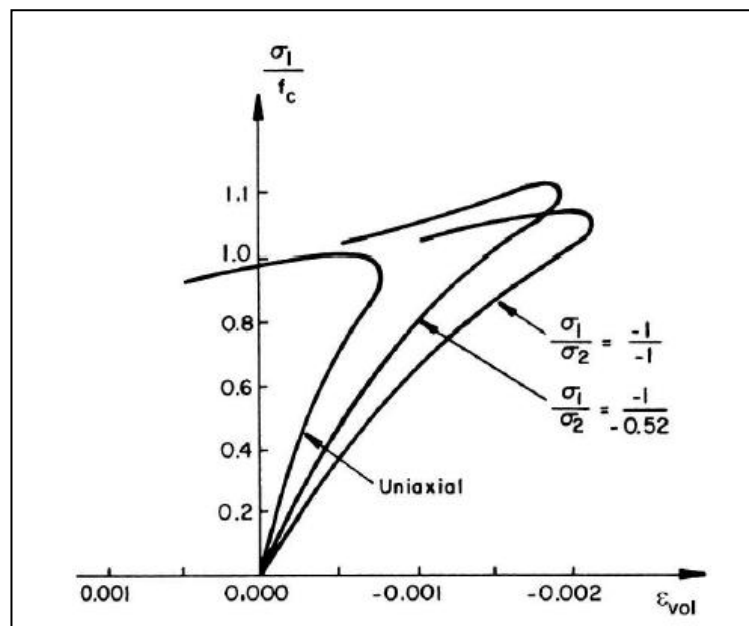


Fig. 4.8: Volumetric strain in a biaxial compression test (Kupfer et al. [J])

4.1.4 Behavior of concrete subject to a state of triaxial state of stress

Figure 4.9 illustrates the stress-strain curve for a triaxial compression test. These curves show that the concrete, as a function of the lateral stress applied, can behave as a brittle material, plastic and plastic hardening. The lateral pressure produces an increase of the compressive strength and in general an increase in the ductility of the element (Fig. 4.10).

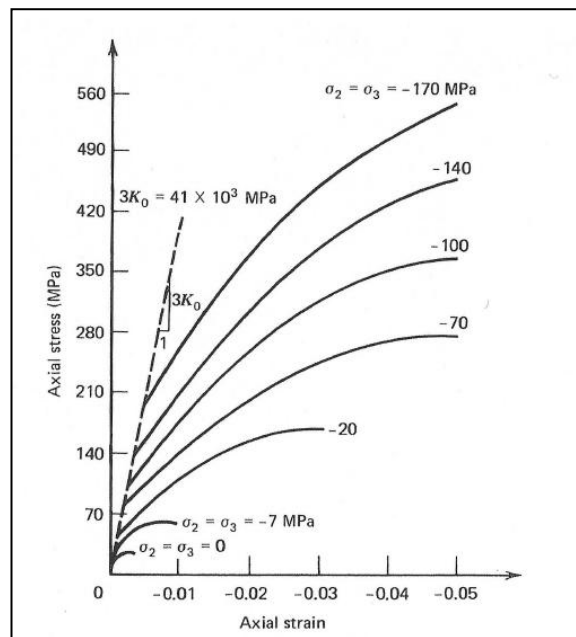


Fig. 4.9: Stress-strain relationship for a triaxial compression (Chen [21])

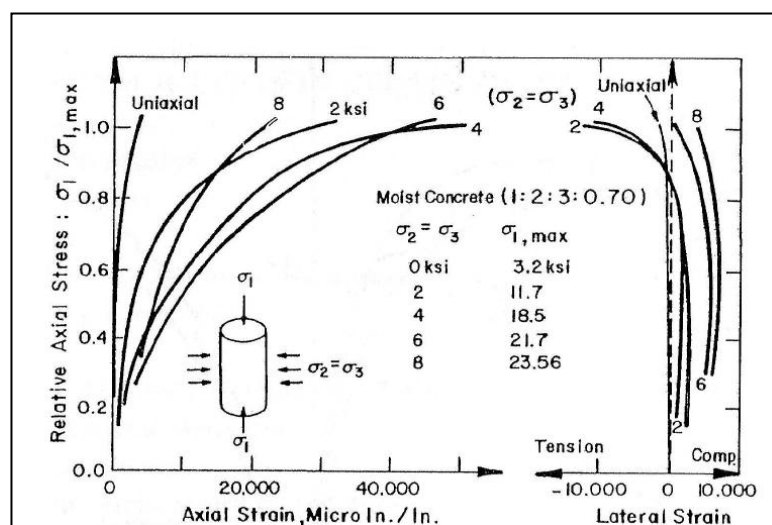


Fig. 4.10: Stress-strain relationship for a triaxial compression (Chen [21])

4.2 Constitutive models for concrete

In recent years many analytical models able to accurately predict the behavior of reinforced concrete structures have been developed. Most of models available in literature are part of one of this three categories: plastic models, models with damage and plastic model coupled with damage. The "plasticity" of concrete is strictly connected with the experimental results obtained in triaxial tests (*Chen [21]*).

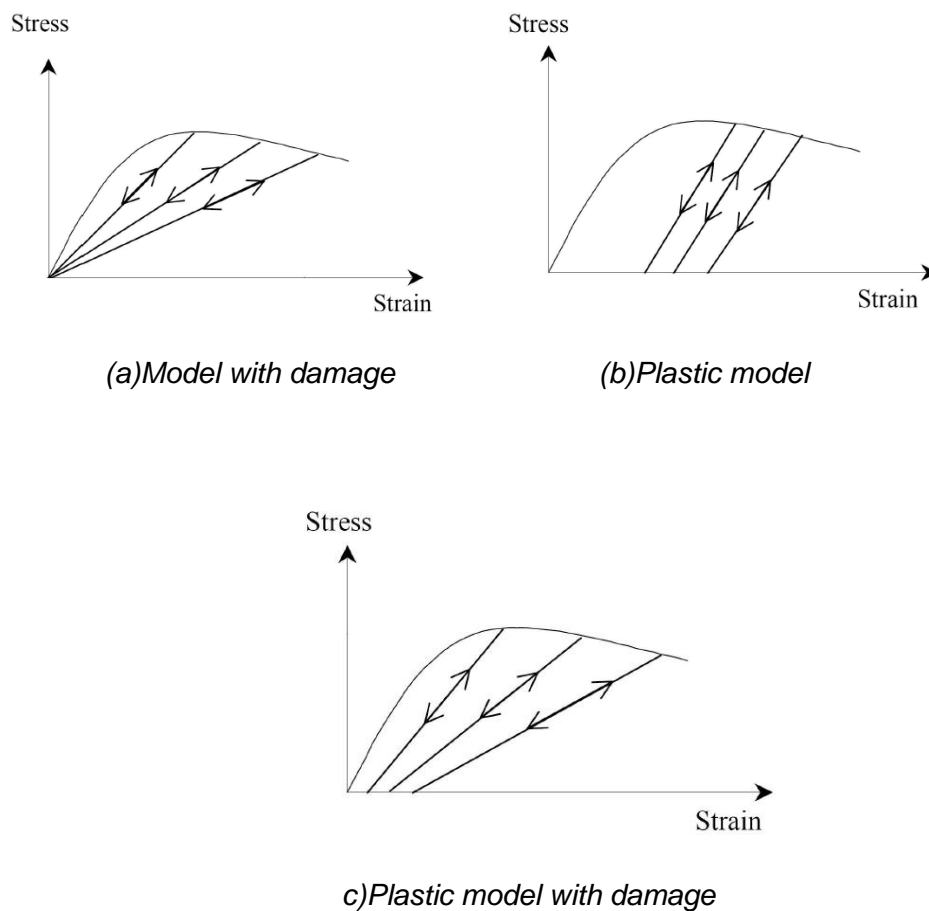


Fig. 4.11: Material behavior

The characteristic of a plastic material is the accumulation of irreversible deformation when it exceeds the yielding point. The previous paragraph introduced how the concrete exhibits plastic deformation when subjected to compression. For this reason, the classical theory of plasticity, originally developed for the description of the behavior of metals, is now widely used to model the non-linear behavior of the concrete. It is of course different the nature of the irreversibility of deformation, due to the movement of dislocations in metals and to the development of cracks in the

concrete. The proposed models are differentiated by the choice of the *yield surface*, which limits the elastic domain, the *hardening law*, which defines the evolution of the yield surface and of the *flow rule*, which determines the orientation of the plastic deformation, which can be associated, therefore normal to the yielding surface or not-associated.

Even if the plastic models describe very well the collapse conditions and the development of irreversible deformation, are not capable of representing the degradation of stiffness due to the growth of micro-cracking . The models based on damage mechanics are relatively recent. They are able to reproduce both the stiffness and the strength degradation, but do not describe the accumulation of permanent deformations. The development of these models requires the definition of a *damage law* that characterizes the orientation and the rate at which damage accumulates. Finally, the most recent models, models with damage criteria, couple both theories catching both the irreversible deformation and the stiffness degradation. Examples of coupled models are those of Lubliner et al.[19], Lee and Fenves [20].

The most critical aspect in the description of the behavior of reinforced concrete structures with the finite element method is the definition of a constitutive model for concrete. One of the most critical is that the model should represent the crack formation. The crack onset implies the presence of a free surface inside the structure, which causes a redistribution of the stress state and a change in the stiffness of the element. The constitutive model should be able to predict the onset and evolution of the crack. The modeling is based on fracture mechanics, and it analyze the bond stress - strain derived from the identification of possible plans of cracking and the definition of the size of the "fracture zones". In the finite element method, there are basically two methods to model the cracks: the discrete crack model ("discrete crack model") and the spread crack model ("smeared crack model").The "discrete crack model" is the method closer to reality. The formation of the crack is represented with two free surfaces, obtained by separating the nodes of the mesh of the finite element model. Obviously, the variation of the mesh, and then the redefinition of the stiffness matrix, results in large computational effort, so this method is not suitable for problems with diffused crack formation. In the "smeared crack model" the cracks are modeled by reducing the principal tensile stress according to a constitutive law of concrete tight. Instead of representing a single

opening, distributed cracks perpendicular to the principal direction of traction are represented. This approximation is quite realistic for concrete, in which the cracking process is preceded by a micro-cracking phase of the material.

4.3 Constitutive models in Abaqus: Concrete Damaged Plasticity model(CDP)

Recently, modeling of failure and fracture became one of the fundamental issues in structural mechanics. The "concrete damaged plasticity" (CDP) model provides a general capability for modeling concrete and other quasi-brittle materials in all types of structures. This model uses concepts of isotropic damaged elasticity in combination with isotropic tensile and compressive plasticity to represent the inelastic behavior of concrete. The CDP model is based on the assumption of scalar (isotropic) damage and is designed for applications in which the concrete is subjected to arbitrary loading conditions, including cyclic loading. The model takes into consideration the degradation of the elastic stiffness induced by plastic straining both in tension and compression. It also accounts for stiffness recovery effects under cyclic loading.

4.3.1 The main features of CDP model

To correctly implement a concrete damage plasticity model four main ingredients must be defined:

- Stress–strain relationship
- Damage and stiffness degradation
- Yield function
- Flow rule

As will be better explained in the following paragraphs the input parameters requested in Abaqus are devoted to the definition of these four laws.

4.3.2 Strain rate decomposition

A strain rate decomposition is assumed for the rate-independent model:

$$\dot{\boldsymbol{\varepsilon}} = \dot{\boldsymbol{\varepsilon}}^{el} + \dot{\boldsymbol{\varepsilon}}^{pl},$$

where $\dot{\boldsymbol{\varepsilon}}$ is the total strain rate, $\dot{\boldsymbol{\varepsilon}}^{el}$ is the elastic part of the strain rate, and $\dot{\boldsymbol{\varepsilon}}^{pl}$ is the plastic part of the strain rate. It's important to underline this aspect also because Abaqus command request as an input only the inelastic part of strain.

4.3.3 Stress-strain relations

The stress-strain relations are governed by scalar damaged elasticity:

$$\boldsymbol{\sigma} = (1 - d)\mathbf{D}_0^{el} : (\boldsymbol{\varepsilon} - \boldsymbol{\varepsilon}^{pl}) = \mathbf{D}^{el} : (\boldsymbol{\varepsilon} - \boldsymbol{\varepsilon}^{pl}),$$

where \mathbf{D}_0^{el} is the initial (undamaged) elastic stiffness of the material; $\mathbf{D}^{el} = (1 - d)\mathbf{D}_0^{el}$ is the degraded elastic stiffness; and d is the scalar stiffness degradation variable, which can take values in the range from zero (undamaged material) to one (fully damaged material). Damage associated with the failure mechanisms of the concrete (cracking and crushing) therefore results in a reduction in the elastic stiffness. Within the context of the scalar-damage theory, the stiffness degradation is isotropic and characterized by a single degradation variable, d . Following the usual notions of continuum damage mechanics, the effective stress is defined as

$$\bar{\boldsymbol{\sigma}} \stackrel{\text{def}}{=} \mathbf{D}_0^{el} : (\boldsymbol{\varepsilon} - \boldsymbol{\varepsilon}^{pl}).$$

4.3.4 Postfailure stress-strain relation in traction

In reinforced concrete the specification of post-failure behavior generally means giving the post-failure stress as a function of cracking strain, $\tilde{\boldsymbol{\varepsilon}}_t^{ck}$. The cracking strain is defined as the total strain minus the elastic strain corresponding to the undamaged material; that is, $\tilde{\boldsymbol{\varepsilon}}_t^{ck} = \boldsymbol{\varepsilon}_t - \boldsymbol{\varepsilon}_{0t}^{el}$, where $\boldsymbol{\varepsilon}_{0t}^{el} = \boldsymbol{\sigma}_t / E_0$, as illustrated in *Figure 4.12*. To avoid potential numerical problems, Abaqus enforces a lower limit on the post-failure stress equal to one hundred of the initial failure stress: $\boldsymbol{\sigma}_t \geq \boldsymbol{\sigma}_{t0}/100$.

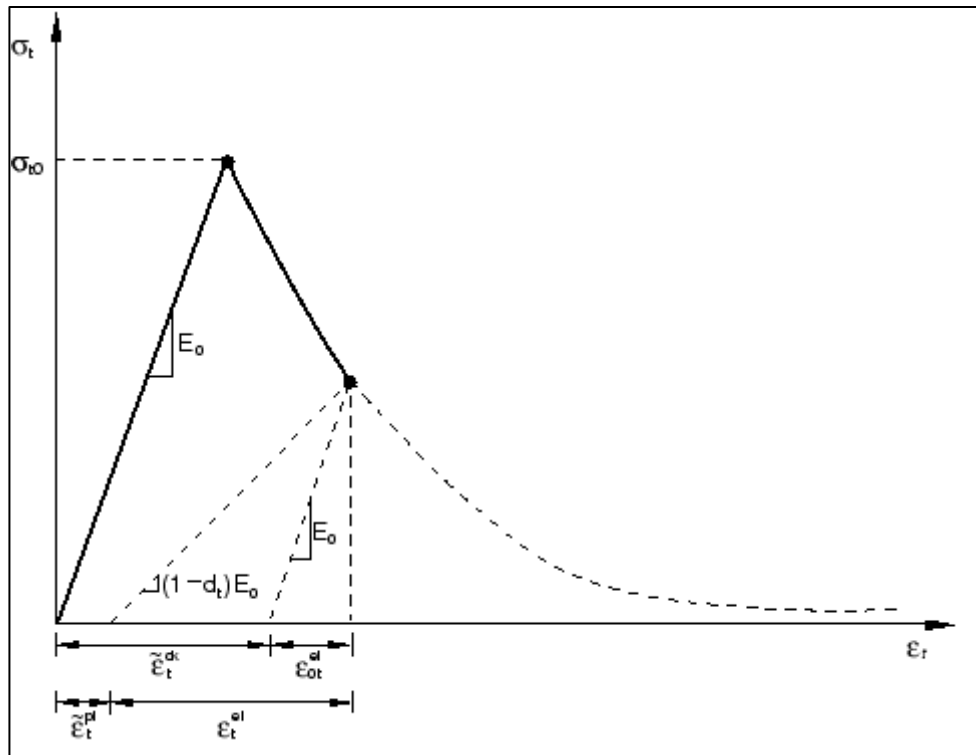


Figure 4.12 Illustration of the definition of the cracking strain $\tilde{\varepsilon}_t^{ck}$ used for the definition of tension stiffening data.

Tension stiffening data are given in terms of the cracking strain, $\tilde{\varepsilon}_t^{ck}$. When unloading data are available, the data are provided to Abaqus in terms of tensile damage curves, $d_t - \tilde{\varepsilon}_t^{ck}$, as discussed below. Abaqus automatically converts the cracking strain values to plastic strain values using the relationship

$$\tilde{\varepsilon}_t^{pl} = \tilde{\varepsilon}_t^{ck} - \frac{d_t}{(1 - d_t)} \frac{\sigma_t}{E_0}.$$

Abaqus will issue an error message if the calculated plastic strain values are negative and/or decreasing with increasing cracking strain, which typically indicates that the tensile damage curves are incorrect. In the absence of tensile damage $\tilde{\varepsilon}_t^{pl} = \tilde{\varepsilon}_t^{ck}$.

The "damage" d_t was defined as:

$$d_t = 1 - \frac{\sigma_t \text{ actual}}{\sigma_{t0}}$$

In cases with little or no reinforcement, the specification of a post-failure stress-strain relation introduces mesh sensitivity in the results, in the sense that the finite element predictions do not converge to a unique solution as the mesh is refined because mesh refinement leads to narrower crack bands. This problem typically occurs if cracking failure occurs only at localized regions in the structure and mesh refinement does not result in the formation of additional cracks. If cracking failure is distributed evenly (either due to the effect of rebar or due to the presence of stabilizing elastic material, as in the case of plate bending), mesh sensitivity is less of a concern.

In practical calculations for reinforced concrete, the mesh is usually such that each element contains rebars. The interaction between the rebars and the concrete tends to reduce the mesh sensitivity, provided that a reasonable amount of tension stiffening is introduced in the concrete model to simulate this interaction. This requires an estimate of the tension stiffening effect, which depends on such factors as the density of reinforcement, the quality of the bond between the rebar and the concrete, the relative size of the concrete aggregate compared to the rebar diameter, and the mesh. A reasonable starting point for relatively heavily reinforced concrete modeled with a fairly detailed mesh is to assume that the strain softening after failure reduces the stress linearly to zero at a total strain of about 10 times the strain at failure. The strain at failure in standard concretes is typically 10^{-4} , which suggests that tension stiffening that reduces the stress to zero at a total strain of about 10^{-3} is reasonable. This parameter should be calibrated to a particular case.

The choice of tension stiffening parameters is important since, generally, more tension stiffening makes it easier to obtain numerical solutions. Too little tension stiffening will cause the local cracking failure in the concrete to introduce temporarily unstable behavior in the overall response of the model. Few practical designs exhibit such behavior, so that the presence of this type of response in the analysis model usually indicates that the tension stiffening is unreasonably low.

4.3.5 Fracture energy cracking criterion

When there is no reinforcement in significant regions of the model, the tension stiffening approach described above will introduce unreasonable mesh sensitivity into the results. However, it is generally accepted that Hillerborg's (1976) fracture energy proposal is adequate to allay the concern for many practical purposes.

Hillerborg defines the energy required to open a unit area of crack, G_f , as a material parameter, using brittle fracture concepts. With this approach the concrete's brittle behavior is characterized by a stress-displacement response rather than a stress-strain response. Under tension a concrete specimen will crack across some section. After it has been pulled apart sufficiently for most of the stress to be removed (so that the undamaged elastic strain is small), its length will be determined primarily by the opening at the crack. The opening does not depend on the specimen's length.

This fracture energy cracking model can be invoked by specifying the postfailure stress as a tabular function of cracking displacement, as shown in *Figure 4.13*.

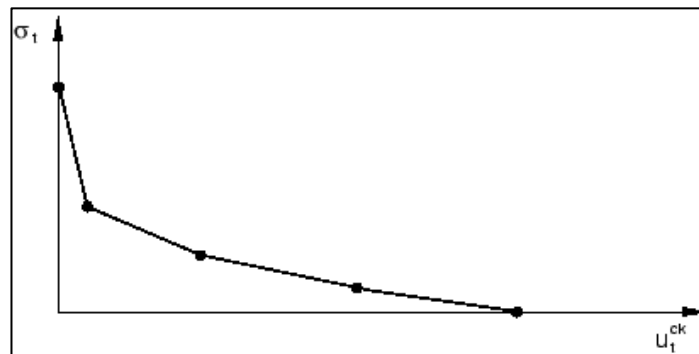


Figure 4.13 Post-failure stress-displacement curve.

Alternatively, the fracture energy, G_f , can be specified directly as a material property; in this case, define the failure stress, σ_{10} , as a tabular function of the associated fracture energy. This model assumes a linear loss of strength after cracking, as shown in *Figure 4.14*.

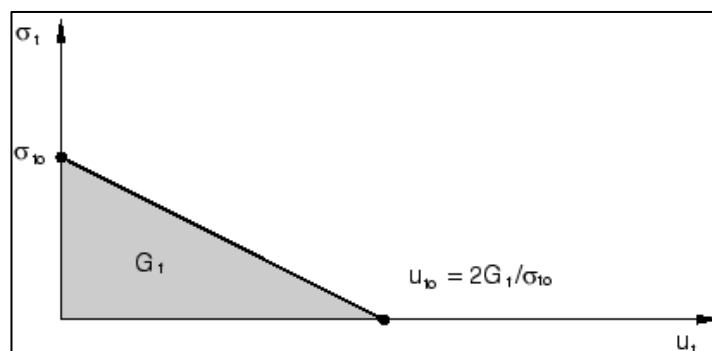


Figure 4.14 Postfailure stress-fracture energy curve.

The cracking displacement at which complete loss of strength takes place is, therefore, $u_{t0} = 2G_f/\sigma_{t0}$. Typical values of G_f range from 40 N/m for a typical construction concrete (with a compressive strength of approximately 20 MPa), to 120 N/m for a high-strength concrete (with a compressive strength of approximately 40 MPa).

If tensile damage, d_t , is specified, Abaqus automatically converts the cracking displacement values to “plastic” displacement values using the relationship

$$u_t^{pl} = u_t^{ck} - \frac{d_t}{(1 - d_t)} \frac{\sigma_t l_0}{E_0},$$

where the specimen length, l_0 , is assumed to be one unit length, $l_0 = 1$.

4.3.6 Defining compressive behavior: σ_{c_inel} - ϵ_{c_inel} ; damage variable d_c

It is of course possible to define the stress-strain behavior of plain concrete in uniaxial compression outside the elastic range. Compressive stress data must be provided as a tabular function of inelastic (or crushing) strain, $\tilde{\epsilon}_c^{in}$, and, if desired, strain rate, temperature, and field variables. Positive (absolute) values should be given for the compressive stress and strain. The stress-strain curve can be defined beyond the ultimate stress, into the strain-softening regime.

Hardening data are given in terms of an inelastic strain, $\tilde{\epsilon}_c^{in}$, instead of plastic strain, $\tilde{\epsilon}_c^{pl}$. The compressive inelastic strain is defined as the total strain minus the elastic strain corresponding to the undamaged material, $\tilde{\epsilon}_c^{in} = \epsilon_c - \epsilon_{0c}^{el}$, where $\epsilon_{0c}^{el} = \sigma_c/E_0$, as illustrated in *Figure 4.15*.

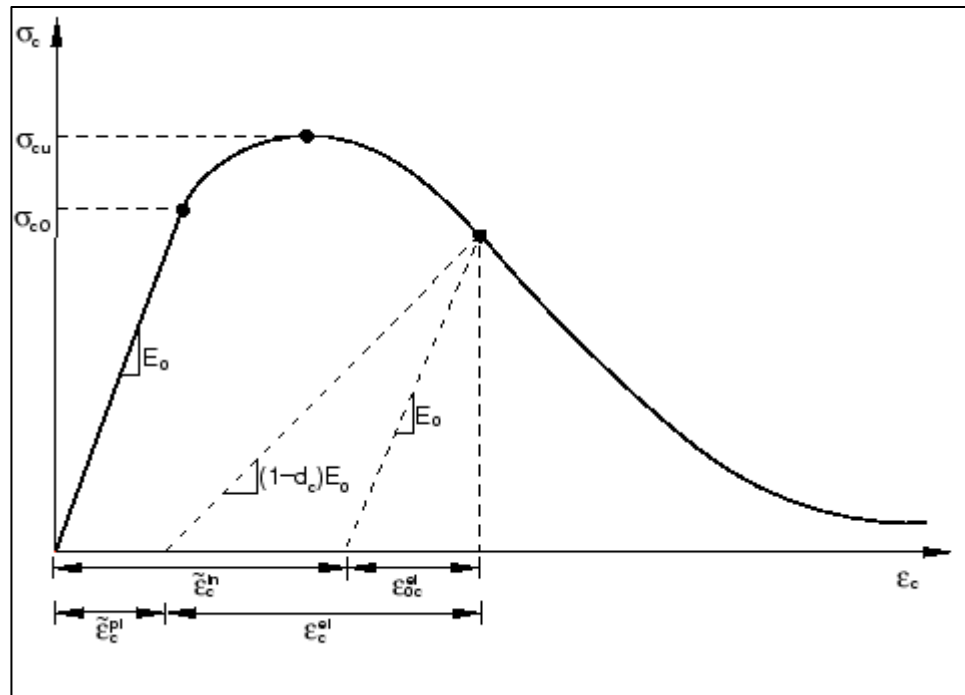


Figure 4.15 - Definition of the compressive inelastic (or crushing) strain $\tilde{\varepsilon}_c^{in}$ used for the definition of compression hardening data.

Unloading data are provided to Abaqus in terms of compressive damage curves, $d_c - \tilde{\varepsilon}_c^{in}$, as discussed below. Abaqus automatically converts the inelastic strain values to plastic strain values using the relationship

$$\tilde{\varepsilon}_c^{pl} = \tilde{\varepsilon}_c^{in} - \frac{d_c}{(1-d_c)} \frac{\sigma_c}{E_0}.$$

Abaqus will issue an error message if the calculated plastic strain values are negative and/or decreasing with increasing inelastic strain, which typically indicates that the compressive damage curves are incorrect. In the absence of compressive damage $\tilde{\varepsilon}_c^{pl} = \tilde{\varepsilon}_c^{in}$.

The choice of the damage properties is important since, generally, excessive damage may have a critical effect on the rate of convergence. It is recommended to avoid using values of the damage variables above 0.99, which corresponds to a 99% reduction of the stiffness.

The "damage" d_c was defined as:

$$d_c = 1 - \frac{\sigma_c \text{ actual}}{\sigma_{cu}}$$

4.3.7 Hardening variables

Damaged states in tension and compression are characterized independently by two hardening variables, $\tilde{\epsilon}_t^{pl}$ and $\tilde{\epsilon}_c^{pl}$, which are referred to as equivalent plastic strains in tension and compression, respectively. The evolution of the hardening variables is given by an expression of the form

$$\tilde{\epsilon}^{pl} = \begin{bmatrix} \tilde{\epsilon}_t^{pl} \\ \tilde{\epsilon}_c^{pl} \end{bmatrix}; \quad \dot{\tilde{\epsilon}}^{pl} = \mathbf{h}(\bar{\sigma}, \tilde{\epsilon}^{pl}) \cdot \dot{\epsilon}^{pl},$$

as described later in this section. Microcracking and crushing in the concrete are represented by increasing values of the hardening variables. These variables control the evolution of the yield surface and the degradation of the elastic stiffness. They are also intimately related to the dissipated fracture energy required to generate micro-cracks.

4.3.8 Yield condition

The plastic-damage concrete model uses a yield condition based on the yield function proposed by Lubliner et al. [] and incorporates the modifications proposed by Lee and Fenves [] to account for different evolution of strength under tension and compression. In terms of effective stresses the yield function takes the form:

$$F(\bar{\sigma}, \tilde{\epsilon}^{pl}) = \frac{1}{1 - \alpha} \left(\bar{q} - 3\alpha\bar{p} + \beta(\tilde{\epsilon}^{pl})\langle \hat{\sigma}_{\max} \rangle - \gamma\langle -\hat{\sigma}_{\max} \rangle \right) - \bar{\sigma}_c(\tilde{\epsilon}_c^{pl}) \leq 0,$$

Equation 1

where α and γ are dimensionless material constants;

$$\bar{p} = -\frac{1}{3}\bar{\sigma} : \mathbf{I}$$

is the effective hydrostatic pressure;

$$\bar{q} = \sqrt{\frac{3}{2} \bar{\mathbf{S}} : \bar{\mathbf{S}}}$$

is the Mises equivalent effective stress;

$$\bar{\mathbf{S}} = \bar{p} \mathbf{I} + \bar{\boldsymbol{\sigma}},$$

is the deviatoric part of the effective stress tensor $\bar{\boldsymbol{\sigma}}$; and $\hat{\sigma}_{\max}$ is the algebraically maximum eigenvalue of $\bar{\boldsymbol{\sigma}}$. The function $\beta(\tilde{\boldsymbol{\varepsilon}}^{pl})$ is given as

$$\beta(\tilde{\boldsymbol{\varepsilon}}^{pl}) = \frac{\bar{\sigma}_c(\tilde{\varepsilon}_c^{pl})}{\bar{\sigma}_t(\tilde{\varepsilon}_t^{pl})} (1 - \alpha) - (1 + \alpha),$$

where $\bar{\sigma}_t$ and $\bar{\sigma}_c$ are the effective tensile and compressive cohesion stresses, respectively.

In biaxial compression, with $\hat{\sigma}_{\max} = 0$, Equation 1 reduces to the well-known Drucker-Prager yield condition. The coefficient α can be determined from the initial equibiaxial and uniaxial compressive yield stress, σ_{b0} and σ_{c0} , as

$$\alpha = \frac{\sigma_{b0} - \sigma_{c0}}{2\sigma_{b0} - \sigma_{c0}}.$$

Typical experimental values of the ratio σ_{b0}/σ_{c0} for concrete are in the range from 1.10 to 1.16, yielding values of α between 0.08 and 0.12 (Lubliner et al. [19]).

The coefficient γ enters the yield function only for stress states of triaxial compression, when $\hat{\sigma}_{\max} < 0$. This coefficient can be determined by comparing the yield conditions along the tensile and compressive meridians. By definition, the *tensile meridian* (TM) is the locus of stress states satisfying the condition $\hat{\sigma}_{\max} = \hat{\sigma}_1 > \hat{\sigma}_2 = \hat{\sigma}_3$ and the *compressive meridian* (CM) is the locus of stress states such that $\hat{\sigma}_{\max} = \hat{\sigma}_1 = \hat{\sigma}_2 > \hat{\sigma}_3$, where $\hat{\sigma}_1$, $\hat{\sigma}_2$, and $\hat{\sigma}_3$ are the eigenvalues of the effective stress tensor. It can be easily shown that $(\hat{\sigma}_{\max})_{\text{TM}} = \frac{2}{3}\bar{q} - \bar{p}$ and $(\hat{\sigma}_{\max})_{\text{CM}} = \frac{1}{3}\bar{q} - \bar{p}$, along the tensile and compressive meridians, respectively. With $\hat{\sigma}_{\max} < 0$ the corresponding yield conditions are

$$\left(\frac{2}{3}\gamma + 1\right)\bar{q} - (\gamma + 3\alpha)\bar{p} = (1 - \alpha)\bar{\sigma}_c, \quad (\text{TM})$$

$$\left(\frac{1}{3}\gamma + 1\right)\bar{q} - (\gamma + 3\alpha)\bar{p} = (1 - \alpha)\bar{\sigma}_c. \quad (\text{CM})$$

Let $K_c = \bar{q}_{(\text{TM})}/\bar{q}_{(\text{CM})}$ for any given value of the hydrostatic pressure \bar{p} with $\hat{\sigma}_{\max} < 0$; then

$$K_c = \frac{\gamma + 3}{2\gamma + 3}.$$

The fact that K_c is constant does not seem to be contradicted by experimental evidence (Lublinter et al. [19]). The coefficient γ is, therefore, evaluated as

$$\gamma = \frac{3(1 - K_c)}{2K_c - 1}.$$

A value of $K_c = \frac{2}{3}$, which is typical for concrete, gives $\gamma = 3$.

If $\hat{\sigma}_{\max} > 0$, the yield conditions along the tensile and compressive meridians reduce to:

$$\left(\frac{2}{3}\beta + 1\right)\bar{q} - (\beta + 3\alpha)\bar{p} = (1 - \alpha)\bar{\sigma}_c, \quad (\text{TM})$$

$$\left(\frac{1}{3}\beta + 1\right)\bar{q} - (\beta + 3\alpha)\bar{p} = (1 - \alpha)\bar{\sigma}_c. \quad (\text{CM})$$

Let $K_t = \bar{q}_{(\text{TM})}/\bar{q}_{(\text{CM})}$ for any given value of the hydrostatic pressure \bar{p} with $\hat{\sigma}_{\max} > 0$; then

$$K_t = \frac{\beta + 3}{2\beta + 3}.$$

Typical yield surfaces are shown in *Figure 4.16* in the deviatoric plane and in *Figure 4.17* for plane-stress conditions.

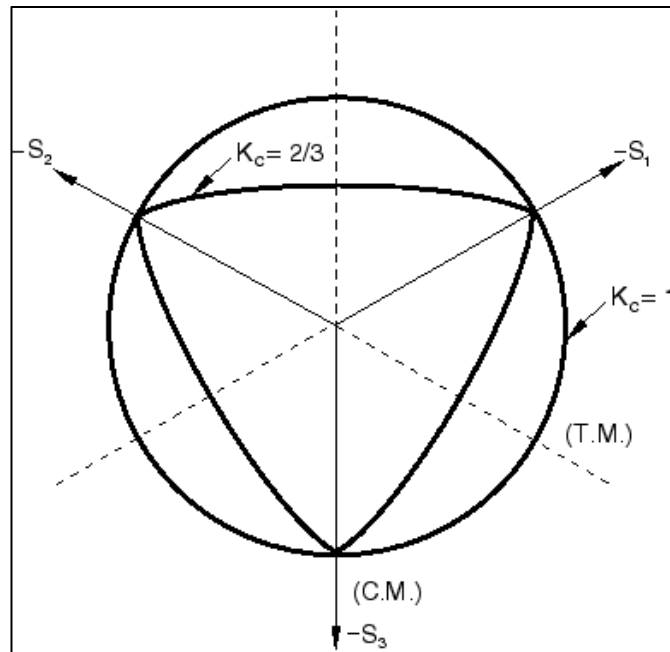


Fig.4.16 Yield surfaces in the deviatoric plane, corresponding to different values of K_c .

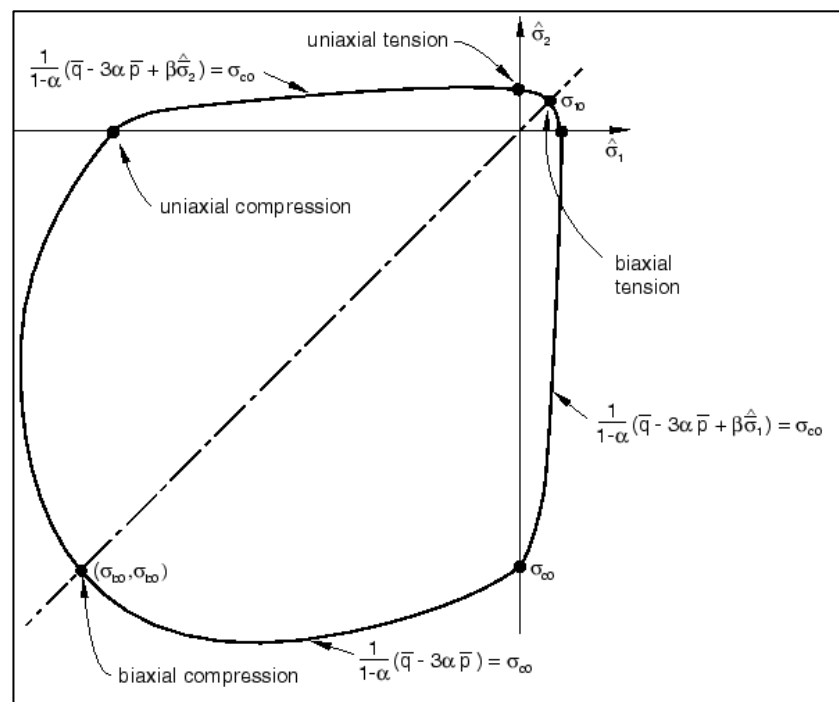


Fig.4.17 Yield surface in plane stress.

4.3.9 The flow rule

The plastic-damage model assumes non-associated potential flow,

$$\dot{\epsilon}^{pl} = \dot{\lambda} \frac{\partial G(\bar{\sigma})}{\partial \bar{\sigma}}.$$

The flow potential G chosen for this model is the Drucker-Prager hyperbolic function:

$$G = \sqrt{(\epsilon \sigma_{t0} \tan \psi)^2 + \bar{q}^2} - \bar{p} \tan \psi,$$

where ψ is the dilation angle measured in the p - q plane at high confining pressure; σ_{t0} is the uniaxial tensile stress at failure; and ϵ is a parameter, referred to as the eccentricity, that defines the rate at which the function approaches the asymptote (the flow potential tends to a straight line as the eccentricity tends to zero). This flow potential, which is continuous and smooth, ensures that the flow direction is defined uniquely. The function asymptotically approaches the linear Drucker-Prager flow potential at high confining pressure stress and intersects the hydrostatic pressure axis at 90° as can be seen in the *Fig. 4.18*.

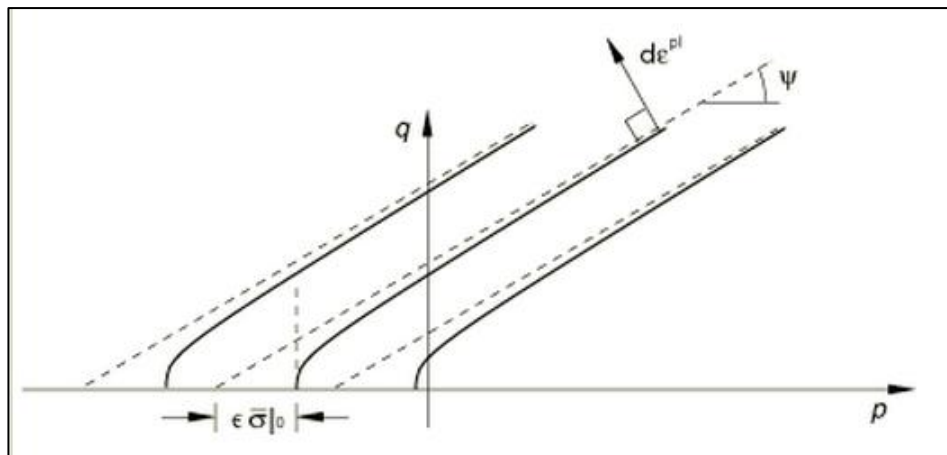


Fig. 4.18: Family of hyperbolic flow potentials in the p - q plane

Because plastic flow is non-associated, the use of the plastic-damage concrete model requires the solution of non-symmetric equations.

4.4 Definition of "plasticity" parameters of CDP

From the menu bar in the **Edit Material** dialog box, select **Mechanical** → **Plasticity** → **Concrete Damaged Plasticity**.

Enter the following data in the **Data** table:

1. **Dilation Angle**

Dilation angle, ψ , in the p - q plane. Enter the value in degrees. **36°**

2. **Eccentricity**

Flow potential eccentricity, ϵ . The eccentricity is a small positive number that defines the rate at which the hyperbolic flow potential approaches its asymptote. The default is $\epsilon = 0.1$.

3. **fb0/fc0**

σ_{b0}/σ_{c0} , the ratio of initial equibiaxial compressive yield stress to initial uniaxial compressive yield stress. The default value is **1.16**

4. **K**

K_c , the ratio of the second stress invariant on the tensile meridian, $q_{(TM)}$, to that on the compressive meridian, $q_{(CM)}$, at initial yield for any given value of the pressure invariant p such that the maximum principal stress is negative, $\hat{\sigma}_{max} < 0$. It must satisfy the condition $0.5 < K_c \leq 1.0$. The default value is **2/3**.

5. **Viscosity Parameter**

Viscosity parameter, μ , used for the visco-plastic regularization of the concrete constitutive equations in Abaqus/Standard analyses. This parameter is ignored in Abaqus/Explicit. The default value is **0.0**. (Units of T.)

4.5 Concrete compression behaviour: Kent-Park formulation

From the compression test mentioned in *Chapter 2*, it was possible to define the peak compression strength. The whole trend of the σ - ϵ curve remained unknown. To overcome this obstacle the Kent-Park [23] formulation was introduced.

The strain at the maximum stress will be assumed to be $\epsilon_0 = 0.002$. This is a commonly accepted assumption for unconfined concrete. Confinement and the presence of strain gradient may increase the strain at maximum stress but as this may be accompanied by a small increase in stress-strain curve will pass close to the assumption point.

Therefore for the first part of the curve can be assumed the following trend:

$$f_c = f'_c \left[\frac{2 \epsilon_c}{\epsilon_0} - \left(\frac{\epsilon_c}{\epsilon_0} \right)^2 \right]$$

in which $\epsilon_0 = 0.002$ and f'_c is the maximum compression strength.

The falling branch of the curve will be assumed to be linear and its slope will be specified determining when the concrete stress has fallen to 0.5 of maximum stress. It is well known that for unconfined concrete the slope of the falling branch increases rapidly with increase in concrete strength.

Fig. shows a plot of the maximum stress, f'_c , and the strain at $0.5f'_c$ of the falling branch for unconfined concrete, ϵ_{50u} . For short-term loading rates the experimental points conform reasonably close to

$$\epsilon_{50u} = \frac{3 + 0.002 f'_c}{f'_c - 1}$$

in which f'_c is expressed in pounds per square inch.

The inclination of the descendant branch is dependent on the presence of confinement.

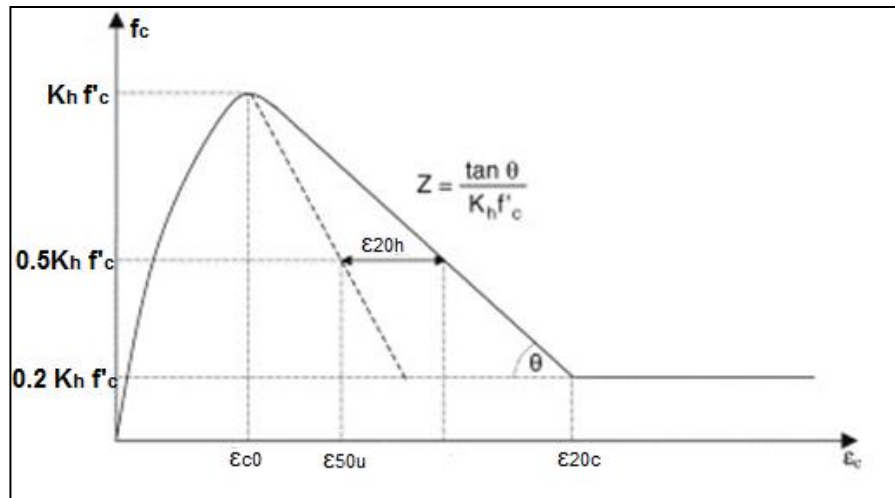


Fig. 4.19: Kent-Park σ - ϵ formulation

4.6 Concrete traction behavior implemented

4.6.1 Cornelissen's theoretical formulation on the post peak traction behavior of concrete(1986)

The post peak traction behaviour of concrete can be expressed in Abaqus or in "stress-stain" terms or in "crack opening- stress" terms.

In general Tensile-strain softening of concrete is defined by the tensile strength of concrete f_t , the area under the softening curve that represents the fracture energy of concrete G_f (that should control the ultimate strain ϵ_0 or the ultimate crack opening w_0) and the shape of the descending branch, as shown in Fig. 4.20.

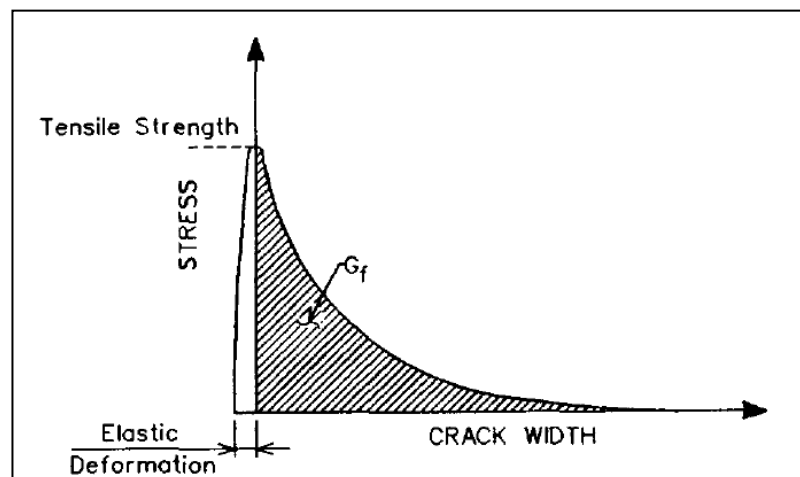


Fig. 4.20: Stress- crack opening displacement

Cornelissen et al. (1986) [24,26] conducted several deformation controlled uniaxial tension tests on normal-weight and lightweight concrete specimens, to determine the actual stress-strain softening characteristics.

For the normalweight concrete, river gravel with a maximum grain size of 8 mm was used, and sintered expanded clay was used for the lightweight concrete. It was concluded that there is a unique relationship between crack opening and ultimate stress for a given concrete; this relationship is not affected by stress or strain history.

The following exponential mathematical model was proposed:

$$\frac{\sigma}{f_t} = f(w) - \frac{w}{w_0} f(w = w_0)$$

where f_t is the maximal tensile strength and $f(w) =$ a displacement function given by:

$$f(w) = \left[1 + \left(\frac{c_1 w}{w_0} \right)^3 \right] \exp \left(-\frac{c_2 w}{w_0} \right)$$

where $w =$ the crack-opening displacement; $w_0 =$ the crack opening at which stress can no longer be transferred; and c_1 and $c_2 =$ material constants (for normal-weight-concrete; $c_1=1.0$ and $c_2= 5.64$; for lightweight concrete; $c_1=3.0$ and $c_2= 6.93$). This model fit the data points of the tensile-strain softening diagram for both type of concrete satisfactorily.

For what concern stress-strain formulations Reinhard and Cornelissen(1986) proposed:

$$\frac{\sigma}{f_t} = \left[1 + \left(\frac{c_1 \varepsilon}{\varepsilon_0} \right)^4 \right] \exp \left(-c_2 \frac{\varepsilon}{\varepsilon_0} \right)$$

where $c_1 =$ a material constant = 9.0; and $c_2 =$ a material constant = 5.0; this formulation was subsequent to Reinhard's proposal(1984):

$$\frac{\sigma}{f_t} = \left[1 - \left(\frac{\varepsilon}{\varepsilon_0} \right)^k \right]$$

where $k = 0.31$; σ = the tensile stress normal to the crack; ε = the strain in the direction of the normal stress; and ε_0 = the ultimate strain of the strain-softening branch.

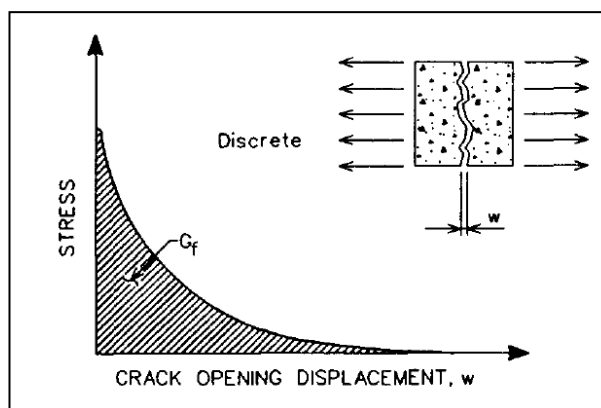
An important relation exist between Fracture Energy G_f and ultimate crack width w . The *crack-opening displacement* w is represented by a crack strain acting over the *crack band width* h within the finite element. Therefore, w is the accumulated crack displacements, as shown in Fig. kkk. *The optimum value for h was determined by Bazant and Oh (1983) as 3 times the maximum aggregate size.* By assuming that the microcracks are uniformly distributed over the crack band width [Fig. 3(b)], w can be expressed as:

$$w = h \varepsilon$$

maximum tensile stress. Since the fracture energy G_f is defined per unit of area of a continuous crack, it is independent of the finite-element mesh size. G_f is released over the full crack band width. The fracture energy of concrete is equal to the area under the stress-crack-opening softening diagram. G_f can therefore be expressed as:

$$G_f = h g_f = h \int_0^{\varepsilon_0} \sigma d\varepsilon$$

where g_f = the area under the stress-strain softening diagram, as shown in Fig. 4.21(b).



a)

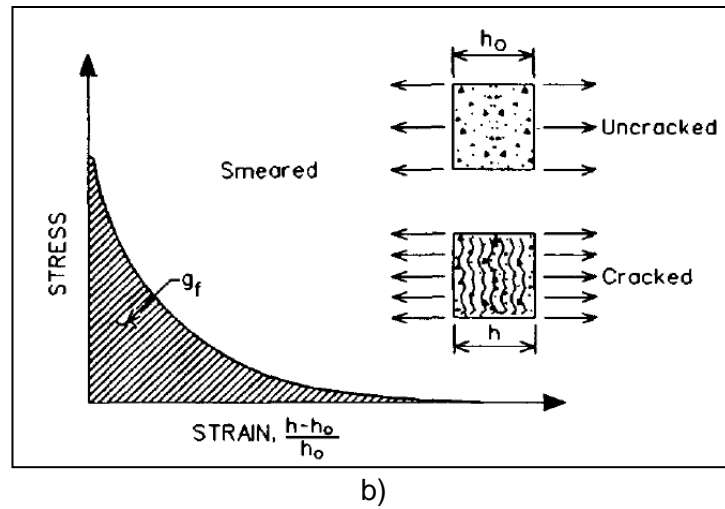


Fig. 4.21: Tensile Stress versus a) crack opening displacement ,
b) crack strain

Since the fracture energy and the tensile strength are material properties of the concrete, it is important to predict the relationship between these material properties and the ultimate crack opening w_0 at which stress can no longer be transferred (Morcos and Bjorhovde 1992b). By using the Reinhardt (1984) mathematical model and substituting in the last integral equation:

$$G_f = h f_t \int_0^{\varepsilon_0} \left[1 - \left(\frac{\varepsilon}{\varepsilon_0} \right)^{0.31} \right] d\varepsilon$$

By performing the integration and substituting for the limits, it is found that

$$G_f = h f_t (0.23664 \varepsilon_0)$$

and the relationship between the ultimate crack opening, the fracture energy, and the tensile strength is:

$$w_0 = 4.226 \frac{G_f}{f_t}$$

The ultimate crack opening is therefore linearly related to the material properties of concrete. w_0 can be determined from the equation above for any concrete mix, provided that the tensile strength and the fracture energy are known.

By using the Cornelissen et al.(1986) exponential mathematical model, the same development leads to the expression

$$w_0 = 5.618 \frac{G_f}{f_t}$$

4.6.2 Experimental results on traction proof on plain concrete specimen

In the previous paragraph the theoretical tools to define the traction behaviour of concrete were provided. All that formulations rely on the definition of 2 important values:

- the maximal tensile stress f_t
- the ultimate strain ϵ_0 or crack opening width w_0

All these parameter should rely on experimental data, the alternative is a long calibration process to find out a traction law that, once inserted in the global model, provide the best fitting between experimental curves and numerical one . An experimental campaign [25] conducted over plain and fiber-reinforced concrete was considered:

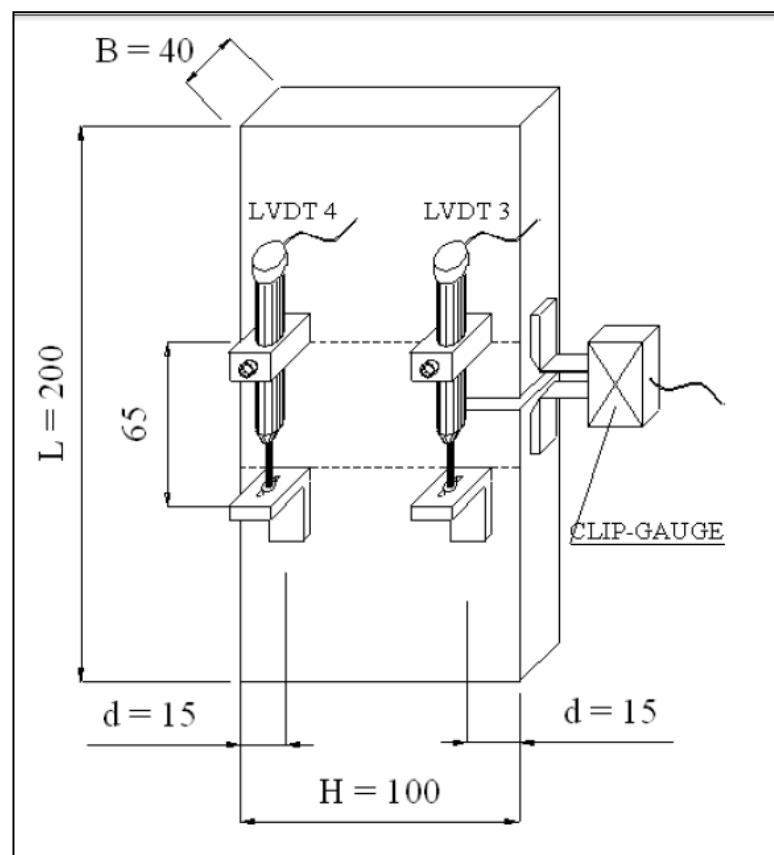


Fig. 4.22: Tensile Stress specimen

in which 4 LVDT were positioned close to the section carved with a measurement base of 65 mm on the front and back surface of the specimen. Neglecting the elastic component, the relative displacements measured by two LVDT closer to the notch have been conventionally considered equal to the crack opening at that point (w [mm]). The output was represented in *Figure 4.23*:

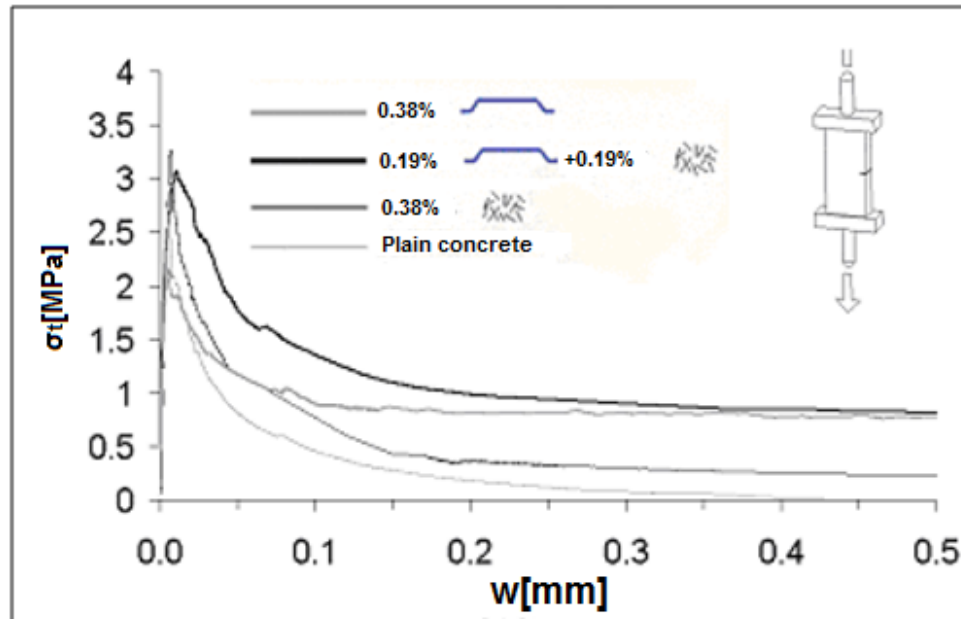


Fig. 4.23 Tensile Stress versus crack opening displacement

4.7 Numerical simulation of a simple tensile test

In order to verify the correct implementation of the traction behavior of the concrete, a numerical simulation of a simple tensile proof was carried out. The goal is to reproduce the experimental results obtained by Reinhardt(1984)[26]. Here below in Fig. the experimental set-up that he used for his experimental campaign is reported.

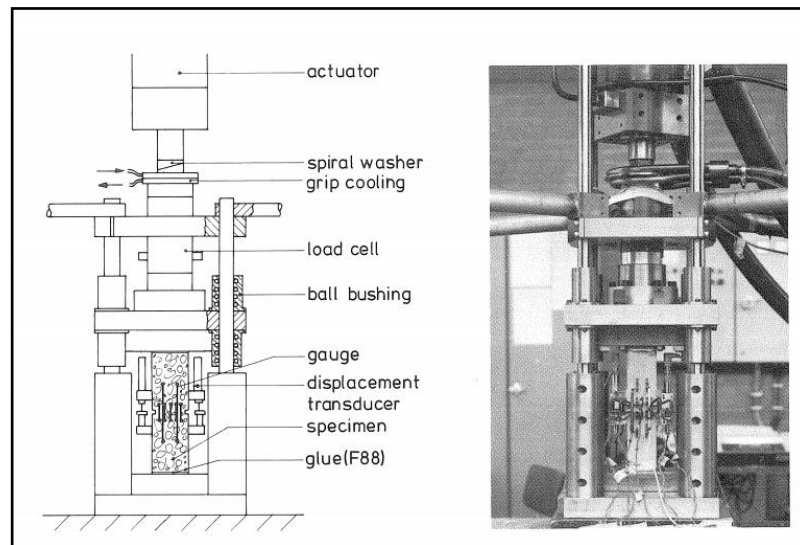


Fig.4.24 - Uniaxial tensile test experimental equipment

In the numerical test specimen having the dimensions proposed in *Fig.4.25* were used .To avoid stress concentrations in correspondence of the corners close to the saw-cuts, the geometries were simplified as reported in *Fig.4.25 b*

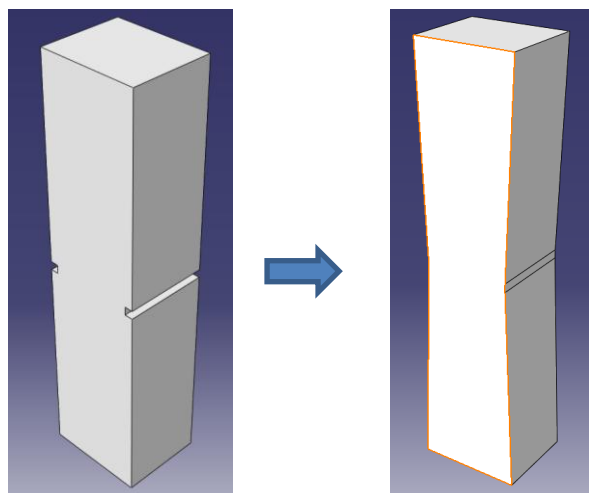


Fig.4.25 Sample geometry

The experiments, conducted in deformation control, were tested on narrow specimen 250 mm x 60 mm x 50 mm, where a saw-cut (5 mm width) reduced the cross section to 50 mm x 50 mm. The specimens have a notch of 5 x 5 mm in both sides so as to locate the process of cracking in the central area of the specimen thus having a section of 50 x 50 mm². In the numerical simulation, to locate the cracking in the central section, it is preferred to replace the two notches present in the experimental test, with a gradual narrowing of the specimen to obtain the same section 50 x 50 mm² in the central area of the specimen. The test consists in applying, with the aid of a load cell a deformation, (in the case of test carried out in displacement control) and through two displacement transducers positioned outside the area of fracture, displacement is measured on the specimen above and below the slatted area. If the measurement length l_0 is sufficiently small, this displacement can be considered coincident with the crack opening width w . In this experiment the measuring distance of transducers is approximately 50 mm. In Fig.4.26, Fig.4.27 are reported the experimental results that the numerical simulation wants to reproduce.

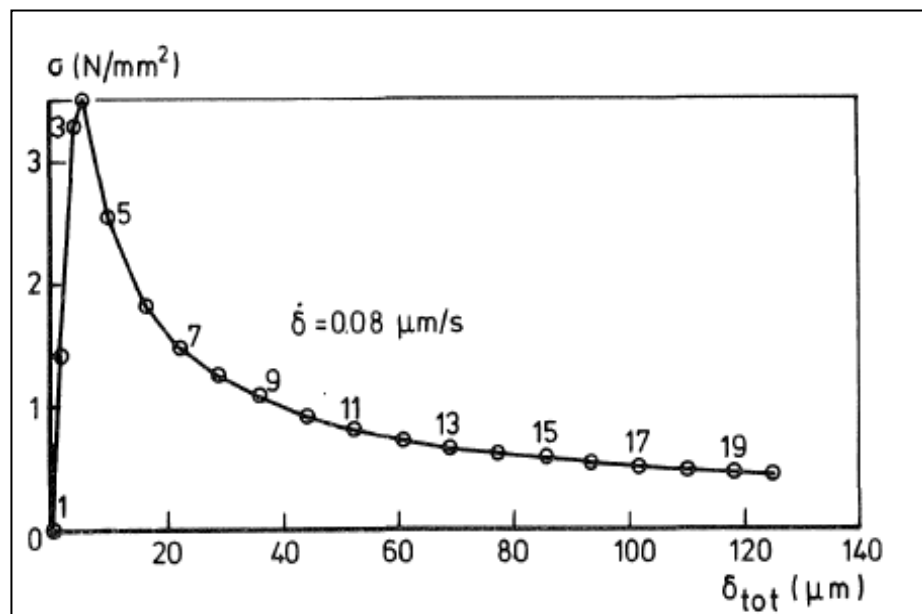


Fig.4.26 Experimental curve σ - w (mean behavior of NC samples)

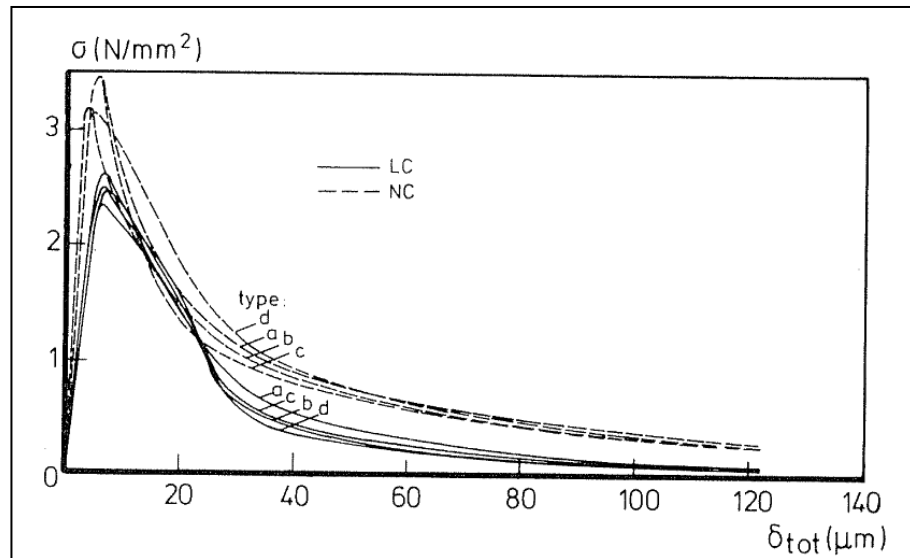


Fig.4.27 Experimental curves σ - w

Once the geometry was created, has been possible to create the element discretization proposed in Fig. . The mesh size is of 6.1 mm with 5 mm of thickness in the central zone. A total top displacement equal to 0.14 mm was imposed. This displacement represents the ultimate displacement and is reached for successive increments of load. An hysostatic boundary condition was imposed at the bottom base to not induce additional hyperstatic stress components.

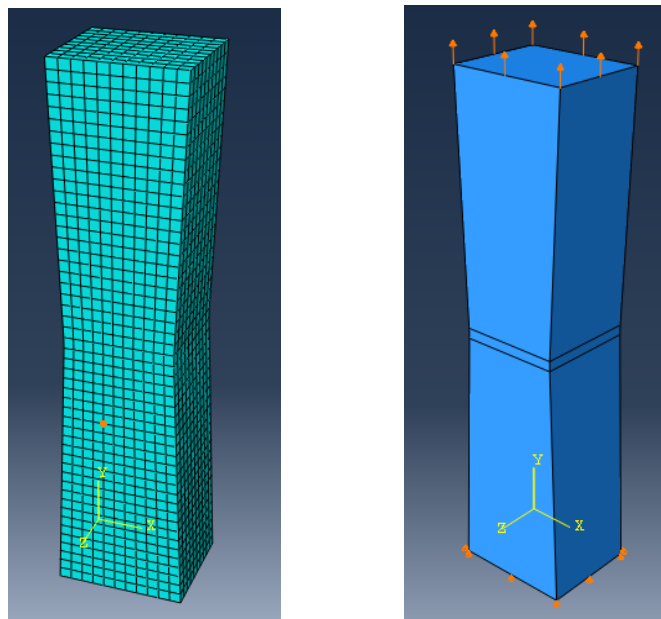


Fig.4.28 The mesh and the boundary conditions

Then the material properties has been defined. The two different concrete constitutive models of Abaqus environment were compared:

- a) Concrete smeared cracking(CSC)
- b) Concrete damaged plasticity(CDS)

The goal of the comparison was to test their performances in reproducing failure behavior and to have an instrument to better understand their calibration process.

To have a brief theoretical insight of these two models, the Paragraph 4.2 with its bibliography is recommended.

4.7.1 Implementation of simple tensile test (Reinhard 1986)with smeared cracking model

To implement this type of constitutive modeling different parameter are requested:

1-Elasticity parameters

The Young's modulus of 39270 MPa and Poisson ration of 0.185 were imposed as reported in *Fig.4.29* and in the reference article [26].

mix proportions	normalweight (kg/m ³)	lightweight (kg/m ³)
Portland cement	375	400
sand 0-2 mm	905	598
sand 2-4 mm	363	-
gravel 4-8 mm	540	-
lightweight aggregate 4-8 mm*	-	732
water	187.5	129
superplasticizer	-	6
density	2370	1865
mechanical properties	(N/mm ²)	(N/mm ²)
compressive strength	47.1 (6.0%)**	48.6 (6.0%)
splitting strength	3.20 (9.4%)	3.66 (8.3%)
direct tensile strength	3.20 (9.7%)	2.43 (8.6%)
Young's modulus (tension)	39270 (8.5%)	22420 (6.1%)

* incl. 17% by weight absorbed water.
** coefficient of variation.

Fig.4.29 Properties of the concrete tested by Reinhard

2-Compressive behavior of concrete

The compressive behavior is not directly involved in this type of proof but Abaqus implementation request it, because in the smeared cracking model the maximum tensile stress is evaluated as a fraction of the maximum compression strength. The input table is in terms of compression stresses σ_c versus "plastic strain", evaluated as the real total strain ϵ minus the strain at the ultimate elastic stress ϵ_{el} . In this case it can be evaluated as 23.55 MPa divided for the Young modulus.

The non-linear part of the compressive behaviour is shown in *Table 4.1*.

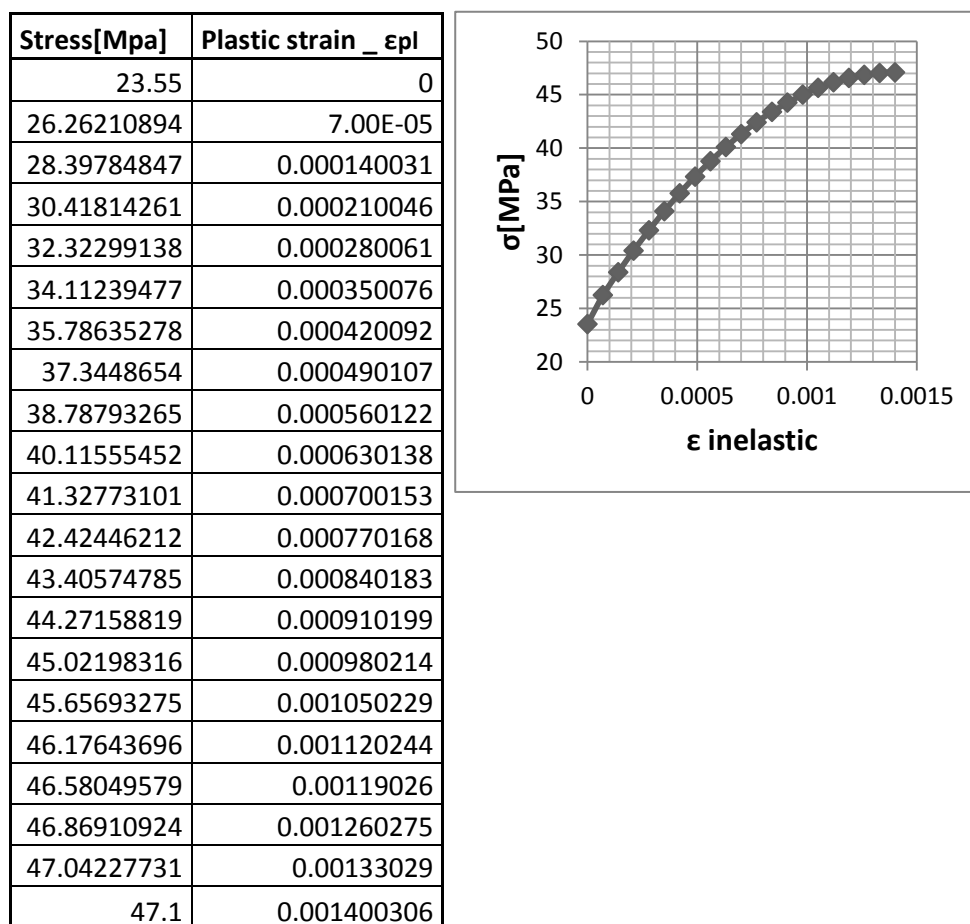


Table 4.1 Non-linear part of the compressive behavior

The parabola follows the σ - ϵ Kent-Park formulation [23].

3- The 4 failure surface parameters

The specification of the failure ratios are necessary to define the shape of the failure surface in the concrete smeared cracking model. Four failure ratios can be specified:

- The ratio of the ultimate biaxial compressive stress to the ultimate uniaxial compressive stress → **1.16**
- The absolute value of the ratio of the uniaxial tensile stress at failure to the ultimate uniaxial compressive stress → **3.2 MPa/47.1 MPa = 0.06794**
- The ratio of the magnitude of a principal component of plastic strain at ultimate stress in biaxial compression to the plastic strain at ultimate stress in uniaxial compression → **1.28**
- The ratio of the tensile principal stress at cracking, in plane stress, when the other principal stress is at the ultimate compressive value, to the tensile cracking stress → **0.33**

4- Tension stiffening

The postfailure behavior for direct straining across cracks is modeled with tension stiffening, which allows you to define the strain-softening behavior for cracked concrete. This behavior also allows for the effects of the reinforcement interaction with concrete to be simulated in a simple manner. Tension stiffening is required in the concrete smeared cracking model. You can specify tension stiffening by means of a postfailure stress-strain relation or by applying a fracture energy cracking criterion. The second approach will be used strictly connected to the definition of ultimate displacement of tension stiffening branch u_0 , that is the ultimate crack opening at which a stress transfer is still possible.

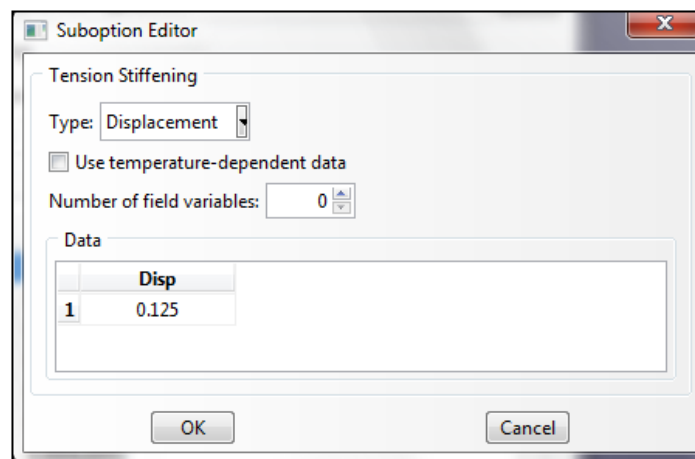


Fig.4.30 Tension stiffening Abaqus editor

Post-failure stress-strain relation

Specification of strain softening behavior in reinforced concrete generally means specifying the post-failure stress as a function of strain across the crack. In cases with little or no reinforcement this specification often introduces mesh sensitivity in the analysis results in the sense that the finite element predictions do not converge to a unique solution as the mesh is refined because mesh refinement leads to narrower crack bands. This problem typically occurs if only a few discrete cracks form in the structure, and mesh refinement does not result in formation of additional cracks. If cracks are evenly distributed (either due to the effect of rebar or due to the presence of stabilizing elastic material, as in the case of plate bending), mesh sensitivity is less of a concern.

In practical calculations for reinforced concrete, the mesh is usually such that each element contains rebars. The interaction between the rebars and the concrete tends to reduce the mesh sensitivity, provided that a reasonable amount of tension stiffening is introduced in the concrete model to simulate this interaction (*Fig.4.31*).

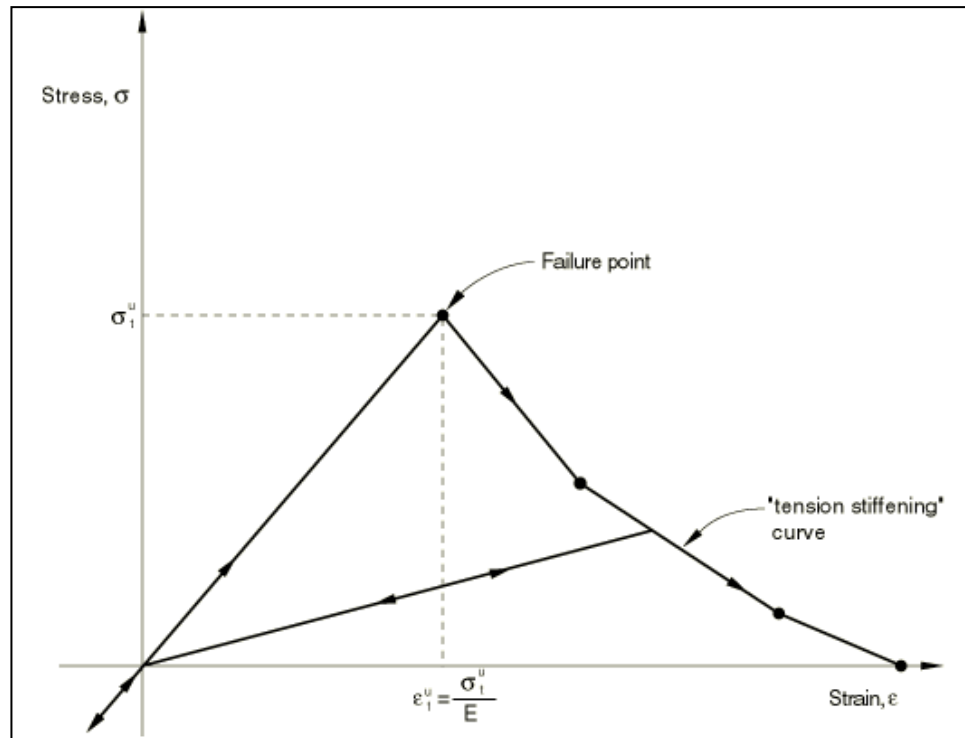


Fig.4.31 "Tension stiffening" model.

The tension stiffening effect must be estimated; it depends on such factors as the density of reinforcement, the quality of the bond between the rebar and the concrete, the relative size of the concrete aggregate compared to the rebar diameter, and the mesh. A reasonable starting point for relatively heavily reinforced concrete modeled with a fairly detailed mesh is to assume that the strain softening after failure reduces the stress linearly to zero at a total strain of about 10 times the strain at failure. The strain at failure in standard concretes is typically 10^{-4} , which suggests that tension stiffening that reduces the stress to zero at a total strain of about 10^{-3} is reasonable. This parameter should be calibrated to a particular case.

The choice of tension stiffening parameters is important in Abaqus/Standard since, generally, more tension stiffening makes it easier to obtain numerical solutions. Too little tension stiffening will cause the local cracking failure in the concrete to introduce temporarily unstable behavior in the overall response of the model. Few practical designs exhibit such behavior, so that the presence of this type of

response in the analysis model usually indicates that the tension stiffening is unreasonably low.

Fracture energy cracking criterion

As discussed earlier, when there is no reinforcement in significant regions of a concrete model, the strain softening approach for defining tension stiffening may introduce unreasonable mesh sensitivity into the results. Crisfield (1986) discusses this issue and concludes that Hillerborg's (1976) proposal is adequate to allay the concern for many practical purposes. Hillerborg defines the energy required to open a unit area of crack as a material parameter, using brittle fracture concepts. With this approach the concrete's brittle behavior is characterized by a stress-displacement response rather than a stress-strain response. Under tension a concrete specimen will crack across some section. After it has been pulled apart sufficiently for most of the stress to be removed (so that the elastic strain is small), its length will be determined primarily by the opening at the crack length (Fig.4.32).

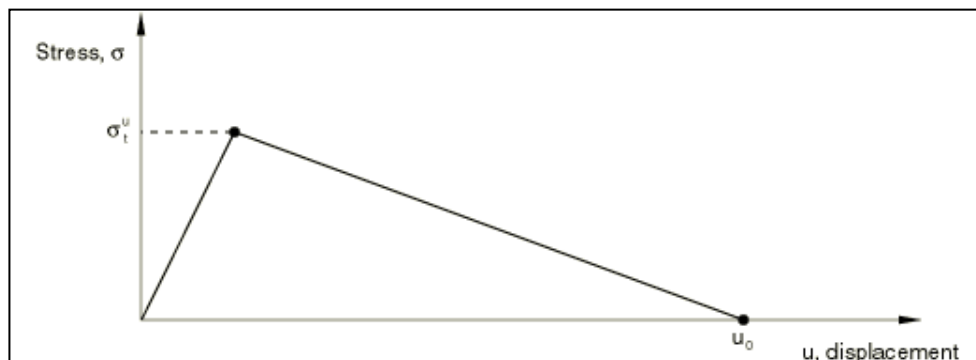


Figure 4.32 Fracture energy cracking model.

Obtaining the ultimate displacement u_0

The ultimate displacement, u_0 , can be estimated from the fracture energy per unit area, G_f , as $u_0 = 2G_f/\sigma_t^u$, where σ_t^u is the maximum tensile stress that the concrete can carry. Abaqus manual states that typical values for u_0 are 0.05 mm for a normal concrete to 0.08 mm for a high strength concrete. A typical value for ϵ_t^u is about 10^{-4} . As a matter of fact this type of values, related to reasonable values of fracture energy per unit area G_f (0.09-0.13 N/mm), don't converge. To find out the correct values of the ultimate displacement u_0 that both:

- converge and

-provide the correct solution,

a trial and error procedure was used. The results are provided in the following pages.

Trial and error procedure to calibrate the u_0 value:

Once the compression behavior and the failure parameters has been implemented is necessary to define the tensile softening branch of the concrete. The difficulty is to find out the correct value of u_0 to find out a convergent and correct solution, because not all the u_0 values provide a solution(in this case Abaqus "abort" the Job) and not all the solution are correct. Different spy-nodes were selected on the numerical specimen: twelve above the critical cross section, twelve below as reported in *Fig.4.33* with a distance of 55 mm between the two lines.

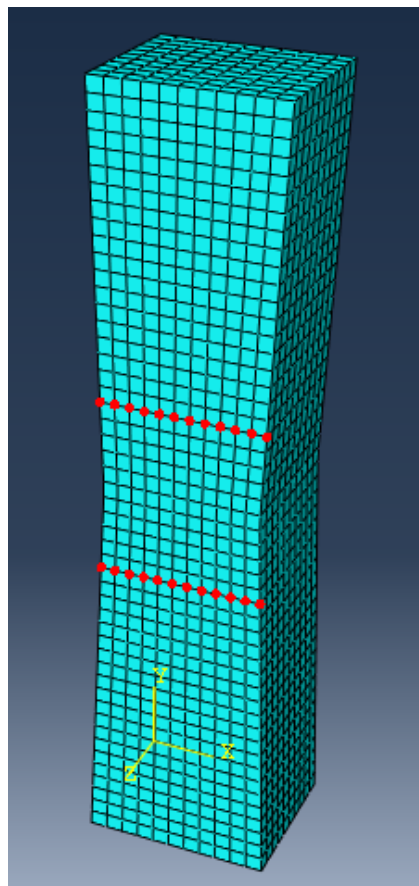


Fig.4.33 Spy-nodes on the numerical specimen

The stress were calculated as the sum of the bottom reaction forces in y direction RF2, divided for the critical area of 2500 mm².

Different values of ultimate displacement were tested: 4 mm , 2 mm , 0.5 mm , 0.125 mm, 0.12 mm, 0.1 mm. Values of 0.05-0.08 mm as suggested in the Abaqus manual don't provide convergent solutions.

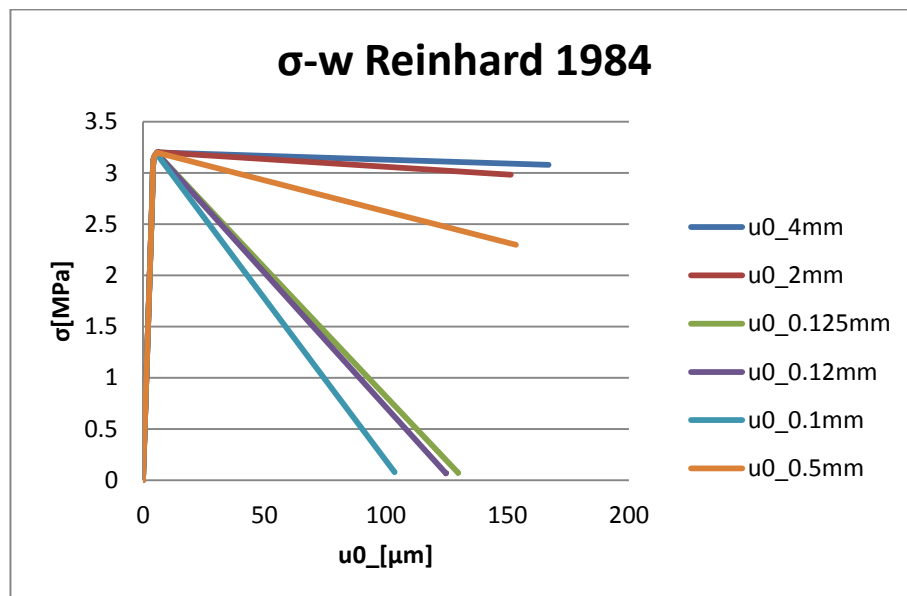


Fig.4.34 Graph σ -Crack Opening dependant on u_0

Overlapping the numerical curve $u_0=0.125$ mm with the experimental one it can noticed how Abaqus reproduce the tensile test:

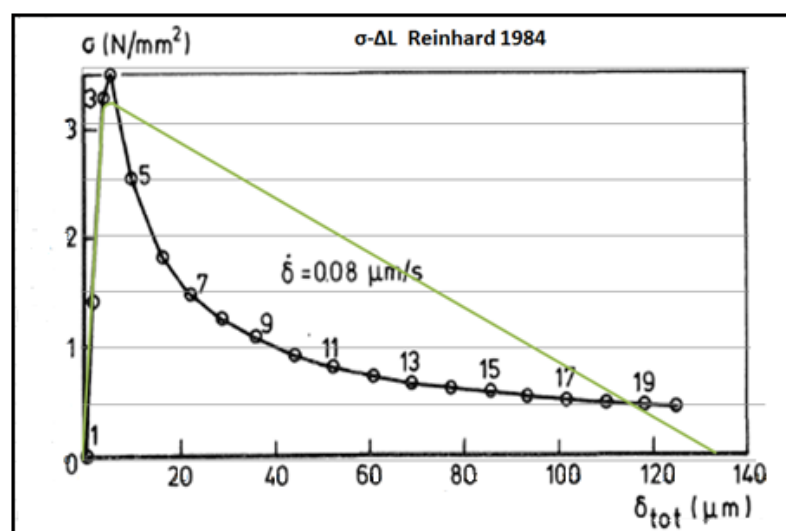


Fig.4.35 Comparison mean experimental σ - Δl curve and numerical - CSC model

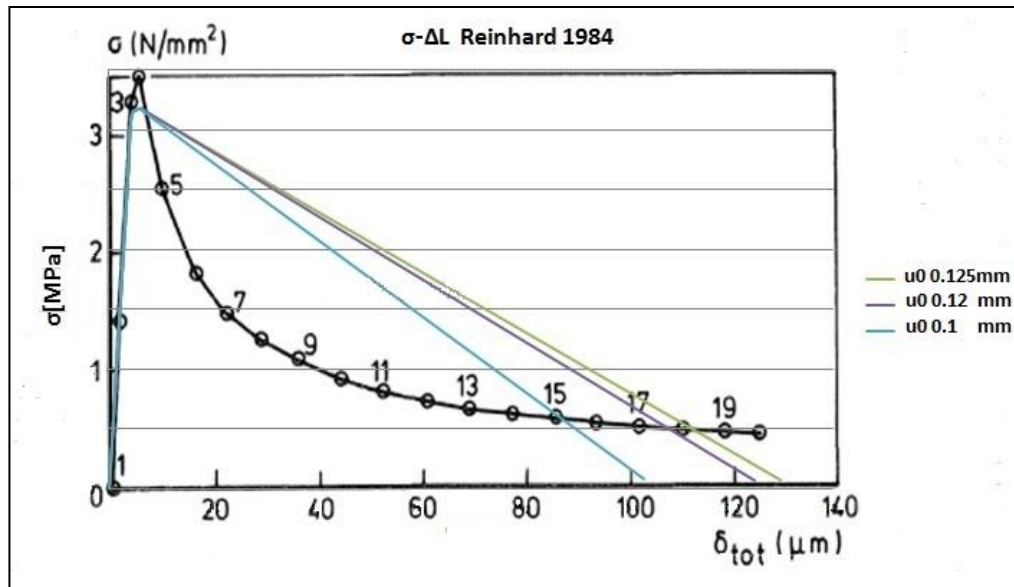


Fig.4.36 Comparison mean experimental σ - Δ curve and numerical - CSC model

The displacement distribution reveal that there is a crack opening in the critical section: at the final state all the deformations are concentrated in that area.

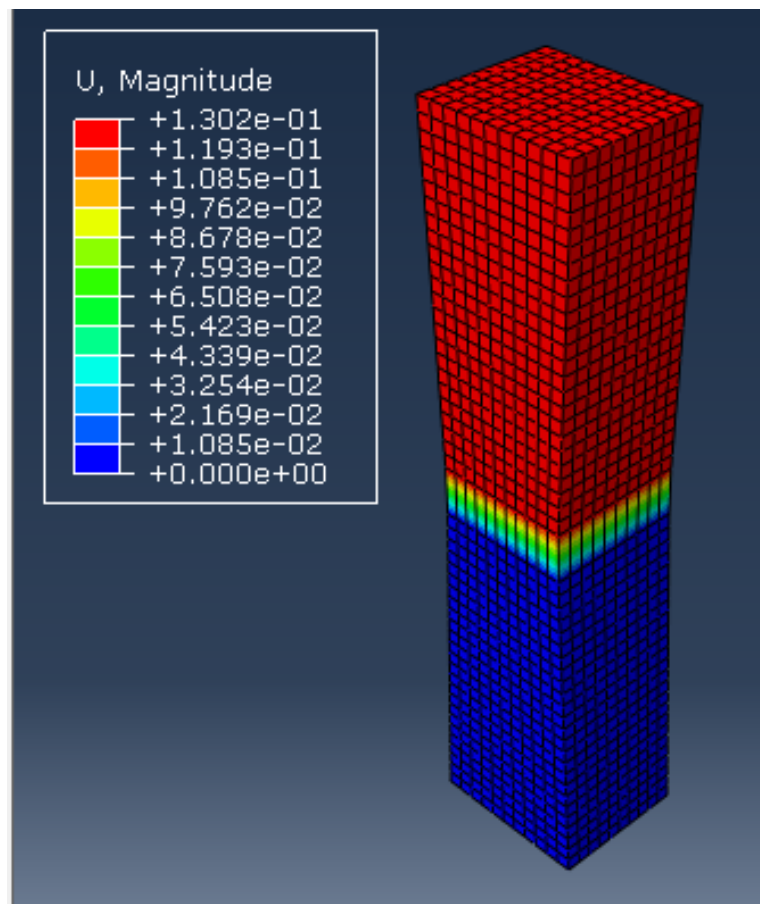


Fig.4.37 Final state of Smearred Cracking specimen (UY - Scale factor x100)

4.7.2 The CDP "concrete damage plasticity" model based on Lee and Fenver theory

Also in the concrete damage model the elastic properties must be defined. As in the previous case a Young modulus of 39270 MPa, a Poisson modulus of 0.185 and a compression behavior in terms of σ_c - ϵ_{pl} were established. The traction law definition for what concern the post peak behavior follows Cornellissen (1986) formulation, as reported in the *Paragraph 4.6.1*. The post peak branch is dependent on the peak stress value equal to 3.2 MPa and on the ultimate strain ϵ_u evaluated as:

$$\epsilon_u = 5.618 \frac{G_f}{h \sigma_t} = 0.0158$$

where h is the extent of the zone that participate to the cracking behavior. From the observation of the previous case the maximum stress and strain concentration before crack opening, where spread over a 1.5 cm of length in the zone close to the critical section; the other two parameters were set as:

$$G_f = 0.135 \text{ N/mm}$$

$$\sigma_t = 3.2 \text{ MPa}$$

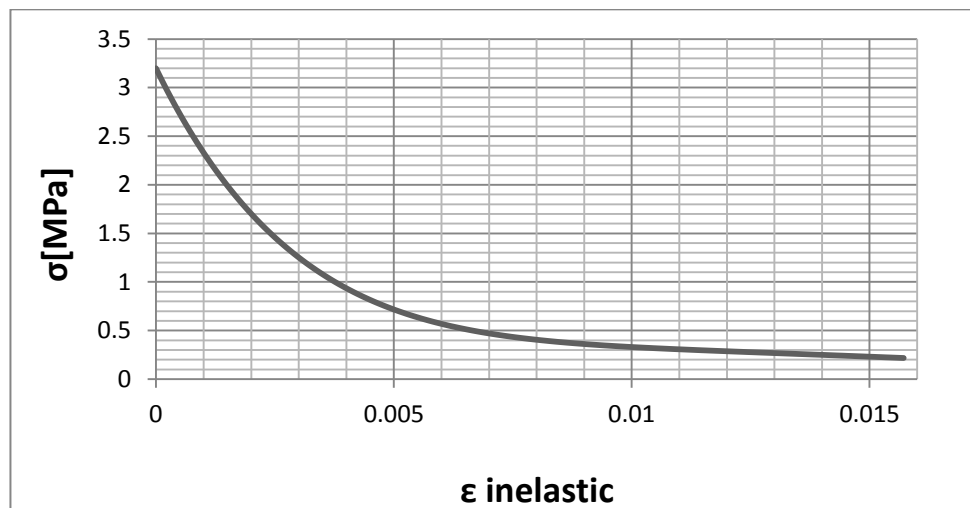


Fig.4.38 Graph σ - ϵ in CDP formulation (Cornellissen)

As reported in the previous paragraph the damage d must be a value between 0 and 1. To not create numerical problems the maximum value should never be bigger than 0.99. For the definition of this variable see paragraph. In Fig. 4.39 is reported the damage trend used in Abaqus traction specimen.

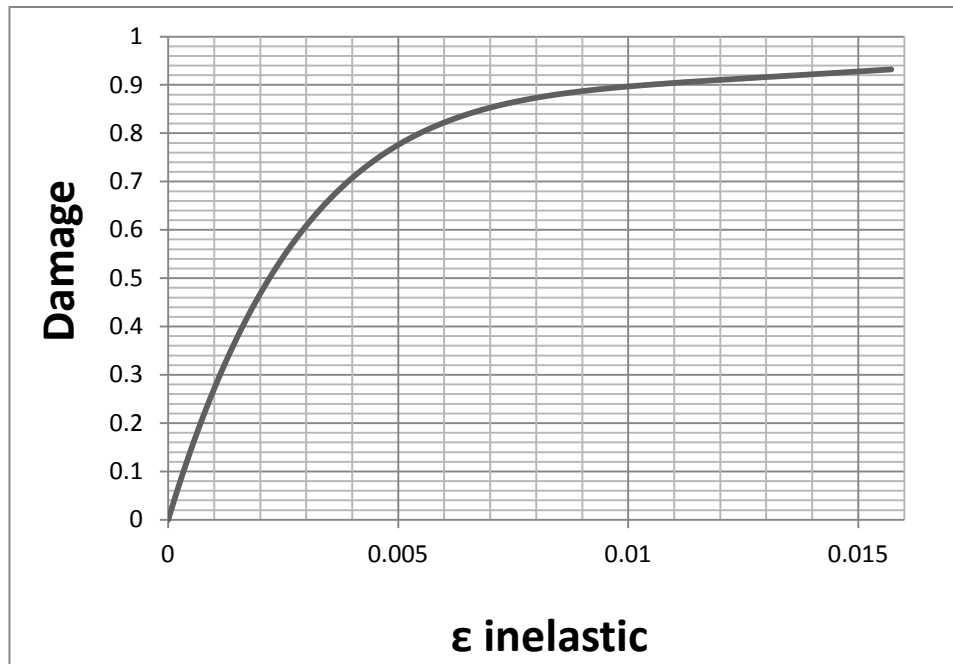


Fig.4.39 Damage variable trend in CDP specimen

For what concern plasticity parameters in Fig. 4.40 is reported the Abaqus editor:

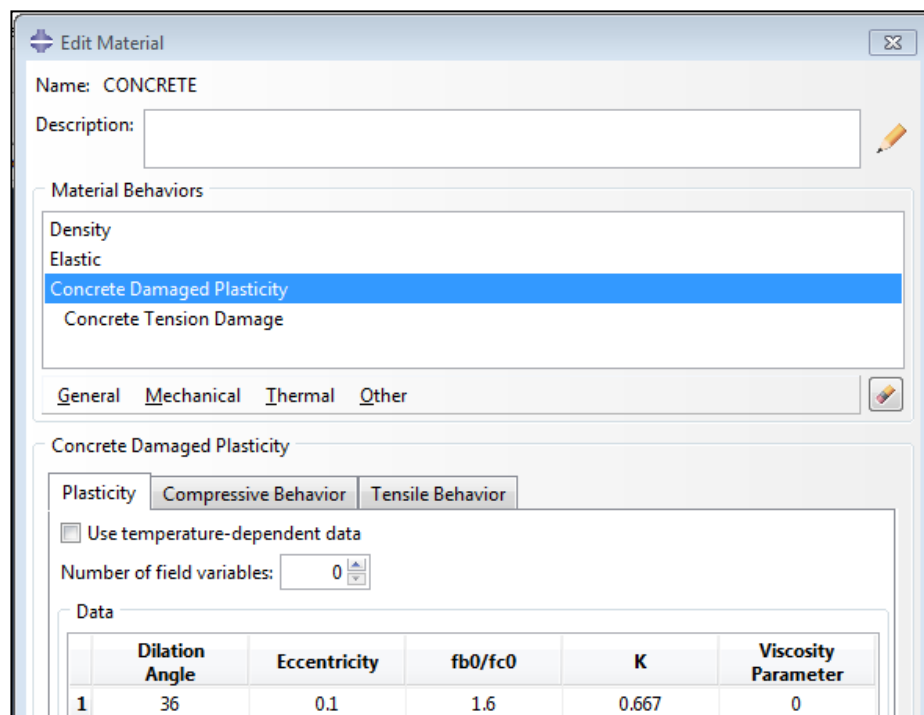


Fig.4.40 Plasticity parameters in CDP specimen

It can be noticed how the numerical model fit the experimental results of the tensile uniaxial experimental test:

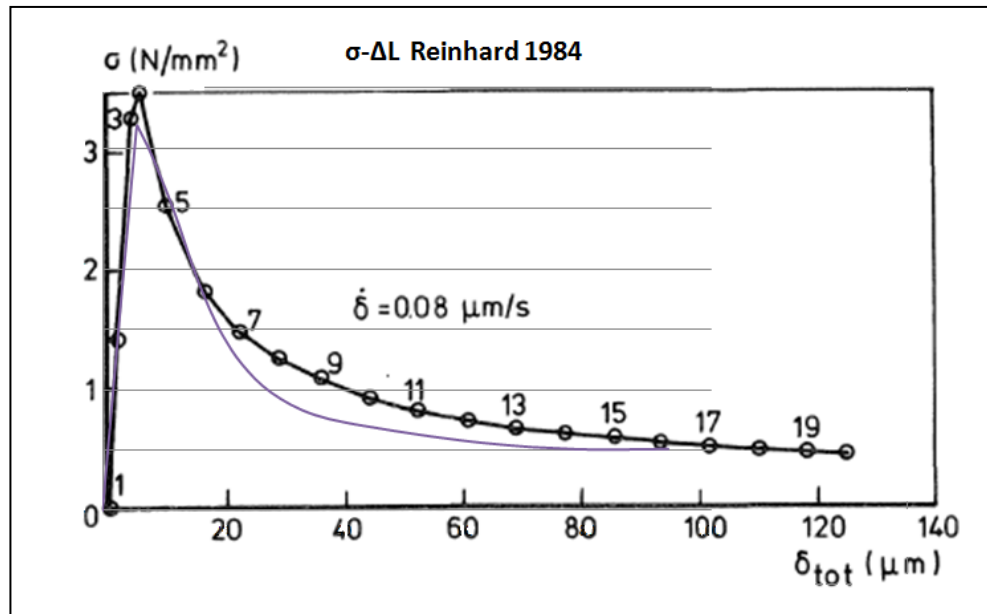


Fig.4.41 Comparison mean experimental σ - Δl curve and numerical - CDP model

Considering the whole set of experiment the results match quite well.

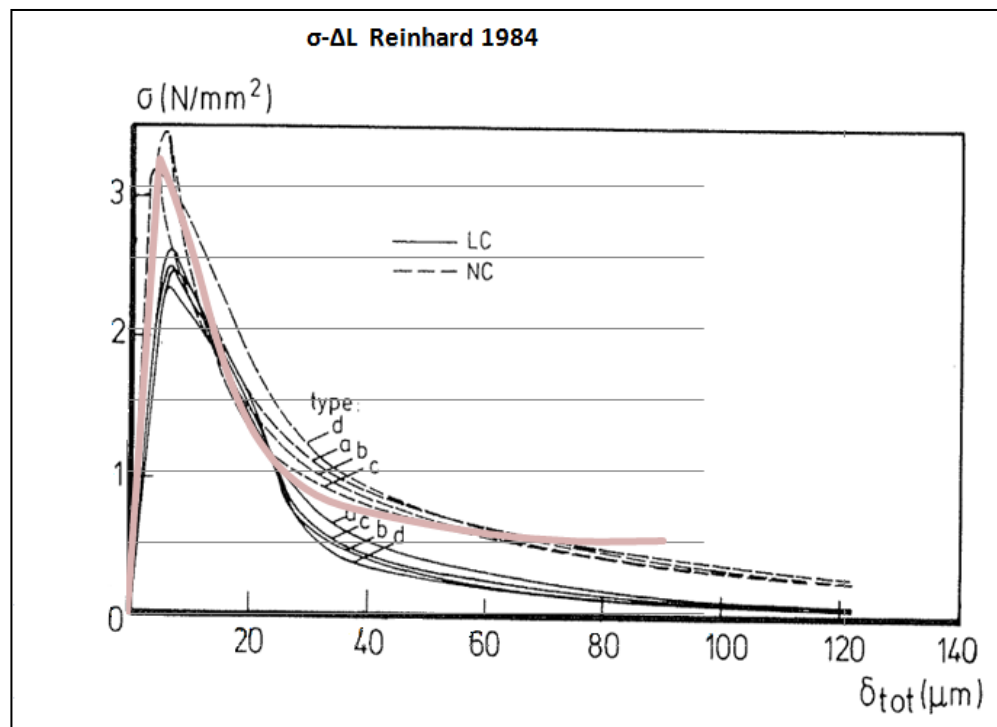


Fig.4.41 Comparison experimental σ - Δl curves and numerical - CDP model

Chapter 5

Bond-slip formulation

Background

The behavior of the bond between the concrete and reinforcing steel in an RC structure is a many-faceted phenomenon which allows longitudinal forces to be transferred from the reinforcement to the surrounding concrete. When studying cracked reinforced concrete, characterization of the bond behavior is one of the most important issues. Once a crack develops, the concrete stress near the crack is relieved, but the tension in the steel can increase considerably. The high level of steel stress at the crack is transferred to the surrounding concrete through the interfacial bond (Won 1991). Therefore, it is helpful to understand the bond behavior and to model it appropriately before simulating the failure behavior of the RC grid wall of interest in this study. This report describes an attempt to accurately model the bond-slip relationship between concrete and rebar using the FE software package ABAQUS.

Object

The primary objective of this study was to develop a finite element model which could correctly simulate the bond-slip relationship in a RC member, and to accurately predict the level of stress and strains transferred by the bond. Other objectives were to develop a better understanding of bond behavior simulation, with the aim to insert in the RC wall model, the best modeling techniques available in Abaqus.

Introduction

The action of the steel/concrete bond is a complex force transfer phenomenon occurring between the reinforcing steel and the surrounding concrete in RC members. The existence of the bond is the basic condition for these two materials to work together as a kind of composite material. The connection between the reinforcing bars and the concrete is also responsible for controlling of the crack opening behavior in an RC member (Filho et al. 2004). Between significant cracks, the concrete still "works" and will absorb part of the tensile load from the rebar because the bond allows the load transfer between these two materials. Consequently, the average and total strains resulting in the rebar are smaller than those that would be experienced under the same load in a plain rebar. This

mechanism, attributed to the bond, reduces the width of the cracks that develop and increases the stiffness of the structure. Because of its importance, the bond-slip relationship is considered in most of the design and analysis efforts involving RC. Researchers have conducted numerous studies to characterize the constitutive bond-slip relationship. In the finite element analysis field, many different methods were also employed to represent the nature of the interaction between the concrete and reinforcement.

5.1 Bond-slip Relationship

The pull-out experiment is perhaps the easiest method used to test the bond-slip relationship. In the state-of-the-art report "Bond of reinforcement in concrete" from CEB-FIP (The International Federation for Structural Concrete), the authors agree that the interaction between the concrete and the rebar subjected to a pull out force is characterized by four different stages, as represented in *Fig 5.1*, and described below (CEB-FIP 2000).

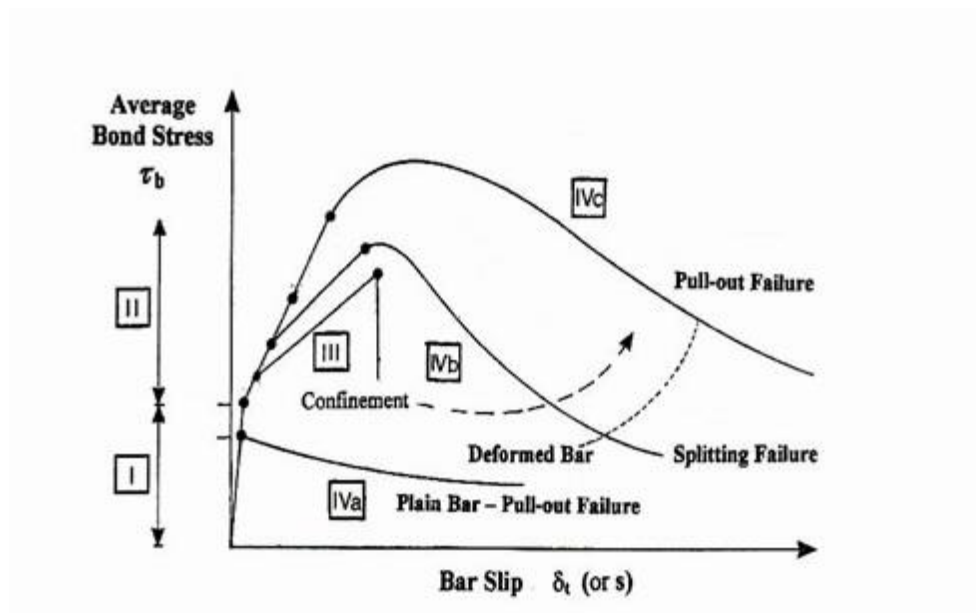


Fig. 5.1 Local Bond Stress-Slip Laws (adapted from CEB-FIP 2000)

In *Stage I* the concrete is uncracked. For the low bond stress levels present in Stage I, bond efficiency is assured mostly by chemical adhesion, and there is little rebar slip, but highly localized stresses arise close to lug tips (CEB-FIP 2000).

Stage II is the stage in which first cracking occurs. For the higher bond stresses present in Stage II, the chemical adhesion breaks down; in deformed bars, the lugs induce large bearing stresses and transverse micro cracks originate at the tips of the lugs, allowing the bar to slip (CEB-FIP 2000). The progression through the relationship for regular reinforced concrete (i.e., including deformed bars) will be from Stage I to Stage II, then either to *Stage III*, or Stage IVb, or Stage IVc, depending on the confinement level and amount of transverse reinforcement present. *Stage IVa*, as indicated in the figure, is a special case for plain bars (i.e., without deformations). Stage IVc is the stage in which deformed bar pull-out failure occurs. In the case of deformed bars confined by sufficient transverse reinforcement, splitting failure does not occur and bond failure is caused by bar pull out, as indicated in *Fig. 5.1* (CEB-FIP,2000). Stage IVb is characterized as the deformed bar-splitting failure stage; in the case of deformed bars confined by light transverse reinforcement, the splitting cracks breakout through the whole cover and between bars, and the bond tends to fail abruptly. On the other hand, a sufficient amount of transverse reinforcement can assure bond efficiency despite of concrete splitting. In this situation, the bond strength reaches a peak and then starts decreasing as slipping value increases, but still the bond strength remains significant at very large slip values, as shown in *Fig. 5.1*. (CEB-FIP 2000) .In Stage III, a more sudden failure occurs in concrete with lighter transverse and confinement. This stage ends as soon as concrete splitting reaches the outer surface of the member (CEB-FIP 2000). Stage IVa is called the plain bar-pull out failure stage: in plain bars, this stage immediately follows the breakage of the adhesive bond. The sliding interface reduces the friction and the bond stress decreases (CEB-FIP 2000). For better use of the bond slip relationship above has been simplified to a linear or bilinear curve by many researchers. There are several popular bilinear models, such as the three segments model (Nilson 1972), the five segments model (Guo and Shi 2003), and the six segments model (Tassios 1982); these three models are illustrated in *Fig. 8.2*. In *Figure 5.2*, τ represents bond stress, while S represents the magnitude of bond slip. In CEB-FIP MC90, a four segment model is suggested, as shown in *Figure 5.3*; *Table 5.1* shows the characteristic values for the different parameters specified in this model.

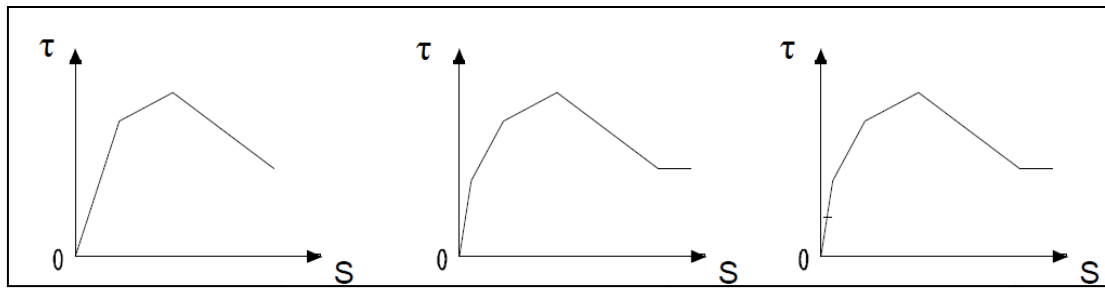


Figure 5.2 Multilinear Bond Slip Relationships

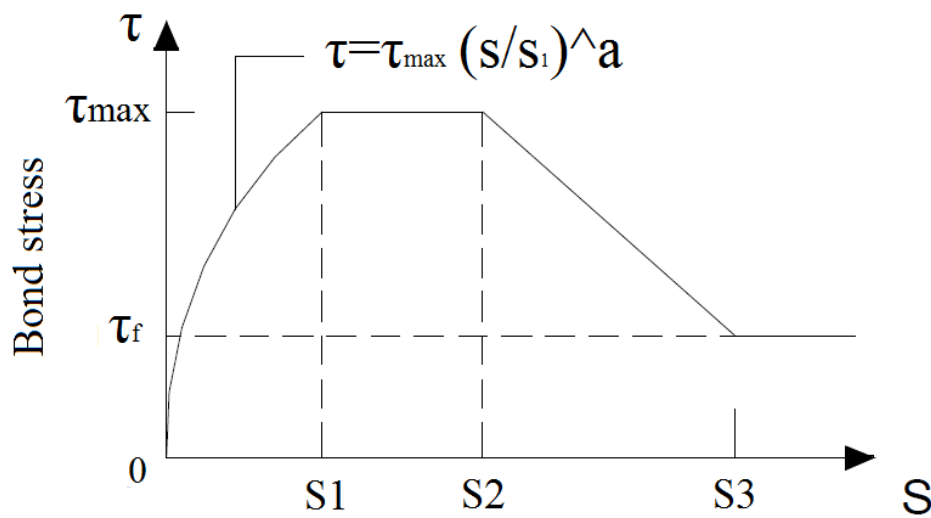


Figure 5.3 CEB-FIP MC90 Model (CEB-FIP, 1993) for Bond-Slip

Table 5.1 Values of Parameters for CEB-FIP MC90 Model

	Unconfined concrete		Confined concrete	
	Good bond conditions	All other bond conditions	Good bond conditions	All other bond conditions
S1	0.6 mm	0.6 mm	1.0 mm	1.0 mm
S2	0.6 mm	0.6 mm	3.0 mm	3.0 mm
S3	1.0 mm	2.5 mm	Clear rib spacing	Clear rib spacing
a	0.4	0.4	0.4	0.4
τ_{max} (MPa)	$2.0\sqrt{f_{ck}}$	$1.0\sqrt{f_{ck}}$	$2.5\sqrt{f_{ck}}$	$1.25\sqrt{f_{ck}}$
τ_f	$0.15 \tau_{max}$	$0.15 \tau_{max}$	$0.40 \tau_{max}$	$0.40 \tau_{max}$

* f_{ck} = characteristic concrete compressive strength, MPa

Engstrom modified the degrading part of the CEB model recently in order to consider the effect of yielding of the rebar (CEB-FIP 2000). He found that the bond stress decreases more when the steel strain exceeds the yield strain than when the steel bar is still elastic because when the reinforcing bar reaches the yield stress, due to the Poisson's ratio, there is a narrowing of the section of the bar, with consequent detachment between the bar and the walls of the concrete. *Fig 5.4* and *Table 5.2* illustrate the different bond slip relationships under these two situations.

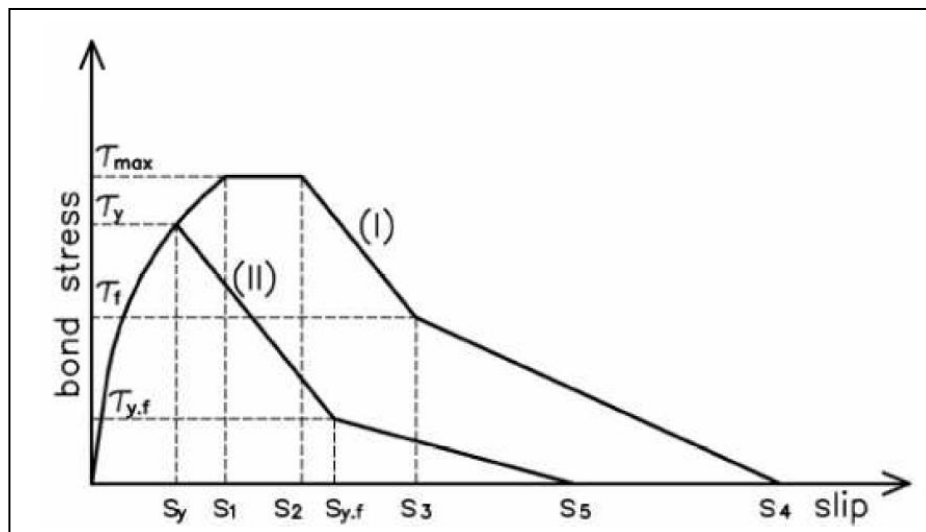


Figure 5.4 Engstrom's Model (CEB-FIP 2000)
 (I) Steel Bar in Elastic Stage (II) Steel Bar in The Plastic Stage

The parameters to define the Elastic curve are:

	S1	S2	S3	S4	τ_{\max}	τ_f	α
Normal strength concrete	1.0mm	3.0mm	Clear rib spacing	3*S3	$0.45f_{cm}$	$0.4\tau_{\max}$	0.4
High strength concrete	0.5mm	1.5mm	Clear rib spacing	3*S3	$0.45f_{cm}$	$0.4\tau_{\max}$	0.3

* f_{cm} = mean value of concrete compressive strength, MPa

Table 5.2 Values of Parameters in Engstrom's Model (CEB-FIP 2000) for Bond-Slip in Elastic phase

Instead the equations that describe the different branches of the Plastic stage are:

$$\begin{aligned}\tau(s) &= \tau_y \left(\frac{s}{s_y} \right)^{0.4} & 0 \leq s \leq s_y \\ \tau(s) &= \tau_y - (\tau_y - \tau_{yf}) \left(\frac{s - s_y}{s_{yf} - s_y} \right) & s_y \leq s \leq s_{yf} \\ \tau(s) &= \tau_{yf} - \tau_{yf} \left(\frac{s - s_5}{s_5 - s_{yf}} \right) & s_{yf} \leq s \leq s_5 \\ \tau(s) &= 0 & s \geq s_5\end{aligned}$$

where:

$$s_y = \text{slip value at yielding phase} = s_1 \left(\frac{\tau_y}{\tau_{\max}} \right)^{0.25} \quad \tau_y = f(s_y) = 0.75 \tau_{\max}$$

$$s_{yf} = s_y + 2.5 \text{ mm}$$

$$\tau_{yf} = 0.2 \tau_{\max}$$

$$s_5 = 2 s_3 \div 15 \text{ mm}$$

5.2 Current Study and Existing Models

5.2.1 FE Model of Reinforced Concrete

Unlike steel and aluminum, which have uniform constitutive properties, reinforced concrete consists of two totally different materials working together to resist various types of loadings. Therefore, it is somewhat complex to predict reinforced concrete behavior that includes the bond-slip relationship using the FE method. Currently there are three different FE models which are widely used to simulate reinforced concrete behavior. They are discrete, distributed and embedded models. For the discrete modeling technique, separate, distinct elements are used to represent the concrete and the reinforcement. For instance, it is sometimes convenient to use a solid finite element to represent the concrete and to use a beam element to simulate the reinforcing bars. In the discrete model, concrete and steel are two totally independent parts. For this modeling technique, special elements must be placed at

the interface between the concrete and steel to represent the bond mechanism. When using the embedded modeling technique, the rebar is considered as an axial member that is built into the concrete element. Because the rebar is embedded, the rebar has the same displacement as the concrete element. Perfect bond is assumed in this modeling technique, so that the two materials are assumed to work together completely as one unit (ASCE 1982). When using the distributed modeling technique, the reinforcement is assumed to be smeared into every element of the concrete. Compared to the embedded model, in which the contribution of the concrete and steel is calculated independently, for the distributed modeling technique, the rebar is transferred to an equivalent amount of concrete and the RC is considered as a homogeneous material in this model. Perfect bond is again assumed for this technique. Each of these three models has its own strong points. The distributed model is frequently used in practical structural design and analysis, based on its simplicity of implementation. However, the internal force of the reinforcement is not available to be quantified in this model since the steel has been smeared. The discrete model is the only model of the three which can consider the bond slip mechanism directly, so it is very useful in more accurate RC simulations, despite the fact that the modeling process for this technique is the most complex. Moreover, it is more convenient to simulate irregular reinforcement in the discrete model, because the concrete and steel are separate entities. The embedded modeling technique falls between the distributed and discrete model in terms of complexity and ease of implementation. It is, in general then, not used as often because it has few distinct advantages over the other techniques. With the development and advancement of computer technology, most finite element software packages such as ABAQUS, ADINA, ANSYS, and MSC/NASTRAN have their own concrete constitutive models, and corresponding concrete and rebar elements. Through the combination of these elements, the users can develop the three basic RC models above, and can then add advanced properties into the model such as the representation of bond, fracture and cracking behaviors.

5.2.2 FE Model of Bond

Based on the different FE models of concrete, there are various corresponding methods to represent the bond behavior. In a discrete concrete model, the bond may be considered as a contact problem between two different materials. Some

dedicated elements have been developed to simulate this contact in earlier research and presently they are widely used in the commercial FE software. In the distributed concrete model, bond phenomena can be represented by a special property of the material, rather than by a connection, since the reinforcement is smeared into the concrete in the distributed model. In ABAQUS code, bond-slip is implicitly approximated by introducing some “tension stiffening” into the concrete model to simulate load transfer through the rebar (ABAQUS 2006). Tension stiffening is a bond-related behavior which decreases the tension in the steel due to bond, and increases the stiffness of the reinforcement, compared to that for a naked bar, after the RC cracks. The user can define the curve in *Figure 5.5* by inputting different tension stiffening parameters. The tensile behavior is defined as having elastic behavior until the stress reaches f_{tu} , the failure point of the material. Then, a linear or nonlinear softening model is used to represent post-cracking behavior including bond effect using the "tension stiffening" option of ABAQUS.

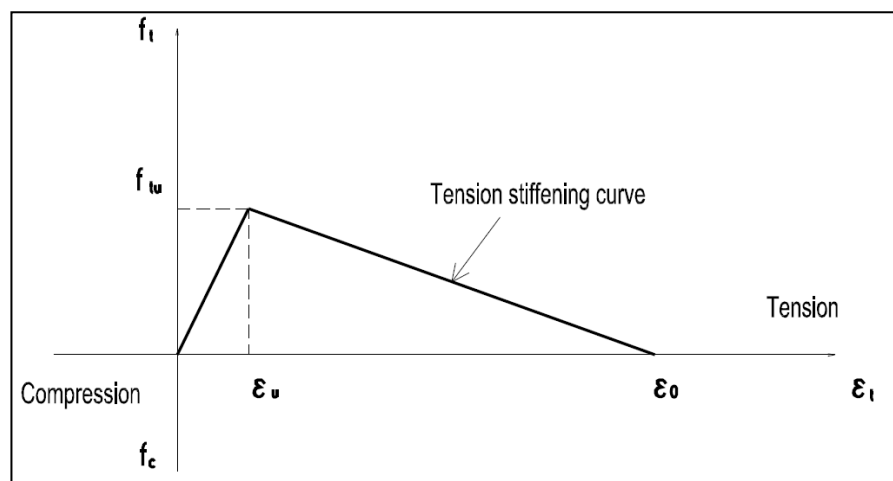


Figure 5.5 Tension Stiffening Behavior in ABAQUS (adapted from ABAQUS 2006)

5.2.3 Interaction Module of ABAQUS

As mentioned earlier, a discrete reinforced concrete model, in which complex bond behavior can be simulated directly was developed for the present study. As such, the first step in producing a model was to select a method for building a contact between concrete and steel. ABAQUS, in its interaction modules, provides various methods for simulating this contact, such as constraints, contact elements, and connector elements. Since bond slip is a force (shear stress) versus displacement

(slip) relationship, and is a surface-based phenomena ,the interaction types in ABAQUS which can couple these two aspects were considered.

5.2.3.1 Friction

Friction is a modeling tool available in ABAQUS that is commonly used to describe the behavior of the contacting surfaces. The basic equation for the friction model is $\tau_{crit} = \mu p$, where τ_{crit} is critical shear stress at which sliding of the surfaces starts, μ is the coefficient of friction and p is the contact pressure between the two surfaces. *Figure 5.6* summarizes the behavior of the friction model in ABAQUS. There is only a very small amount of slip allowed between the two contact faces before the shear stress across the interface equals the limiting frictional stress, μp .

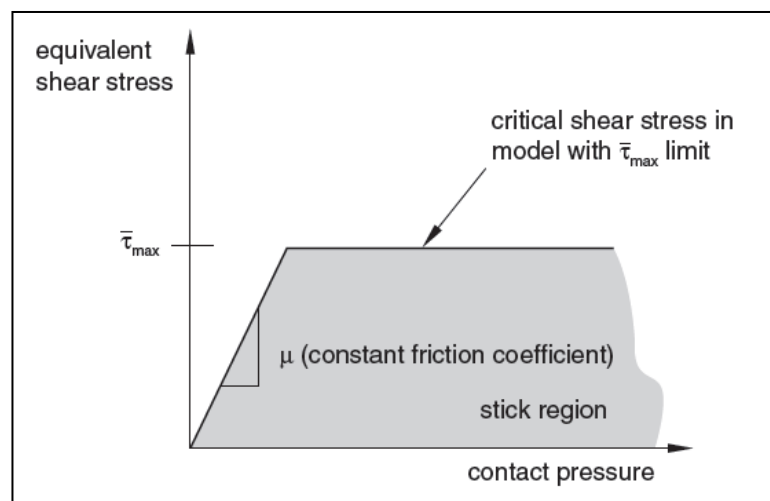


Fig. 5.6 Frictional Behavior in ABAQUS

The transmission of the shear forces caused by friction is very similar to the bond behavior exhibited between concrete and steel. Comparing the curve in Figure 5.6 with the bond-slip relationships in previous pages, it seemed obvious that the friction model would seem a good choice for simulating a linear bond phenomenon. The advantage of using a friction model is that it is defined through a face-to-face contact. A friction model's shortcoming, though, is also very obvious. Friction can simulate neither the non linear bond behavior, nor the degradation portion of the bond behavior. Furthermore this type of modeling is not convenient in my model: I chose to reproduced “equivalent-area -squared bars”, this imply that only the upper

and the bottom work, reproducing incorrectly the bonding phenomena. The best choice results “cohesive based surface modeling”.

5.2.3.2 Cohesive based surface modeling

Surface-based cohesive behavior is defined as surface interaction properties between two contact pairs (two surfaces coupled by a relationship master-slave) that can be used to model delamination at interfaces directly in terms of traction versus separation, where traction and separation must be conceived in the three directions as it will be better explained after the introduction of traction-separation matrix. It can be used to model sticky contact and it assumes a linear-elastic traction-separation law prior to damage. It's enforced as a node-to-face interaction in Abaqus/Explicit or as a surface-to surface formulation in Abaqus/Standard. Considering the latter a “small sliding” approach must be enforced. The model rely on three components: a linear traction separation law that describe the ascendant part of the law, a damage initiation criteria and a damage evolution law for the post peak. The elastic behavior is written in terms of a constitutive matrix that relates the normal and the shear stresses to the normal and shear separation across the interface. The nominal traction stress vector, \mathbf{t} , consists of three components (two components in two-dimensional problems): t_n , t_s , and (in three-dimensional problems) t_t , which represent the normal (along the local 3-direction in three dimensions and along the local 2-direction in two dimensions) and the two shear tractions (along the local 1- and 2-directions in three dimensions and along the local 1-direction in two dimensions), respectively. The corresponding separations are denoted by δ_n , δ_s , and δ_t . The elastic behavior can then be written as

$$\mathbf{t} = \begin{Bmatrix} t_n \\ t_s \\ t_t \end{Bmatrix} = \begin{bmatrix} K_{nn} & K_{ns} & K_{nt} \\ K_{ns} & K_{ss} & K_{st} \\ K_{nt} & K_{st} & K_{tt} \end{bmatrix} \begin{Bmatrix} \delta_n \\ \delta_s \\ \delta_t \end{Bmatrix} = \mathbf{K}\boldsymbol{\delta}.$$

An uncoupled behavior, that means to define only the diagonal elements of the matrix, has been considered. Moreover to restrict the cohesive constraint to act along the contact tangential direction only, the normal stiffness term, K_{nn} , has been set to zero; as a consequence an “hard contact” behavior in the normal direction has been imposed to not allow penetration between steel and concrete.

The next step has been to define the damage, that means simulate the degradation and the eventual failure of the bond between two cohesive surfaces. The failure mechanism consist of two ingredients: a damage initiation criterion and a damage evolution law. Damage initiation refers to the beginning of degradation of the cohesive response at a contact point. The process of degradation begins when the contact stresses and/or contact separations satisfy certain damage initiation criteria that you specify. Several damage initiation criteria are available but a “quadratic stress criterion has been chosen”. This criterion recall the ellipsoid domain and can be represented as

$$\left\{ \frac{\langle t_n \rangle}{t_n^o} \right\}^2 + \left\{ \frac{t_s}{t_s^o} \right\}^2 + \left\{ \frac{t_t}{t_t^o} \right\}^2 = 1.$$

The damage evolution law describes the rate at which the cohesive stiffness is degraded once the corresponding initiation criterion is reached. A scalar damage variable, D , represents the overall damage at the contact point. It initially has a value of 0. If damage evolution is modeled, D monotonically evolves from 0 to 1 upon further loading after the initiation of damage. The contact stress components are affected by the damage according to

$$t_n = \begin{cases} (1 - D)\bar{t}_n, & \bar{t}_n \geq 0 \\ \bar{t}_n, & \text{otherwise (no damage to compressive stiffness);} \end{cases}$$

$$t_s = (1 - D)\bar{t}_s,$$

$$t_t = (1 - D)\bar{t}_t,$$

where \bar{t}_n , \bar{t}_s , and \bar{t}_t are the contact stress components predicted by the elastic traction-separation behavior for the current separations without damage. There are two components to the definition of damage evolution. The first component involves specifying either the effective separation at complete failure, δ_m^f , relative to the effective separation at the initiation of damage, δ_m^o ; δ_m^o ; or the energy dissipated due to failure, G^C .

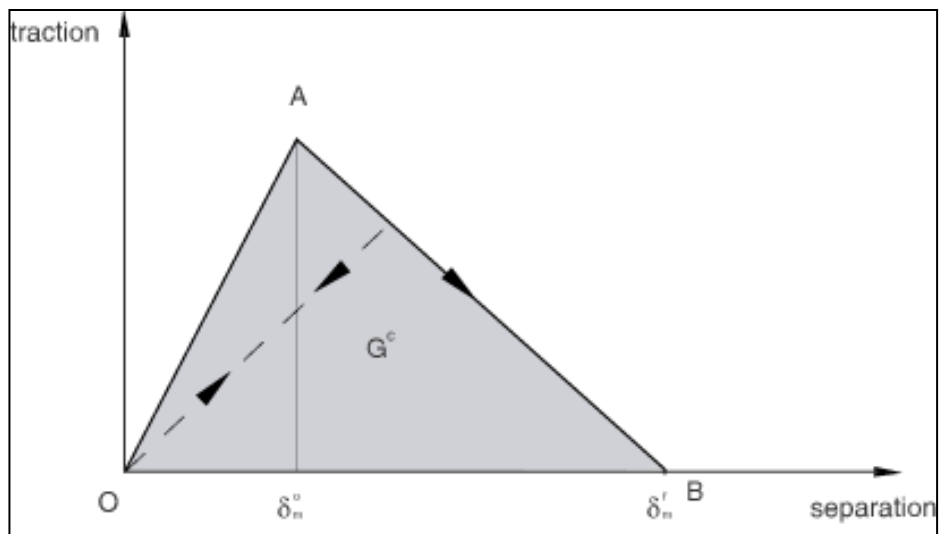


Figure 5.7 Traction-separation response implemented in Abaqus

The figure above represent the bond-slip behavior that can be modeled in Abaqus.

5.3 The pull-out test

5.3.1 The test equipment

A 3D finite element model is discussed in this paragraph. The geometry of this model was simplified from the specimen of the pull-out experiment detailed in E. Perry and J. Thompson's article "Bond stress distribution on reinforcing steel in beams and pullout specimens" (Perry and Thompson 1966). *Figure 5.8* shows the simplification employed.

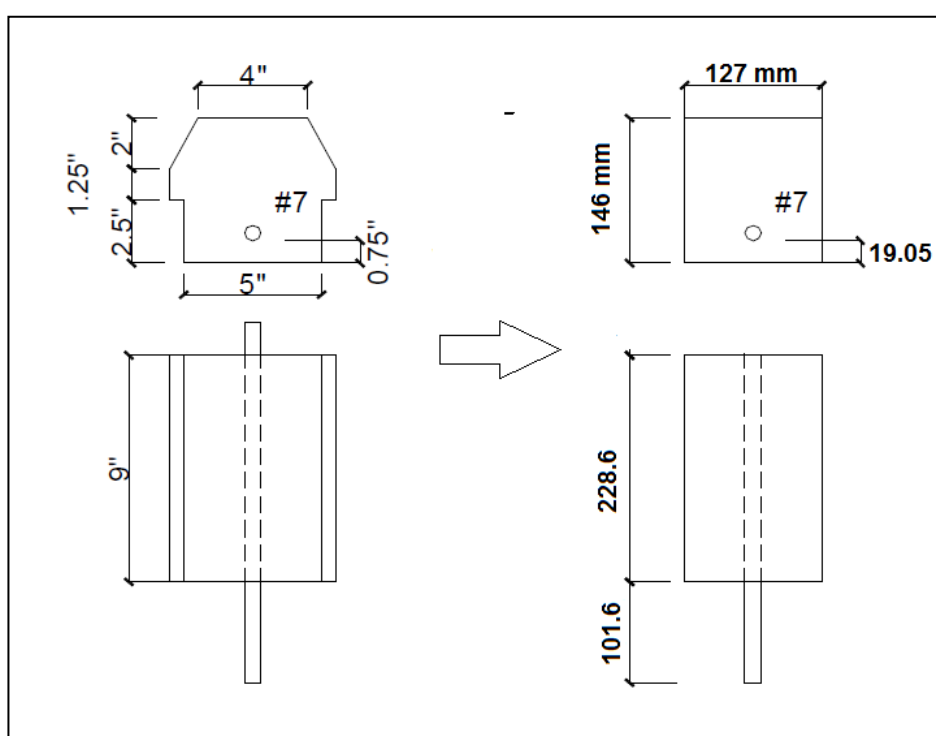


Figure 5.8 Pull-out experimental set up: the simplification reported

As can be seen, a standard No.7 steel bar was embedded into a concrete prism. It correspond to a

R fi 7 USA	0.4375	inch	1.11125	cm	FI 22 ITA
-------------------	--------	------	---------	----	------------------

An equivalent are criteria was used obtaining a lateral edge of 19.5 mm.

Figure 5.9 shows the 3D profile of the model in the CAE environment of ABAQUS.

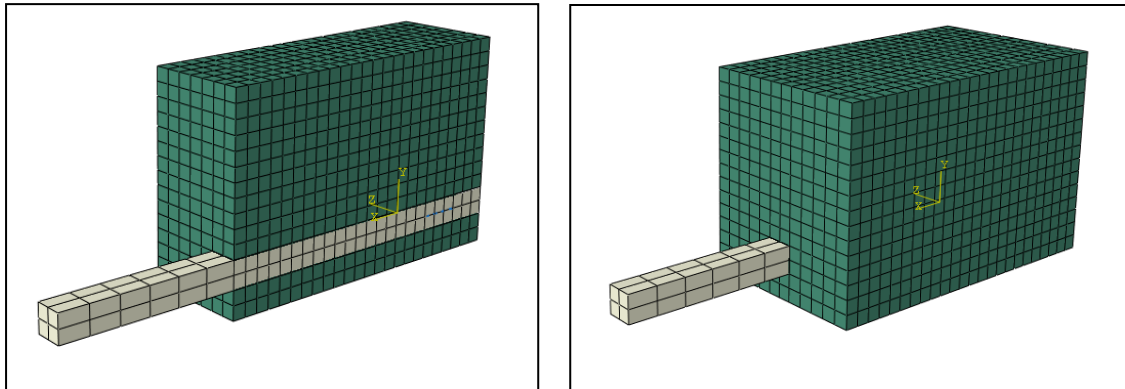


Figure 5.9 Geometry and mesh in Abaqus

Elastic material properties were used for both concrete and reinforcement in this model since the focus of the model was to investigate the bond between these two materials, rather than the response of the materials themselves.

Concrete			Steel		
E	30474.84	Mpa	E	199948	MPa
v	0.15		v	0.32	
density	2380.463	kg/m³	density	7916.423	kg/m³

Table 5.3 Material properties

5.3.2 Load and boundary condition

The applied loading consisted of an axial surface pressure of 142.005 MPa imposed at the exposed end of the rebar, applied in the pull out direction, which generated a slip that moved the rebar for a certain distance. The load was applied in small increments to overcome numerical instability difficulties that could have occurred: a Linear- Static RIKS analysis was used.

To accurately simulate the effect of bearing on the block in the pull out test, a fixed boundary condition was also assigned at the surface of the concrete specimen to fix the concrete; moreover an upper pressure of 0.1 MPa was introduced to best simulate the conditions in the macro model that will be presented in the Chapter 6.

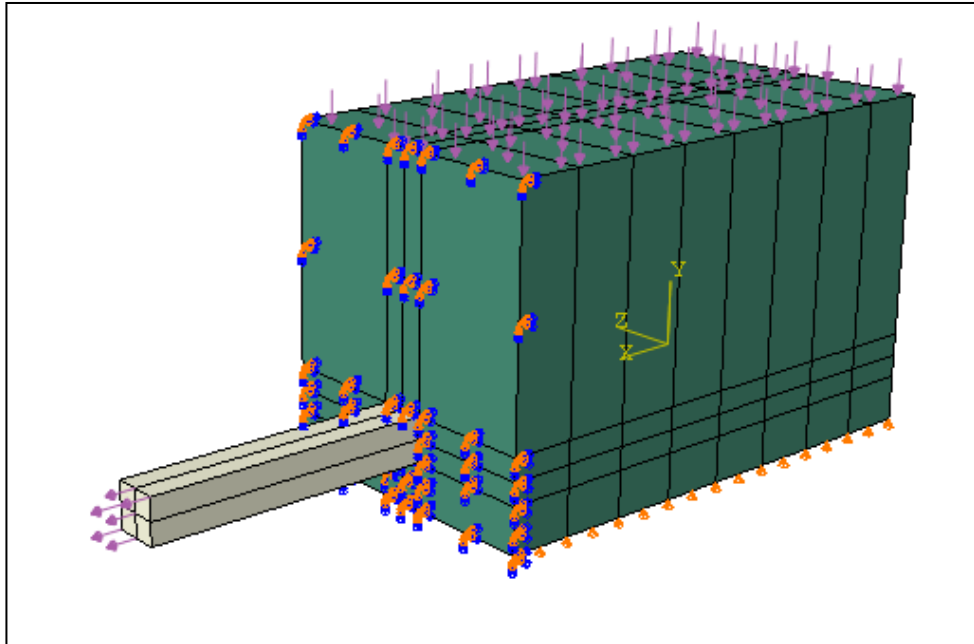


Figure 5.10 Load and boundary conditions in the Pull-out test

5.3.4 Bond-slip formulation in the pull-out test

As a special interaction available in ABAQUS, "*Cohesive based surface modeling*" was selected to simulate the bond phenomena between concrete and steel in this model as shown in Figure 5.11.

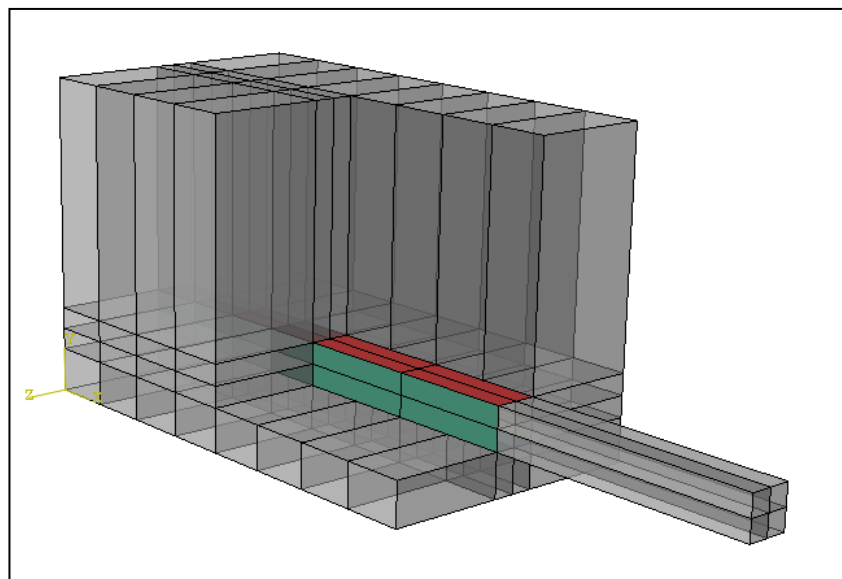


Figure 5.11 View-cut on 2 contact-pairs (in green and in red) on which was applied the "*Cohesive based surface behavior*"

These contact pairs (involving a master-slave relationship on the 4 edges of the bar) were used to insert and interaction between the concrete and steel (along the length of the rebar) with a τ -slip behavior in the longitudinal (pull out) direction. A *hard-contact* was employed in normal direction on the same pairs, to not allow penetrations between concrete and steel.

5.4 Bond-slip law implemented in the Pull-out test

The mathematical bond-slip relationship CEB-FIP,2000 was used as reference, and was associated to contact pairs in a simplified version due to the bilinear trend of Abaqus implementation(see *Figure 5.7*). Referring to *Figure 5.4* and *Table 5.2* (CEB-FIP 2000), the values that were used in the model are:

f_{cm}	31.3	Mpa
T_{max}	14.085	Mpa
T_y	10.56375	Mpa
s₁	1	mm
s₂	3	mm
s_y	0.9306049	mm
s_{yf}	3.4306049	mm
s₃	3	mm
s₄	9	mm
a	0.4	

Table 5.4 Parameters for CEB-FIP curve designation

Once implemented in an Excel-spread sheet:

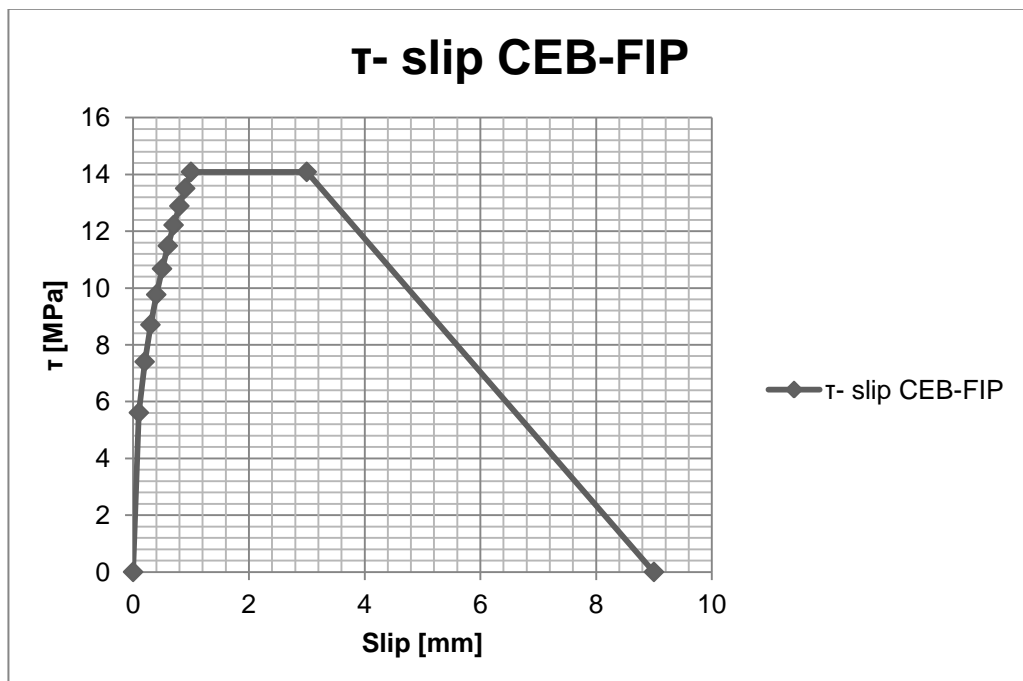


Figure 5.12 Bond-slip relation

This law was conceived on a fi 8 rebar as the macro model presented in Chapter 6 required. This choice could seem incorrect but from the bond-slip curves provided by Abaqus as output(see next *Par 5.4*) it can be noticed how the implementation resulted not affected by the Area. It is reminded that the goal of this specific model was to test the reliability of "based cohesive surface" interaction, not to study the stress-strain field developed.

The interaction was transferred to the contact pairs by defining the stiffness in the ascendant linear branch OA reported in *Figure 5.7* and reproduced in *Fig. 5.13.*, a damage initiation criterion and a damage evolution criterion. All the step to implement in Abaqus this type of behaviour are reported in *Chapter 6 Par.6.5*.

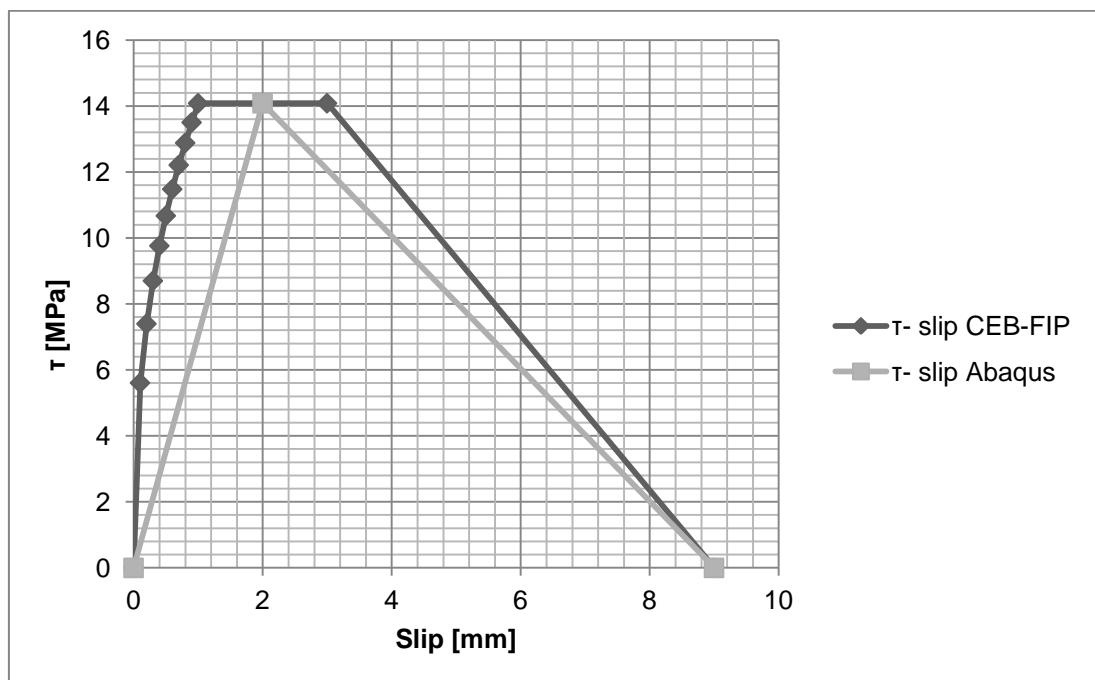


Figure 5.13 Bond-slip relation implemented in the pull-out test

5.5 The results of the Pull-out numerical test

To verify the reliability of this type of implementation the CTF1 (Contact total force in direction 1, the horizontal one) on the 4 concrete master surfaces was requested as output. To catch the slip-trend, another single spy-node in the center bottom-surface of the steel bar was considered and the horizontal displacement history U1 of this node was requested.

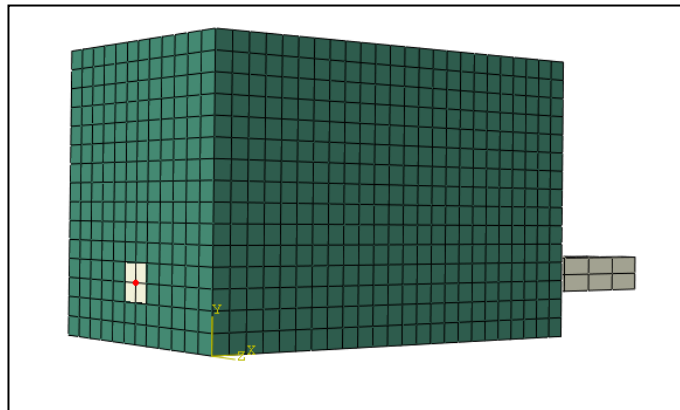


Figure 5.14 The spy node (in red)

The CTF1 of the 4 concrete master surfaces were summed and divided for the lateral area of the steel bar in contact (equal to 17830.8 mm²) to have a τ in MPa. Implementing the whole history output "U1spy_node - Sum 4_CFT1/Lat_Area " :

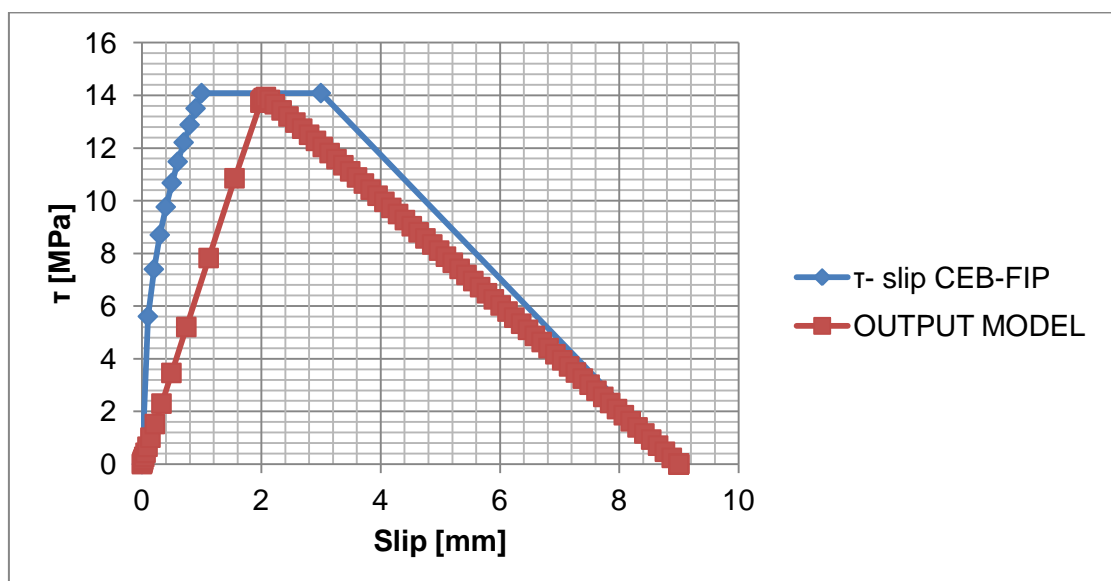


Figure 5.15 Bond-slip output of the numerical pull-out test in comparison with the code one

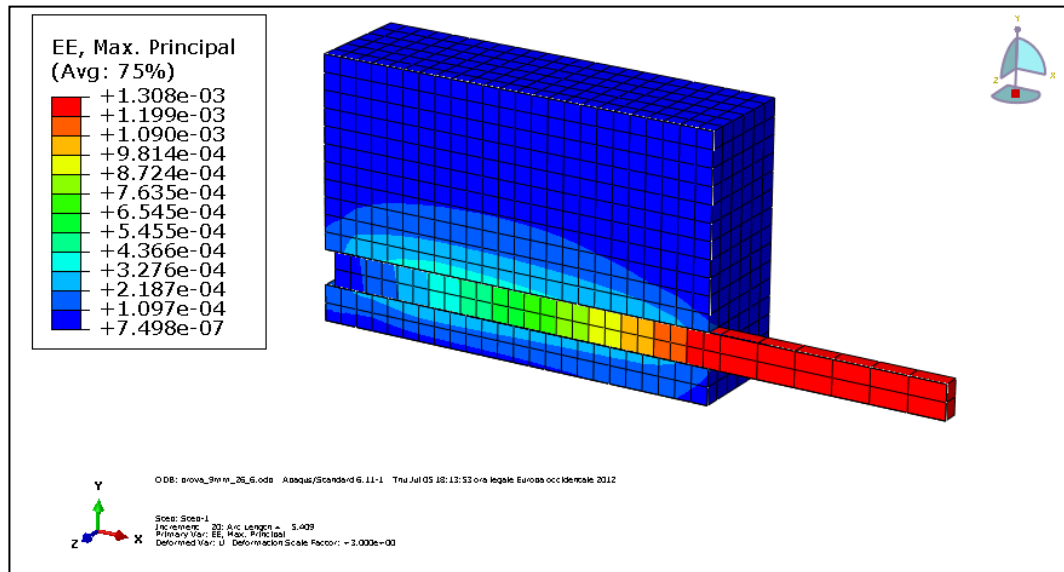


Figure 5.16 Elastic strain distribution in the middle plain

5.6 Bond-slip law implemented in the grid wall

The macro model that will be presented in the next Chapter 6 is reinforced with $\Phi 8$ steel bars only. Reinforcing bars were simplified with "equivalent area squared section bars". Through this simplification the mesh around the bars resulted less complex. This assumption leads to an increase of the lateral surface of the bar and therefore a greater surface on which develop the adhesion between concrete and reinforcement. This effect was taken into account considering a decrease of the τ_{\max} proportional to the ratio of the two different lateral areas. In the next *Figure 5.17* the bond-slip implemented was reported.

f_{cm}	31.3	Mpa
τ_{\max}	14.085	Mpa
τ_y	10.56375	Mpa
s1	1	mm
s2	3	mm
s_y	0.9306049	mm
s_{yf}	3.4306049	mm
s3	3	mm
s4	9	mm
a	0.4	

Table 5.5 Parameters CEB-FIP for a $\Phi 8$ bar

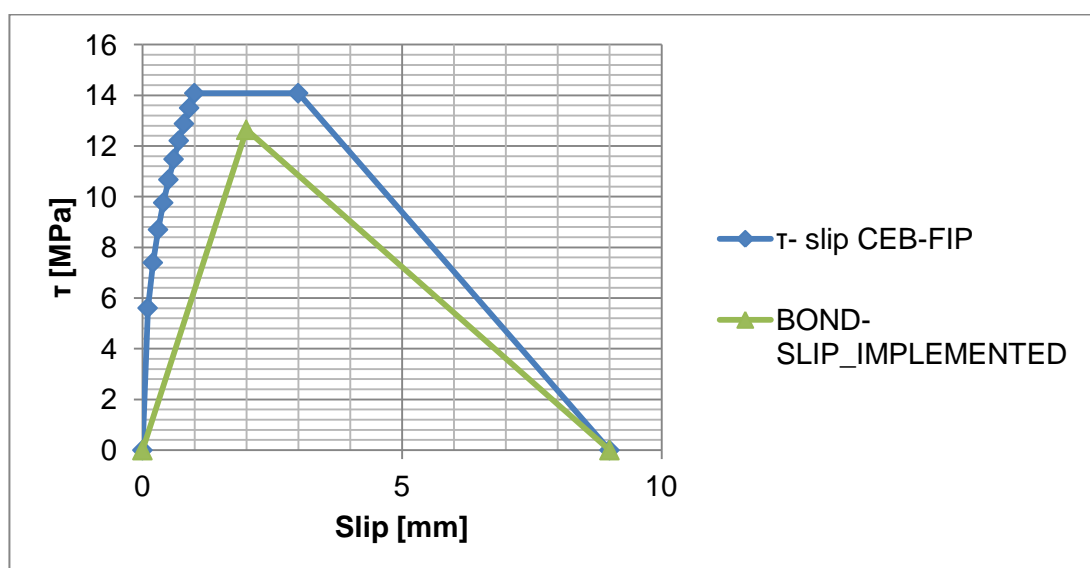


Figure 5.17 The bond-slip implemented in green.

Chapter 6

Numerical model in Abaqus

Background

“The model is intended as a self-contained set of rational relations aimed at giving a closed –form response on the basis of a set of input data” (Fib, 2000).

Every complete finite-element analysis consists of 3 separate stages:

- Pre-processing or modeling: This stage involves creating an input file which contains an engineer's design for a finite-element analyzer (also called "solver").
- Processing or finite element analysis: This stage produces an output visual file.
- Post-processing or generating report, image, animation, etc. from the output file: this stage is a visual rendering stage.

The use of FE software package ABAQUS is strictly connected with its powerful solver component. Furthermore the presence of two packages for concrete modeling made this software interesting for the numerical analysis that this work wants to explore. Abaqus/CAE is capable of pre-processing, post-processing, and monitoring the processing stage of the solver; however, the first stage can also be done by other compatible CAD software, or even a text editor. Abaqus/Standard, Abaqus/Explicit or Abaqus/CFD are capable of accomplishing the processing stage. The scheme below simplify these concepts:

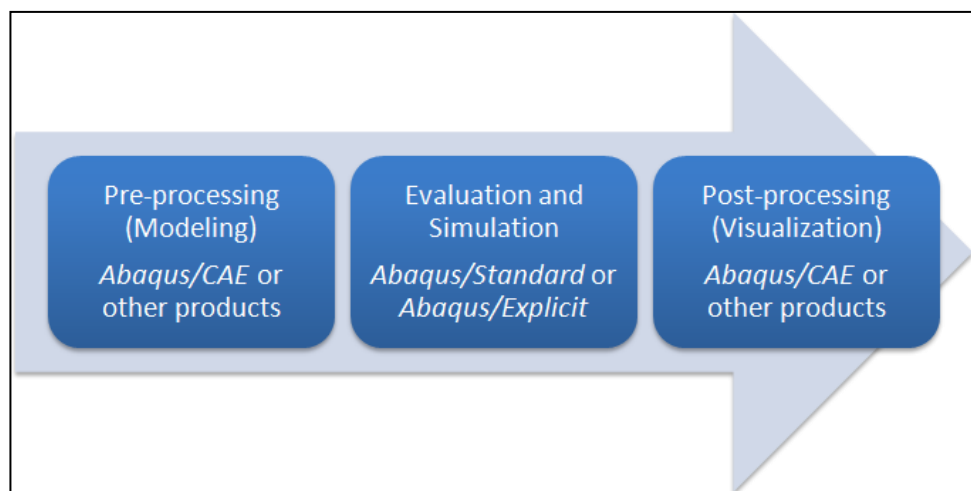


Figure 6.1 The 3 blocks of FE analysis in Abaqus

Object

The primary object of this study was to develop a finite element model which could correctly simulate the experimental test conducted on 1 m x 1 m grid-wall subjected to compression, for an in deep understanding of the collapse phase. The experimental outputs provide lots of information, but the stress-strain distribution inside the wall and the coactive state between steel and concrete remain essentially unknown. The model, that wants to fill this gap, include the bond-slip relationship between steel-bars and concrete and non-linear constitutive laws both in tension and in compression for the concrete. The goal was to capture the ultimate state and the mechanisms that aid the collapse of the wall. In this chapter all the building phases of the model will be shown and analyzed. The experimental test chosen to be reproduced was the *CC14_02* because it shown the most reliable data of the experimental campaign.

Introduction

To create the model the Abaqus/CAE was used. Abaqus/CAE, means "Complete Abaqus Environment" (an acronym with an obvious root in Computer-Aided Engineering).

The set-up of this chapter reflect the sequence of the different steps presented by Abaqus/CAE for the modeling purposes.

The generation of a geometric model represents a fundamental step for the creation of a FE model in Abaqus, because the generation of the mesh rely on the geometric model. A geometric model, is essentially a set of various geometric entities (*Part module*), available in Abaqus. Once geometric entities has been build, their properties must be defined (*Property Module*) and it is necessary to assign the spatial relations between geometric entities (*Assembly module*). It follows the choice of the resolution-algorithm and of the interesting output(*Step module*). A mesh must be created (*Mesh module*) and interactions between parts must be assigned (*Interaction module*). If all these steps have been set with sufficient accuracy, it is possible to create an input file (*inp.file* with Job module) to be analyzed by the

Abaqus solver that provide an *odb.file* in which all the output requested can be visualized(*Visualization module*).

Since this is a three-dimensional model, *Solid deformable elements* were used for creating the geometric model.

In the model creation it was decided to apply the following simplification compared to the actual structure to be tested:

- Reinforcing bars of squared section: through this simplification the mesh around the bars resulted less complex. To not compromise the results on the stress state of the bars, a squared section with equivalent area was adopted. This assumption leads to an increase of the lateral surface of the bar and therefore a greater surface on which develop the adhesion between concrete and reinforcement . This effect was considered in *Par 5.6*.



Circular section	Squared equivalent section
Diameter[mm]	Edge lenght[mm]
8	7.1

Another important aspect is that, nonlinear analysis is characterized by the non-proportional nature of the load-deformation behaviour, which means that the structural response against an incremental loading is affected by the instantaneous loading level and the deformed geometry of the structure. In other words, the stiffness matrix of the structure is a function of element force as well as the deflection of the structure and, therefore, for medium to huge size problems, the instantaneous stiffness equation can only be solved numerically by an incremental and iterative procedure allowing for the geometrical change of the structure. These aspects will be analyzed in the xx paragraph concerning the definition of the "Step Module".

FE model for panels subjected to centered axial compression

6.1 The "Part" module

The real model consist of 32 different elements:

- 2 high strength reinforced concrete bases(top one and bottom one)
- 1 core made of 4 pillars and 4 joist(the grid-wall)
- 8 horizontal steel bars
- 8 vertical steel bars
- 12 different wood-concrete cores that fill the "holes" of the grid-wall
- 1 top steel plate for load-diffusion purposes

In the following *Figure 6.2* the real specimen with the test set-up and the numerical model are reported:

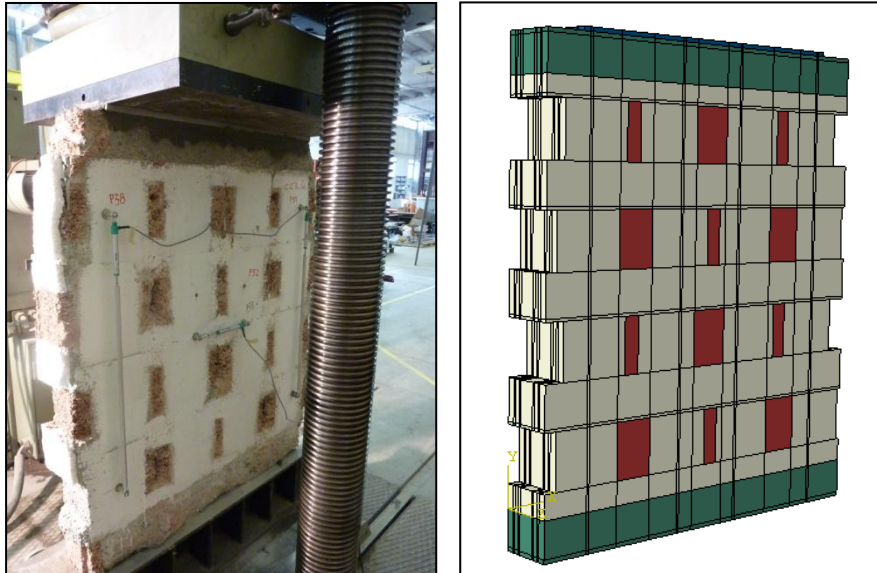


Figure 6.2 The real model and the numerical one

Even if 32 different element compose the specimen, only 8 different Parts (geometrical entities) are necessary to define the whole geometry; as a matter of fact can be used only 1 Part to define the 8 different vertical steel bars, and 1 Part for the horizontal steel bars. The same for the wood-concrete elements: there's the need of only 1 Part for smaller one and another for the bigger elements.

6.1.1 The Units

In Abaqus CAE before starting to define any model, it is necessary to decide which system of units to use. ABAQUS has no built-in system of units. All input data must be specified in consistent units.

In the model everything was consistent with [N] and [mm].

6.1.2 The two bases

The dimension of the two bases were identical: 1m x 0.1m x 0.14 m of width. Their main function was to create a sort of anchorage-length for the vertical bars and to provide a diffusive zone for the load and the boundary. With the "Cut:extrude" command the holes for the vertical steel were recreated.

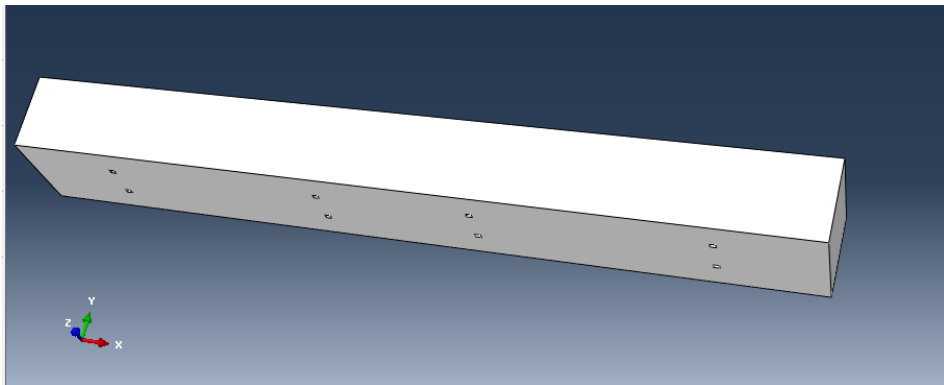


Figure 6.3 The Part representing the upper base

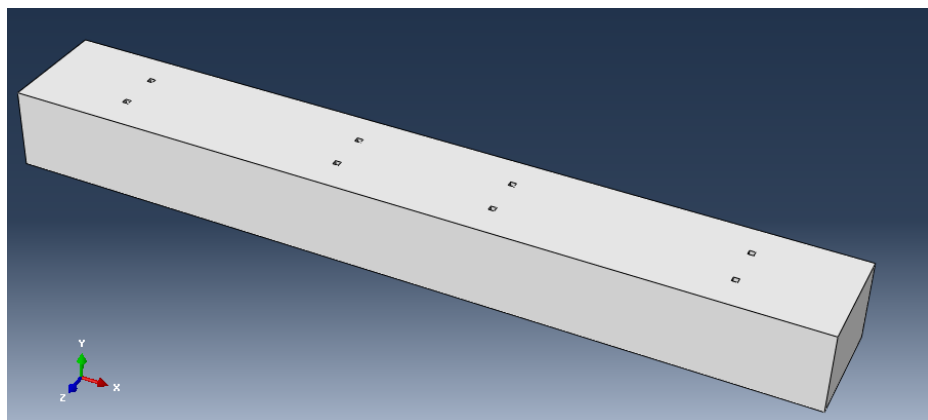


Figure 6.4 The Part representing the bottom base

6.1.3 The concrete core

It represent the most important element of the entire model. It is the grid-wall made of 4 pillars and of 4 connector beams 12 cm high, that the campaign want to test. Also in this case the "Cut:extrude" command was used to reproduce the wood-concrete holes and the place of both vertical and horizontal bars.

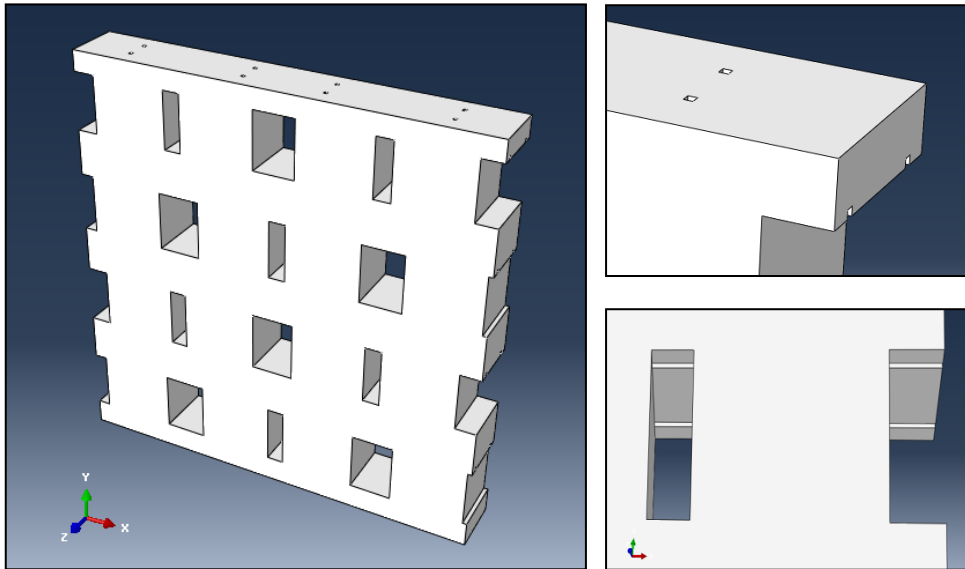


Figure 6.5 The concrete core with the place for bars

The main dimensions are 1 m x 1m x 0.14 m and the "holes-pattern" try to reproduce the real one observed in laboratory.

6.1.4 The steel bars

In the model-creation it was decided to apply the following simplification compared to the actual structure: reinforcing bars of squared section. Through this simplification the mesh around the bars resulted less complex. To not compromise the results on the stress state of the $\Phi 8$ bars, a squared section with equivalent area was adopted (7.07 mm of edge). The following *Figure 6.6* report the positioning of the bars inside the concrete core. The vertical bar is 1.18 m long (with anchor. length), the horizontal is 1 m long.

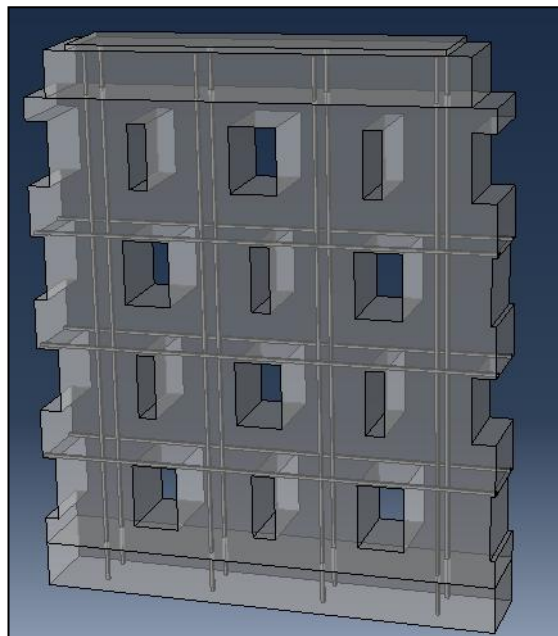


Figure 6.6 The position of the bars inside the concrete core

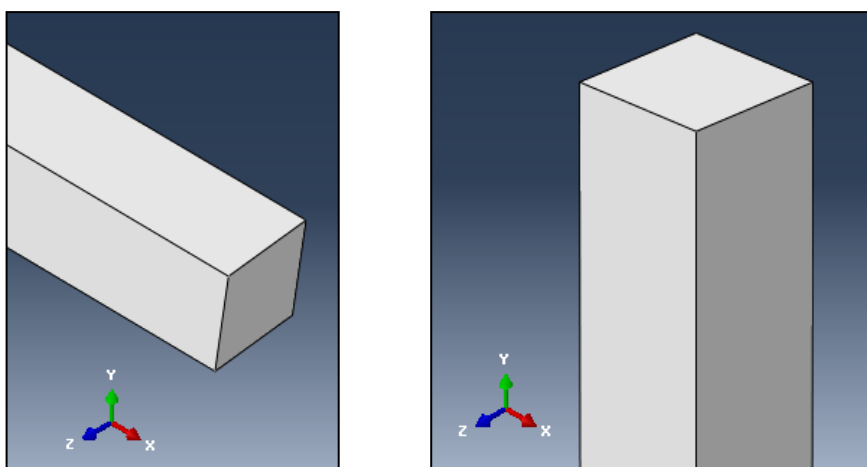


Figure 6.7 The Horizontal Bar Part and the Vertical Bar Part

6.1.5 The wood-concrete cores

They represent what remain of the wood-concrete formwork block removed to focus on the structural part of the grid wall and to underline the cracking pattern.

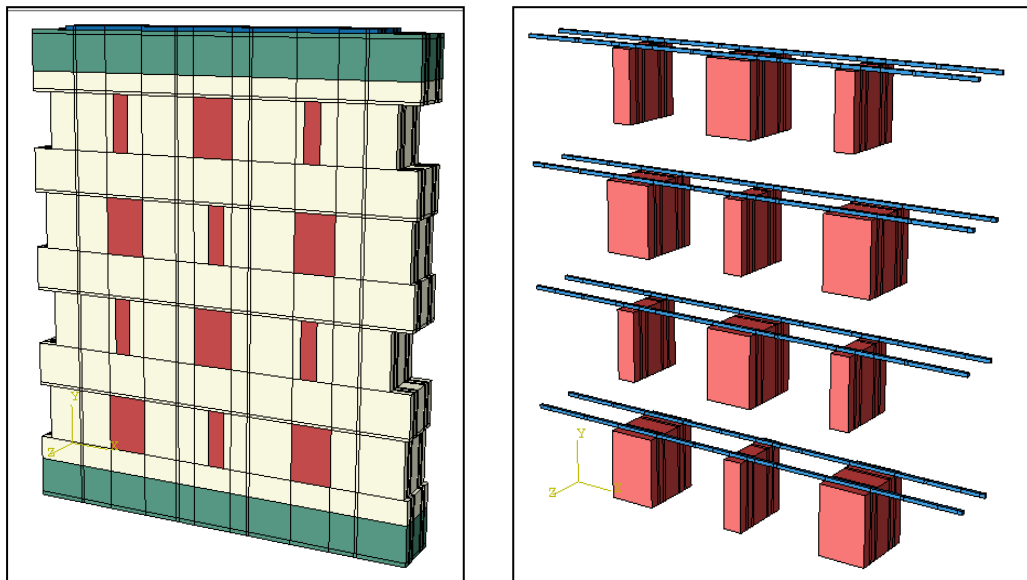


Figure 6.8 The Wood-concrete cores in the model

The bigger one have a base of 10 cm for 14 cm of height. The smaller are 4 cmx 14 cm.

6.2 Mechanical characterization of the materials

One of the most challenging and tricky modules of the whole modeling process involved the calibration of the constitutive laws of the materials used. The results were strongly influenced by the definition of the laws implemented. When the information about the material are scarce the only way to proceed is to rely on the few experimental information, to make reference to literature review and to start a long calibration process. The experimental information are collected in *Chapter 2*; the constitutive laws proposed by the literature are reported in *Chapter 4*.

6.2.1 Steel

The reference is Chapter 2 *par.* 2.2.2 where the 3 tensile tests conducted on three different $\Phi 8$ bars allowed the definition of the main parameters:

$$f_{ym} = 500 \text{ MPa}$$

$$f_{tm} = 550 \text{ MPa}$$

$$E = 200000 \text{ Mpa}$$

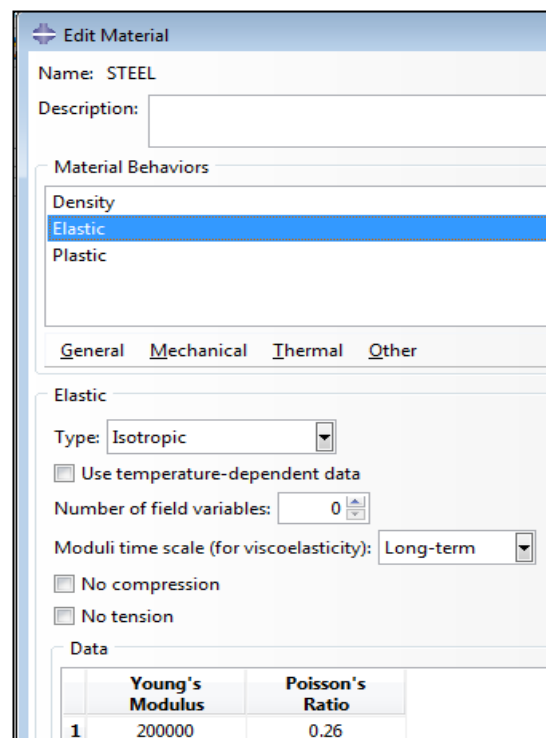
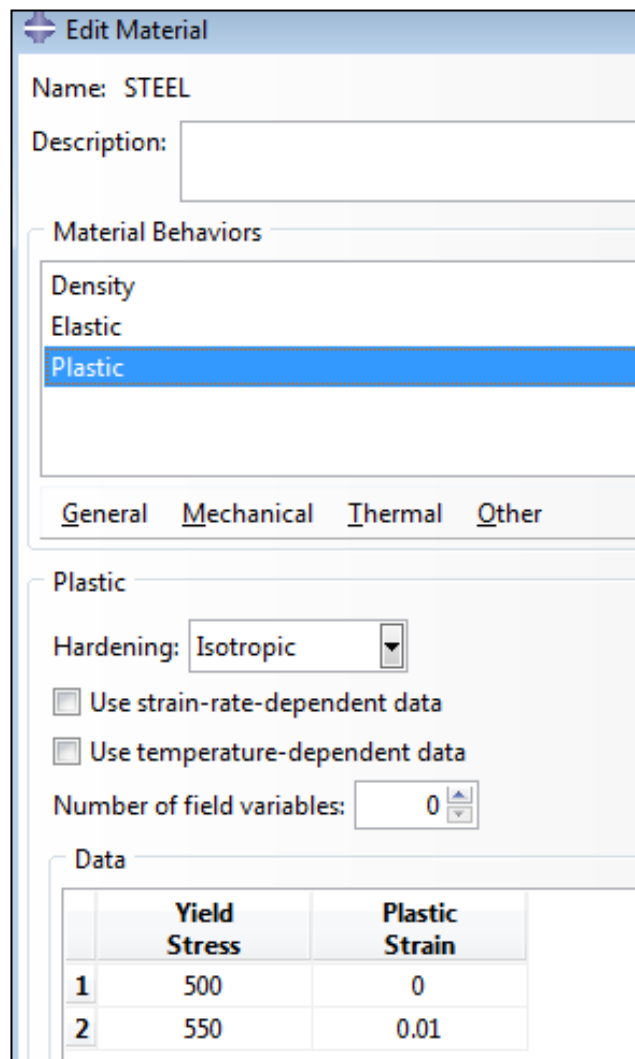


Figure 6.9 The Elastic material editor for STEEL

The definition of the material "STEEL" requests also the density that was simply defined as 7850 kg/m^3 , inserted in Abaqus in N/mm^2 and the definition of the plastic properties as reported in *Figure 6.10*.



The screenshot shows the 'Edit Material' dialog box for the material 'STEEL'. The 'Plastic' behavior is selected. The 'Hardening' is set to 'Isotropic'. The 'Number of field variables' is set to 0. The 'Data' table shows two rows of plastic data.

	Yield Stress	Plastic Strain
1	500	0
2	550	0.01

Figure 6.10 The Plastic material editor for STEEL

The Isotropic Hardening was set. Furthermore each Abaqus inelastic editor, mandatory requests that the 1st Plastic strain is set to zero.

6.2.2 Concrete

6.2.2.1 Kent-Park formulation implemented for compressive behaviour

The theoretical framework was reported in *Par 4.5*. The descendant branch of σ - ϵ curve of concrete is strictly related to the presence of confinement. The base Kent-Park formulation *without confinement* was built on the base of the results of compressive tests on cubic specimen reported in *Table 2.1* of *Chapter 2*.

Here below the curve without confinement is reported:

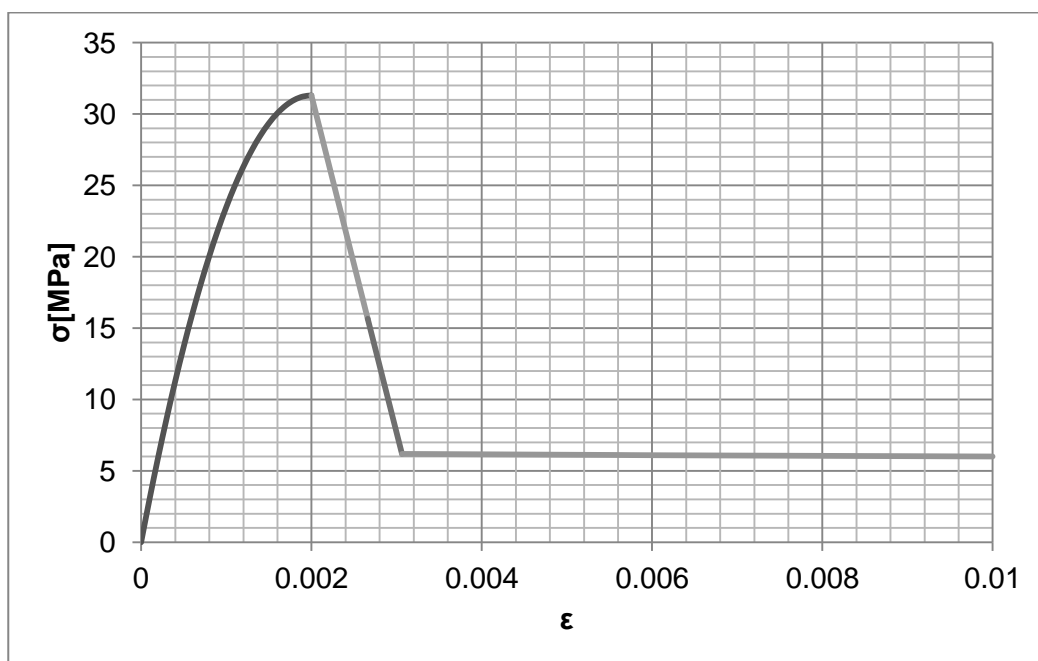


Fig. 6.11: Kent-Park σ - ϵ formulation w/o confinement

In the following table the σ - ϵ *inelastic* definition of the ascendant branch is reported:

KENT-PARK Constitutive Concrete		ϵ_0	0.002	
EPS	SIGMA			
0	0			
0.0001	3.052424102			
0.0002	5.948313636			
0.0003	8.687668599			
0.0004	11.27048899			
0.0005	13.69677482			
0.0006	15.96652607			

Pro_abaqus	INELASTIC STRAIN	dc
E[Mpa]		
26610.8768	0	0

0.0007	18.07974276		2.05882E-05	0
0.0008	20.03642488		4.70588E-05	0
0.0009	21.83657243		7.94118E-05	0
0.001	23.4801854		0.000117647	0
0.0011	24.96726381		0.000161765	0
0.0012	26.29780765		0.000211765	0
0.0013	27.47181692		0.000267647	0
0.0014	28.48929162		0.000329412	0
0.0015	29.35023175		0.000397059	0
0.0016	30.05463732		0.000470588	0
0.0017	30.60250831		0.00055	0
0.0018	30.99384473		0.000635294	0
0.0019	31.22864659		0.000726471	0
0.002	31.30691387	f'cm	0.000823529	0

Table. 6.1: Kent-Park σ - ε formulation W/O confinement

The insertion of this type of curve, with a connected damage law didn't provide good results. So an amount of confinement was inserted. The final σ - ε inelastic (as Abaqus request) was reported in Figure 6.12:

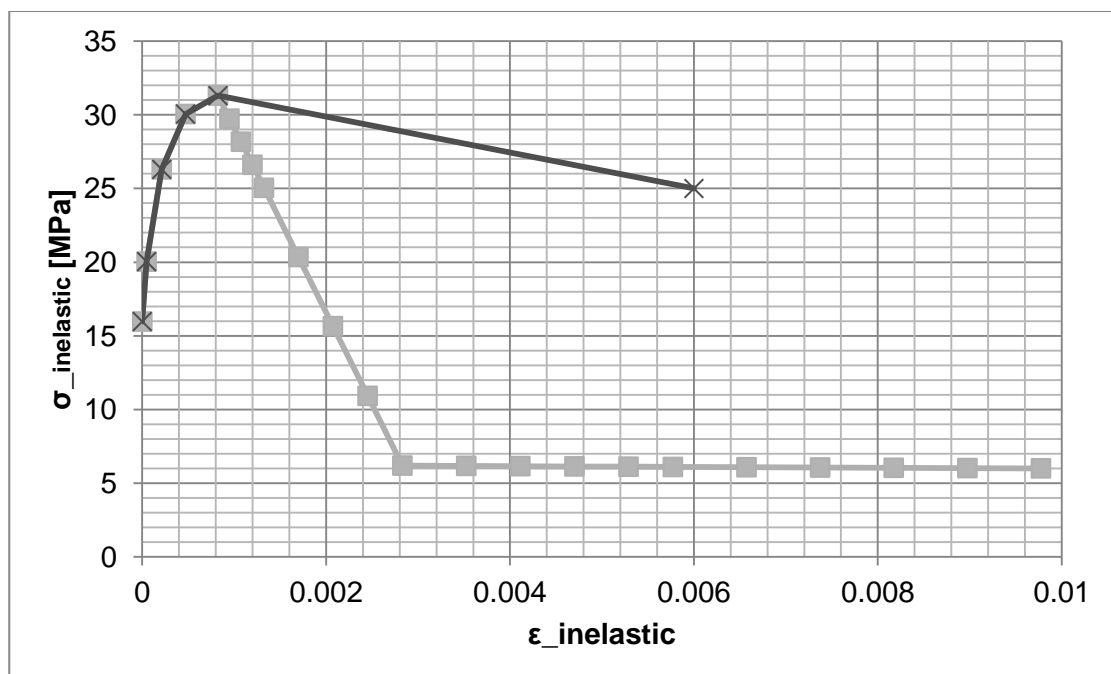


Fig. 6.12: Kent-Park σ - ε formulation implemented

For the inelastic quantities definition the *Par 4.3.1* can be consulted as reference. In Table 6.2 are reported the used quantities.

COMPRESSION				
SIGMA	EPS INEL		DAMAGE	EPS_INEL
15.9665	0		0	0
20.0364	4.71E-05		0	4.71E-05
26.2978	0.000212		0	0.000212
30.0546	0.000471		0	0.000471
31.3069	0.000824		0	0.000824
25	0.006		0.201454	0.006

Table. 6.2: Kent-Park σ - ε inelastic formulation implemented in the CDP formulation

6.2.2.2 Formulation implemented for traction behavior

Considering:

- the tension stiffening effects in *Par 4.3.1.2*
- the experimental curves reported in *Par. 4.6.2*.

the traction behavior of concrete implemented was:

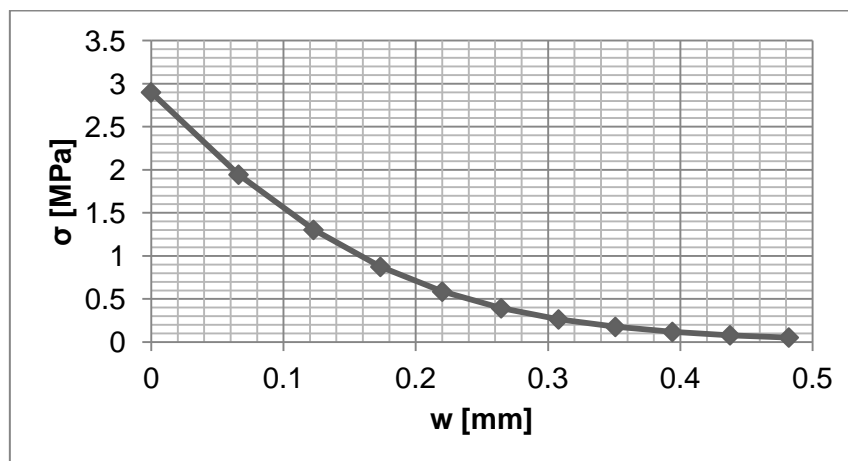


Fig. 6.13: Post-peak traction law σ - w [mm] implemented

With a peak resistance of 2.9 MPa. In the following table the values implemented are reported:

TENSION				
SIGMA	DISPL_INEL		DAMAGE	DISPL-INEL
2.9	0		0	0
1.94393	0.066185		0.381217	0.066185
1.30305	0.12286		0.617107	0.12286
0.873463	0.173427		0.763072	0.173427
0.5855	0.22019		0.853393	0.22019
0.392472	0.264718		0.909282	0.264718
0.263082	0.308088		0.943865	0.308088
0.176349	0.35105		0.965265	0.35105
0.11821	0.394138		0.978506	0.394138
0.079239	0.437744		0.9867	0.437744
0.053115	0.482165		0.99177	0.482165

Table 6.3: Concrete traction behavior implemented in the CDP model

To edit the material property "CONCRETE" the following editor was set:

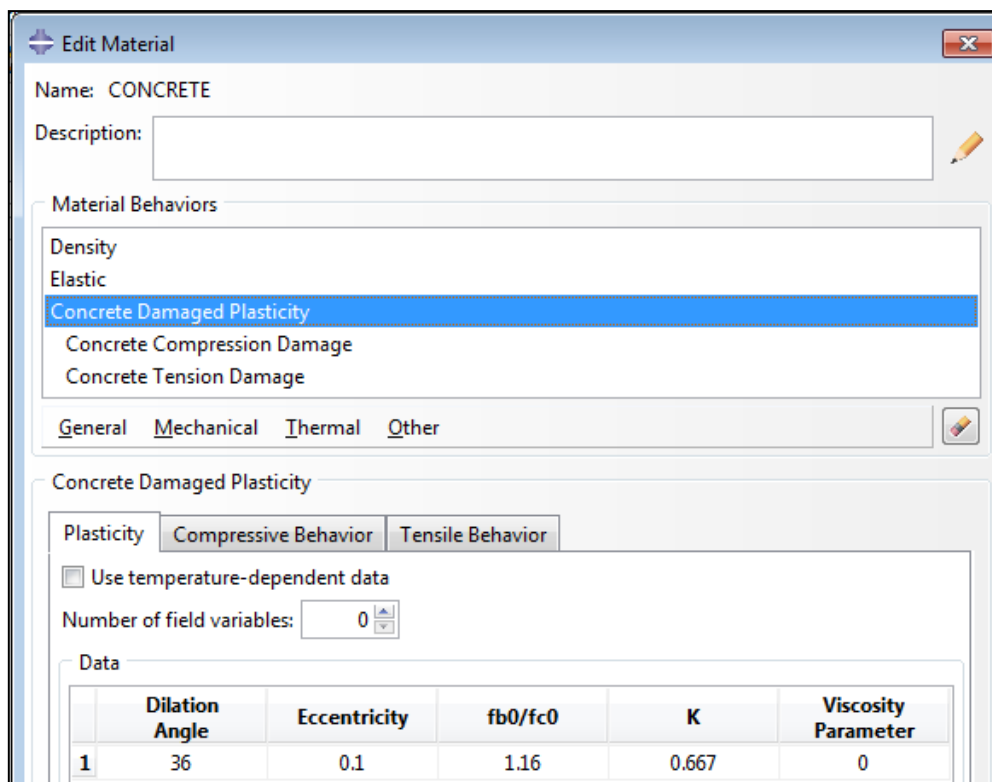


Fig. 6.14: Post-peak traction law σ - w [mm] implemented

For what concern "Compressive behavior" editor and "Tensile behavior" editor the reference values were reported in Table 6.2 and Table 6.3.

6.2.3 The high strength concrete bases

The two different bases, inserted for diffusion and anchoring purposes, were reinforced in the laboratory tests. The presence of the steel bars was neglected in the model but taken into account inserting a Young's modulus of 500000 MPa.

	Young's Modulus	Poisson's Ratio
1	500000	0.26

Fig. 6.15: Material editor for the 2 bases

The value of 500000 MPa was chosen considering a high value, but not too high to not introduce numerical problems.

6.2.4 The wood-concrete elements

To define the properties of the wood-concrete strength, a bad masonry was considered; a f_{cm} of 1.5 MPa with a Young's modulus of 300 MPa found in literature was inserted.

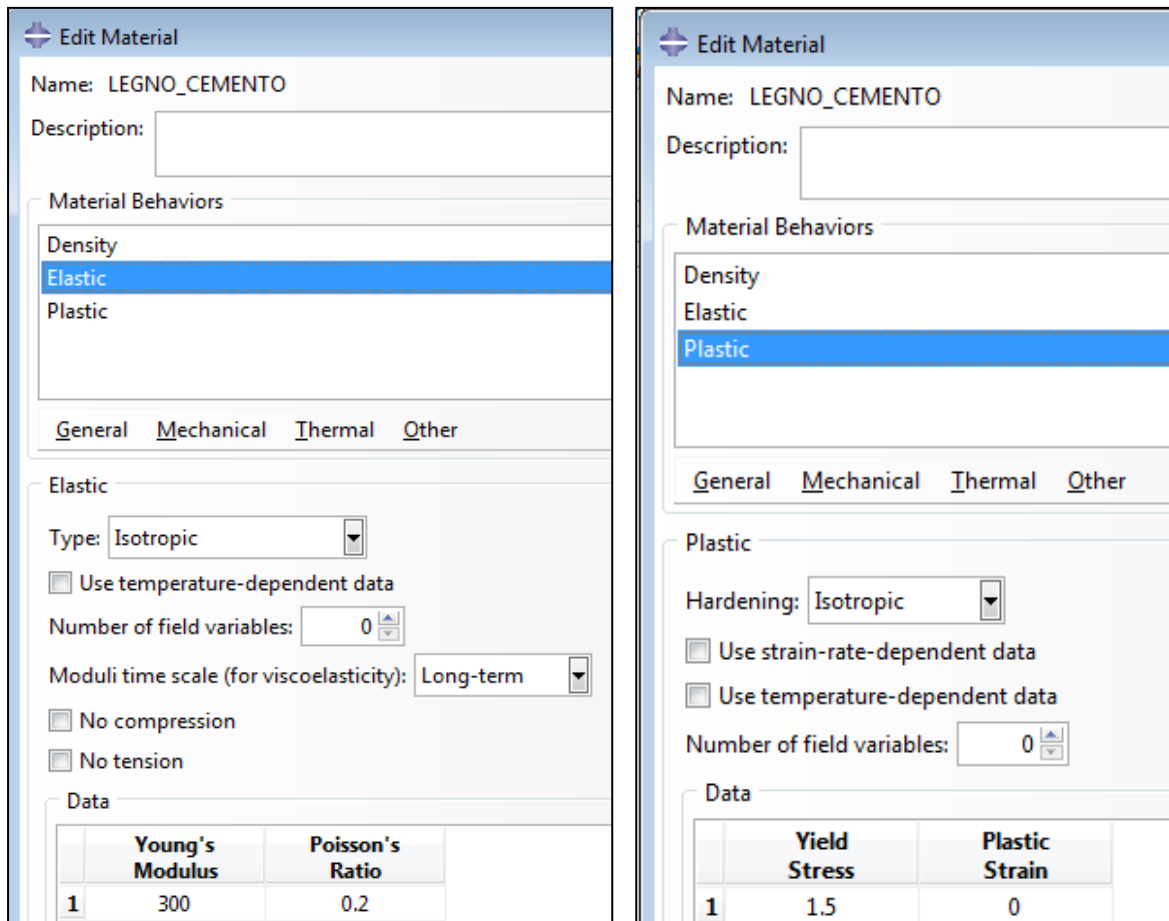


Fig. 6.16: Elastic properties of wood-concrete elements

Once the Materials were defined, different "Sections" were created to assign the material property to the different "Parts":

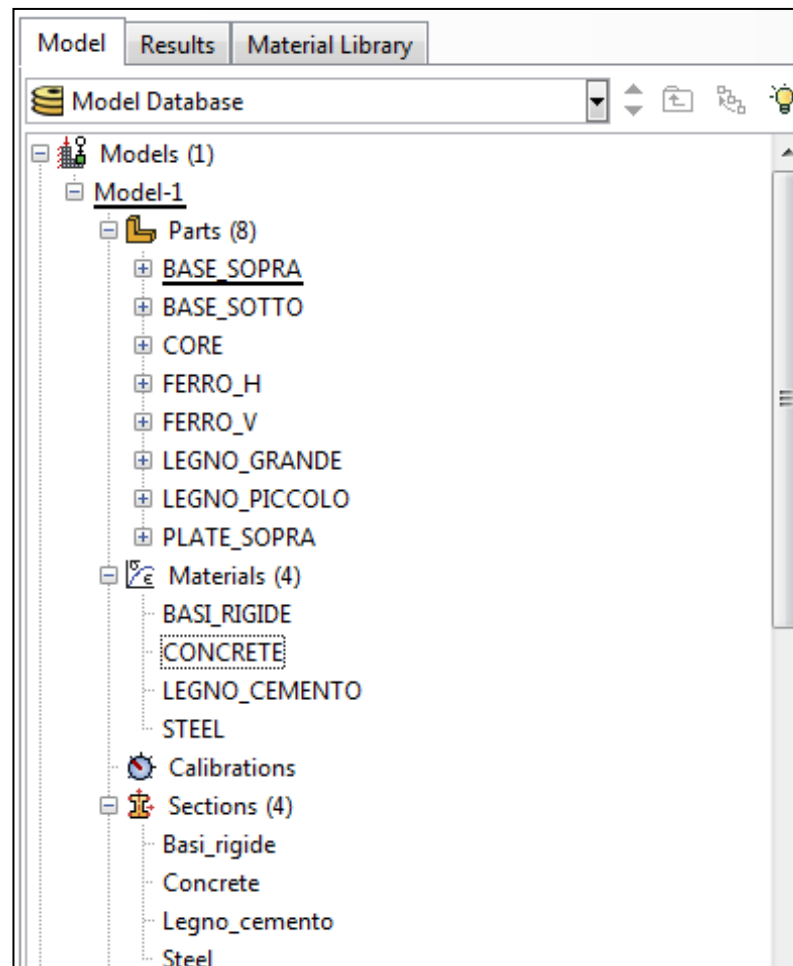


Fig. 6.17: Section editor

6.3 The assembly

Despite of the different figures used to better show the single elements in the entire context, after "Part" and "Material" modules, all the elements were still conceived as isolated. This module was used to *assemble* the model and to create all that "sets" useful for the definition of the next modules.

Recalling the 8 different Parts, **32 Instances** was identified and assembled with "**Coincident point constraint**". This type of "Position-constraint" allow a simple localization between instances that share the location of a chosen point.

The Part is a geometrical entity that can be recalled more than one time, the Instance is a single element of the final model to which a mesh is assigned. The "independent mesh" was set for each instance. The alternative was to define the mesh on Parts.

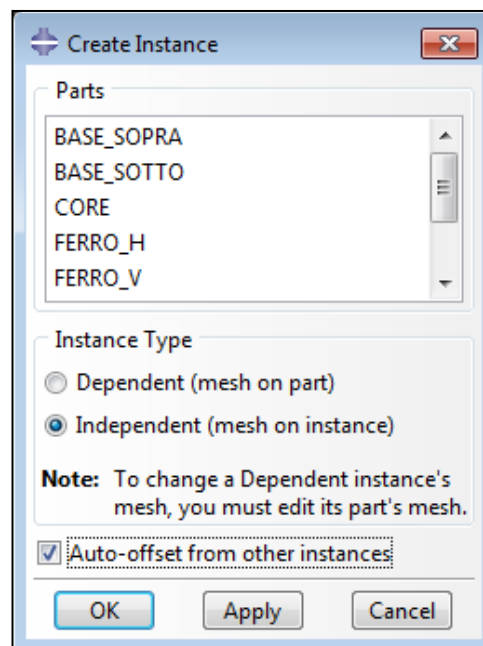


Figure 6.18 Instance editor in Abaqus

The use of "Independant mesh" on instances was the first step for a simplification in the creation of the global mesh.

The different surfaces necessary to implement the contact interaction between steel and concrete were created. More information are given in the "Interaction module" paragraph 6.5.

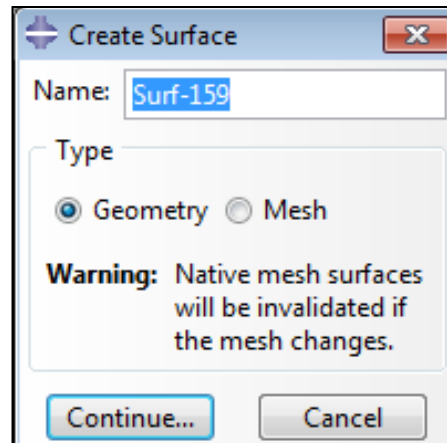
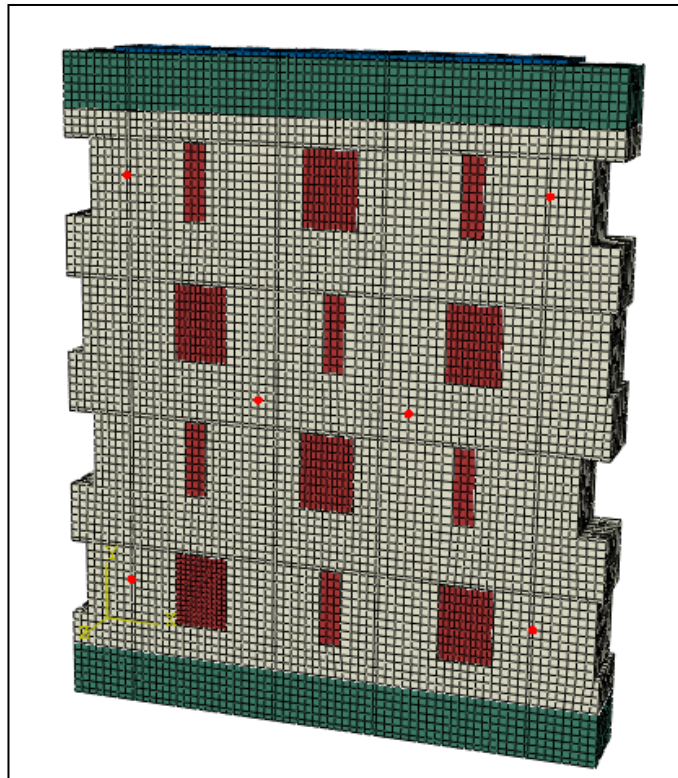


Figure 6.19 Surface editor in the Assembly module

Quite important is the definition of the "spy-nodes", that are "Set" of the Assembly module. The goal was to reproduce the vertical shortening and horizontal lengthening measured by the LVDT as will be reported in *Chapter 7*. The red points reported in the following figures were considered for both sides of the wall.



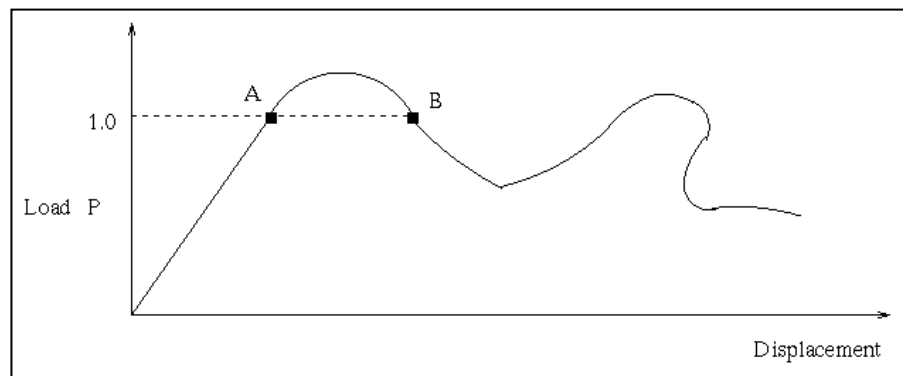
The spy-nodes to monitor ΔL_v and ΔL_h

6.4 The "Step" module

This module allowed the selection of the *type of analysis* to be performed on the model (defining also the associated parameters) and the selection of the *variables to be included in the output files*.

For what concern the type of analysis two ingredients must be mentioned: the use of "Non linear geometric option" called "**NLGEOM**", and the use of "Modified Riks Method" called "**RIKS**". The "Non linear geometric option" request to be set in a large deformation analysis, where it is necessary to take into account the changes in geometry during the steps. The stiffness matrix will be calculated using the current configuration that means using the current position of the nodes.

Modified RIKS algorithm is generally used to obtain nonlinear static equilibrium solutions for unstable problems, where the load-displacement response can exhibit the type of behavior sketched in *Figure 6.20* —that is, displacement may decrease as the solution evolves.



. *Figure 6.20 Typical unstable static behaviour*

"Modified Riks Method" is one of the evolutions of the **arc-length method** proposed by Wempner (1971), Riks (1979) and Ramm (1980; 1981) for nonlinear analysis. The basic concept of this spherical arc-length method is to constrain the load increment so that the dot product of displacement along the iteration path remains a constant in the 2-dimensional plane of load versus deformation, as can be seen in *Fig. 6.21*.

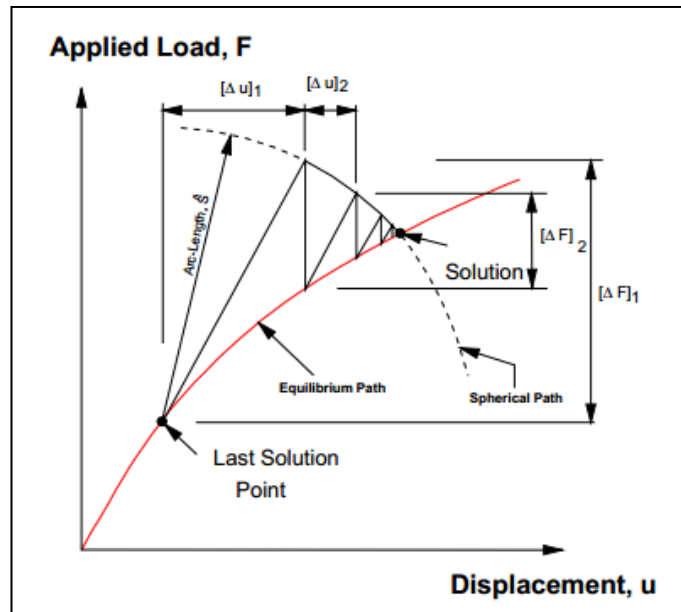


Figure 6.21 .- Typical Arc-length method algorithm

It is assumed that the loading is proportional - that is, that all load magnitudes vary with a single scalar parameter as it happens in experimental compression test.

$$P_{\text{total}} = P_0 + \lambda(P_{\text{ref}} - P_0),$$

where P_0 is the “dead load,” P_{ref} is the reference load vector, and λ is the “load proportionality factor.” The load proportionality factor is found as part of the solution. In addition, it is assumed that the response is reasonably smooth - that sudden bifurcations do not occur. Several methods have been proposed and applied to such problems. The most successful seems to be the modified Riks method - see, for example, Crisfield (1981), Ramm (1981), and Powell and Simons (1981) - and a version of this method has been implemented in Abaqus. The essence of the method is that the solution is viewed as the discovery of a single equilibrium path in a space defined by the nodal variables and the loading parameter. Development of the solution requires that we traverse this path as far as required. The basic algorithm remains the Newton method; therefore, at any time there will be a finite radius of convergence. Further, many of the materials (and possibly loadings) of interest will have path-dependent response. For these reasons, it is essential to limit the increment size. In the modified Riks algorithm, as it is implemented in Abaqus, the increment size is limited by moving a given distance (determined by the standard, convergence rate-dependent, automatic incrementation algorithm for static case in Abaqus/Standard) along the tangent line to the current solution point

and then searching for equilibrium in the plane that passes through the point thus obtained and that is orthogonal to the same tangent line.

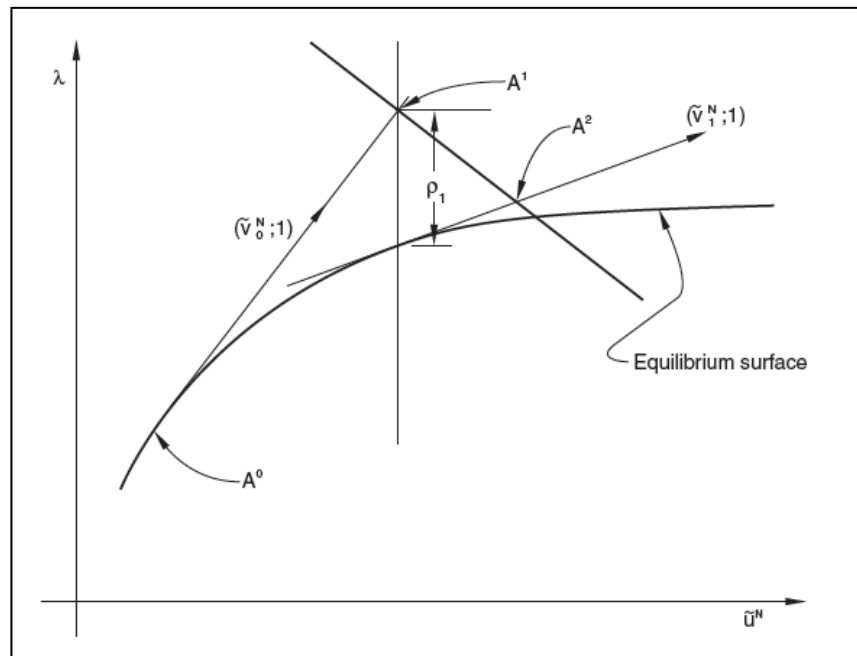


Figure 6.23 Modified Riks algorithm

All these concepts are implemented in Abaqus in the step editor reported in the Fig. 6.24 and Fig.6.25 where the choice of the step is also reported.

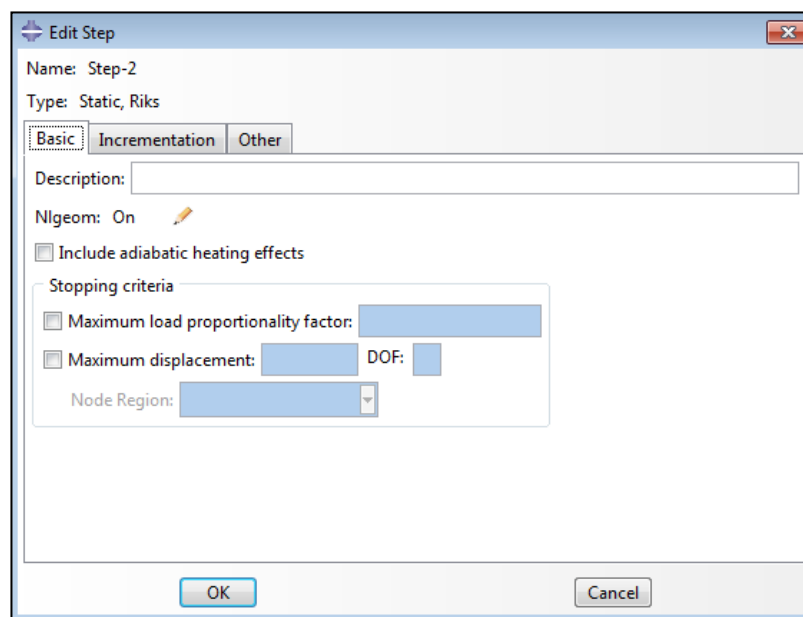


Figure 6.24 NLGEOM editor

Abaqus/Standard uses Newton's method to solve the nonlinear equilibrium equations. The Riks procedure uses only a 1% extrapolation of the strain increment. The user should provide an initial increment in arc length along the static equilibrium path, Δl_{in} , when the step must be defined. The initial load proportionality factor, $\Delta \lambda_{in}$, is computed as

$$\Delta \lambda_{in} = \frac{\Delta l_{in}}{l_{period}},$$

where l_{period} is a user-specified total arc length scale factor (typically set equal to 1). This value of $\Delta \lambda_{in}$ is used during the first iteration of a Riks step. For subsequent iterations and increments the value of λ is computed automatically, so the user have no control over the load magnitude. The value of λ is part of the solution. Minimum and maximum arc length increments, Δl_{min} and Δl_{max} , can be used to control the automatic incrementation.

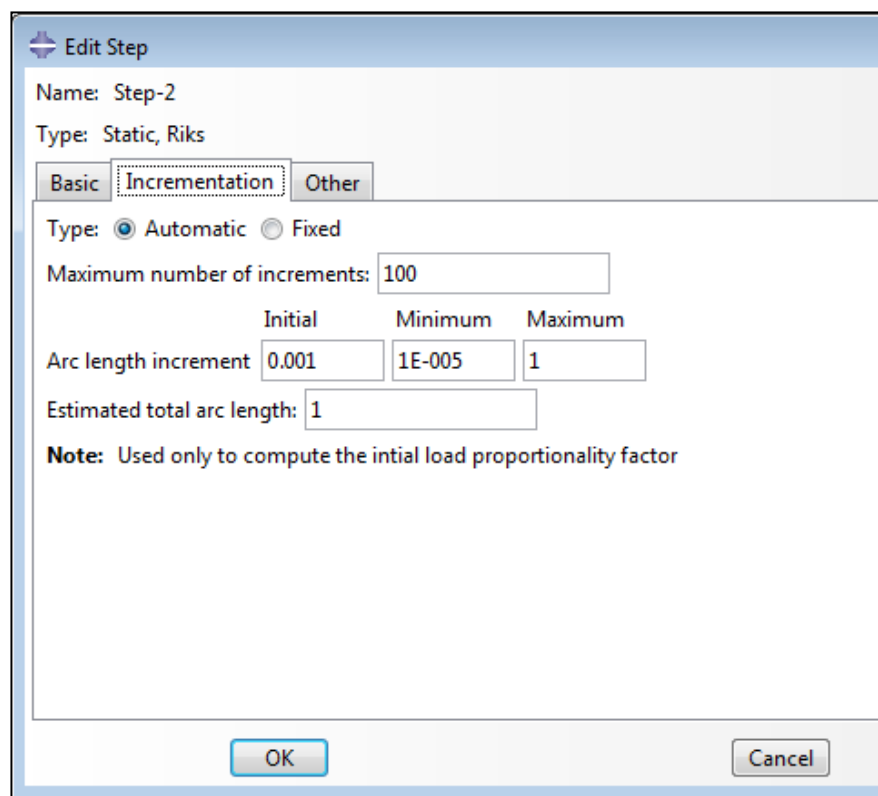


Figure 6.25 Riks increment step editor

For what concerns the selection of the *output files*, in Fig.26 was reported the "Field output request editor" for the whole model.

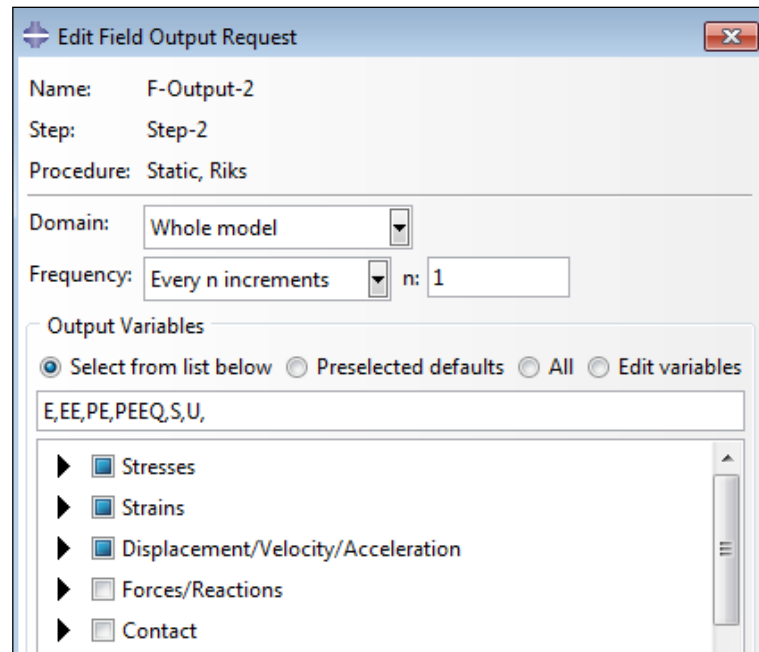


Figure 6.26 Field output request for the whole model

Finally, the "History output Request" editor allow to define the output story of a predefined sets of points called "spy nodes" that will be better defined in the Mesh Module paragraph.

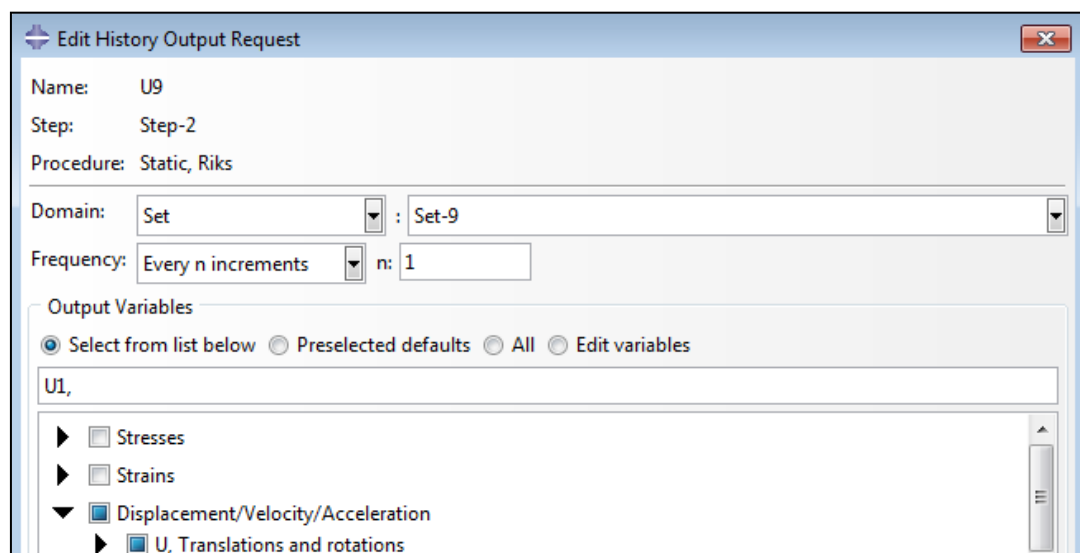


Figure 6.27 History output editor

6.5 The "Interaction" Module

In the model two type of interactions were introduced:

-*"tie constraint"* between the bases in high-strength concrete and the concrete core, and to connect the wood-concrete elements to the concrete close to them.

-*surface based cohesive interactions* between steel bars and concrete

The theoretical framework under bond-slip interactions was fully examined in *Chapter 5*. Here below the Abaqus steps for the implementation are reported only.

Contact interactions for contact pairs and *general contact* are defined by specifying surface pairings. All these surfaces were defined in the Assembly module.

For what concern *"steel bars-concrete interaction"* one surface was defined for each of the 4 sides of the 16 steel-bars. For each side of the bars a concrete-pair surface was defined.

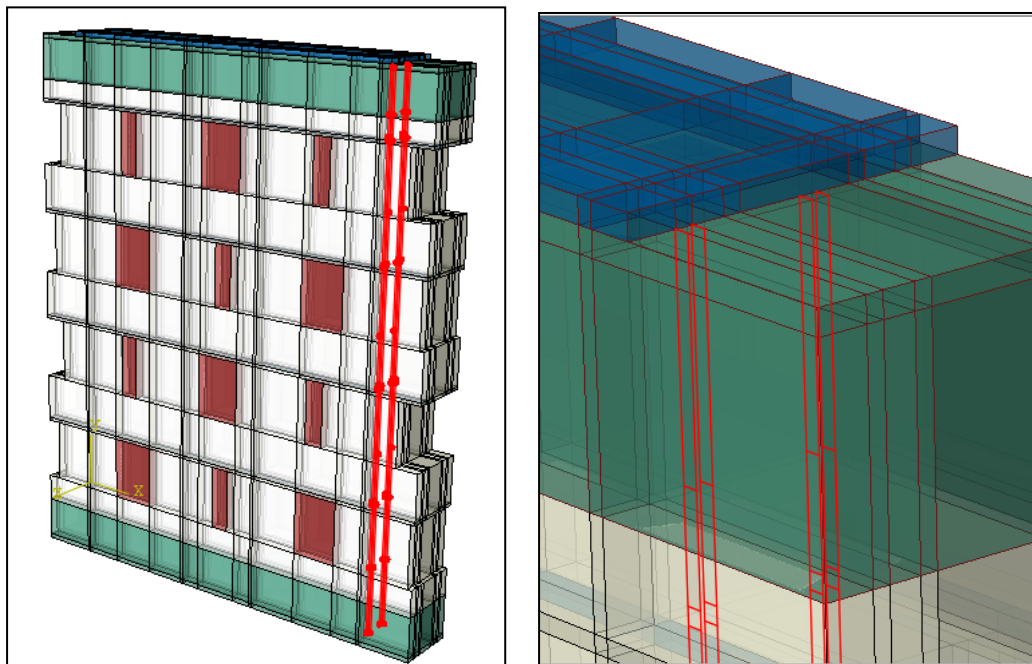


Figure 6.28 Some surfaces of the steel-bars

After the definition of the surfaces, the "Interaction Property" was defined, as proposed in *Paragraph 5.4*, in the three main steps reported in the following *Figure 6.29*, *Fig. 6.30*, *Fig. 6.31*, *Fig. 6.32*:

- Normal behaviour: to block the penetration between bars and concrete an "Hard contact" was introduced
- Cohesive behaviour: to define the ascendant part of the bond-slip law.
- Damage: that define the descending branch of the bond-slip law.

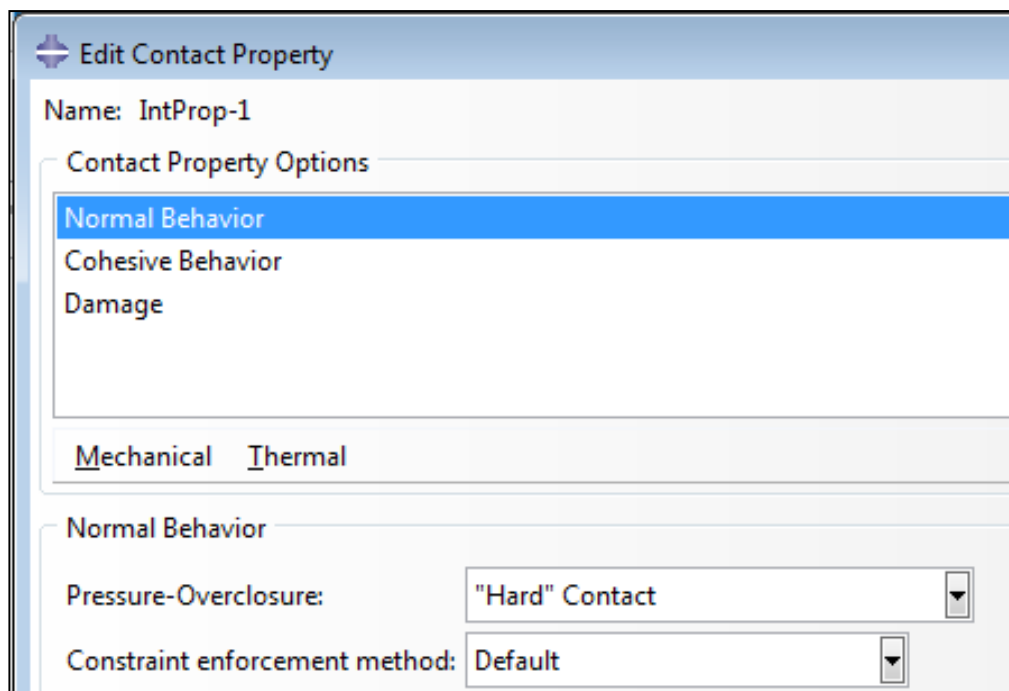


Figure 6.29 Normal behaviour in the Contact Property editor

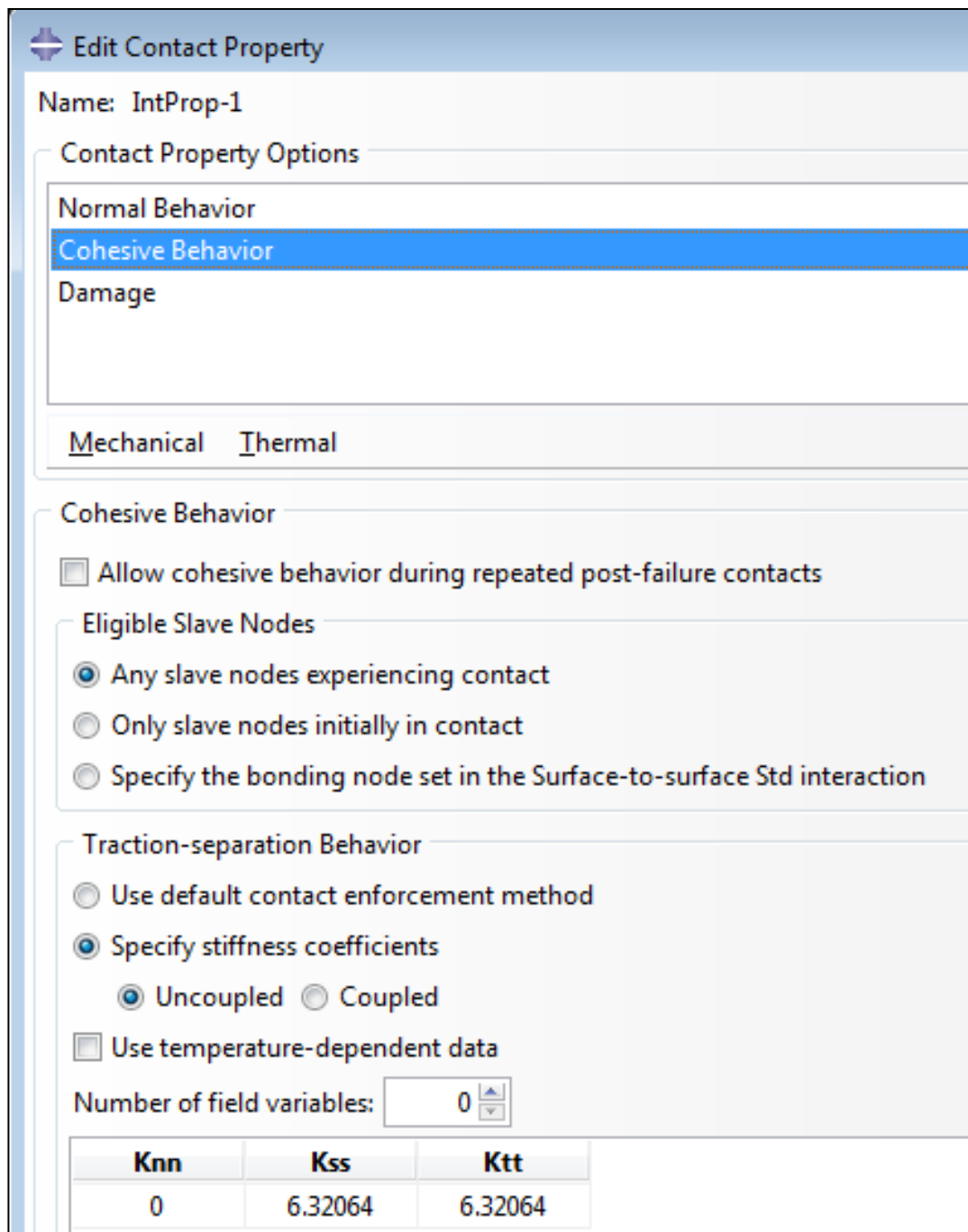
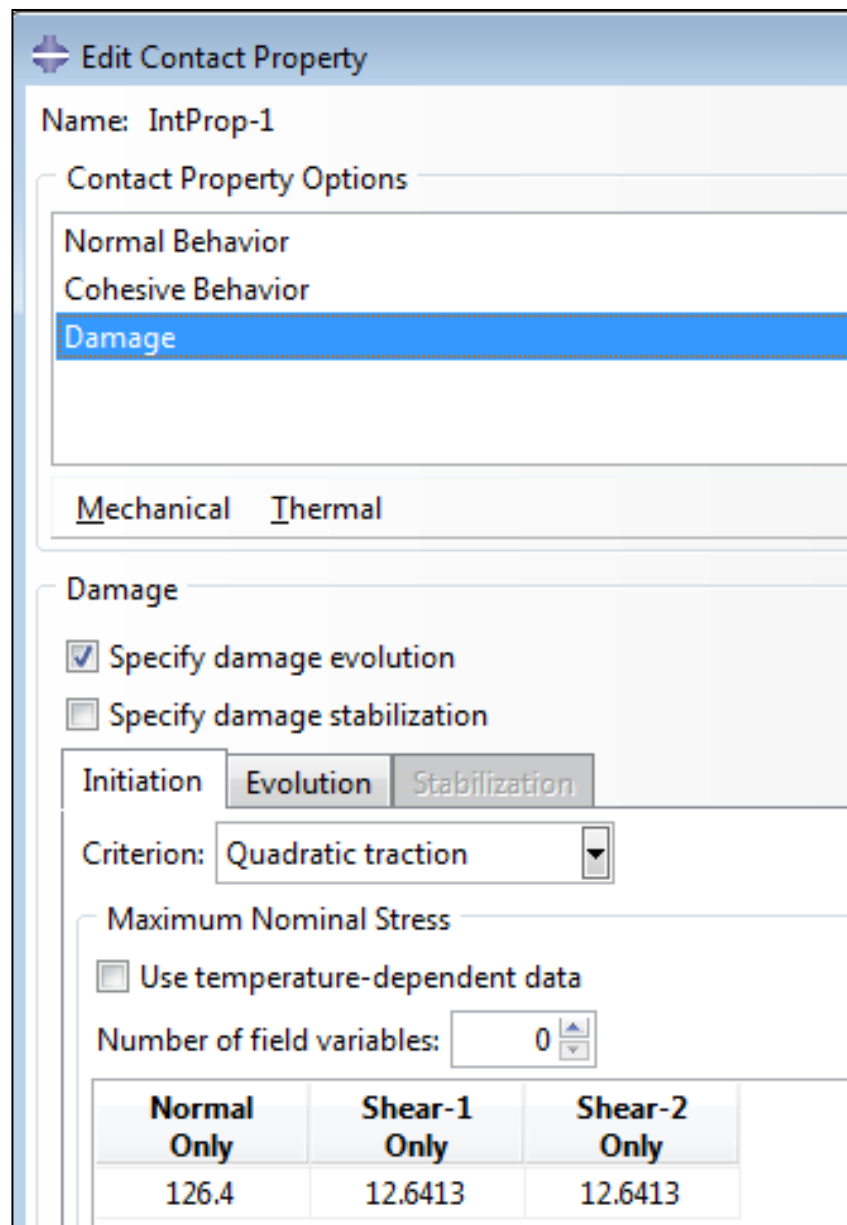


Figure 6.30 Cohesive behaviour in the Contact Property editor



Edit Contact Property

Name: IntProp-1

Contact Property Options

- Normal Behavior
- Cohesive Behavior
- Damage**

Mechanical Thermal

Damage

Specify damage evolution

Specify damage stabilization

Initiation Evolution Stabilization

Criterion: Quadratic traction

Maximum Nominal Stress

Use temperature-dependent data

Number of field variables: 0

Normal Only	Shear-1 Only	Shear-2 Only
126.4	12.6413	12.6413

Figure 6.31 Damage Cohesive behaviour in the Contact Property editor: the initiation criterion

Edit Contact Property

Name: IntProp-1

Contact Property Options

- Normal Behavior
- Cohesive Behavior
- Damage**

Mechanical Thermal

Damage

Specify damage evolution

Specify damage stabilization

Initiation **Evolution** Stabilization

Type: Displacement Energy

Softening: Linear Exponential Tabular

Specify mixed mode behavior:

- Tabular Power law Benzeggagh-Kenane

Mode mix ratio: Energy Traction

Specify power-law/BK exponent:

Displacement at Failure

Use temperature-dependent data

Number of field variables:

Total/Plastic Displacement
7

Figure 6.32 Damage Cohesive behaviour in the Contact Property editor: the linear evolution criterion

Same procedure for the wood-concrete elements and for the contacts between the bases and the core. In this case a simple *tie constraint* was used. A tie constraint doesn't need the perfect compatibility between meshes: Abaqus "ties" the d.o.f. of the nodes that are close one to another within a prescribed tolerance. The relation is a "master-slave" one as can be seen in the *Constraint editor* reported in *Figure 6.33*.

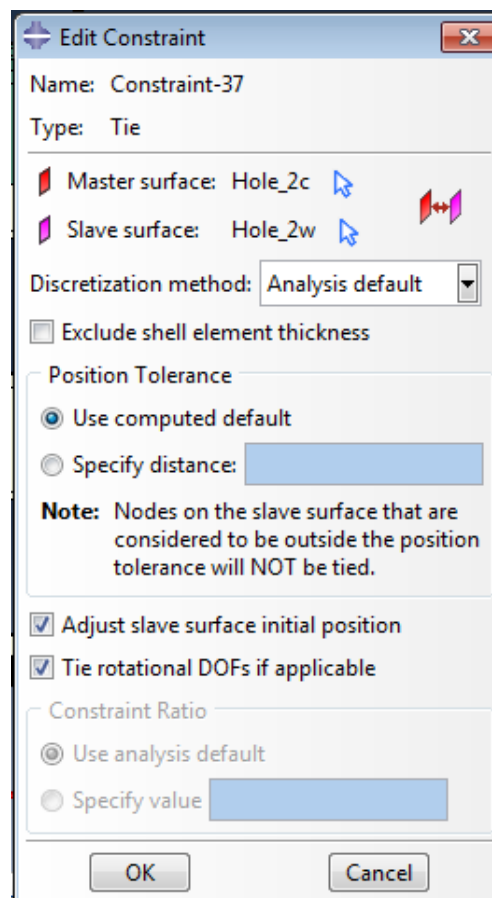


Figure 6.33 Tie constrain editor

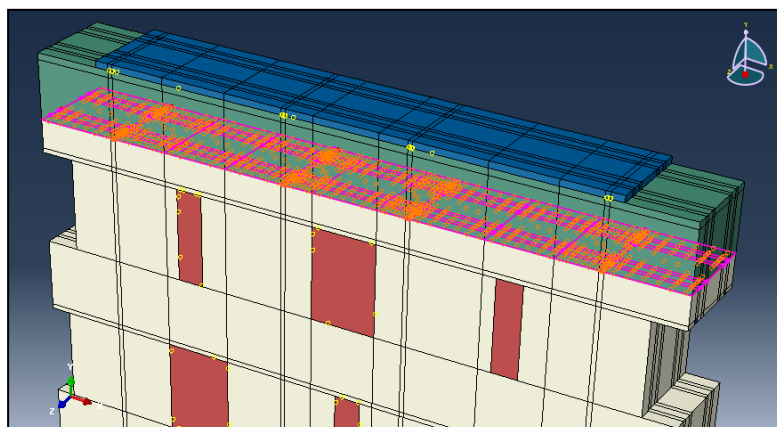


Figure 6.34 Tie constrain between upper base and concrete core

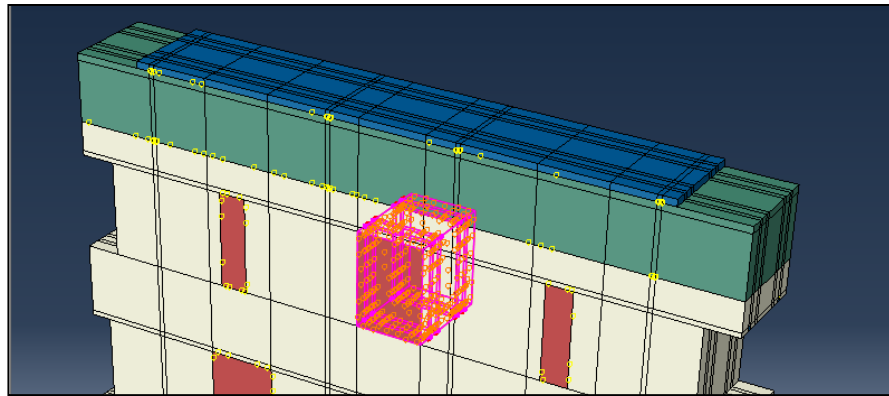


Figure 6.35 Tie constrain between a wood-concrete core and the main concrete core

6.6 Load and the boundary conditions

The Load History of *CC14_01 test* reached a peak value of 2497 kN. To reproduce the experimental proof a pressure of

$$p = \frac{2500 \text{ kN} \times 1000}{1000 \text{ mm} \times 140 \text{ mm}} = 17.857 \text{ MPa}$$

on the top-surface of the concrete core was applied. The solver divide the Load History in steps. The RIKS method is able to capture also higher values than the maximum provided, but the analysis can also "abort" at smaller values.

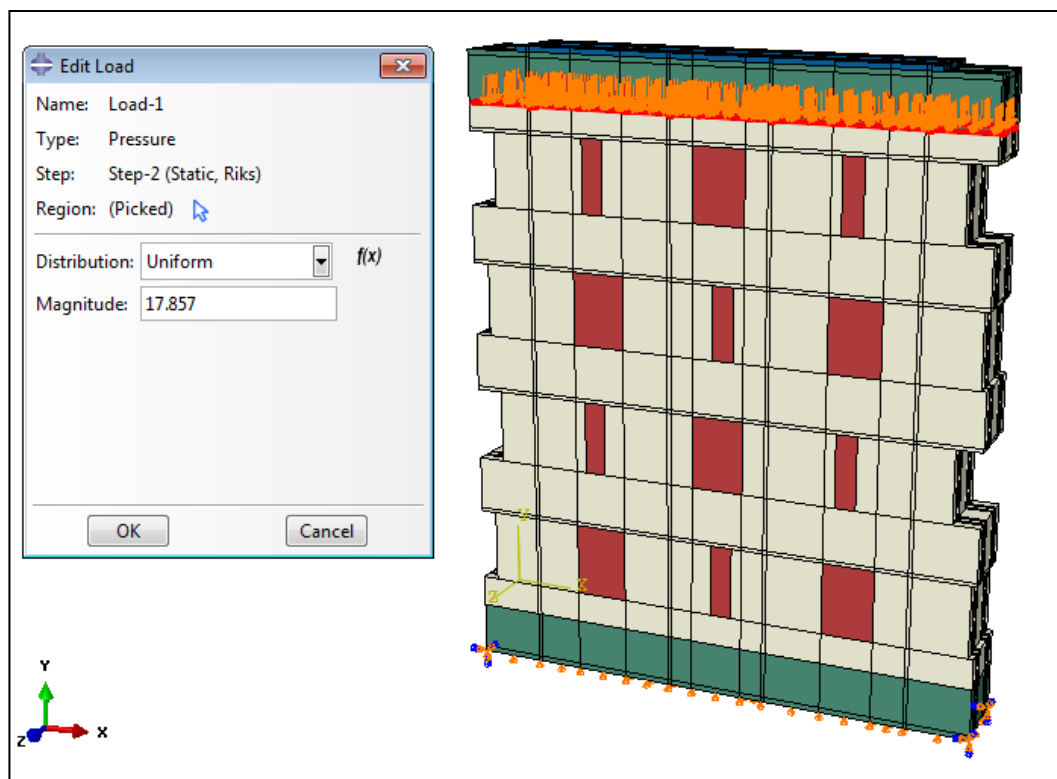


Figure 6.36 Load conditions

For what concerns the boundary conditions, the vertical displacements of the lower face of the bottom base were prevented. Moreover the 4 point corners were blocked.

6.7 The mesh

The goal was to create a so called *structured mesh* in *Abaqus* environment.

The *Mesh module*, assign one color to the regions of the model according to the method it will use to generate the mesh:

- Green indicates that a region can be meshed using *structured methods*.
- Yellow indicates that a region can be meshed using *sweep methods*.
- Orange indicates that a region cannot be meshed using the default element shape assignment (hexahedral) and must be partitioned further. The alternative is to mesh the model by assigning tetrahedral elements to the model and using the free meshing technique. The mesh could obviously results very irregular.

The assembly was partitioned to obtain only region in which apply *Structured Technique*.

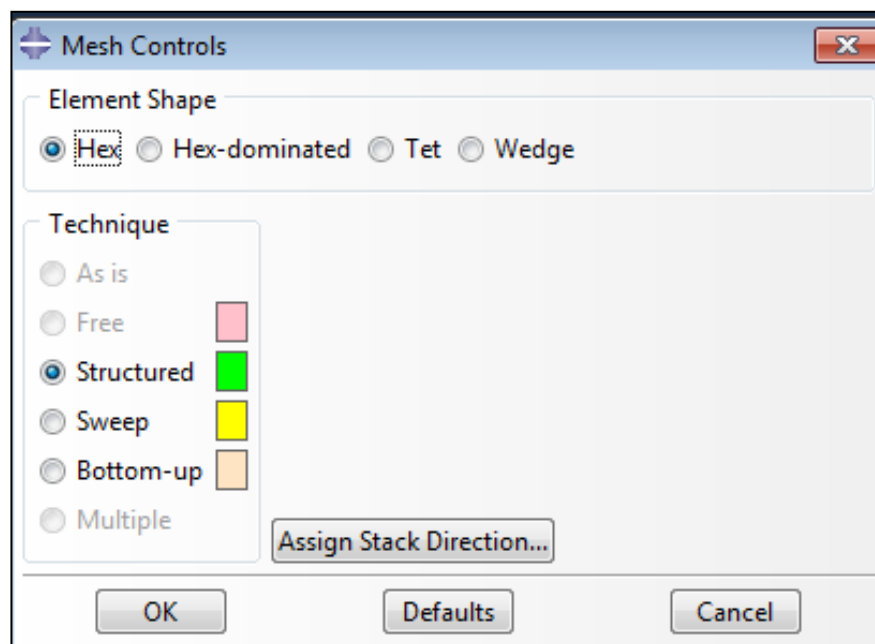


Figure 6.37 Mesh control editor

In a structured mesh the nodes of the "grid" are generated by the intersection of two families of lines belonging to specific systems of Cartesian coordinates or curvilinear (it is similar to the grids made by the method of finite differences). Using "grids" of this type it is easy to carry out a "rational" numbering of the nodes.

To mesh the assembly the following operations were performed:

- the Assembly was partitioned to create regular zones in which structured mesh can be build.

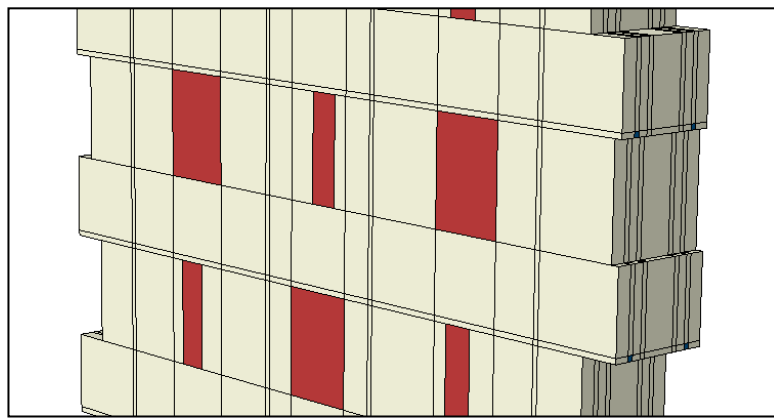


Figure 6.38 Partitioning lines

To partitions the assembly it means to create prismatic shaped regions without cavities.

- the "mesh attributes" were assigned to the part instances, that means to choose which FE element to use. The choice was "Hex8" elements with "reduced integration" option to reduce the time to solve.

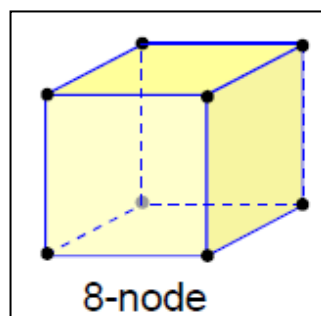


Figure xx Elementary FE used

- the part instances were seeded. The seed are the reference point on which the mesh was built.

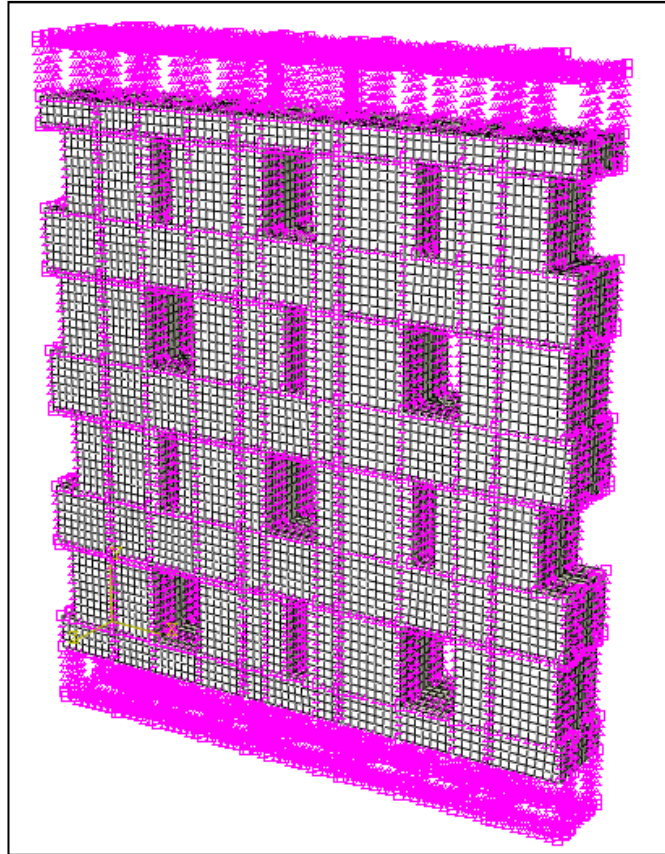


Figure 6.39 The Seeds of the Mesh

- the entire assembly was meshed as a single Region with the command "Mesh Region". To proceed in this way the choice of "Independent mesh" on Instance during Assembly Module was required.

Some particulars of the mesh obtained can be seen in *Figure 6.40,6.41* . The mean dimension of the FE elements was 13.1 mm.

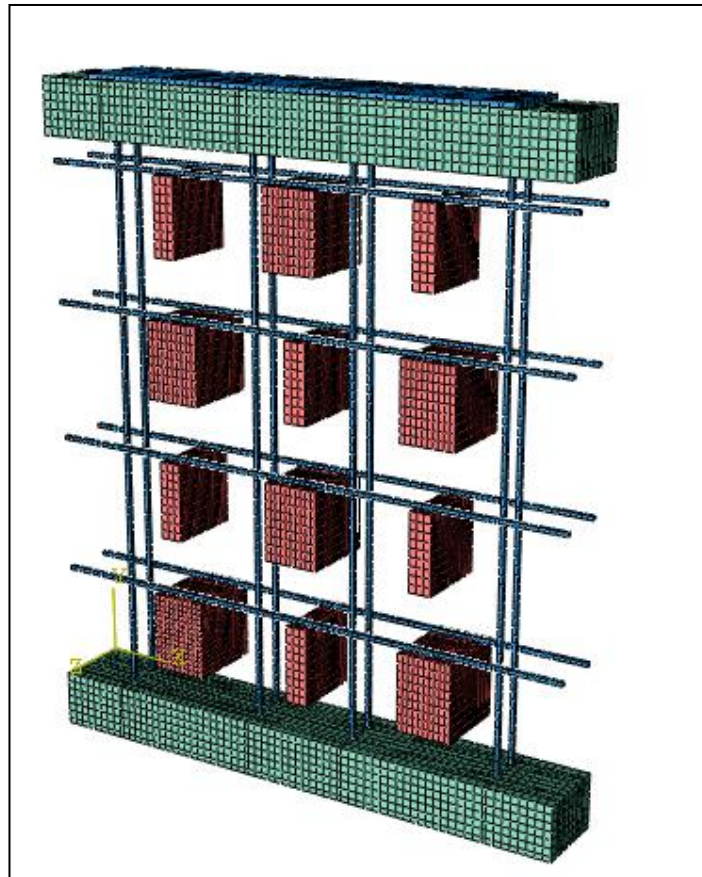


Figure 6.40 The mesh on the bases, on the Wood Cores and steel

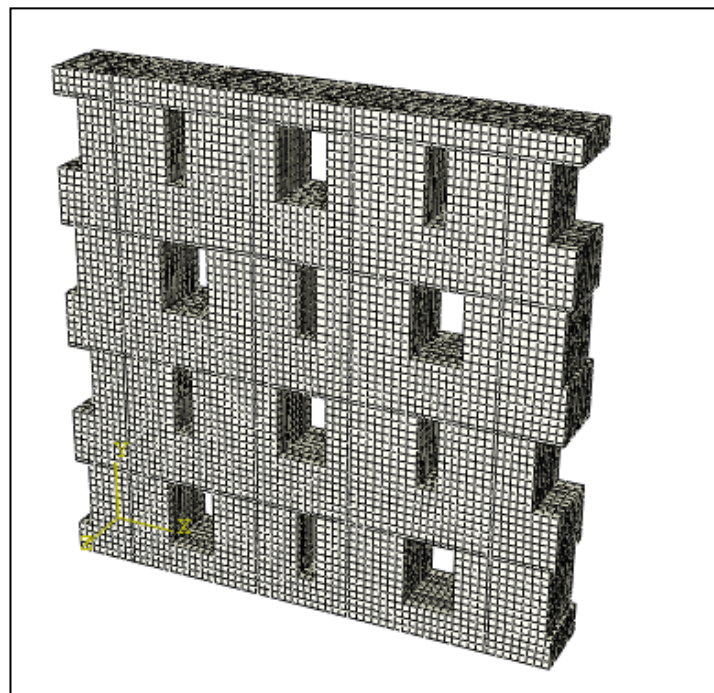


Figure 6.41 The mesh on the main Concrete Core

Chapter 7

Results of the numerical model in Abaqus

Introduction

In this chapter the numerical results obtained are analyzed in order to compare the output-data of the model with experimental observations and measurements obtained during the investigation performed at the Laboratory of CIRI-Building Department of the University of Bologna.

The experimental tests on which this Chapter are focused were the compressive tests *CC14_01* and *CC14_02*, the results of which are reported in *Chapter 3*.

It is reminded that the geometry of the model tried to reproduce the CC14_02 specimen, because it shown to be the most reliable test.

The insertion of bond-slip behavior allowed a better understanding of the stresses into the steel bars, moreover the comparison between experimental results and numerical one showed a good agreement in terms stress concentration in the cracking zones.

7.1 Comparison P- Δ curves

As reported in *Paragraph 6.3* the differential settlement of different spy-nodes was monitored to reproduce the *Load- ΔL* pattern of the experiment both in horizontal and vertical direction.

7.1.1 P- Vertical ΔL comparison

If the numerical test is compared with the *test CC14_02* that the simulation wants to reproduce it can be noticed how the model is able to capture the peak load with a difference of 0.6%.

Experimental Peak Load: 2497 kN

Numerical Peak Load: 2512 kN

Also the general trend showed a very good matching.

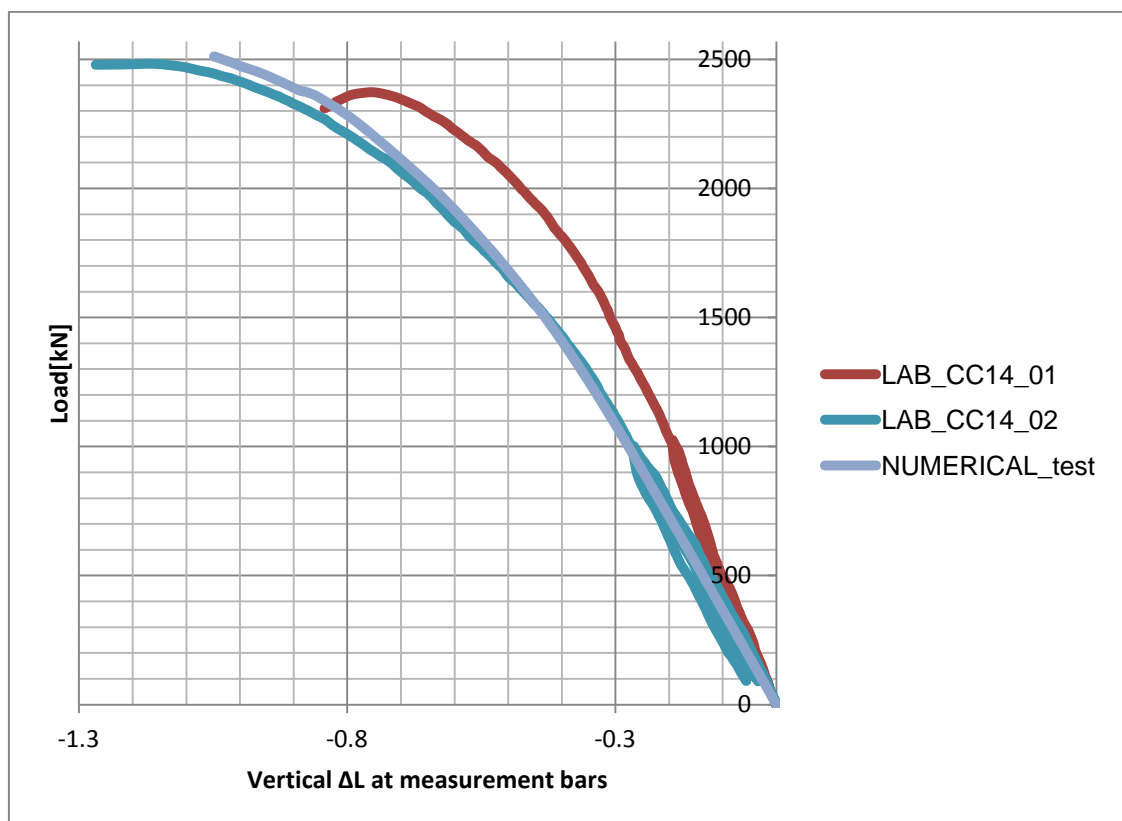


Figure 7.1 P- ΔL Vertical comparison

7.1.2 P-Horizontal ΔL comparison

For what concern the Load- ΔL Horizontal *Figure 7.2(a) and (b)* can be considered:

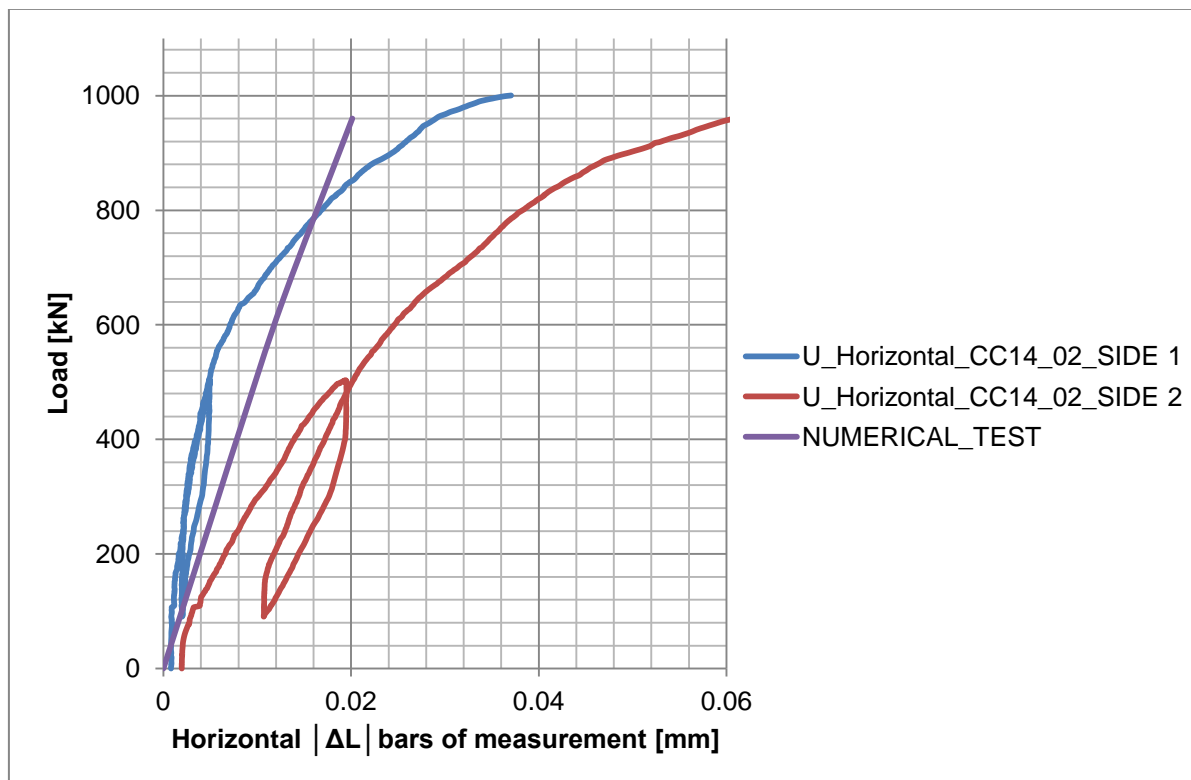


Figure 7.2(a) Load - ΔL Horizontal in elastic phase. Comparison between test and

In blu and in red the experimental results of the two horizontal LVDT on the two sides of the grid-wall, in purple the numerical output. During the *linear-elastic* phase the model response was perfectly in between the two experimental curves that means that the model was able to capture the horizontal expansion of the specimen, but only in the linear elastic phase. The presence of the wood-concrete elements, probably didn't allow a real lateral expansion of the model. The strength and the mechanical characteristics of wood-concrete elements were derived from unofficial literature, the only available. The whole trend of the *Load - ΔL Horizontal* graph is presented in Figure 7.2(b).

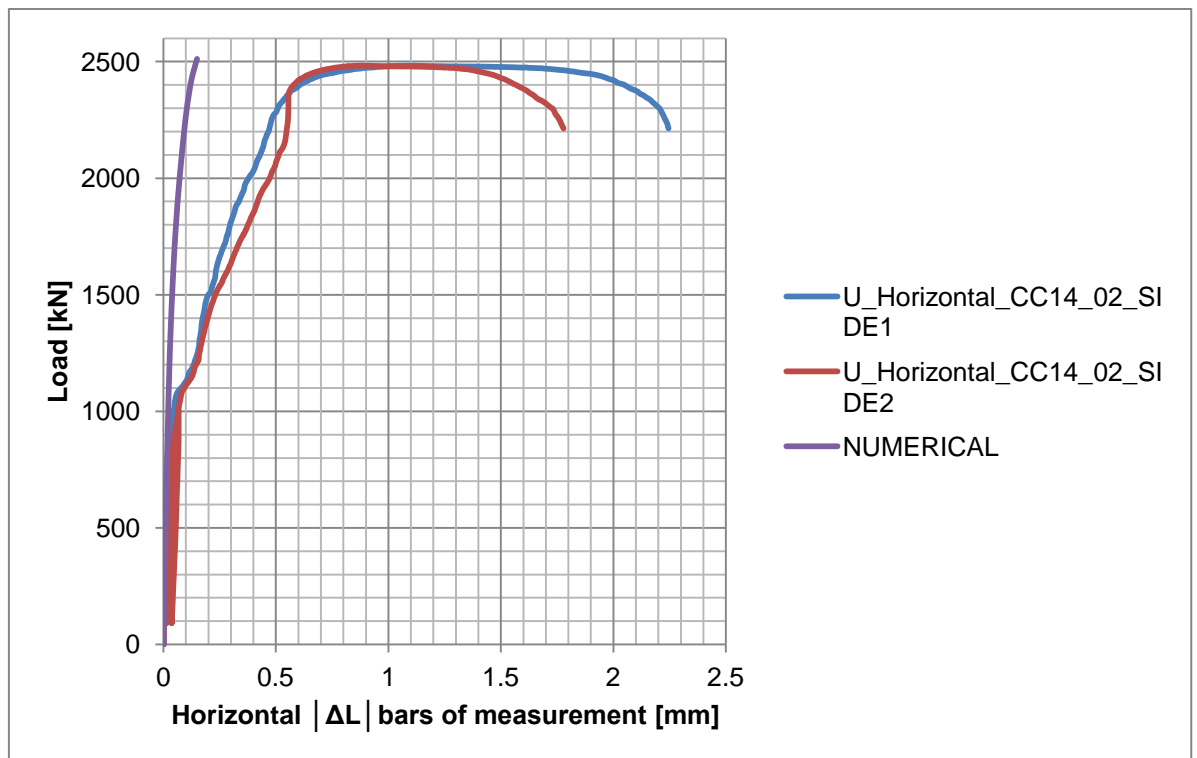


Figure 7.2(b) Load - ΔL Horizontal comparison

7.2 Active yield flag

The active yield flag is a so called "yes or no" variable. Indicates where one of the stress components reaches the inelastic strain. As a matter of facts it can be noticed that the values assumed are 1 (Red zone) or 0 (Blue zone).

The raise of the first "yielded elements" was detected between step 13 and 14 (between 645 kN and 960 kN) that is the ultimate load of perfectly elastic phase as can be noticed in *Fig.7.1*.

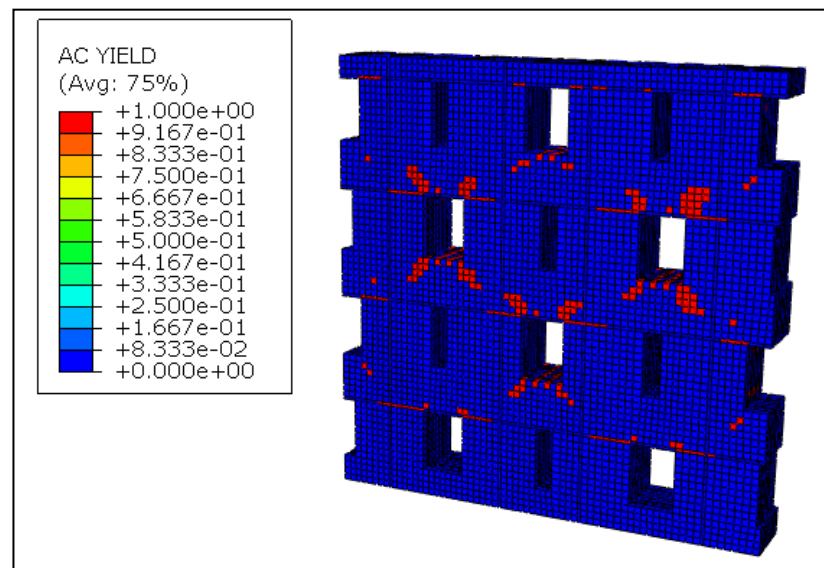


Figure 7.3 Active Yield Flag at 960 kN(step 14)

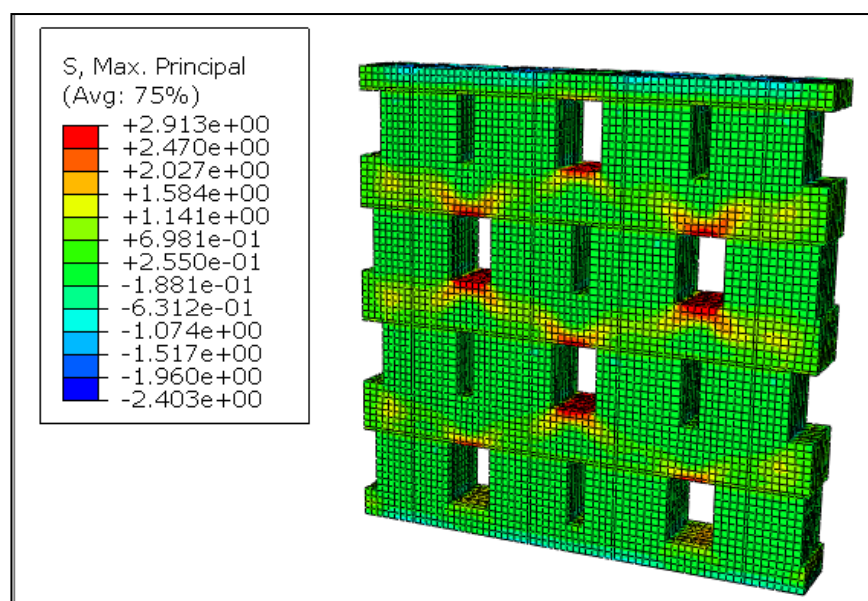


Figure 7.4 Stress distribution(max. principal) at 960 kN

From Fig.7.4 can be noticed how the raise of the AC YIELD is strictly related to the fact that the concrete close to the tensioned steel bars reach the maximum tensile stress: 2.9 MPa as implemented and reported in Fig.7.4.

At step 16 that correspond to 1225 kN it can be saw how the critical zones are close to the biggest holes, venues of the wood-concrete elements.

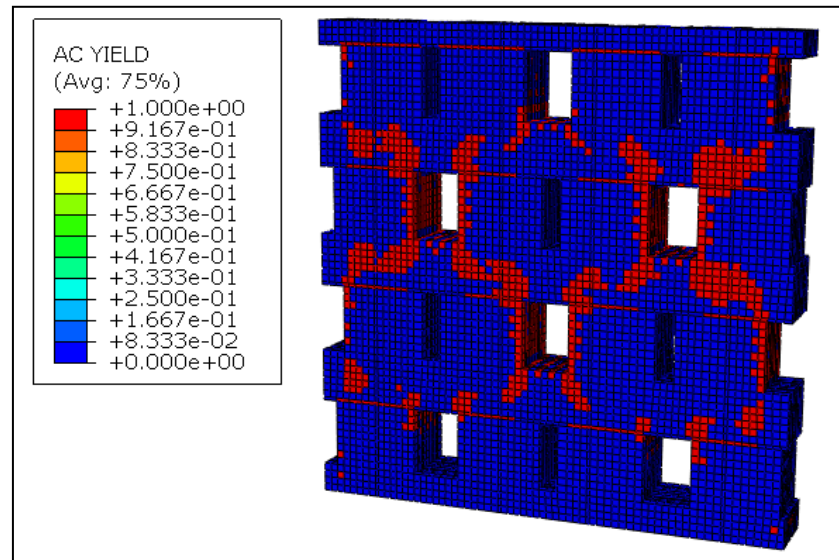


Figure 7.5 Active Yield Flag at 1225 kN(step 16)

At the step 21 that correspond to 1500 KN. The collapse is studied in Par. 7.7 ,7.8.

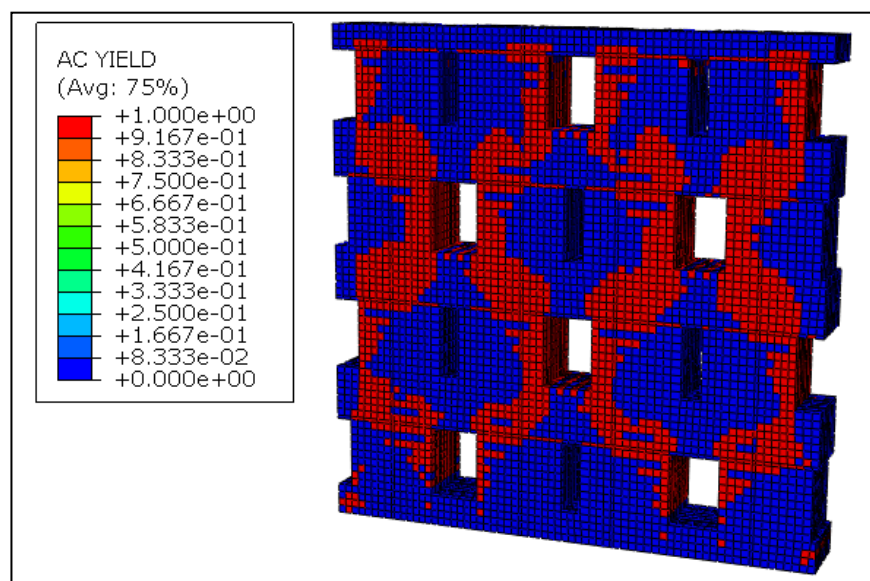


Figure 7.6 Active Yield Flag at 1500 kN(step 21)

7.3 Main stresses on the pillars

At the ultimate state, the stress distribution of the sigma σ_{22} (in vertical direction) in the middle plain is represented in Fig. 7.7. The units of the legend is in MPa and it can be noticed how the model reproduce reliable values of stresses: in a range in between 2.45 MPa in tension and 31.3 MPa in tension. It's also interesting to notice how the stress path in Figure 7.7 recall the one presented in Fig.7.6.

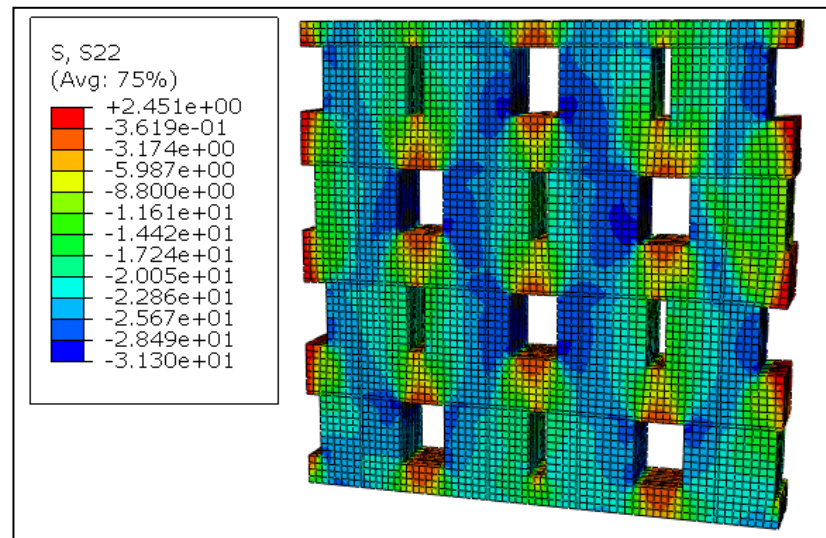


Figure 7.7 Stress σ_{22} distribution

The symbolic representation makes more evident the stress path on a generic cross section.

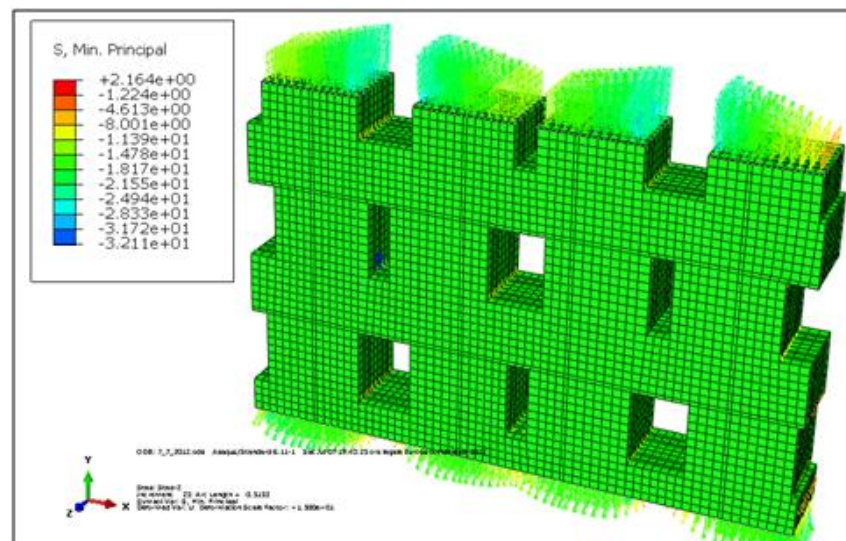


Figure 7.8 Stress σ_{22} distribution over a cross-section of the pillars

7.4 Main stresses on the connector-beams

As literature suggests, the connector -beams-behavior follows a *strut and tie* scheme: the composition of the *Sigma max-principal* [MPa] and of the *Sigma min-principal*[MPa], reported in the following figures suggested the presence of a compressed strut in the zone close to the bigger holes. Making a cut view it can be noticed how the stresses are distributed in connector beams in horizontal direction.

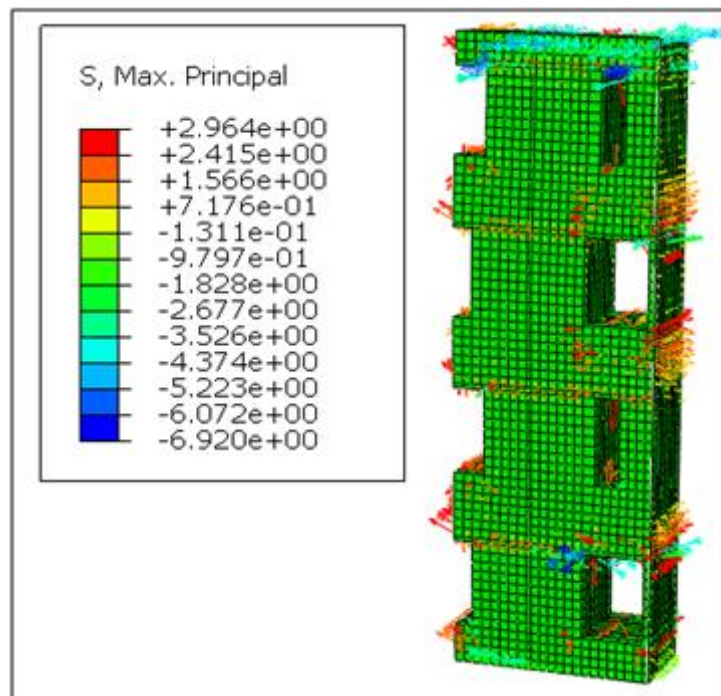


Figure 7.9(a) Principal Max Stress distribution inside the connector beam

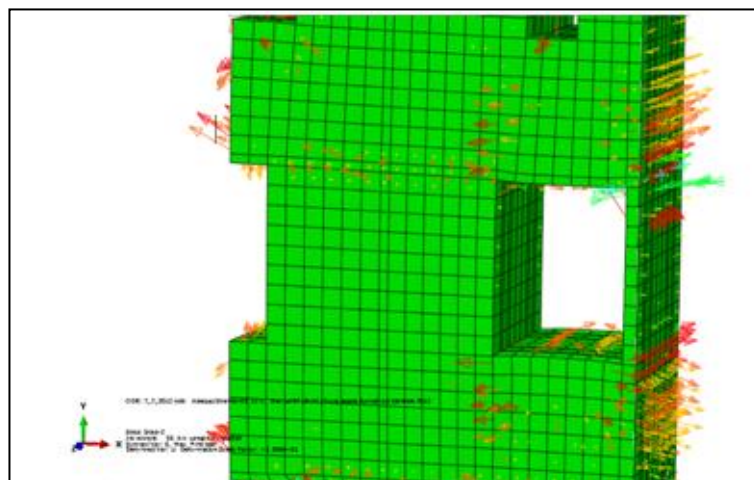


Figure 7.9(b) ZOOM of Principal Max Stress distribution inside the connector beam

In vertical direction the stresses are of compression as can be expected.

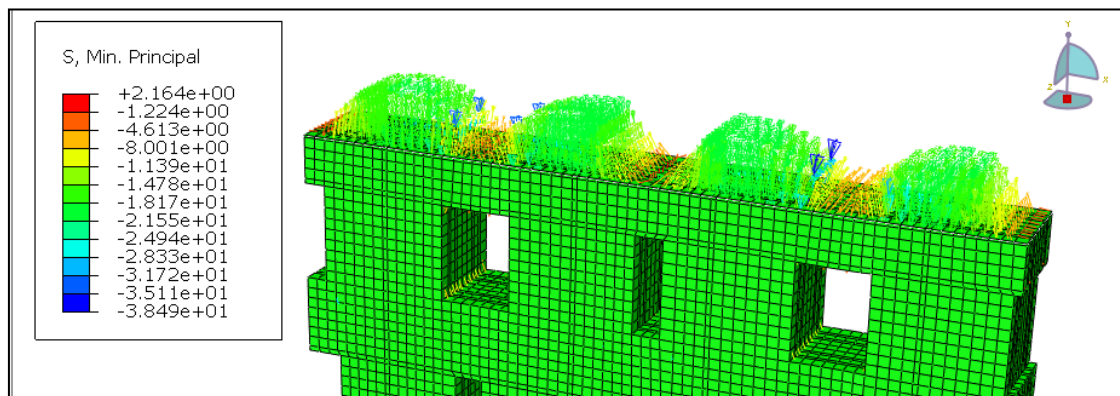


Figure 7.10 Vertical Stress distribution on a joist-longitudinal cross-section

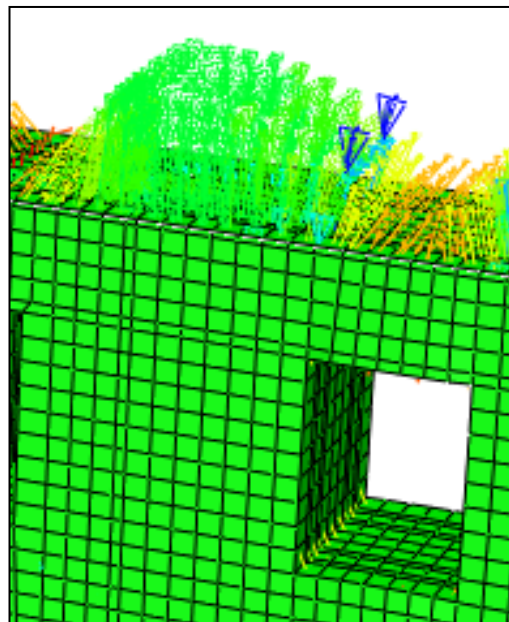


Figure 7.11 Zoom of Vertical Stress distribution on a joist-longitudinal cross-section

7.5 Main stresses on the wood-concrete elements

The peak values of these stress maps are reasonable: 0.27 MPa in tension, 1.6 MPa in compression as can be expected by a fragile material. For action-reaction principle the wood-concrete elements develops in the external corners stress-distribution with equal direction to the one that will be presented in *section 7.7* on the adjacent concrete core.

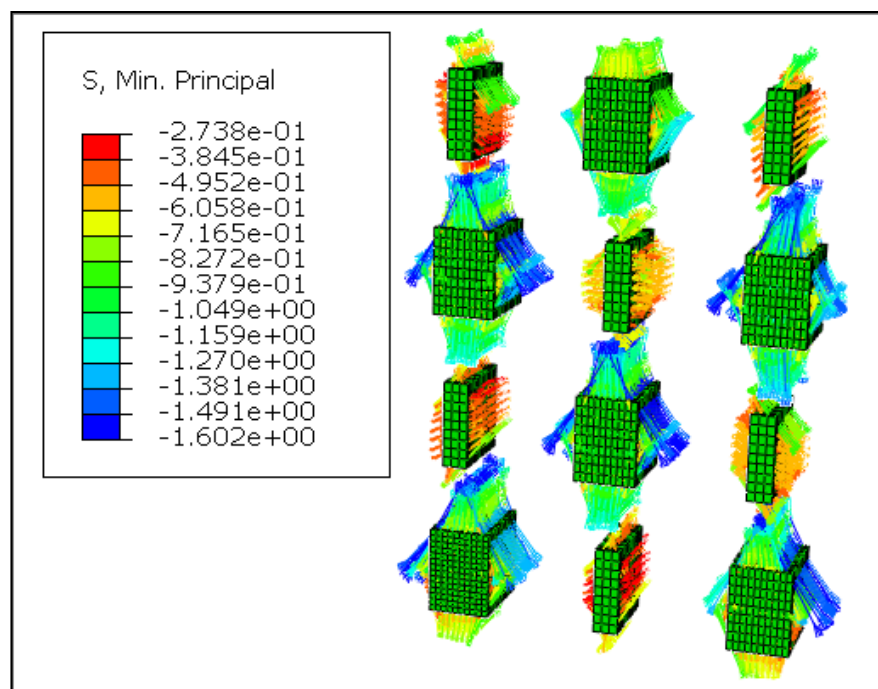


Figure 7.12 Stress distribution in the Min. Principal direction on wood-concrete elements

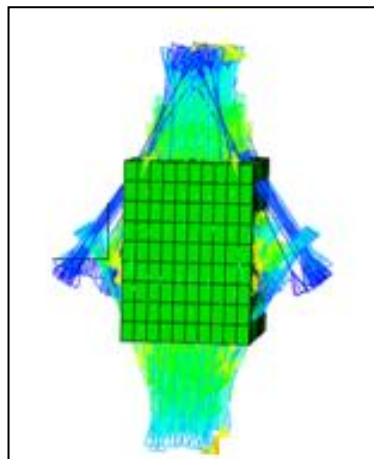


Figure 7.13 ZOOM of Stress distribution in the Min. Principal direction on the central element

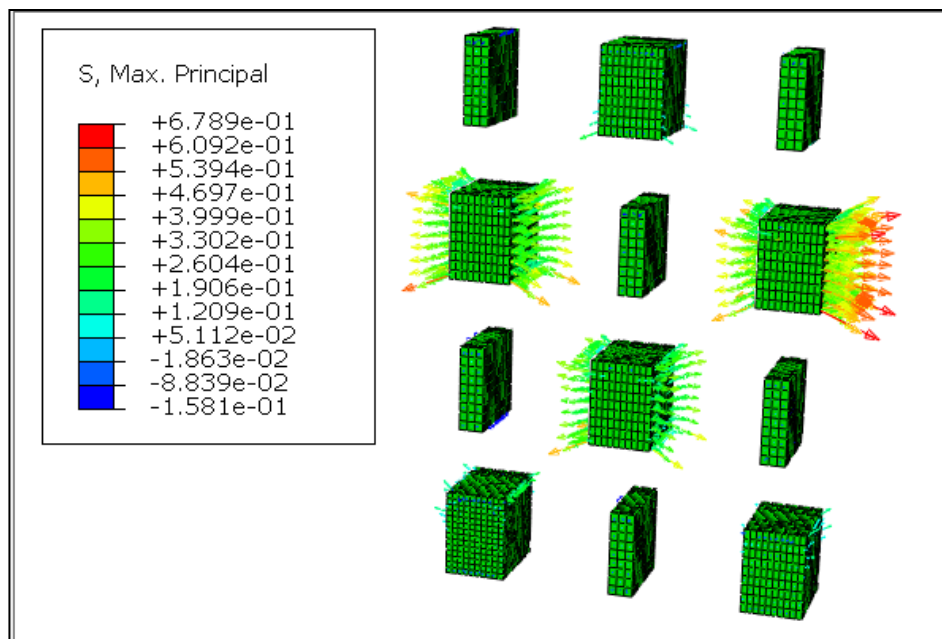


Figure 7.14 Stress distribution in the Min. Principal direction on wood-concrete elements

The lateral expansion can be noticed also in the following Figure 7.15.

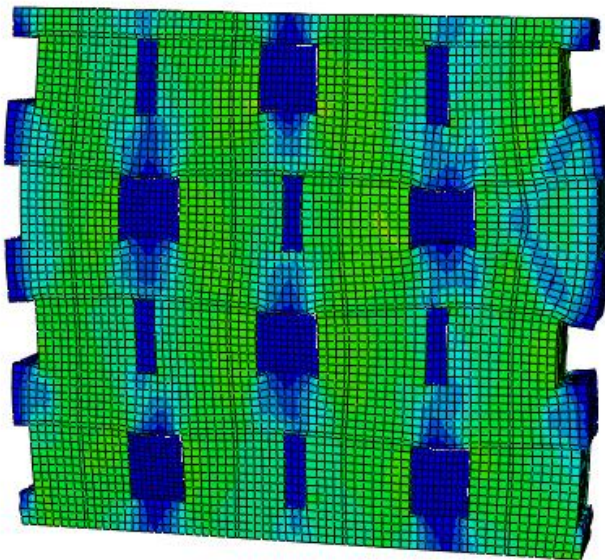


Figure 7.15 Deformed configuration in the ultimate state

7.6 Strain distribution on concrete grid-wall

The software divide the elastic strain(EE) of the order of 10^{-4} from the plastic strain (PE) of the order of 10^{-3} as can be correctly expected in concrete.

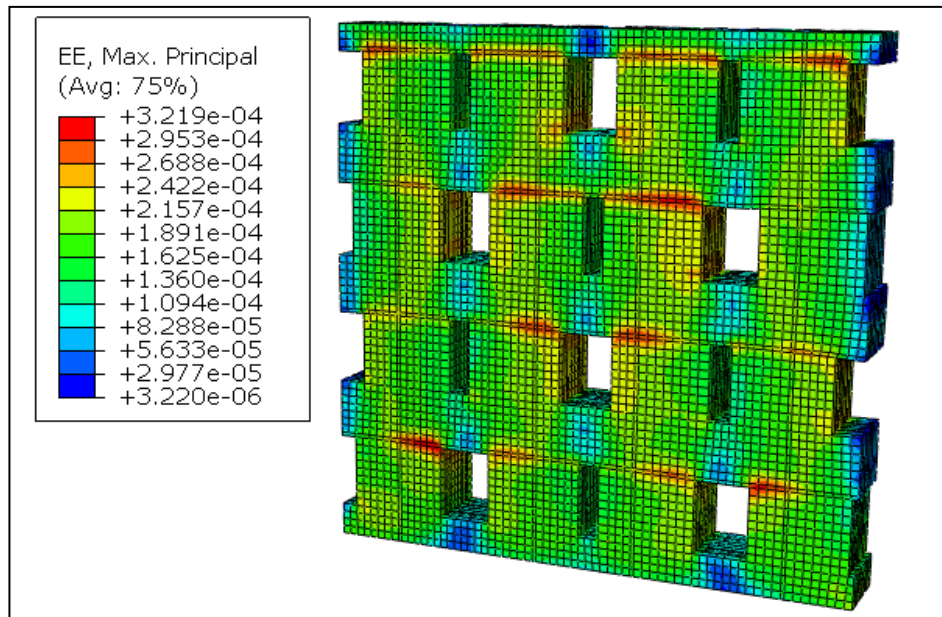


Figure 7.16 Stress distribution in the Min. Principal direction on wood-concrete elements

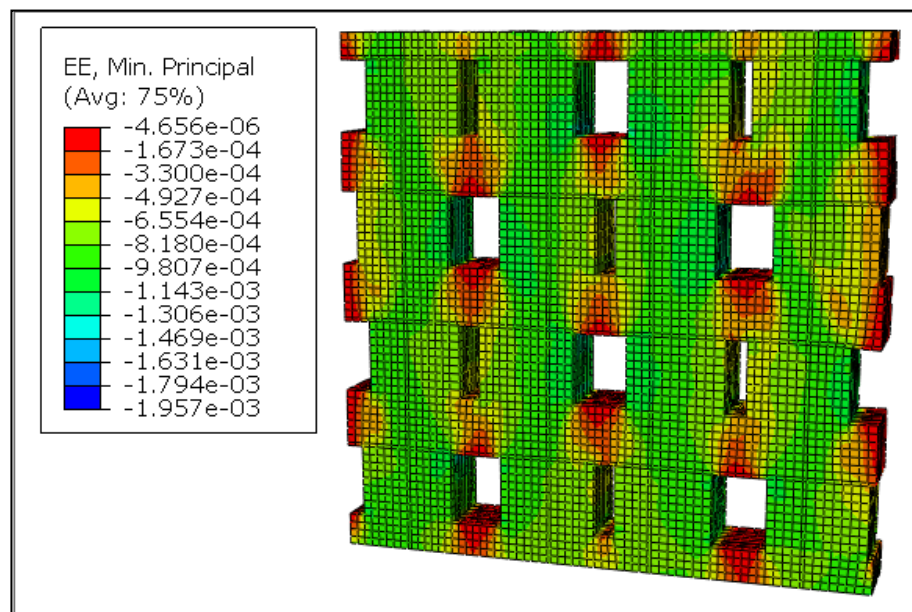


Figure 7.17 Stress distribution in the Min. Principal direction on wood-concrete elements

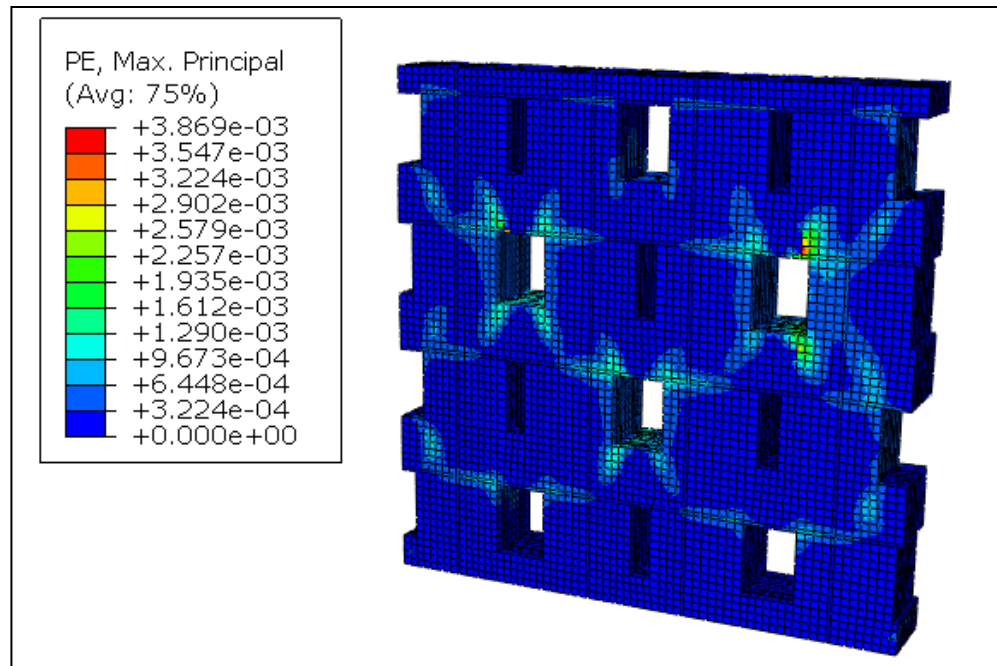


Figure 7.18 Plastic strain at ultimate state

7.7 Comparison between cracking pattern of the test and numerical results

In almost all the compression tests the cracking-patterns presented the same diagonal direction as can be seen in *Figure 7.19* , *Figure 7.20*, *Figure 7.21*, *Figure 7.22*. The 45° diagonal crack between bigger holes are present in all the cases reported below.



Figure 7.19 Cracking pattern of one compression test CC14_01

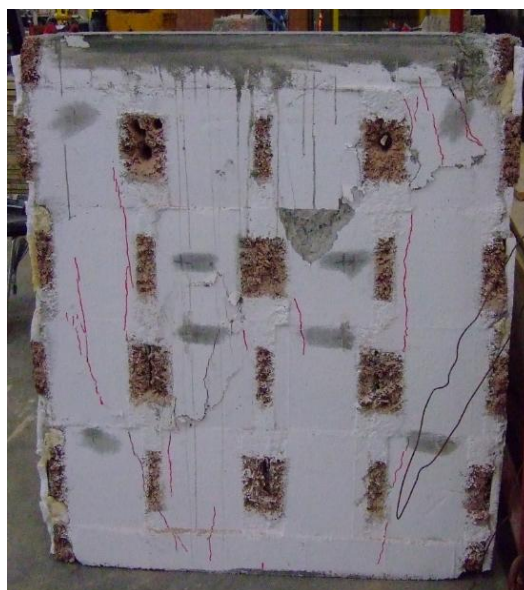


Figure 7.20 Cracking pattern of one compression test



Figure 7.21 Cracking pattern of one compression test CC4_14(CC14_02)



Figure 7.22 Cracking pattern of one compression test CC1_18

Unlike concrete models based on the smeared crack approach, the concrete damaged plasticity model does not have the notion of cracks developing at the material integration point. However, it is possible to introduce the concept of an **effective crack direction** with the purpose of obtaining a graphical visualization of the cracking patterns in the concrete structure. Different criteria can be adopted within the framework of scalar-damage plasticity for the definition of the direction of cracking. Following Lubliner et. al. (1989), it can be assumed that cracking initiates at points where the *tensile equivalent plastic strain* (PEEQ) is greater than zero, $\epsilon_t^{pl} > 0$, and the maximum principal plastic strain (PE, Max principal) is positive. The direction of the vector normal to the crack plane is assumed to be parallel to the direction of the maximum principal plastic strain. This direction can be viewed in the Visualization module of Abaqus/CAE as reported in the following figures.

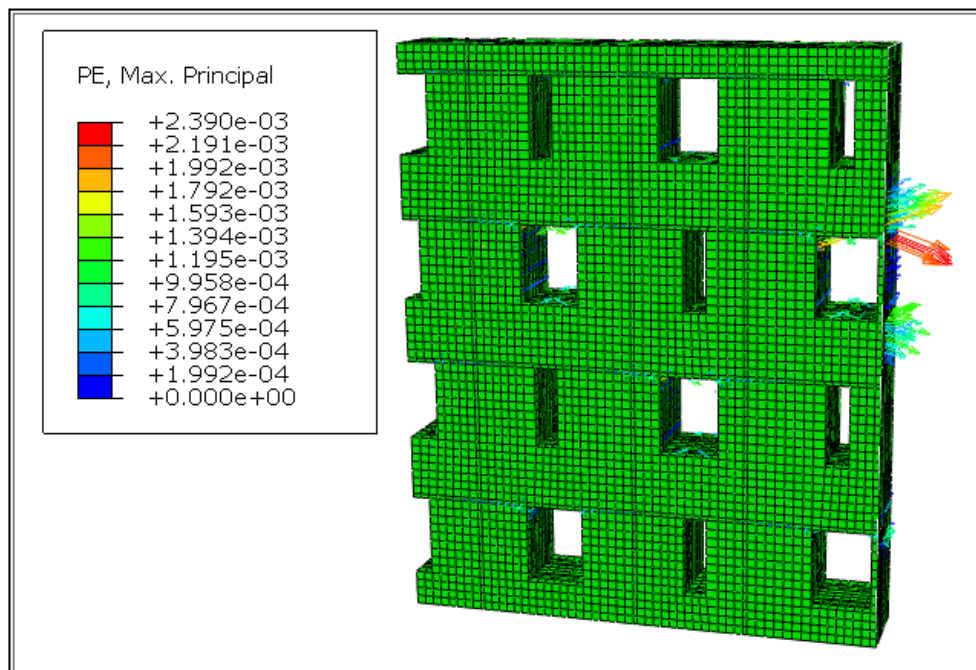


Figure 7.23 Plastic strain in the Maximum principal direction in the symbolic visualization

A *view cut* command scanned in all the wall length, showed that the maximum plastic strain concentration is in correspondence of the corners of the bigger cavities. *Figure 7.23* and *Figure 7.24* and *7.25* shows this evidence.

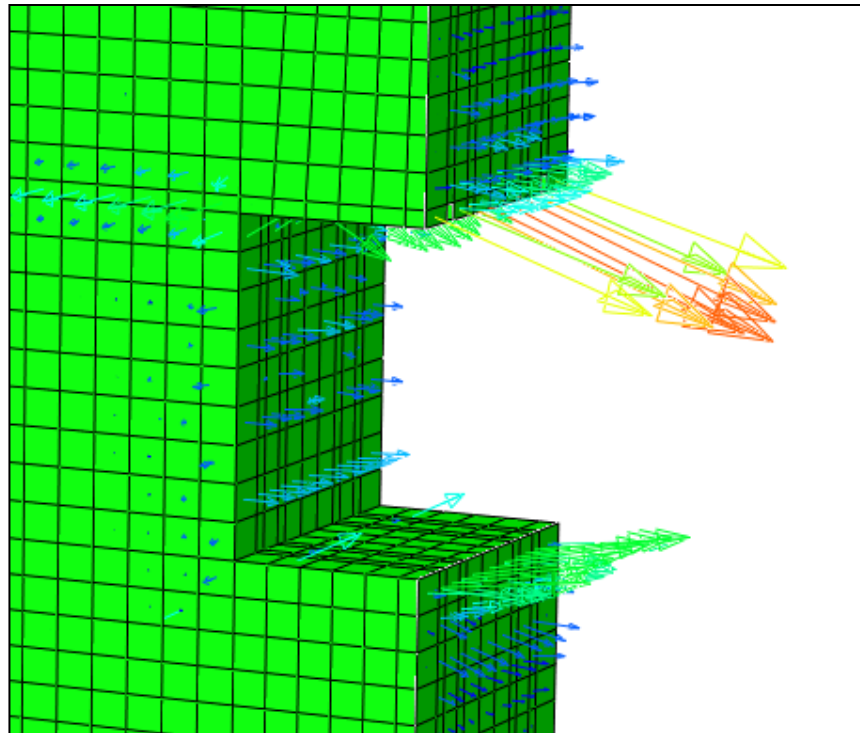


Figure 7.24 ZOOM of Maximum principal plastic strain symbolic visualization

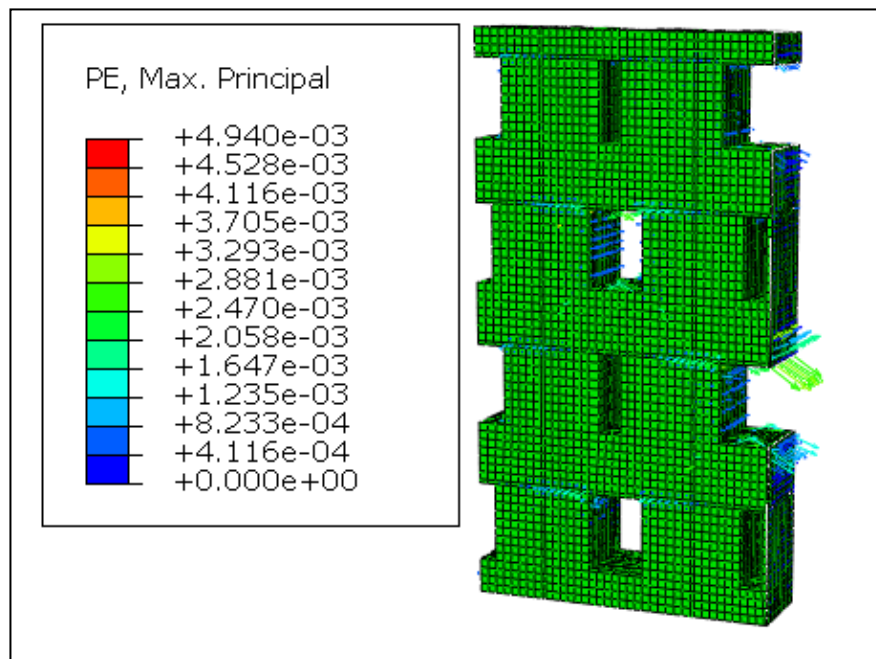


Figure 7.25 Maximum principal plastic strain symbolic visualization

Considering also *Figure 7.18* that represents the zones in which the PEEQ are present and bigger than zero we can notice how the model is able to capture the cracking pattern related to the collapse phase.

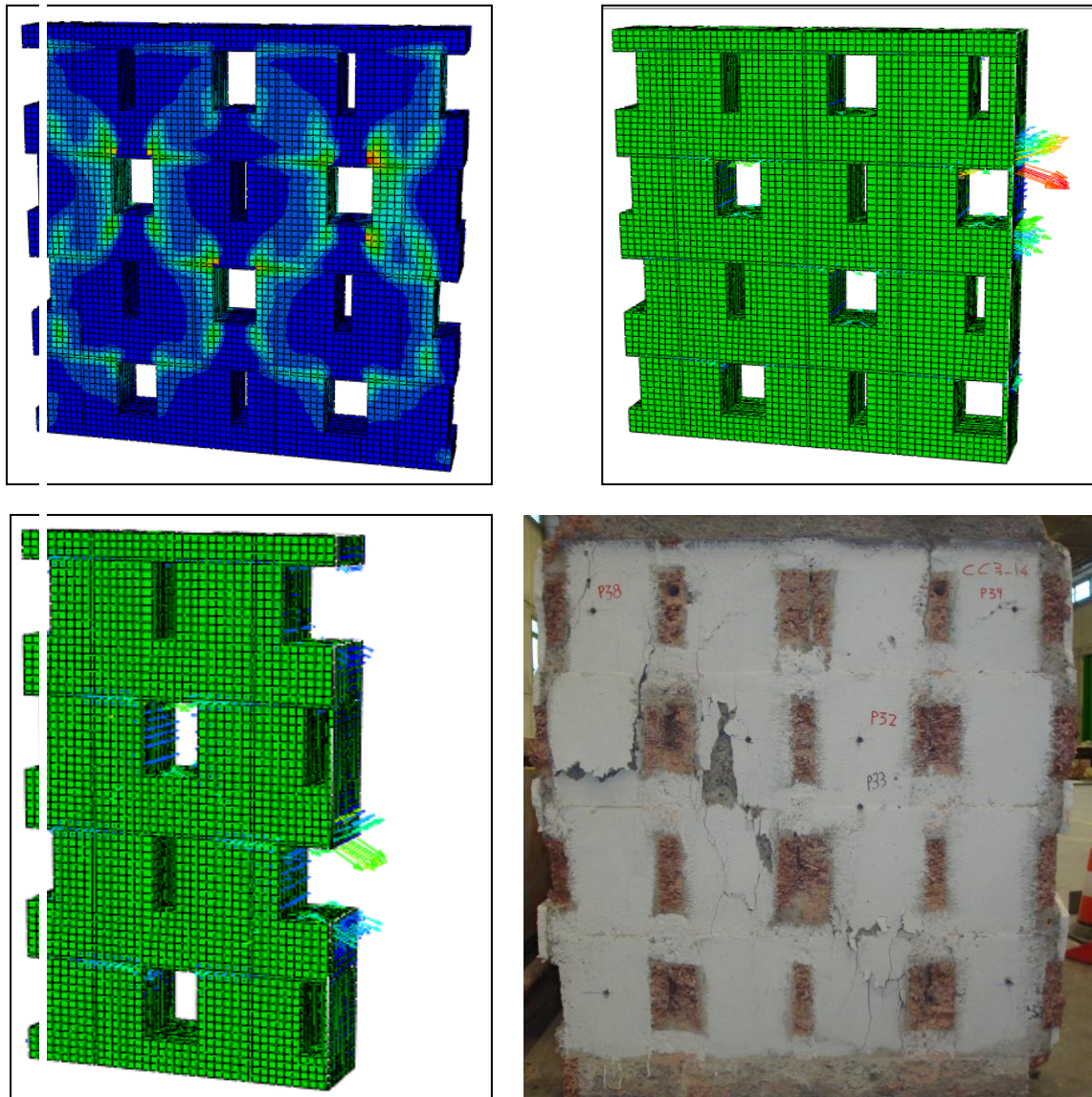


Figure 7.26 Ability of CDP model to catch the cracking pattern

7.8 Collapse mechanism and stress history on steel bars

The presence of misaligned pillars, intrinsically connected with the building technology, create a collapse mechanism that is well captured by the *stress history output* of the steel bars and here reported in its main steps.

At step 23, that correspond to 1780 kN the vertical bars are equally compressed with a $\sigma_{yy \max}$ of 127.7 MPa of compression (*Figure 7.27 in blue*)horizontal steel bar are in tension with $\sigma_{xx \max}$ of 33.8 MPa. (*Figure 7.28 in red*).

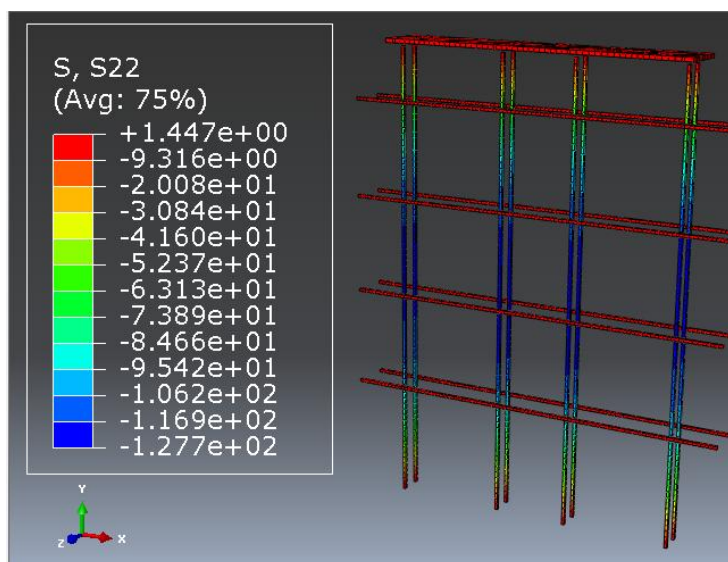


Figure 7.27 Stress $\sigma_{yy \max}$ of 127.7 MPa at 1780 kN

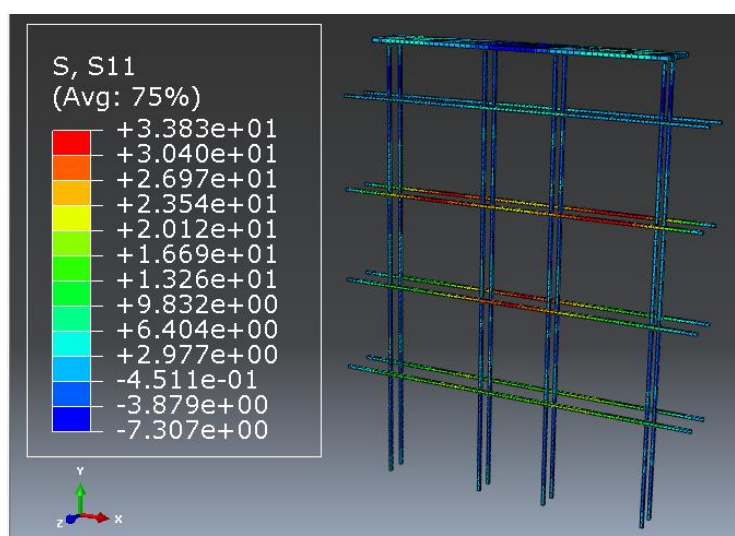


Figure 7.28 Stress $\sigma_{xx \max}$ of 33.8 MPa at 1780 kN

At step 49, that correspond to a load of 2490 kN the situation is changed: the load is no more equally distributed in the 4 pillars and even the σ_{xx} distribution is no more symmetric.

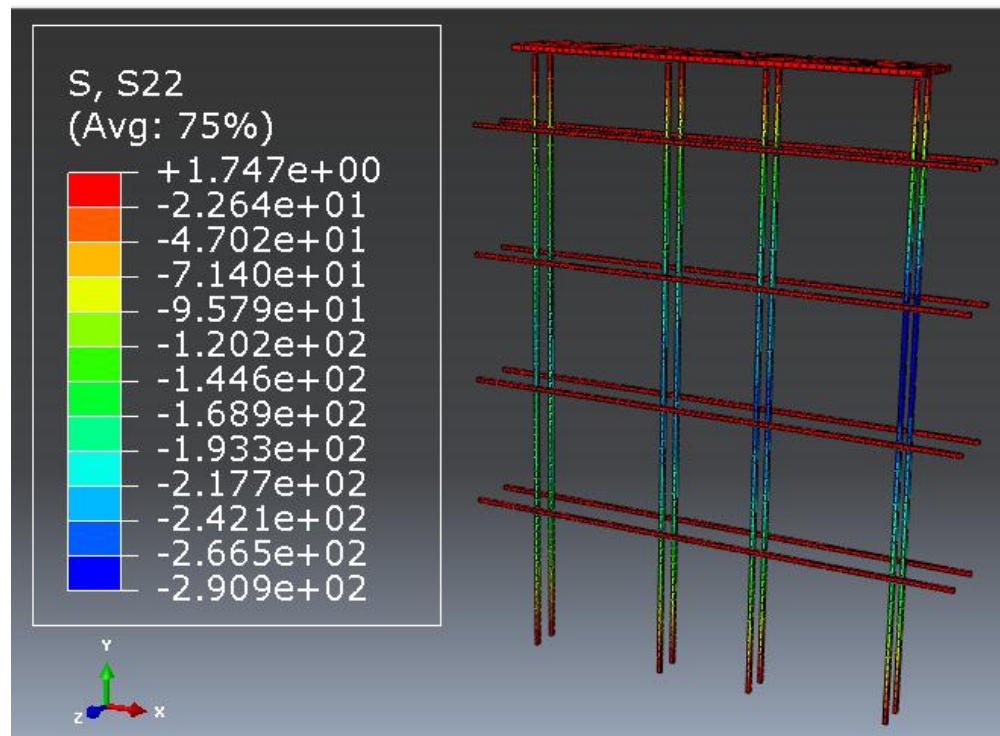


Figure 7.29 Stress σ_{yy} max of 290 MPa at 2490 kN

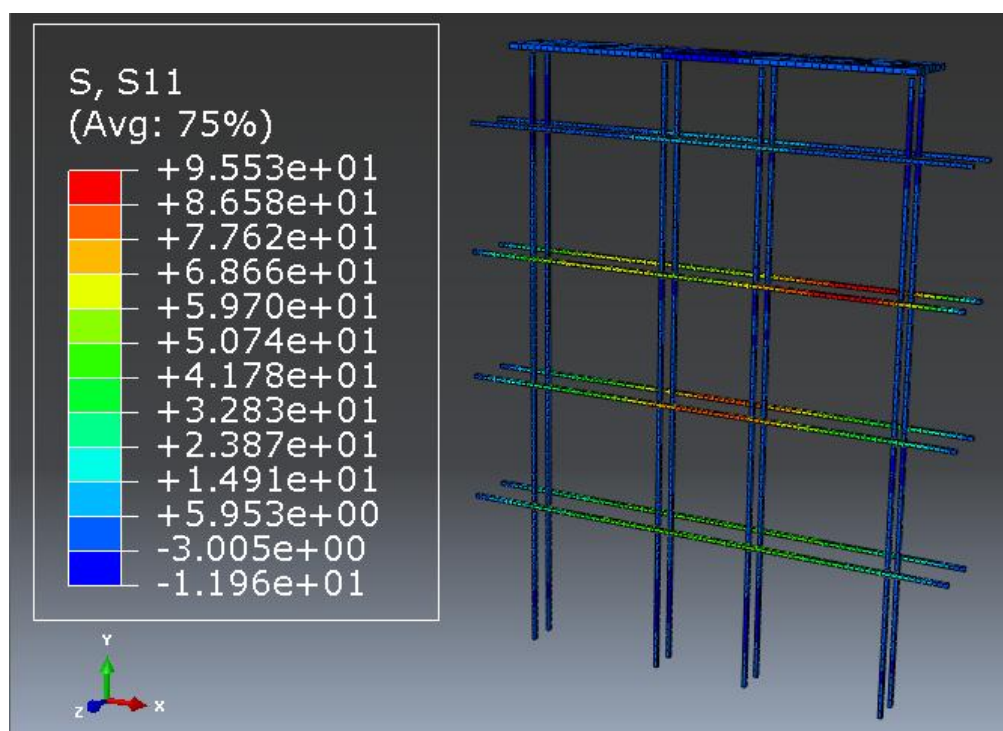


Figure 7.30 Stress σ_{xx} max of 95.5 MPa at 2490 kN

At ultimate load of 2512 kN the situation is the following.

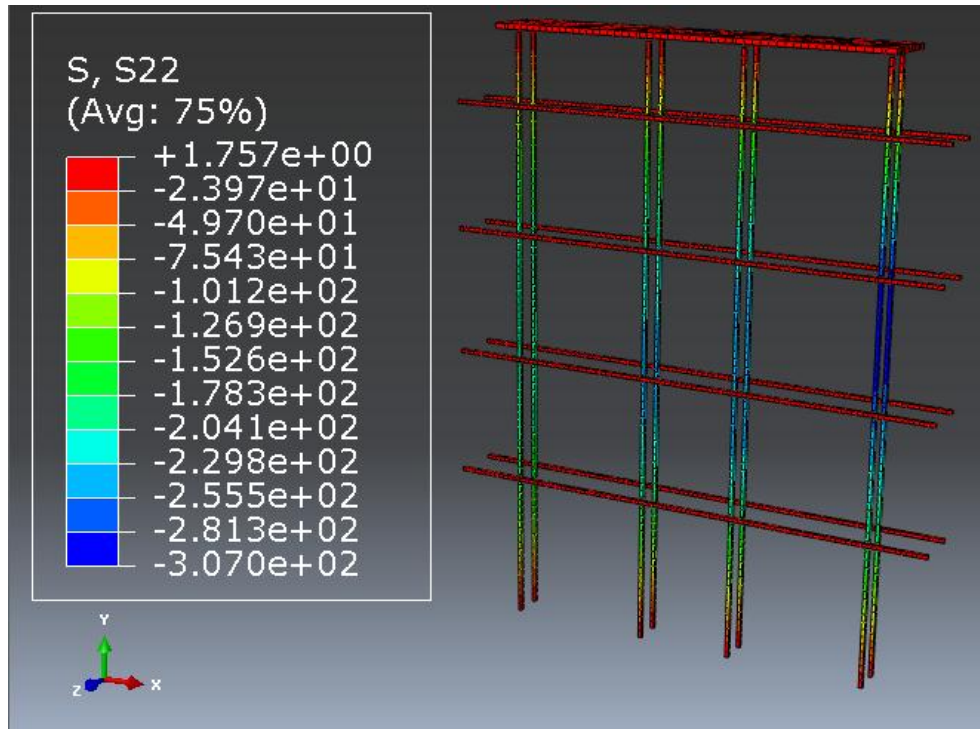


Figure 7.31 Stress $\sigma_{yy \max}$ of 307 MPa at 2512 kN

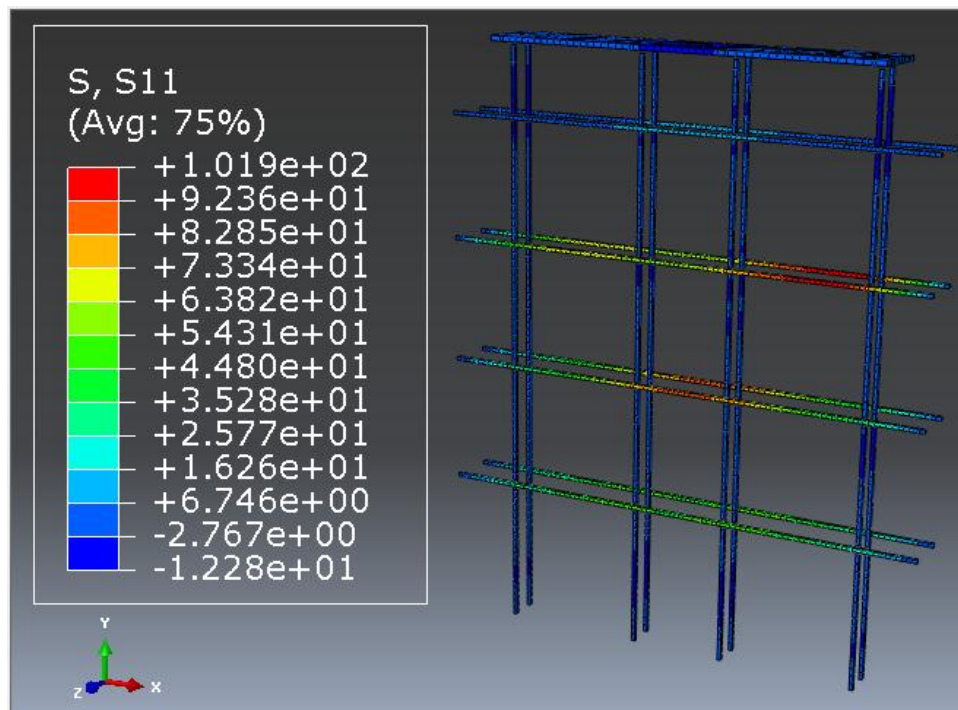


Figure 7.32 Stress $\sigma_{xx \max}$ of 101.9 MPa at 2490 kN

This behavior suggest the direction of the global collapse mechanism.

Chapter 8

Summary, conclusions, recommendations for future study

Summary

The structure of this Thesis concerning "Grid-type wall systems" can be divided into two main parts: the first considered some experimental tests with particular attention on the results aimed at defining the equivalent continuous wall in linear-elastic field. The second part was focused on the building of a non-linear numerical model.

The grid-wall objective of this thesis were so introduced, described and inserted in the National and ultra-national normative context (*Chapter 1*); followed a brief description of the test aimed at characterize the material used and the experimental test suggested by the CSLP Italian Guidelines (*Chapter 2*). Exploiting the experimental output the characteristics of the equivalent continuous wall in linear-elastic field were defined (*Chapter 3*).

The crucial aspect in the modeling phase was to correctly choose the necessary parameters to define the constitutive properties of concrete. In particular, the softening branch both in compression and in tension was set, comprehensive of damage laws, considering the few information from the test on the two materials(*Chapter 2*) and literature reviews(*Chapter 4*). The bond-slip relation between concrete and steel-bars was considered, analyzed in detail (*Chapter 5*) and reproduced in the numerical model of the grid-wall. The model was build trying to obtain mesh-compatibility between the steel-bars and the adjacent concrete, not necessary in Abaqus environment, but almost imposed once the assembly was correctly partitioned (*Chapter 6*). The results of the numerical model (*Chapter 7*) showed that the finite element model developed with the program Abaqus was able to accurately describe the non-linear response up to failure. The comparison and the agreement between numerical and experimental curves showed the reliability of the model and the ability to capture also the collapse mechanism.

Conclusions

During the preliminary design phases there' s the need of simple tools for an immediate and effective global elastic analysis; the characteristics of the equivalent continuous linear elastic panel were so evaluated. Considering the experimental compression tests on 1m x 1 m grid-walls conducted in CIRI was possible to evaluate both for 14 cm and 18 cm panels:

-the equivalent geometric thickness s_{eg}

-the corrective coefficient α and β to be applied respectively on the elastic Modulus E and G

-the implementation of a *simple traction proof* allowed an in-deep understanding of the functioning of the two constitutive models implemented in Abaqus for concrete

- a *pull-out test* was numerically reproduced to calibrate the bond-slip behavior between steel bars and concrete; the cohesive based surface model showed to be a reliable tool to be used in the *numerical grid-wall model*

-the grid wall model, after an accurate calibration process, furnished detailed stress and strain maps for a better understanding of the mechanisms occurred during the collapse phase,

- the loading conditions of the steel bars were also captured

- With an appropriate choice of the constitutive model was possible to reproduce with sufficient accuracy, the experimental collapse mechanism noticed in more than one centered compressive tests.

-This CDP model can then be eligible to develop a study on the failure load and on the micro behavior of concrete.

Recommendations for future study

-One aspect that could be deepened is the effective contribution of the wood-concrete layers both on the bearing capacity and on the field of deformation of the grid-wall. The lack of data didn't allow a detailed study of this aspect.

-more detailed tests on concrete specimens (triaxial tests, tension test..) to restrict the calibration process to a few number of parameters could be conceived.

-a smeared cracking approach could be calibrated to have another confirmation about the results obtained

-a real scale building could be implemented to test the reliability of the correction coefficient found to conceive the grid walls as simple the equivalent continuous walls in linear elastic field.

Bibliography

[1] Gasparini, Trombetti, Silvestri, Ceccoli, Malavolta – “Results of pseudo-static tests with cyclic horizontal load on R.C. panels made with wood concrete caisson block” *The 14th World Conference on Earthquake Engineering October 12-17,2008 , Beijing, China*

[2] Oregon University System, “Capital Construction: Key Investments Related to Access and Sustainability”, Issue Brief, Office of the Chancellor, 2007.

[3] “Edifici zero energia, un mercato che nel 2035 frutterà 1300 MLD \$” – Articolo CasaClima 17 febbraio 2012.

http://casaclima.com/index.php?option=com_content&view=article&id=10631:edifici-zero-energia-un-mercato-che-nel-2035-fruttera-1300-mld&catid=1:latest-news&Itemid=50

[4] In-Plane Shear Resistance of Insulating Concrete Form Walls - Prepared by: NAHB Research Center, Inc. Upper Marlboro, MD - April 2001

[5] Elnashai, A.S., Pilakoutas, K., and Ambraseys, N.N., “Experimental Behavior of Reinforced Concrete Walls Under Earthquake Loading”, *Earthquake Engineering and Structural Dynamics*, Vol. 19, pp. 389-407, 1990.

[6] Prescriptive Method for Insulating Concrete Forms in Residential Construction, Prepared for the U.S. Department of Housing and Urban Development, the Portland Cement Association, and the National Association of Home Builders by the NAHB Research Center, Inc., Upper Marlboro, Maryland, 1998.

[7] International Residential Code (IRC), International Code Council, Reston, VA, 2000.

[8] Mau, S.T. and Hsu, T.C., “Shear Behavior of Reinforced Concrete Framed Wall Panels with Vertical Loads”, *ACI Structural Journal*, Vol. 84, No. 3, pp. 228-234, 1987.

[9] Cardenas, A.E., Russel, H.G., and Corley, W.G., “Strength of Low Rise Structural Walls”, Publication SP-63, American Concrete Institute, Detroit, MI, 1980.

- [10] Osterle, R.G., Shiu, K.N., and Corley, W.G., "Web Crushing of Reinforced Concrete Structural Walls", ACI Journal, Vol. 81, pp. 231-241, 1984.
- [11] Uniform Building Code, Vol. 2, International Council of Building Officials, Whittier, CA, 1997.
- [12] Taylor, C.P., Cote, P.A., and Wallace, J.W., "Design of Slender Reinforced Concrete Walls with Openings", ACI Structural Journal, Vol. 95, No. 4, pp. 420-433, 1998.
- [13] Ali, A. and Wight, J.K., "Reinforced Structural Walls with Staggered Opening Configurations Under Reversed Cyclic Loading", Report No. UMCE 90-05, Department of Civil Engineering, University of Michigan, Ann Arbor, MI, 1990.
- [14] Wallace, J.W., "New Methodology For Seismic Design of RC Shear Walls", Journal of Structural Engineering, ASCE, Vol. 120, No. 3, 1994.
- [15] Lefas, I.D., Kotsovos, M.D., and Ambraseys, N.N., "Behavior of Reinforced Concrete Structural Walls: Strength, Deformation Characteristics, and Failure Mechanism", ACI Structural Journal, Vol. 87, No. 1, pp. 23-31,
- [16] Marisa Pecce, Fabio Antonio Bibbò – "Comportamento sismico di edifici realizzati con pareti estese debolmente armate" - Atti convegno ANIDIS 2011
- [17] Malavolta - Strutture a pareti portanti in c.a. caratterizzate da elevate prestazioni " p.415-418 - 2008
- [18] Designation: E519/E519M – 10: " Standard Test Method for Diagonal Tension (Shear) in Masonry Assemblages
- [19] "A Plastic-Damage Model for Concrete," International Journal of Solids and Structures, vol. 25, no.3, pp. 229–326, 1989. Lubliner, J., J. Oliver, S. Oller, and E. Oñate,
- [20] Jeeho Lee and Gregory L.Fenves, Member ASCE - "Plastic damage model for cyclic loading of concrete structures"
- [21] W.F. Chen - Plasticity of reinforced concrete - McGraw-Hill, New York 1982

[22] Van Vliet, M.R.A., Van Mier, J.G.M. "Softening behaviour of concrete under uniaxial compression," Proc., 2nd Int. Conf. on Fracture Mechanics of Concrete and Concrete Structures (FRAMCOS), Zurich, Switzerland, 383-396, 1996.

[23] Kent D.C, Park R " Flexural members with confined concrete" - Publisher: American Society of Civil Engineers

[24] Sherif S. Morcos, I Associate Member, ASCE, and Reidar Bjorhovde, 2 Fellow, ASCE - "Fracture modeling of concrete and steel"

[25] Luca G. Sorelli Università di Brescia , Alberto Media, Università di Bergamo Giovanni A. Plizzari, Università di Bergamo "LEGAME COSTITUIVO DI CALCESTRUZZI RINFORZATI CON SISTEMI DI FIBRE IBRIDE" extracted from the documents of 15° Congresso C.T.E. Bari, 4-5-6 novembre 2004

[26] – H. A. W. Cornellissen , D.A. Hordijk and H.W. Reinhardt - "Experimental determination of crack softening characteristics of normalweight and lightweight concrete" , Heron publications